Rapid Induction of the Unfolded Protein Response and Apoptosis by Synthetic Oestrogen Mimic TTC-352 and Naturally-Occurring Oestrogen Oestetrol for the Treatment of Endocrine-Resistant Breast Cancer

Balkees Abderrahman

Submitted in accordance with the requirements for the degree of Doctor of Philosophy

The University of Leeds

School of Molecular and Cellular Biology, Faculty of Biological Sciences

8 September 2020

The rationale for pursuing an alternative style PhD thesis is that Balkees Abderrahman's PhD bibliography meets the criteria of the alternative style PhD thesis by the University of Leeds, Faculty of Biological Sciences (FBS). She is the sole, lead, first or primary author on two submitted peer-reviewed publications in academic journals that are appropriate for the field of research, and with an impact factor >3. Her contribution is significant starting with study design, to study implementation, and ending with study write-up. The work of these two publications is derived only from original research undertaken whilst registered for her doctoral study at the University of Leeds, and constitutes a continuous body of work, which is a coherent and continuous thesis, not a series of disconnected publications.

For the convenience of all parties involved, a legend for referencing the two publications in this additional required document that slightly expands on them, has been agreed upon with the internal PI (Prof. John Ladbury) and external PI (Prof. V. Craig Jordan), and in concordance with the University of Leeds, FBS's recommendations for the alternative style

PhD thesis. Whereby, *PAP1* refers to paper 1: Abderrahman B et al. Pharmacology and Molecular Mechanisms of Clinically-Relevant Estrogen Estetrol and Estrogen Mimic BMI-135 for the Treatment of Endocrine-Resistant Breast Cancer. Molecular Pharmacology (American Society for Pharmacology and Experimental Therapeutics journal) 2020 (Online). *PAP2* refers to paper 2: Abderrahman B et al. Rapid Induction of the Unfolded Protein Response and Apoptosis by Estrogen Mimic TTC-352 for the Treatment of Endocrine-Resistant Breast Cancer. Molecular Cancer Therapeutics (American Association for Cancer Research journal) 2020 (Online).

The contribution of the candidate and the other authors to this work has been explicitly indicated below. Balkees Abderrahman was responsible for: cell viability and proliferation assays, real-time polymerase chain reaction, luciferase reporter assays, chromatin immunoprecipitation assays, immunoblotting, human UPR RT^2 PCR profiler arrays, live cell microscopic imaging and analysis, and annexin V staining assays. The contribution of the other authors was: docking and molecular dynamics simulations (Ramona F. Curpan), X-ray crystallography (Sean W. Fanning and Geoffrey L. Greene), ERE DNA pull downs (Yue Chen and Charles E. Foulds), mass spectrometry (Anna Malovannaya and Antrix Jain), resources (Philipp Y. Maximov), and administrative assistance (Jay S. Hanspal and Ping Fan).

Abstract

Patients with long-term oestrogen-deprived (LTED) breast cancer (BC), after resistance to tamoxifen or aromatase inhibitors develops, can experience tumour regression when treated with oestrogens. Oestrogen's anti-tumour effect is attributed to apoptosis via the oestrogen receptor (ER). Oestrogen treatment can have unpleasant gynecological, as well as non-gynecological adverse events, and thus the development of safer oestrogenic agents remains a clinical priority. Here, we study synthetic selective oestrogen mimics (SEMs) BMI-135 and TTC-352, and the naturally-occurring oestrogen oestetrol (E_4), which are proposed as safer oestrogenic agents compared to 17β-oestradiol (E_2), for the treatment of endocrine-resistant BC. TTC-352 and E_4 are being evaluated in advanced BC clinical trials. Cell viability assays, real-time polymerase chain reaction, luciferase reporter assays, chromatin immunoprecipitation, immunoblotting, ERE DNA pull downs, mass spectrometry, X-ray crystallography, docking and molecular dynamics simulations, live cell microscopic imaging and analysis, and annexin V staining, were conducted in 11 biologically-different patient-derived BC models and a human endometrial cancer model. Results were compared with the potent full agonist E_2, less potent full agonists oestrone and oestriol, the benchmark partial agonist triphenylethylene bisphenol (BPTPE), antagonists or Selective ER modulators 4-hydroxytamoxifen, endoxifen, and raloxifene, and Selective ER Downregulator fulvestrant. This work reports ERα's regulation and coregulators' binding profiles with SEMs and E_4. It also describes SEMs and E_4's pharmacology as weak full agonists, and anti-tumour molecular mechanisms through the unfolded protein response (UPR) and apoptosis. These studies highlight the phenolic OH of TTC-352's benzothiophene scaffold and E_4's A ring that yield an H-bond with Glu353, which allows Asp351-to-helix 12 (H12) interaction; sealing ERα's ligand binding domain (LBD), recruiting E_2-enriched coactivators, and triggering rapid ERα-induced UPR and apoptosis, as the basis of its anti-cancer properties. By contrast,

BPTPE's phenolic OH yields an H-Bond with Thr347, which disrupts Asp351-to-H12 interaction; not sealing ERα's LBD properly, not recruiting many E_2-enriched coactivators, and triggering delayed ERα-induced UPR and apoptosis. Such delay might increase the risk of metastasis, clonal evolution, and acquired resistance. Overall, this work concludes the structural, pharmacological, and mechanistic constituents of an effective oestrogen for the treatment of LTED advanced BC.

Table of Contents

Abbreviations

4-hydroxytamoxifen (4OHT)

Adverse events (AEs)

Aromatase inhibitors (AIs)

Activating transcription factor 6 (ATF6)

Breast cancer (BC)

Triphenylethylene bisphenol (BPTPE)

Oestrone (E_1)

17β-oestradiol (E_2)

Oestriol (E_3)

Oestetrol (E_4)

Effective concentration (EC50)

Endoxifen (Endox)

Endoplasmic reticulum (EnR)

E1A binding protein p300 (EP300)

Oestrogen receptor (ER)

Endoplasmic reticulum associated degradation (ERAD)

Oestrogen responsive elements (EREs)

Human epidermal growth factor receptor 2 (HER2)

Intensity-based absolute quantification (iBAQ)

ICI 182,780 fulvestrant (ICI)

Inositol-requiring enzyme 1 (IRE1α)

Lysine Methyltransferase 2D (KMT2D)

Ligand-binding domain (LBD)

Long-term oestrogen deprivation (LTED)

Metastatic breast cancer (MBC)

Mediator complex (MED)

messenger RNA (mRNA)

Nuclear receptor co-activator-3 (NCOA3)

Nuclear extract (NE)

Protein kinase regulated by RNA-like endoplasmic reticulum kinase (PERK)

Progesterone receptor (PgR)

Raloxifene (Ralox)

Root-mean-square deviations (RMSD)

Root-mean-square fluctuation (RMSF)

Selective oestrogen mimic (SEM)

Selective oEstrogen Receptor Modulators (SERMs)

Selective oEstrogen Receptor Downregulators (SERDs)

Selective Human oEstrogen Receptor Partial Agonists (ShERPAs)

 Steroid receptor coactivator -3 (SRC-3)

Tamoxifen (TAM)

Thioflavin T (ThT)

Triphenylethylene (TPE)

Unfolded protein response (UPR)

Women's Health Initiative (WHI)

I. Introduction

IA. Historical background

In 1944, Scottish pathologist Sir Alexander Haddow used high-dose synthetic oestrogen (diethylstilbestrol (DES) and triphenylchloroethylene) therapy to treat metastatic breast cancer (BC) (MBC) (Haddow et al., 1944). Women can achieve oestrogen deprivation either naturally after menopause (average age of menopause in the U.S. and UK is 51 years old), or through long-term adjuvant endocrine therapy with tamoxifen (TAM) or aromatase inhibitors (AIs). Tamoxifen blocks oestrogen action at the level of the breast oestrogen receptor (ER), whereas, AIs inhibit oestrogen synthesis at the level of the breast aromatase enzyme system (Jordan and Brodie, 2007). In Haddow's study, women were long-term oestrogen-deprived (LTED) (≥5 years past menopause), and had a 30% response rate on receipt of the treatment (Haddow, 1970).

High-dose oestrogen therapy was, subsequently, used for 30 years prior to the successful introduction of TAM (Jordan, 2003) (Figure. 1). Tamoxifen was used rather than oestrogen therapy because of the lower incidence of adverse events (AEs) such as those gynecological (i.e., vaginal bleeding and endometrial hypertrophy) and non-gynecological (i.e., hot flashes and thromboembolism-related) (Cole et al., 1971, Ingle et al., 1981). In the 1970s, adjuvant endocrine therapy was successfully advanced with the proposal of long over short-term adjuvant TAM therapy (Jordan and Allen, 1980, Jordan et al., 1979) (Figure. 1). This translational research strategy helped establish TAM as the agent of choice for adjuvant anti-hormone therapy (Early Breast Cancer Trialists' Collaborative Group, 1998).

Beforehand in 1941, Canadian-American physiologist and Nobel Laureate Charles Huggins, and American physician Clarence Hodges, used androgen therapy to treat metastatic prostate cancer (PC) (Huggins and Hodges, 1941). Men were androgen-deprived

either through surgical castration (bilateral orchiectomy), or medical castration with high-dose synthetic oestrogen therapy (DES) that suppresses testosterone levels to the castrate range (Huggins and Hodges, 1972, Huggins and Hodges, 1941). A 50% response rate has been reported on receipt of the treatment (Schweizer et al., 2015, Huggins and Hodges, 1972, Huggins and Hodges, 1941). Huggins and Hodges's work marked the first successful chemical therapy, and awarded Huggins his Nobel Prize for Physiology or Medicine in 1966. Huggins, Hodges, and Haddow's work marked the first successful use of hormones to treat cancer.

Androgen therapy was, subsequently, used for 45 years until the successful introduction of the first luteinizing hormone (LH) releasing hormone (LHRH) analogue, leuprolide, in the 1980s (Garnick, 1984). Leuprolide was used rather than androgen therapy because of the lower incidence of AEs such as gynecomastia and serious cardiovascular-related AEs (Cox and Crawford, 1995, Blackard et al., 1970). Other successful treatment modalities followed such as: anti-androgens (e.g., bicalutamide) that block androgen action at the level of the testes androgen receptor (AR) (Chen et al., 2009), and inhibitors of the testes CYP17 enzymes (e.g., abiraterone acetate) that block androgen synthesis (Reid et al., 2008) (Figure. 1).
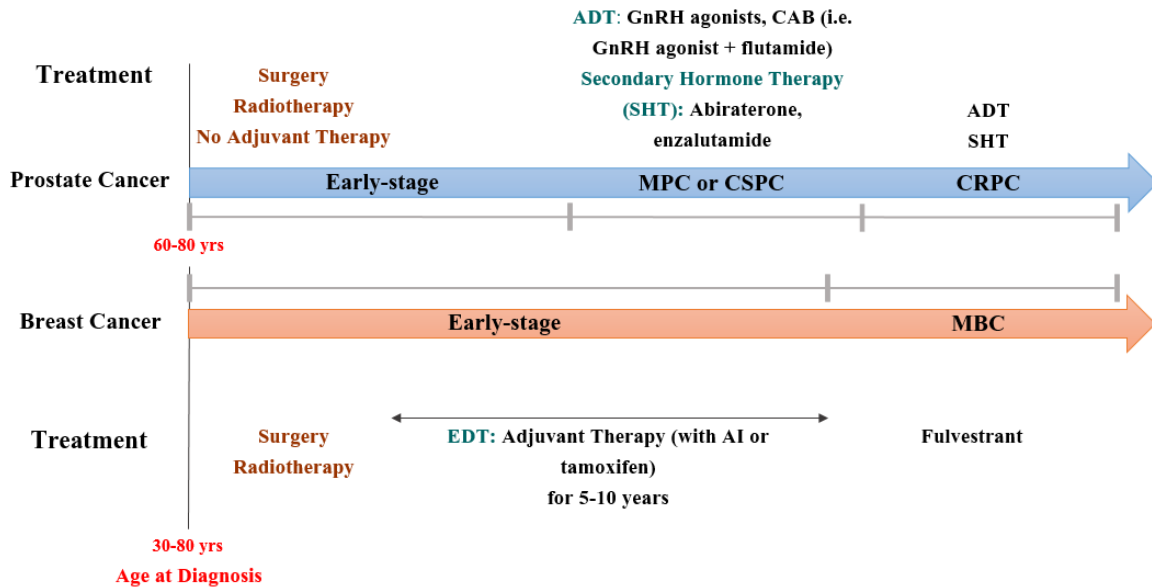
Figure 1 | **Schematic representation of the treatment paradigms used clinically for breast and prostate cancers.** (Panel above) early-stage prostate cancer (PC) is usually approached with active surveillance, and local treatments such as: surgery and radiation therapy. Hormone therapy can be given for early-stage PC men at high-risk, or if they cannot undergo surgery or radiation therapy. The newer treatments for early-stage PC are: Intensity-Modulated Radiation Therapy, Proton beam therapy, and Cryosurgery. If early-stage PC progresses to metastatic PC (MPC), or what is known as castration-sensitive PC (CSPC), it will be treated with androgen deprivation therapy (ADT); using GnRH agonists, or complete androgen blockade (CAB) with a GnRH agonist plus flutamide as one example, or secondary hormone therapy (SHT) using abiraterone, or enzalutamide as an another example. If CSPC progresses to castration-resistant PC (CRPC), it will be treated with ADT or SHT. About 60% of PC is diagnosed in men >65, with 97% in men age >=50. The median age at the time of diagnosis in the U.S. is about 66. (Below panel) early-stage BC can be treated with local treatments such as: surgery and radiotherapy, or systemic treatments such as: hormone therapy. What sets early-stage BC treatment apart from prostate cancer treatment is adjuvant therapy with tamoxifen or AIs for 5–10 years. If early-stage BC progresses to metastatic BC (MBC), one therapeutic option is fulvestrant. Breast cancer rates increase after age 40 and are highest in women >70. The median age of diagnosis of BC for women in the U.S. is 62.

IB. Breast and prostate cancer epidemiology

Breast cancer is the most common cancer in women, and the second leading cause of cancer death in females, in the United States and United Kingdom (Siegel et al., 2020, Cancer Research UK, 2014) (Figure. 2). In 2014 in Great Britain, 31 women died every day from BC (Cancer Research UK, 2014). In 2012 in Europe, more than 131,000 women died from BC (Cancer Research UK, 2014). England ranks 14th in Europe in regards to the highest BC related-mortality rates (Cancer Research UK, 2014). Whereas, by 2019 in the United States, an estimate of 41,760 women were expected to die from BC (2019b). Rosenberg and colleagues projected BC cases to double between 2011 and 2030 in the United States (Rosenberg et al., 2015). In this projection, the majority of BC cases will be ER-positive (Rosenberg et al., 2015), which has a high risk of recurrence and residual relapse even with clinically low-risk disease (T1N0) (Schroeder et al., 2017).
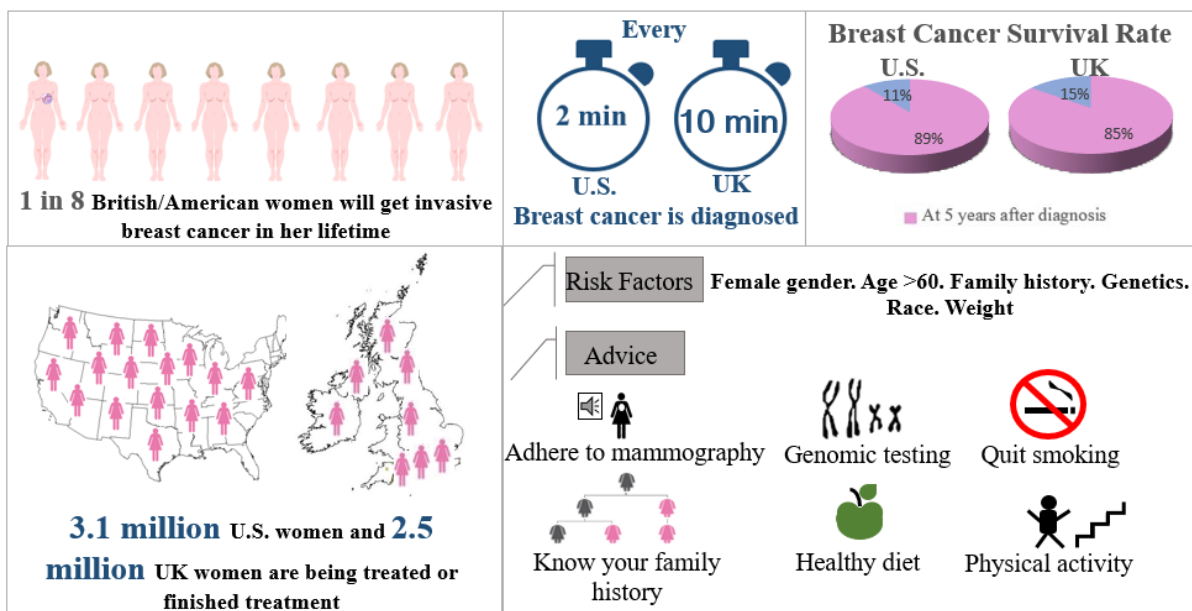
Figure 2 | **Schematic representation of the epidemiology of breast cancer in the United States and United Kingdom.**

Prostate cancer is the most common solid-organ malignancy in men in the United States and the United Kingdom, and the second most common worldwide (Siegel et al., 2015,

Ferlay et al., 2015, Cancer Research UK, Siegel et al., 2020). It is also the second leading cause of cancer death in males in the United States and the United Kingdom (American Cancer Society, Cancer Research UK, Siegel et al., 2020). Between 2014-2016 in Great Britain, 31 men died every day from PC (Cancer Research UK). Whereas, in 2019 in the United States, approximately 91 men died every day from PC (2019a).

IC. Oestrogen and androgen receptor signal transduction pathways

The ER has two subtypes (Thomas and Gustafsson, 2011): ERα which was discovered in the late 1950s, and ERβ identified in 1996. ERα is a product of the gene ESR1, and ERβ is a product of ESR2 on a different chromosome (Thomas and Gustafsson, 2011). The ER has several structural and functional domains (Thomas and Gustafsson, 2011) (Figure. 3): the amino-terminal A/B region contains a transactivation domain (AF-1), which is pivotal to the transcriptional activity of ERα through a ligand-independent function, and a co-regulatory domain responsible for co-activators and co-repressors recruitment. ERβ is truncated and lacks AF-1. The C region represents the DNA-binding domain (DBD), which is the most conserved region among ERα and ERβ. This region is crucial for binding to specific oestrogen response elements (EREs) in the proximal promoter region or at distal regulatory elements of ERE. The D region (or the hinge region) is part of the ligand-dependent activating domain and the nuclear localization signal. The regions E and F, contain the ligand-binding domain (LBD), a coregulatory binding surface, the dimerization domain, second nuclear localization signal, and activation function 2 (AF-2).

Both AF-1 and AF-2 act together at the promoter region for a full oestrogen-like activity in ERα, but ERβ does not have an active AF-1 site (Figure. 3). As there is no AF-1 in ERβ, heterodimerization of ERα and ERβ causes anti-oestrogenic effects. The amino acids Leu384 and Met421 in the LBD regions of ERα are replaced by Met336 and Ile373 in ERβ,

respectively. This similarity in the LBD of ERα and ERβ created problems for targeting

ligands to a specific ER. Human ERα and ERβ isoforms are expressed differently in

malignant tissues, which impacts cancer biology, and exerts opposite effects on cellular

proliferation and apoptosis. Isoform ERα-36 (Wang and Yin, 2015) (Figure. 3), also known

as the "dwarf or truncated ER", lacks both *trans*-activation domains. ERα-36 maintains a

"nongenomic" signaling pathway through mitogen-activated protein kinase, and is resistant to

TAM treatment.
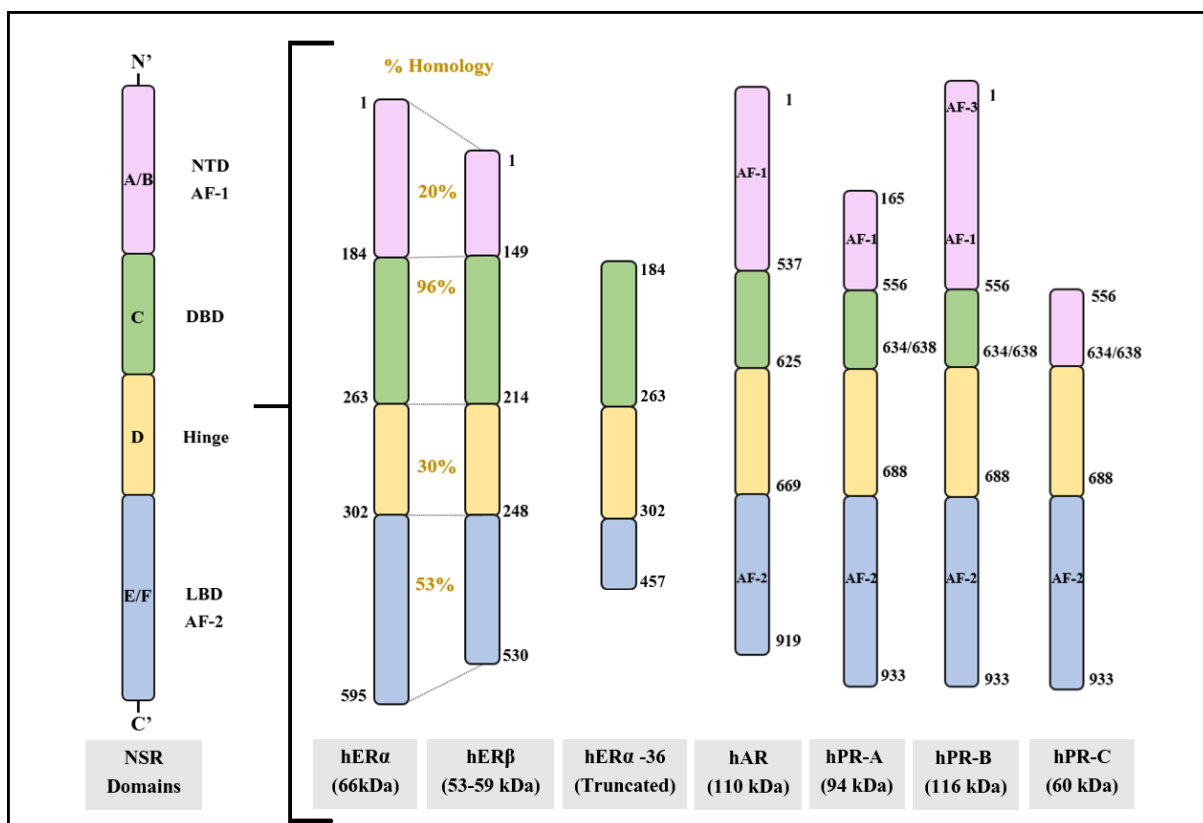
Figure 3 | **Schematic representation of structural and functional domains of the nuclear steroid receptor (NSR) super family, including: ERα, ERβ, ERα-36, and AR.** The structural domains of ERα and ERβ are depicted A–F, with the amino acid numbers indicated above. The percentage amino acid homologies between wild-type oestrogen receptor-α (ERα) and ERβ are also shown. The structural domains for hAR, and hPR are depicted A–F, with the amino acid numbers indicated above. The diagram demonstrates the molecular weight of all receptors.

The expression level and stability of ER is modulated by oestrogens and anti-oestrogens. Two regulatory mechanisms that govern the steady-state of ER messenger RNA (mRNA) and protein levels in BC cells were reported (Pink and Jordan, 1996) (Figure. 4). Model I ER regulation reflects the rapid down-regulation of the steady-state of ER mRNA and protein levels upon oestrogen exposure, and is exemplified in MCF-7:WS8 BC cell line, ovarian carcinoma line (PEO4) (Langdon et al., 1993), and the mouse and rat uterus (Medlock et al., 1991). Model II ER regulation reflects the up-regulation of the steady-state level of ER mRNA, alongside the maintenance of the ER protein level upon oestrogen exposure, and is exemplified in T47D:A18 BC cell line (Pink and Jordan, 1996).
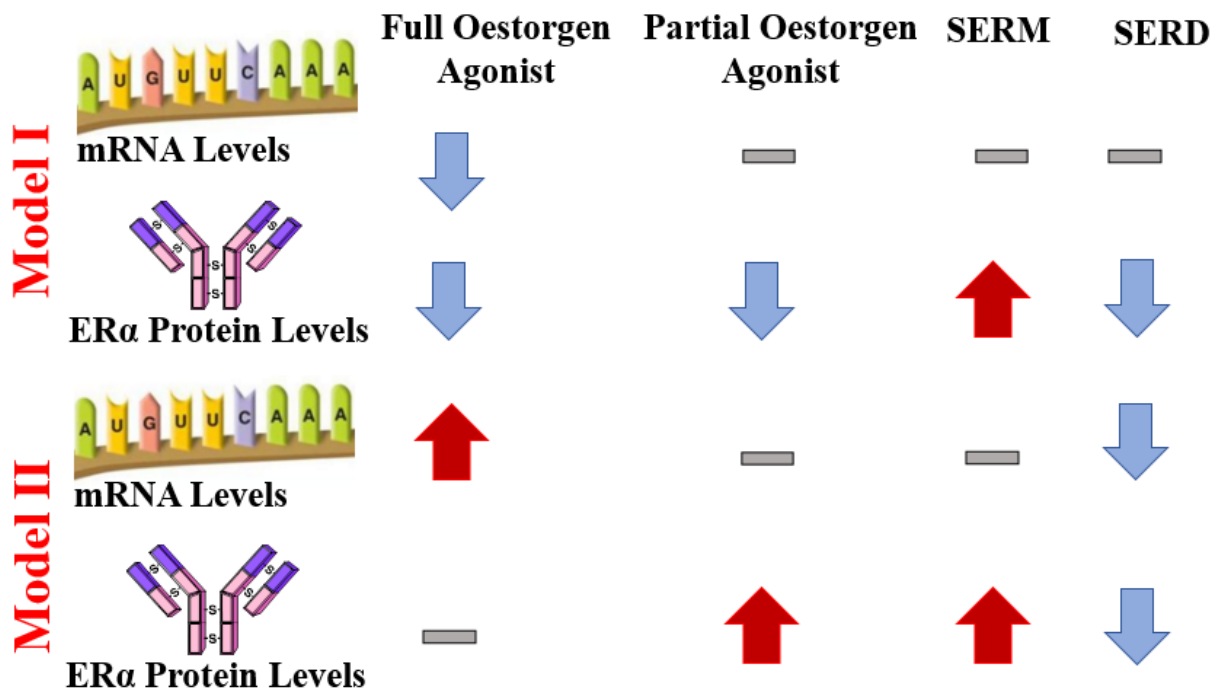
Figure 4 | **Schematic representation of Model I and Model II of ERα regulation with ligands.**

In basic terms, once the ligand binds to the ER in the cytoplasm, ER dissociates from heat shock proteins (HSPs), dimerizes, gets phosphorylated and relocates within nucleus (Thomas and Gustafsson, 2011) (Figure. 5). The ligand-ER complex then binds to a gene specific ERE, and recruits corresponding co-activators or co-repressors. This, in turn, initiates or inhibits a cascade of transcription and translation (Figure. 5).

ERα's transcriptional control of diverse downstream gene expression (Feng and O'Malley, 2014) is dictated by its ability to properly recruit and assemble (Heery et al., 1997, Shiau et al., 1998a, Brzozowski et al., 1997) primary steroid receptor coactivators (e.g., p160 family proteins like steroid receptor coactivator -3 (SRC-3); also known as nuclear receptor co-activator-3 [NCOA3] or A1B1), followed by secondary coactivators (e.g., histone acetyltransferases like p300/E1A binding protein p300 [EP300]), in what's known as minimal receptor-coactivator complex (Yi et al., 2015). This facilitates chromatin remodeling and transcriptional activation. A model was proposed for the assembly mechanism of the quaternary complex (of ERE-bound ERα, SRC-3, and p300/EP300): the two ligand-bound ERα monomers each, independently, recruits one SRC-3 protein through the transactivation domain of ERα, and the two SRC-3s, subsequently, bind to different regions of one p300 protein via multiple contacts (Yi et al., 2015).

Resistance to endocrine therapies can be attributed to ample factors, such as: increased activity of downstream kinase pathways (Jordan et al., 2004), or overexpression of growth factor receptors (Schiff et al., 2005), or increased phosphorylation of ER, or mutations at the level of ER (Roodi et al., 1995).

Androgen synthesis is finely regulated by the hypothalamic–pituitary–gonadal axis. Upon the stimulation of the hypothalamus, LHRH is produced. This hormone works in a pulsatile fashion to stimulate the release of LH by the anterior pituitary. This, in turn, induces the synthesis of androgen at the testicular level. Moreover, LHRH also stimulates the production of adrenocorticotropic hormone by the anterior pituitary, which augments overall androgen production, but at the adrenal gland level.

Testosterone is metabolically converted to dihydrotestosterone by enzyme 5α reductase, which then binds to AR causing the dissociation of corresponding HSPs, and

subsequent dimerization and phosphorylation of the AR (Figure. 5). The AR has three

distinctive functional domains: N-terminal domain, the DBD and the LBD (Wong et al.,

2014) (Figure. 5). In the nucleus, the androgen-AR complex (Edwards and Bartlett, 2005)

binds to androgen response elements/genes including *TMPRSS2:ERG* and prostate-specific

antigen. This, in turn, recruits the DNA transcriptional machinery to initiate gene

transcription (Edwards and Bartlett, 2005). Although the AR is the essential mediator to

regulate normal growth, it also participates in promoting the oncogenic fusion genes

especially E-twenty-six family (Wang et al., 2009).
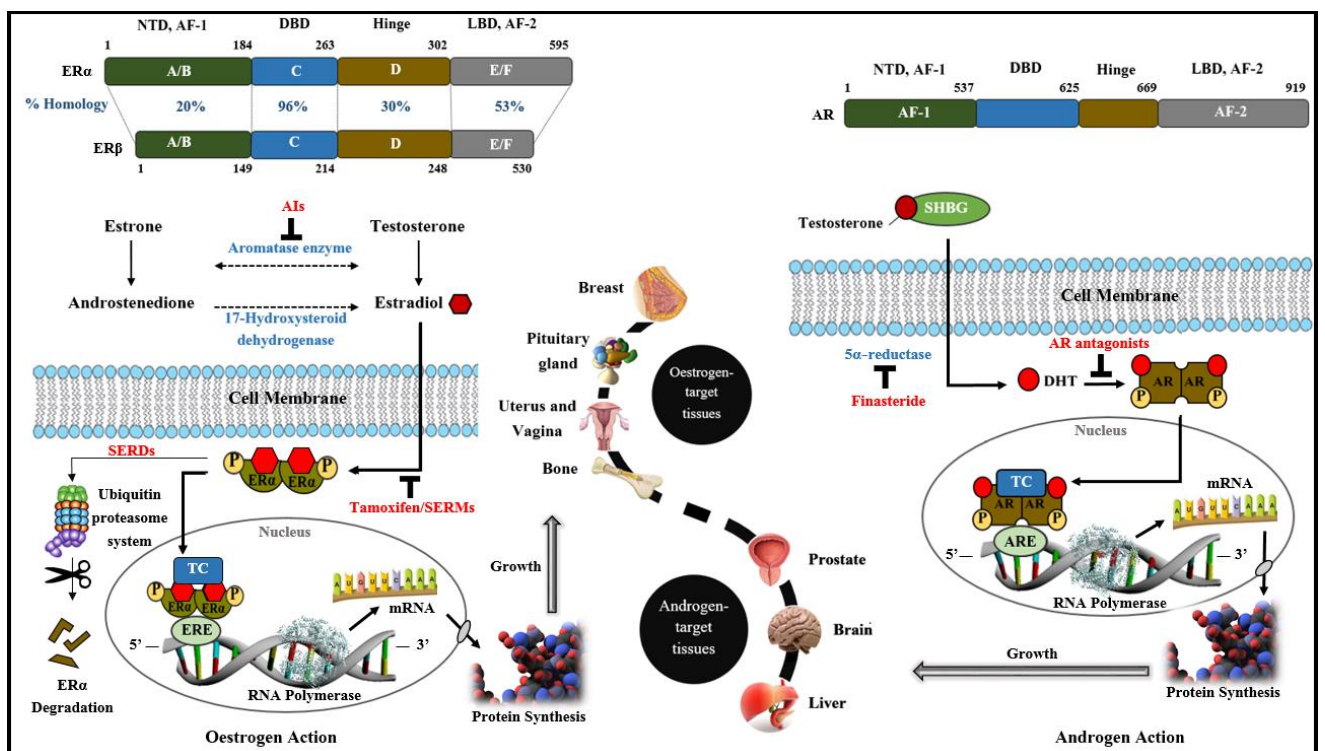
Figure 5 | **Schematic representation of the ER and AR structural and functional domains, their corresponding signal transduction pathways, commonly used therapeutic agents, and target tissues.** The DBD is most conserved among ERα and ERβ with a homology of 96%. Oestrone is

converted to androstenedione, and testosterone is converted to oestradiol through the aromatase

enzyme system, which is inhibited by AIs. Androstenedione, in turn, is converted to oestradiol

through 17-hydroxysteroid dehydrogenase. Tamoxifen/SERMs competitively inhibit oestrogen

binding to the ER, while SERDs destroy the ER through the ubiquitin proteasome system. Oestrogen

binding to the ER initiates a cascade of events throughout the ER signal transduction pathway. Similarly, the binding of DHT to the AR, after it's synthesis from testosterone by 5α-reductase, initiates a cascade of events throughout the AR signal transduction pathway. Finasteride inhibits 5α-reductase, and AR antagonists competitively inhibit the binging of androgens to the AR.

Mechanisms of maintained AR signaling in castration-resistant prostate cancer (CRPC) have been identified (Ryan and Tindall, 2011, Attard et al., 2011), such as: increased AR signaling whether it was increased AR expression or gene amplification, point mutations in AR LBD, expression of active AR splice variants, cross-talk with other pathways, presence of residual androgens, and changes in co-regulator proteins.

A unique transcription factor termed forkhead-box A1 (FOXA1), plays a critical role in chromatin remodeling and decompaction (Yang and Yu, 2015). This allows the genomic access by the nuclear hormone receptors such as the AR and ER. The complex of FOXA1-AR remains in equilibrium states in the nucleus, and defines the prostatic AR binding profile. In prostate cancer, this equilibrium is disturbed with FOXA1 and/or AR de-regulation (Yang and Yu, 2015). A recent meta-analysis (Shou et al., 2016) showed that higher levels of FOXA1 expression is associated with a better prognosis in BC.

ID. Oestrogen synthesis and metabolism

There are four naturally-occurring forms of oestrogen: oestrone (E_1), E_2, oestriol (E_3), and oestetrol (E_4) (Figure. 6). 17β-oestradiol is the most potent and biologically-active oestrogen, which is primarily secreted by the ovarian granulosa cells (positioned next to theca cells), under the influence of the follicle-stimulating hormone (FSH) (Cui et al., 2013). Oestriol is the major oestrogen in pregnant women given its production in large quantities by the placenta, is the most abundant oestrogen in the urine of all women, and is not used in long-term oral oestrogen therapy as it has a very short oral elimination half-life. Oestetrol is

exclusively produced by the fetal liver during pregnancy, and reaches maternal circulation through the placenta (Holinka et al., 2008). Overall, E_1 is generally 12 times weaker than E_2, and E_3 is generally 80 times weaker than E_2.

Oestrone is reversibly converted to E_2 through the enzyme 17β-hydroxysteroid dehydrogenase (Ryan, 1959) (Figure. 6). Androstenedione, produced in the theca cells during the follicular phase of the menstrual cycle, acts as a precursor for E_1 and testosterone in the ovaries and peripheral tissues (Cui et al., 2013). Testosterone is then converted to E_2 through the aromatase enzyme in the peripheral tissues (Figure. 6). Aromatase (CYP19; encoded by the *CYP19A1* gene) is the rate-limiting enzyme in converting androgens to oestrogens (Tsuchiya et al., 2005). Oestriol is produced by the hydroxylation of E_2 or 16α-hydroxyoestrone, while E_4 is produced from E_2, E_3, and other precursors from the fetal liver and adrenal gland (Figure. 6). In premenopausal women, E_2 is synthesized in the ovaries, and is considered the dominant oestrogen. In postmenopausal women, oestrone is synthesized in peripheral tissues, and is considered the dominant oestrogen.

17β-oestradiol is metabolized by three competitive pathways involving irreversible hydroxylations by the NADPH-dependent cytochrome P450 (CYP) enzymes (CYP1A1, CYP1B1, and CYP1A2) (Samavat and Kurzer, 2015). Catechol oestrogens are further metabolized to methoxyestrogens (2-methoxyestrone, 4-methoxyestrone, 2-methoxyestradiol and 4-methoxyestradiol) by the catechol-O-methyltransferase (COMT) enzyme (Samavat and Kurzer, 2015).
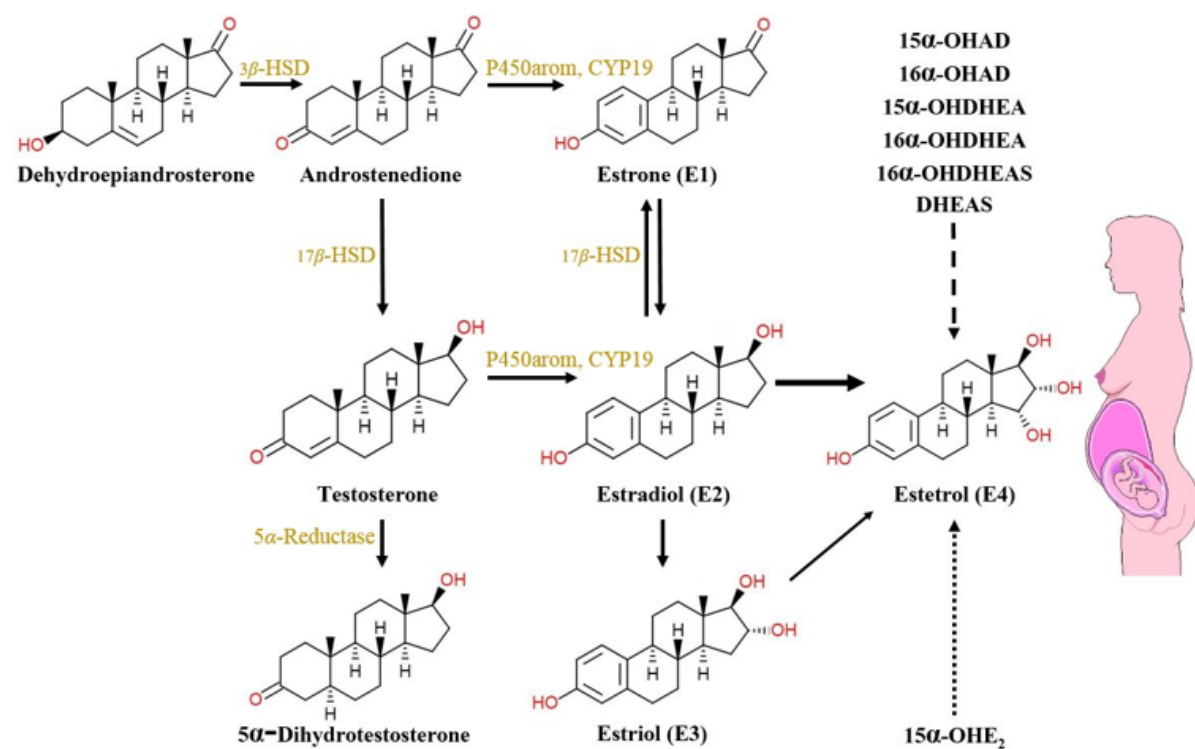
Figure 6 | **Schematic representation depicting the synthesis of different oestrogens.**

Other than methylation, parent oestrogens and catechol oestrogens are conjugated with glucuronic acid and sulfate by hepatic phase II enzymes (UDP-glucuronosyltransferases and sulfotransferases, respectively). Such conjugation makes oestrogens become either water soluble to be excreted in the urine or feces, or turn them into a more lipophilic moiety with prolonged half-lives (Lakhani et al., 2003).

Sulfation remains the main pathway for oestrogen metabolism, and is involved in the inactivation of oestrogens in target tissues; through converting oestrogens to 17b-estra-1,3,5-trien-3,17-diol 3-sulfateno, which cannot interact with the oestrogen receptors (Kotov et al., 1999). In specific, SULT1E1 and PAPSS (PAPSS1 and PAPSS2) are responsible for the oestrogen sulfation, through providing the catalyzing enzyme and universal sulfate donor. Dietary flavonoids were shown to influence the bioavailability of endogenous oestrogens through inhibiting steroid sulfatase (Harris et al., 2004).

Overall, the ratio of circulating oestrogens could be indicative of the woman's dynamic metabolism, in terms of the balance between oestrogen synthesis and deactivation (through metabolism of E_2 to the less-potent forms E_1 or E_3, and sulfation of E_2 by oestrogen sulfotransferase).

IE. Breast and prostate cancer therapeutics

More than 70% of BC is ER–positive (Clark et al., 1984), which is effectively targeted with endocrine therapies (Abderrahman and Jordan, 2016e), such as: Selective ER Modulators (SERMs) (e.g., TAM) (Maximov et al., 2013), or AIs (e.g., anastrozole, exemestane, and letrozole) (Jordan and Brodie, 2007).

Tamoxifen (Figure. 7) is a competitive inhibitor of oestrogen at the level of the ER, and causes a G1 blockade in BC cell cycle (Sutherland et al., 1983, Osborne et al., 1983). On the other hand, AIs inhibit the BC aromatase enzyme system CYP19, blocking the conversion of androstenedione or testosterone to oestrogens in peripheral tissues (Jordan and Brodie, 2007). Neither TAM nor AIs are cytotoxic and, therefore, do not cause cellular apoptosis (Jordan, 2015a, Bhattacharya et al., 2017). Tamoxifen is used to treat all stages of ER-positive BC, for long-term adjuvant therapy, and chemoprevention (Abderrahman and Jordan, 2015, Abderrahman and Jordan, 2016c, Abderrahman and Jordan, 2016a). It can be administered to pre-and-post-menopausal women, and has serious but *rare* AEs such as: endometrial cancer and thromboembolic events. Such AEs were observed particularly in postmenopausal women (Vogel et al., 2010).

Aromatase inhibitors (Figure. 7) are now the treatment of choice in BC, because there are fewer AEs compared to TAM, but are used only to treat post-menopausal women, except those who are at risk of osteoporosis. Nevertheless, AIs can have unpleasant musculoskeletal

symptoms (Khan et al., 2010), cause osteoporotic fractures (Hadji et al., 2017), and lead to significant urogenital atrophy including vaginal atrophy (Melisko et al., 2017).

Pure anti-oestrogens, or Selective ER Downregulators (SERDs) (e.g., ICI 182,780 fulvestrant [ICI]) (Figure. 7), exert a proteasomal degradation of the ERα protein through the ubiquitin proteasome system (McDonnell et al., 2015). Fulvestrant is used in post-menopausal women with MBC, but given its route of administration being intramuscular injections (Robertson, 2007, Ellis et al., 2015, Robertson et al., 2016), it has an unfavorable AE of pain and swelling at the injection site.
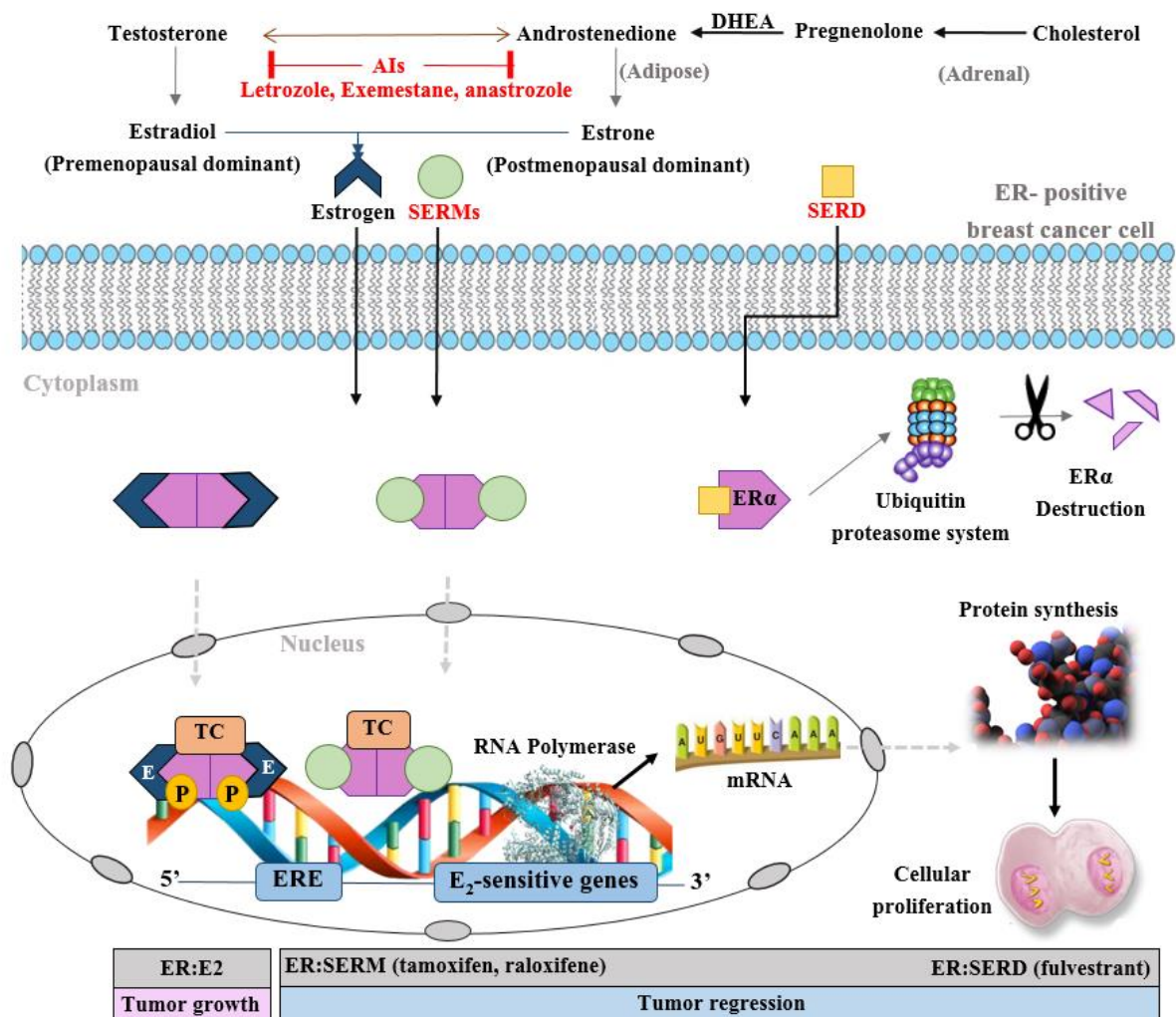
Figure 7 | **Schematic representation of the signal transduction pathways in ER-positive breast cancer cells and their targeted therapeutics.** At the adrenal level, adrenal androgen *de novo* steroidogenesis occurs. Cholesterol is produced and converted to Pregnenolone with the aid of

CYP11A1 enzyme. Pregnenolone is converted to dehydroepiandrosterone (DHEA) with the aid of CYP17A1. Finally, DHEA is converted to androstenedione (AD) with the aid of 3-β hydroxysteroid dehydrogenase enzyme. Then, AD is converted to testosterone via 17-β hydroxysteroid dehydrogenase. At the adipose tissue level, both androstenedione and testosterone are converted with the aid of the aromatase enzyme system to oestrone (predominant in postmenopausal women), and oestradiol (predominant in premenopausal women), sequentially. Oestrogen normally binds to the ER in the cytoplasm, the oestrogen:ER complex translocates to the nucleus, gets phosphorylated, and binds to oestrogen responsive elements (EREs) with the recruitment of coactivators. This creates a transcription complex (TC). This in turn, will initiate a cascade of protein synthesis and subsequent tumour proliferation through the activation of oestrogen-sensitive genes. Whereas, SERMs:ER follows a similar pattern, but recruits corepressors and inhibits protein synthesis; causing tumour regression. For SERDs, they bind to the ER causing an alien conformation, which leads to the destruction of the ER through the ubiquitin proteasome system; subsequently tumour regression.

Patients with MBC, who have failed prior endocrine therapy with TAM, AIs, or ICI, can be treated with mammalian target of rapamycin (mTOR) inhibitors (e.g., everolimus) (Vicier et al., 2014), or Cyclin-dependent kinase 4/6 (CDK4/6) inhibitors (e.g., palbociclib) (O'Leary et al., 2016, Xu et al., 2017). Both mTOR and CDK4/6 inhibitors are expensive (Abderrahman and Jordan, 2016e), costing patients ~$10,000-11,000 per month out-of-pocket expense. In addition, they have undesirable toxicity profiles with grade 1/2 AEs (e.g., stomatitis) for mTOR inhibitors (Paplomata and O'Regan, 2014), and grade 3/4 AEs (e.g., non febrile neutropenia) for CDK4/6 inhibitors (Finn et al., 2016). Endocrine therapies often fail to achieve their therapeutic targets because of acquired resistance (Musgrove and Sutherland, 2009, Jeselsohn et al., 2015), or patients' non-adherence from toxicity and/ or other factors (Osterberg and Blaschke, 2005, Abderrahman, 2017a, Abderrahman, 2017b).

Prostate cancer has followed a similar treatment strategy to that of BC, in essentially exploiting the clues and principles established for BC treatment. Androgen deprivation can

still be achieved by gonadectomy and high-dose oestrogen therapy, however, they are now replaced by the use of sustained release of an LHRH superagonist. This effectively suppresses the release of gonadotropins, which, in turn, suppresses androgen synthesis in the testes. Anti-androgens (Figure. 8) that bind to and block the AR, have been refined and improved over the past three decades, based on the experiences with the modulation of the ER. The next generation "anti-androgenic" blocking agents (abiraterone acetate and enzalutamide), have significantly prolonged survival in patients with CRPC (Wong et al., 2014). Abiraterone acetate is considered a first-in-class inhibitor of cytochrome P-450c 17 (Figure. 8), which is responsible for androgen synthesis at the testicular and extragonadal level, and has shown to improve overall survival, and delay the initiation of chemotherapy in metastatic CRPC (Ryan et al., 2013). The combination of abiraterone acetate and prednisone is used for CRPC after exposure to docetaxel (de Bono et al., 2011).
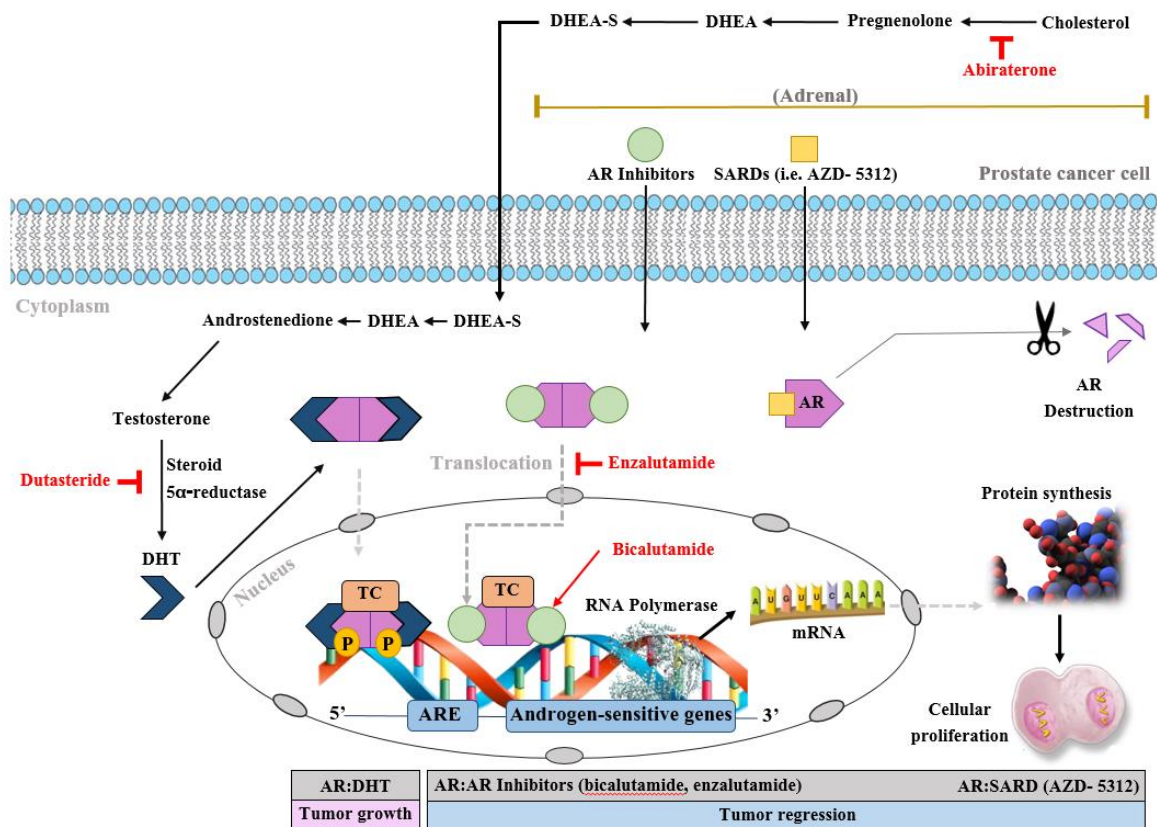
Figure 8 | **Schematic representation of the signal transduction pathways in prostate cancer cells and their targeted therapeutics.** At the adrenal level, adrenal androgen *de novo* steroidogenesis occurs. Cholesterol is produced and converted to Pregnenolone with the aid of CYP11A1 enzyme. Pregnenolone is converted to dehydroepiandrosterone with the aid of CYP17A1. Finally, DHEA is converted to DHEA-S with the aid of following enzymes: steryl-sulfatase (STS) and bile salt sulfotransferase. At the prostae level, DHEA-S in Leydig cells is converted back to DHEA via STS, and then DHEA is converted to AD via enzyme 3β-HSD. Then, AD is converted to testosterone via enzyme AKR1C3, and finally to DHT via steroid 5α-reductase. Dihydrotestosterone normally binds to the AR in the cytoplasm, the DHT:ER complex translocates to the nucleus, gets phosphorylated, binds to androgen responsive elements (AREs) with the recruitment of coactivators. This creates a transcription complex (TC), which initiates a cascade of protein synthesis and subsequent tumour proliferation; through the activation of androgen-sensitive genes. Whereas, AR inhibitors:AR complex follows a similar pattern, but recruits corepressors and inhibits protein synthesis; causing tumour regression. For SARDs, they bind to the AR causing the degradation of the receptor; subsequently tumour regression. Androgen receptor inhibitors vary in their mechanisms of action. For example, enzalutamide competitively inhibits the AR binding to DHT, inhibits nuclear translocation of AR, and DNA and cofactor binding. Whereas, bicalutamide is a highly selective, competitive and a silent antagonist of the AR, which was also found to accelerate AR degradation. Abiraterone inhibits CYP17A1 and subsequently adrenal androgen *de novo* steroidogenesis. Dutasteride is a 5α-reductase inhibitor that blocks testosterone conversion into DHT.

IF. Long vs. short-term adjuvant tamoxifen therapy

The use of adjuvant TAM therapy was initially short-term; limited to 1-2 years (Jordan, 1990). This cautious approach by the clinical community was based upon their experience with TAM being effective for 2-3 years in the treatment of 30% of MBC, and that resistance might develop with long-term treatment. The first question was: what would happen if TAM treatment is extended beyond 2 years? The Swedish Breast Cancer

Cooperative Group trial catered to answering this question (1996). It showed that 5 years of TAM is more beneficial than 2 in the treatment of postmenopausal women with ER-positive, early stage, invasive BC (1996).

The second question was: what is the duration of therapy necessary to maintain the maximum benefit, and what is the nature and severity of AEs from prolonged treatment? The National Surgical Adjuvant Breast and Bowel Project (NSABP) filled in these gaps by evaluating the outcomes of patients in the NSABP B-14 trial through 10 years of follow-up, and evaluating the effects of 5 years versus more than 5 years of TAM therapy in ER-positive lymph node-negative BC patients (Fisher et al., 1996). The trial concluded that the 5-year-benefits from TAM treatment persisted through 10 years of follow-up, and that the TAM-extended arm had a higher incidence of thromboembolic AEs, but not endometrial cancer.

The third question was: if 5-year-TAM treatment is better than 2, would 10 years be better than 5, especially when at least 50% of BC recurrences occur more than 5 years after diagnosis, according to the Oxford overview analyses (Early Breast Cancer Trialists' Collaborative et al., 2011)? The Adjuvant Tamoxifen Longer Against Shorter (ATLAS) trial demonstrated both a reduction in BC recurrence and mortality, when TAM treatment is continued to 10 years in ER-positive BC women (Davies et al., 2013). These effects were more pronounced after 10 years (Davies et al., 2013). The ATLAS trial alongside other previous trials, suggested that 10 years of TAM treatment can halve BC mortality during the second decade after diagnosis (Davies et al., 2013) (Figure. 10). A similar trial but UK-based, referred to as adjuvant Tamoxifen Treatment offers more (aTTom) (Gray et al., 2013) (Figure. 10), has reaffirmed ATLAS's conclusions. Pooled data from the ATLAS and aTTom trials accentuated the tremendous clinical benefit of long-term adjuvant TAM treatment up to 10 years (Schiavon and Smith, 2014). These findings changed clinical practice. The American Society of Clinical Oncology guidelines now recommend that women with ER-

positive BC should consider 10 years of TAM treatment (Abderrahman and Jordan, 2018). Investigators, subsequently, provided a guide (Sgroi et al., 2013) to improve the risk-benefit of long-term adjuvant endocrine therapy in concordance with the patient's individualized risk for early- versus late-distant recurrence.

Earlier scientific studies dovetailed with clinical trials in demonstrating that TAM can reduce the risk of BC, whereby TAM in animal models was capable of preventing chemical carcinogenesis in rats, and spontaneous mammary carcinogenesis in high-risk strains of mice (Jordan, 1976, Jordan et al., 1991). They also showed that TAM treatment might yield occult endometrial cancer, which warrants gynecological screening (Gottardis et al., 1988).

The fourth and last question was: can AIs replace TAM in short or long-term adjuvant endocrine therapy for BC? Several clinical trials (Baum et al., 2002, Howell et al., 2005, Breast International Group 1-98 Collaborative et al., 2005, Coates et al., 2007, Coombes, 2004, Boccardo et al., 2005, Goss et al., 2003b, Goss et al., 2005) (Figure. 10) answered this question with a "yes"; showing equal clinical benefits to TAM, if not superior in certain patient populations. However, there seems to be a general outlook that 3 years of TAM followed by 2 years or more of AIs is cost-effective, well-tolerated, and improves event-free and recurrence-free survival in postmenopausal patients with early BC (Boccardo et al., 2005).

IG. Acquired resistance to endocrine therapy in breast cancer

Laboratory studies demonstrated the unique properties of acquired resistance to anti-oestrogen therapy *in vivo* in ER-positive BC. Acquired resistance to TAM therapy initially involves the growth of BC populations, within 1 to 2 years, which are TAM and oestrogen-dependent (Gottardis and Jordan, 1988, Gottardis et al., 1989b) (Figure. 10). Further studies of resistance *in vivo* demonstrated that >5 years of TAM treatment (mimicking the period of

the standard of care at the time), leads to cell selection pressure during oestrogen deprivation

(Figure. 9), of new BC populations that grow with TAM, but now die with physiologic levels

of oestrogen (Yao et al., 2000, Wolf and Jordan, 1993). This discovery provided an

explanation of why high-dose oestrogen therapy was only effective ≥5 years past menopause

in Haddow's studies (Haddow, 1970).
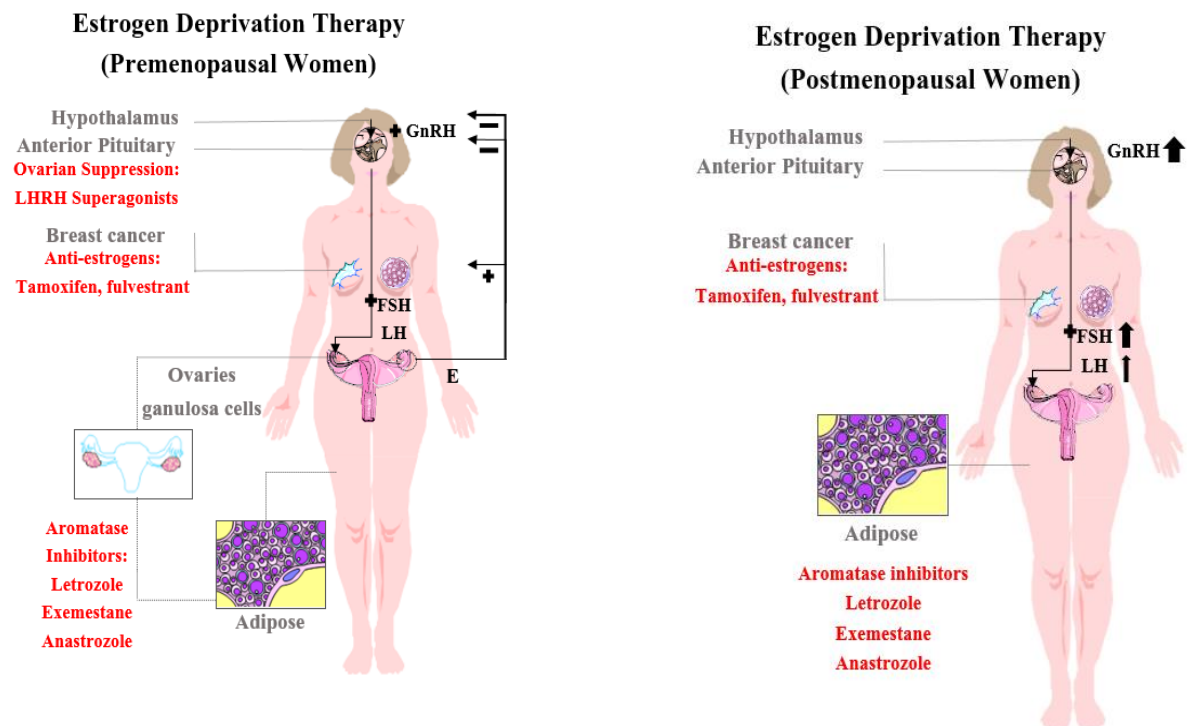
Figure 9 | **Schematic representation of the oestrogen deprivation therapy in pre- and
postmenopausal women with breast cancer.** (Left) The hypothalamic–pituitary–gonadal axis in
premenopausal women with breast cancer and their therapeutic targets. The hypothalamus produces
gonadotropin-releasing hormone (GnRH), which stimulates the adenohypophysis of the pituitary to
produce luteinizing hormone (LH) and follicle-stimulating hormone (FSH). This in turn, stimulates
the granulosa cells in the ovarian follicles to produce oestrogen. However, FSH in particular
stimulates the granulosa cells to produce inhibin, which suppresses FSH in a feedback loop and
activin; a peripherally produced hormone that stimulates GnRH cells. Oestrogen stimulates the growth
of breast cancer cells, and exerts a negative feedback loop onwards to the hypothalamus and pituitary.

Ovarian suppression can be achieved with LHRH superagonists such as goserelin, which is an analogue of LHRH, and a GnRH or LHRH agonist. Goserelin initiates a flare of LH production and ultimately leads to receptor downregulation. Anti-oestrogens can be oestrogen receptor (ER) competitive blockers such as the Selective ER Modulators (SERMs, i.e., tamoxifen), or pure anti-oestrogens or what is known as a Selective ER Downregulators (SERDs, i.e., fulvestrant). Third-generation aromatase inhibitors (i.e., anastrozole, letrozole, exemestane) selectively block the aromatase enzyme system at the breast cancer level and, therefore, suppress oestrogen synthesis. (Right) The hypothalamic–pituitary–gonadal axis in postmenopausal women with breast cancer and their therapeutic targets. The differences from premenopausal women is that the ovarian follicles are depleted, therefore, there is no active production of oestrogen and progesterone. This leads to a dramatic increase in GnRH, and an increase in FSH serum level relatively to that of LH through the feedback loops. Ovarian suppression is not used as a treatment option anymore.

The effect of physiologic oestrogen on LTED BC *in vitro*, was shown to trigger a cellular stress response, named the unfolded protein response (UPR), and, subsequently, induce mitochondrial apoptosis (Ariazi et al., 2011, Lewis et al., 2005a, Song et al., 2001) (Figure. 10). Hosford and colleagues (Hosford et al., 2019) confirmed the involvement of the UPR and apoptosis in patient-derived oestrogen-deprived ER-positive xenografts when treated with 17β- oestradiol (E_2). This UPR-and-apoptosis-paired biology, underlining oestrogen-induced tumour regression in LTED BC, not only explains the earlier observational clinical science (Haddow, 1970), but also forms the pillar of oestrogen's therapeutic potential for the treatment of advanced endocrine-resistant BC.
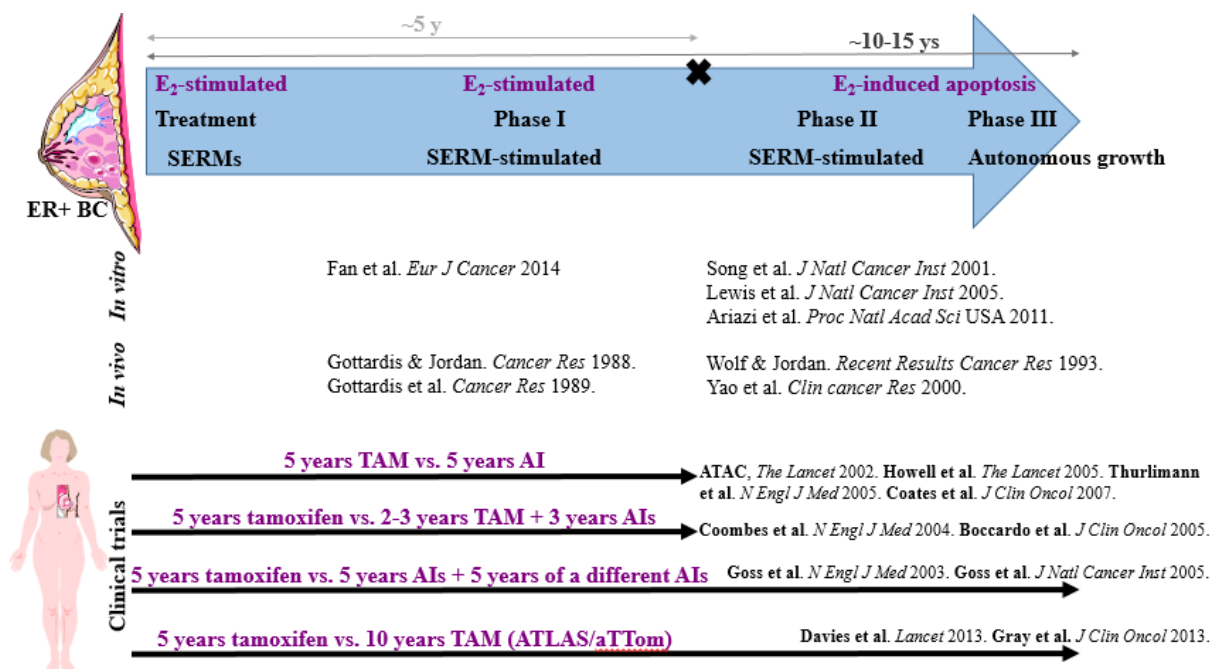
Figure 10 | **Schematic representation of the** *in vitro* **and** *in vivo* **studies of tamoxifen resistance alongside the landmark clinical trials that evaluated tamoxifen versus AIs (over 5 and 10 years).**

IH. Acquired resistance to endocrine therapy through ER mutations

Under normal physiologic conditions, the planar steroid oestradiol is positioned in the LBD of the WT ERα by Glu353, Arg394, and His524 (Figure 11B). This allows H12 to seal the LBD (Figure 11B). The amino acids Tyr537, which gets phosphorylated to ensure an efficient oestrogenic action of the ligand:ERα complex and was shown to influence the turnover and activation of ERα, as well as Asp538 have become of interest. *ESR1* somatic mutations, Y537S and D538G, stabilize ERα in the agonist state, and are linked to acquired resistance to endocrine therapies (Fanning et al., 2016) (Figure. 11A). Mutations Tyr537Ser and Asp538Gly were most prevalent in BC metastases (Toy et al., 2013b), especially AI-resistant BC patients, and contribute to roughly 25% of overall resistance to endocrine therapies. These mutations improve the closure of H12 over ERα's LBD, through interacting with Asp351, and recruiting coactivators in the absence of oestrogen, which increases the estrogen-like properties of the complex (Toy et al., 2013b, Jordan et al., 2015). These

mutations are positioned on the external view of the E₂:ERα complex, and are closely aligned with Asp351 in the LBD (Jordan et al., 2015) (Figure. 11C and E).

The prognostic and predictive value of circulating *ESR1* mutation, and its kinetics before and after progression on AI treatment, was evaluated. *ESR1* circulating D538G and Y537S/N/C mutations were shown to be independent risk factors for poor outcome after AI failure, and were frequently detectable before clinical progression (Clatot et al., 2016).
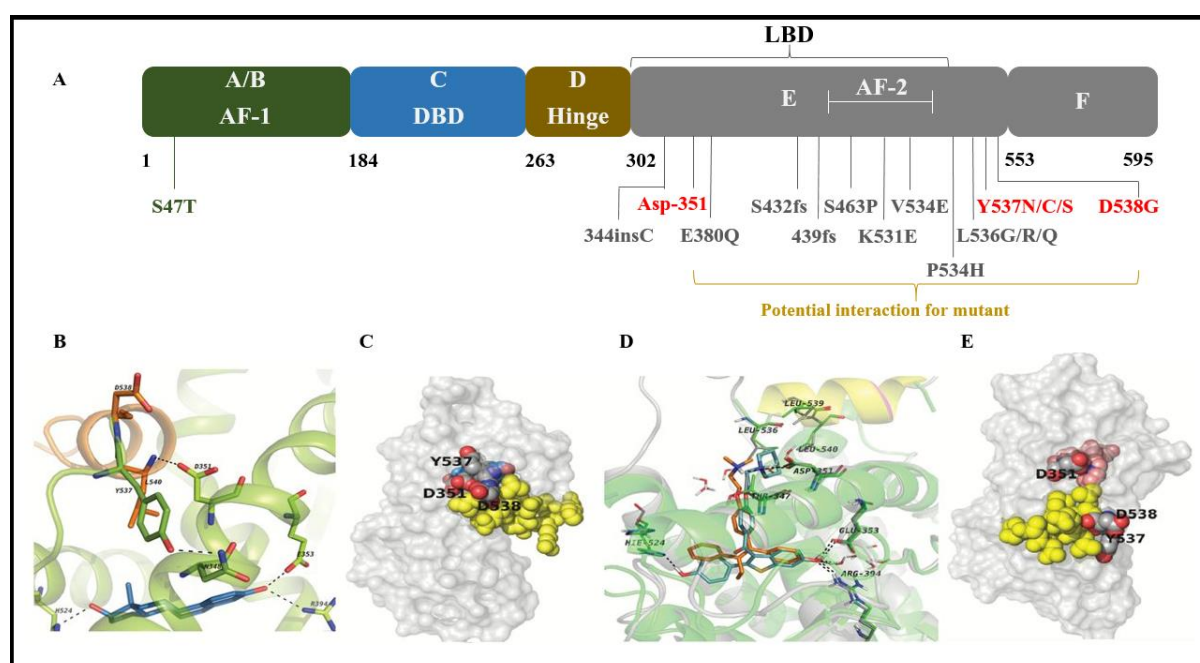
Figure 11 | **Schematic representation of ERα's mutations and the molecular interactions of the oestradiol (E₂)–oestrogen receptor (ER) complex. A)** Schematic representation of the wild-type human ER cDNA. The position initially known for the natural single-point mutations, such as Asp351Tyr is indicated. The activating function (AF) – 2 region, and various mutant receptors generated by random chemical or site-directed mutagenesis are shown, which either cause loss of AF-2 activity (i.e., 537, 538), or an increase in oestrogenic activity if the receptor is unliganded or liganded with an anti-oestrogen (other mutations). The **orange line** connecting 537, and 538 to the anchor Asp351 illustrates the current finding of Toy et al. (Toy et al., 2013a) that D538G interacts and closes the empty ER pocket. The most common and important mutations in the LBD are highlighted in red. **B)** The interaction of E₂ (**blue**) in the ligand-binding domain (LBD) with relevant amino acids

and the associated amino acids in the vicinity from helix 12 (Brzozowski et al., 1997). **C)** A space filled model from the top of the E_2 LBD showing the closed helix 12 (**yellow**) securing E_2 within. Three amino acids of relevance are indicated on the surface of the LBD complex: Asp(D)351, Tyr(Y)537, and Asp(D)538. **D)** The selective ER modulators 4-hydroxytamoxifen (4-OHT) and raloxifene (Ral) secured within the LBD of the ER by the same two amino acids, Glu353 and Arg394, via a phenolic hydroxyl on both 4-OHT and Ral, as noted with the 3 phenolic hydroxyl on ring A of E_2 (B). **E)** A space filler model from the top of the Ral LBD showing helix 12 pushed back (**yellow**), and the piperidine ring of Ral-neutralizing Asp(D)351.

II. Oestrogen-induced BC regression in clinical trials

In 2001, Lonning and colleagues (Lonning et al., 2001) successfully used high-dose oestrogen therapy in postmenopausal women with advanced endocrine-resistant BC, who were exhaustively treated with multiple endocrine therapies (median of deprivation 4 years). In 2004, the conjugated equine oestrogen arm in the Women's Health Initiative (WHI) trial (Anderson et al., 2004), and its long-term follow-up (Chlebowski et al., 2019, Jordan, 2020), unwittingly, revealed the tremendous clinical benefit of oestrogen-induced tumour regression (Abderrahman and Jordan, 2016d). The WHI trial had more than 75% of the postmenopausal women (aged 50 to70 years) LTED (i.e., 10 years past menopause). When given oestrogen hormone replacement therapy (HRT), there were significant decreases in both BC incidence and mortality (Roehm, 2015, Anderson et al., 2004). In 2009, Ellis and colleagues (Ellis et al., 2009), compared and contrasted high-and-low-dose oestrogen therapy in postmenopausal women with advanced adjuvant AIs-resistant BC (deprivation ≥ 2 years). These clinical trials combined (Lonning et al., 2001, Ellis et al., 2009) demonstrated a 30% response rate on receipt of the treatment, and reaffirm the earlier laboratory findings that oestrogen treatment after LTED leads to BC regression (Yao et al., 2000). Iwase and colleagues (Iwase et al., 2013) using ethinyloestradiol in MBC patients (median age 63 years), had a 50% response

rate, a 56% clinical benefit rate, and reported no severe AEs. Chalasani and colleagues (Chalasani et al., 2014) using low-dose E_2 during 3-month exemestane breaks in MBC patients, had measurable clinical activity with minimal toxicity.

Taken together, these *in vivo*, *in vitro* studies, and clinical trials, support the clinical benefit of using oestrogen alone, or potentially in combination with growth inhibitors and/ or apoptosis promoters, for the treatment of endocrine-resistant BC. Nonetheless, concerns regarding AEs require the research and development of safer oestrogens or oestrogen mimics.

IJ. Hormones causing regression of other cancers

Chuu and colleagues (Chuu et al., 2011) showed that CRPC (e.g., LNCaP, ARCaP, and PC-3 cells over-expressing AR), becomes vulnerable to androgens, and dies with androgen-induced apoptosis, after long-term androgen deprivation (Chuu et al., 2011) (Figure. 12). In androgen-induced tumour regression, the response rate was 50% (Salonen et al., 2008, Schweizer et al., 2015) on receipt of the treatment. Laboratory studies *in vitro* and *in vivo* confirm this phenomenon, however, additional clinical trials are underway (Michaud et al., 2015, Schweizer et al., 2015).

In a retrospective study of epithelial ovarian cancer patients over 20 years, Eeles and colleagues (Eeles et al., 2015) showed that women, who were put on oestrogen-containing preparations to treat postmenopausal symptoms, had a doubled survival rate, compared to those who did not (Figure. 12). The survival benefits even continued after oestrogen was stopped (Abderrahman and Jordan, 2016b). Syed and colleagues (Syed and Ho, 2003) demonstrated that progesterone induces apoptosis in immortalized normal, and malignant human ovarian surface epithelia cells, by enhancing the expression of FasL (i.e., extrinsic pathway of apoptosis).

IK. Hormones causing apoptosis in developmental biology

The UPR is involved in many processes that are part of developmental biology. Song and colleagues (Song et al., 2002) demonstrated that hormonal withdrawal of oestrogen and progesterone, after the proliferative and secretory phases in a woman's menstrual cycle, leads to the observed shedding in the uterine wall, through the extrinsic pathway of apoptosis (Figure. 12). The study also showed that the dysregulation of the Fas/FasL could be involved in endometrial cancer (Song et al., 2002).

Krum and colleagues (Krum et al., 2008) demonstrated *in vivo* and *in vitro* that bone-resorbing osteoclasts undergo oestrogen-induced apoptosis. This explains how oestrogen maintains bone health in women through fueling the survival and proliferation of osteoblasts, which build bone, and killing off extra osteoclasts, which destroy bone. Several studies supported this notion, and showed that oestrogen specifically kills pre-osteoclasts before they evolve into mature osteoclasts (Nakamura et al., 2007, Kameda et al., 1997, Imai et al., 2009, Xing and Boyce, 2005, Wang et al., 2015) (Figure. 12).

Patel and colleagues (Patel et al., 2015) demonstrated *in vitro* that cytotrophoblasts undergo oestrogen-induced apoptosis to maintain the balance of normal placental development, remodeling, and implantation of the fertilized ovum (Figure. 12). This occurs specifically when oestrogen levels are elevated during a narrow window in the first trimester of pregnancy. This also explains why premature or abnormal elevation in oestrogen concentration leads to abnormal placentation and preeclampsia (Patel et al., 2015). Matsuura and colleagues (Matsuura et al., 2004) demonstrated *in vivo* that oestradiol benzoate at physiological doses in pregnant rats, leads to fetoplacental growth retardation via trophoblastic apoptosis, and degeneration of placental labyrinth (i.e., the branching layer of

placental trophoblasts, which is situated between the maternal and fetal blood vessels) (Figure. 12).
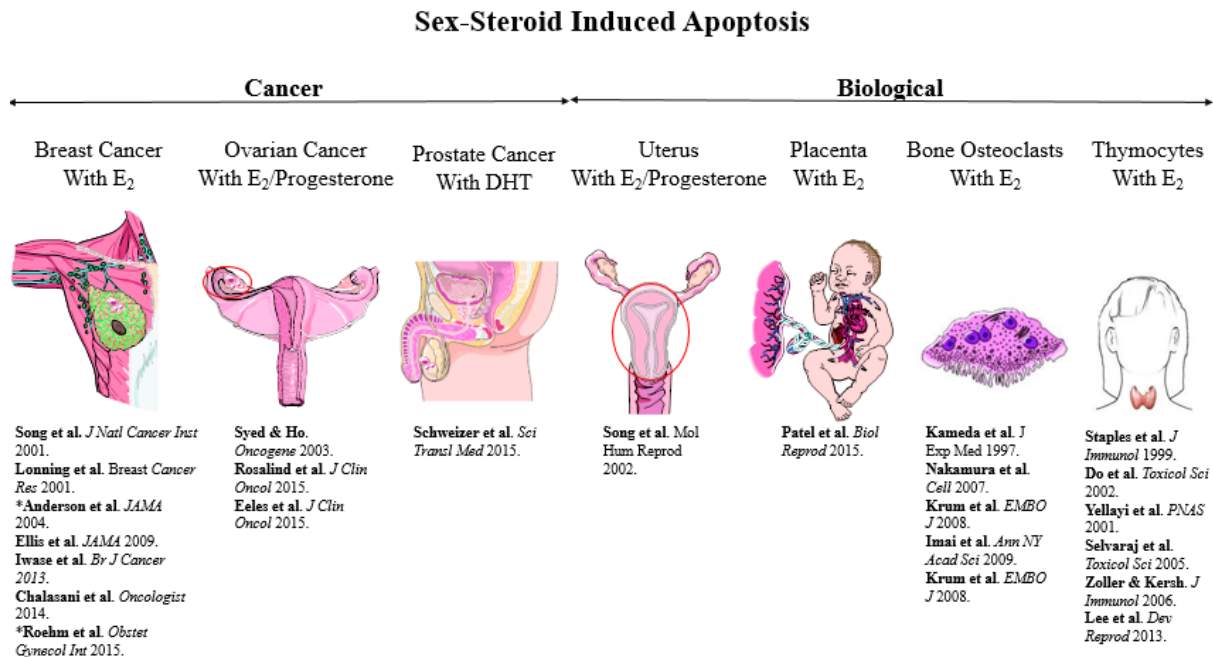
Figure 12 | **Schematic representation of sex-storied induced-apoptosis in cancer and non-cancer tissues.**

Rijhsinghani and colleagues (Rijhsinghani et al., 1996) showed *in vivo* that CD4 and CD8 thymocyte T cells, specifically CD4+/CD8+, undergo oestrogen-induced apoptosis to maintain the balance of the immune system cells, at the level of the thymus gland. This explains why oestrogen causes a dramatic decrease in thymic size and cellularity. Oestrogen specifically kills double positive T cells (CD4+/CD8+) before they evolve into single positive T cells (CD4+/CD8- or CD4-/CD8+). Other studies *in vivo* (Lee et al., 2013, Do et al., 2002, Staples et al., 1999) reaffirm this conclusion (Figure. 12).

The phenomenon of oestrogen-induced apoptosis is prevalent in normal cells, as part of developmental biology, but appears to be an acquired vulnerability in 30% of LTED BC and 50% of androgen-deprived PC. Understanding the molecular mechanisms that underline sex-steroid-induced apoptosis, and leveraging that understanding to identify switch

mechanisms to cancer cell death, can lead to novel therapeutic advances applied to treating a wide range of cancers.

IL. Endoplasmic reticulum stress: a prelude to apoptosis

Under normal or disease conditions, cells face environmental or intracellular stress. Initially, cells respond with instigating a protective endoplasmic reticulum (EnR) stress regulation (i.e., integrated stress response [ISR], and UPR), in an attempt to defend themselves against the insult and eventually recover (Fulda et al., 2010, Pakos-Zebrucka et al., 2016) (Figure. 13). However, if the insult creates a maximum or a prolonged and unresolved EnR stress, then organisms choose to sacrifice these irreparable cells, through triggering a terminal ISR or UPR regulation, and, subsequently, proceeding into irreversible programmed cell death (apoptosis) (Fulda et al., 2010, Hetz, 2012) (Figure. 13). The ISR and UPR are part of the cellular stress responses. Whereas, apoptosis is part of cellular stress-induced death (Fulda et al., 2010). The UPR usually leads to the activation of intrinsic apoptosis in the mitochondria (Walter and Ron, 2011). The nature and duration of the stress alongside the cell type were shown to be key to this decision-making; for cells to either persist with a protective ISR or UPR, or flip to a pro-apoptotic one (Hetz, 2012, Pakos-Zebrucka et al., 2016). This survival response against stress is highly conserved throughout evolution, and is embedded in the EnR of all organisms (Maly and Papa, 2014).

The ISR and UPR are involved in the development, differentiation, function, and survival of immune cells (Pierre, 2019), and ample diseases, such as: cancers, neurodegenerative diseases, cardiovascular diseases, ocular disorders, and diabetes type 1, among others (Cybulsky, 2017, Hetz and Saxena, 2017b, Grootjans et al., 2016, Walter and Ron, 2011). The UPR is also involved in many inflammatory diseases. Jing and colleagues (Jing et al., 2012) demonstrated that glaucoma, diabetic retinopathy, and age-related macular

degeneration create an EnR stress that leads to the activation UPR, and eventually apoptosis of retinal vascular and neuronal cells (Shimazawa et al., 2007, Ryoo et al., 2007, Yang et al., 2008). This was observed in both cultured retinal cells (i.e., vascular endothelial cells, pericytes, ganglion cells, Muller cells, and RPE cells), and in the retina from animal models of various diseases. In retinitis pigmentosa, the role of EnR stress and UPR were central to photoreceptor cell death, and retinal degeneration (Rebello et al., 2004, Yang et al., 2008).
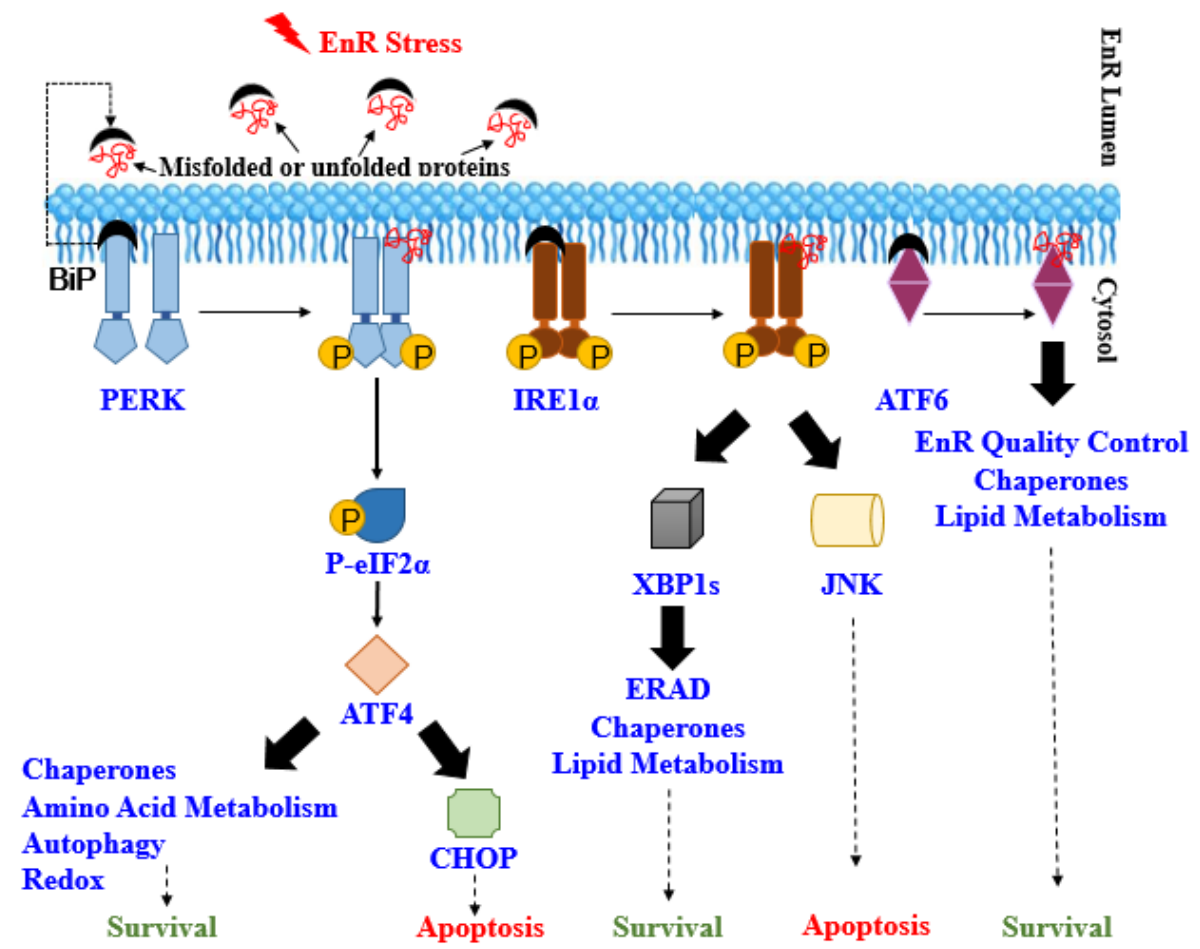
Figure 13 | **Schematic representation of the UPR and its connection to survival or apoptosis in cells.**
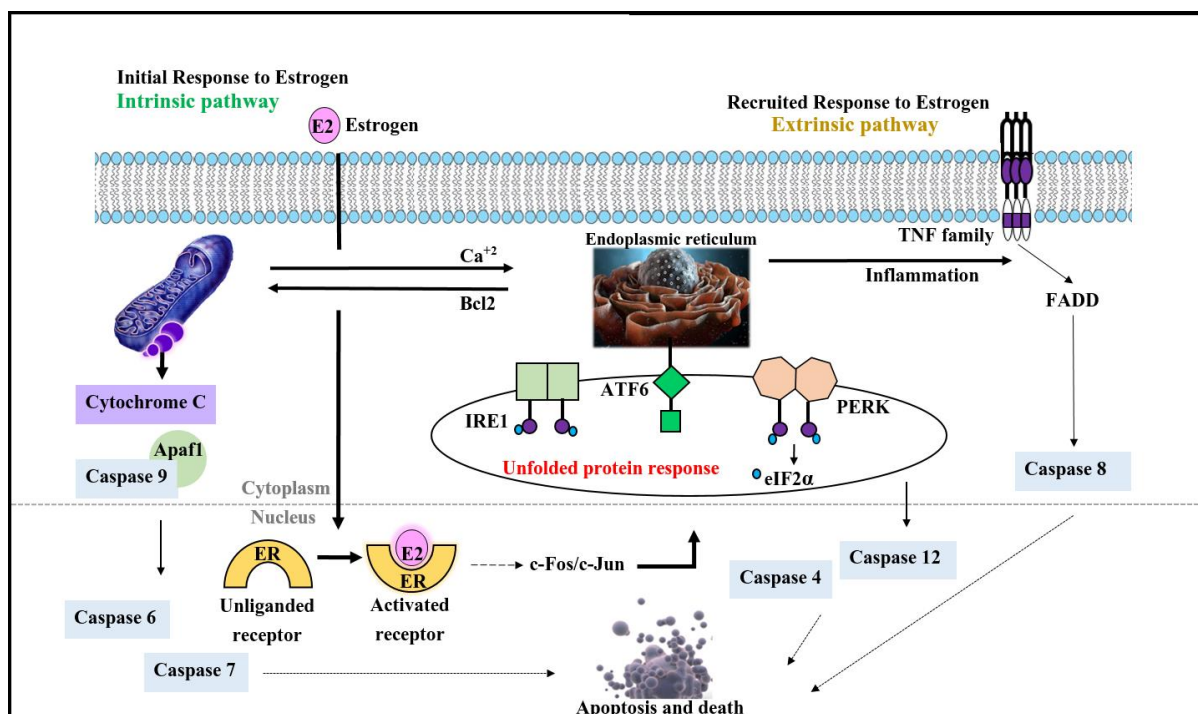
Figure 14 | **Schematic representation of the UPR in breast cancer.**

In addition, a chronic EnR stress was found to repress the synthesis of synaptic proteins, and result in neuronal loss, with implications on cognition, memory, and autism spectrum disorder (Hetz and Saxena, 2017a). The UPR was shown to be at the center of Alzheimer's disease, Parkinson's disease, amyotrophic lateral sclerosis, Huntington's disease, prion-related disorders, and some myelin-related disorders.

The UPR is activated when cells are exposed to a stress stimuli, such as: glucose starvation, inhibition of protein glycosylation, Ca^{2+} depletion as one form of Ca^{2+} disequilibrium, oxygen deprivation, DNA damage, and cytokine deprivation, among others. The EnR is considered the chief site for generating and tailoring mature proteins in all cells (Walter and Ron, 2011). This protein synthesis process is guarded by the ISR and UPR. Under normal circumstances, proteins within the EnR undergo posttranslational processing (i.e., glycosylation, disulfide bond formation, correct folding, and oligomerization) (Walter and Ron, 2011). If cells are under extrinsic or intrinsic stress insults, proteins will not undergo this process efficiently and, therefore, a buildup of misfolded or unfolded proteins

will follow (Walter and Ron, 2011). These defective proteins will be sensed by the 4 transducers of the ISR: PERK, PKR, GCN2, and HRI (Pakos-Zebrucka et al., 2016), or the 3 transducers of the UPR: PERK, IRE1α, and ATF6 (Schroder and Kaufman, 2005, Ron and Walter, 2007, Walter and Ron, 2011).

During the UPR activation, PERK is activated rapidly, followed by ATF6, and lastly IRE1α (Figures. 13 and 14). Studies suggest that IRE1α could be the "switch transmitter", whereby the "time" of IRE1α activation is hypothesized to be a switch mechanism to flipping the UPR trajectory from pro-survival to pro-apoptotic (Lin et al., 2007). The potential mechanisms include: IRE1 inducing p58^{IPK} (Szegezdi et al., 2006), and IRE1α-dependent activation of ASK1, and its downstream target JNK. Many studies show that an EnR stress that leads to a tonic or a maximum activation of the UPR sensors is credited with the UPR switching from a protective to a terminal UPR regulation. This naturally begs the question: how can we leverage the molecular switch mechanisms to cell death, in this stress-death associated biology, to enhance the clinical responses seen in anti-hormone resistant BC and PC patients, when treated with the stress-inducing sex-storied hormones?

IM. New promising oestrogenic agents for endocrine-resistant BC treatment

Oestetrol is proposed as a promising oestrogen for the treatment of advanced BC (Bennink et al., 2017, Singer et al., 2014, Verhoeven et al., 2018, Schmidt, 2020), advanced PC (Dutman et al., 2017), and for use in HRT (Coelingh Bennink et al., 2016, Donesta Bioscience, 2016, Gerard et al., 2015) as well as oral contraception (Apter et al., 2017) (Figures. 15 and 16). The combination of E_4 and progestin drospirenone is subject to FDA approval, with the possibility of E_4 becoming the first natural oestrogen approved in a contraceptive product in the US, and the first new oestrogen introduced in the U.S. in 50 years. Oestetrol is devoid of ERα Membrane Initiated Steroid Signaling in the endothelium,

which conveys an atheroprotective effect in an ERα-dependent manner (Abot et al., 2014).

It's also associated with a low risk of drug-drug interactions (CYP450 family) as well as a

neutral impact on risk markers of venous thromboembolism. In preclinical models, E_4

selectively activates the nuclear ERα, which plays a prominent role in the vasculoprotective

action of oestrogens (Abot et al., 2014). An ongoing phase I/IIA clinical trial of E_4 (Schmidt,

2020), to treat advanced BC, shows that the majority of patients experienced favorable

subjective effects on wellbeing. One patient of such completed both the phase 1/IIA with

stable disease after 24 weeks of treatment. The 20 mg dose E_4 allowed dose escalation to 40

mg per day.

E4 (left) and ShERPA TTC-352 (right)

In Patients:
- Safety, Tolerability and Pharmacokinetics of Estetrol (E4) After Single and Multiple Oral Doses in Healthy Female Volunteers
  ClinicalTrials.gov Identifier: NCT03075956
- Effect of Food on the Bioavailability of 30 mg Estetrol (E4) Tablet in Healthy Postmenopausal Female Volunteers
  ClinicalTrials.gov Identifier: NCT03798197
- Estetrol, the Next Generation of Hormone Therapy: Results of a Phase 2b Dose-finding Study in Postmenopausal Women (E4 Relief)
  Presented at the 29th Annual Meeting of The North American Menopause Society October 3-6, 2018, San Diego, CA

In industry:
- Pantarhei Bioscience, the Netherlands ➔ BC, PC
- Mithra Pharmaceuticals, Belgium ➔ HRT

E_4 Pros over E_2:
- Induction of an atheroprotective effect in an ERα-dependent manner.
- Not eliciting major endothelial actions known to be membrane ERα dependent, namely an increase in eNOS phosphorylation, in NO production, or an acceleration of reendothelialization.
  "Improved cardiovascular safety"

In Patients:
- Study of TTC-352 in Patients With Metastatic Breast Cancer Progressing on Endocrine Therapy
  ClinicalTrials.gov Identifier: NCT03201913

In industry:
- TTC Oncology, LLC ➔ BC

ShERPAs Pros over E_2:
- Three ShERPAs (including BMI-135 and TTC-352) were shown not to cause significant estrogen-like uterine growth, when tested in xenograft models of TAM-resistant BC.
  "Improved endometrial safety"

Figure 15 | **Schematic representation of the new generations of oestrogenic therapies, their clinical trials, and superior AEs' profile compared to E_2.**

Three Selective Human ER Partial Agonists (ShERPAs; including pilot BMI-135 and

clinically-tested TTC-352) were shown not to cause significant uterine growth in certain

TAM-resistant BC models, and are proposed as safer oestrogen mimics for the treatment of

endocrine-resistant BC (Molloy et al., 2014, Xiong et al., 2016) (Figures. 15 and 16). TTC-

352, an orally-bioavailable ShERPA, caused growth inhibition in 3 TAM-resistant ER-positive BC cultures (Molloy et al., 2014, Xiong et al., 2016). Moreover, preclinical 7-day repeated dose studies conducted in 2-gender Sprague-Dawley rats and in dogs, demonstrated TTC-352's efficacy, tolerability, and rapid absorption (Tonetti et al., 2017). A phase 1 clinical trial using TTC-352 in metastatic hormone receptor-positive BC patients, who had progressed on at least two lines of endocrine therapy (with one that included a CDK 4/6 inhibitor), has been completed (Dudek et al., 2020). It shows that TTC-352 has manageable safety and early clinical evidence of activity in patients with MBC progressing on endocrine therapy. The 180 mg BID dose is recommended for further testing. Both compounds have further clinical trials planned.
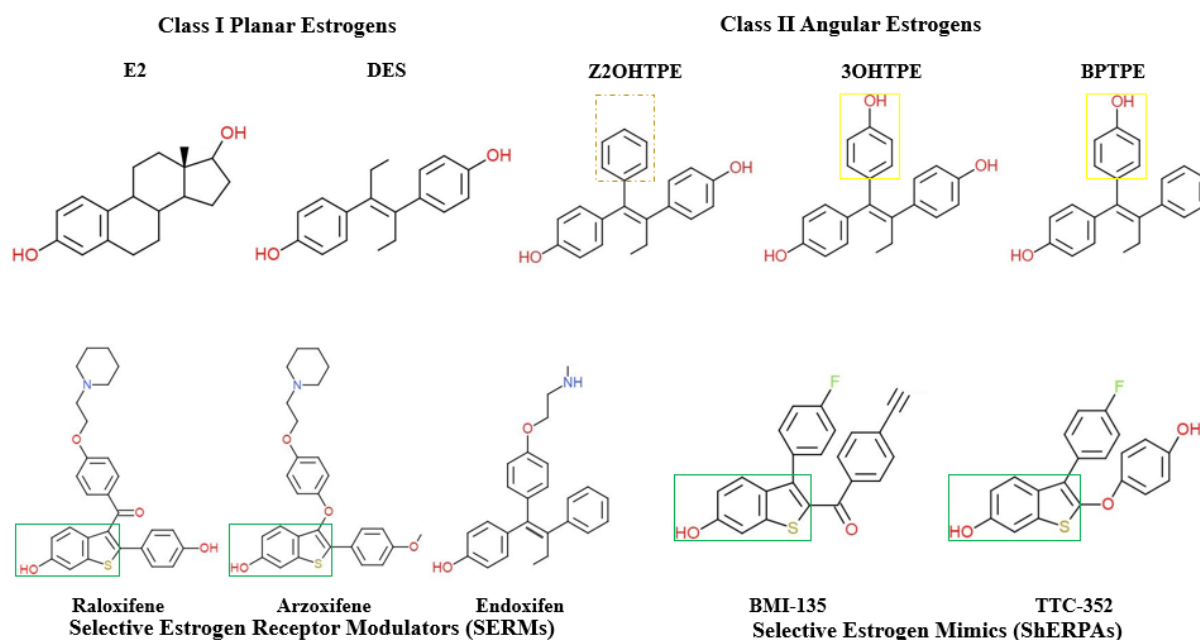
Figure 16 | **Schematic representation of the chemical structures of planar oestrogens, angular oestrogens, SERMS, and ShERPAs.** The box (in green) highlights the benzothiophene scaffold embedded in raloxifene and arzoxifene structures, of which the ShERPAs' structures were based upon. The *continuous* box (in yellow) highlights the phenyl ring bearing OH of triphenylethylenes (TPEs): trihydroxytriphenylethylene (3OHTPE) and BPTPE (Maximov et al., 2020), which makes them angular oestrogens/partial agonists. The *dashed* box (in brown) highlights the absence of OH on

the phenyl ring of the Z-isomer of dihydroxytriphenylethylene (Z2OHTPE), which makes it an angular oestrogen/full agonist like E_2 and diethylstilbestrol (DES) (Maximov et al., 2020).

IN. Rationale for research

Given the unpleasant gynecological and non-gynecological AEs of oestrogen treatment, the development of safer oestrogens for the treatment of endocrine-resistant BC, or for use in HRT, remains a priority. The naturally-occurring oestrogen E_4 and synthetic oestrogen mimic TTC-352 are being put forward as such, and are currently being evaluated in endocrine-resistant MBC patients. The rationale for this research (i.e., two peer-reviewed publications) lies in the fact that ShERPAs and E_4 currently lack: (i) thorough structural studies, (ii) molecular mechanistic studies on how they cause tumour regression in LTED BC patients, and (iii) thorough pharmacological studies in a wide range of patient-representative BC models, as previous studies used either 1-2 models or an engineered model that does not necessarily reflect patients' tumour heterogeneity. This evaluation is necessary to guide the future clinical trials of ShERPAs and E_4, and provide accurate structural, pharmacological, and mechanistic insights into what an "effective and safer oestrogenic agent to treat advanced drug-resistant BC" looks like.

To fill in these specific gaps, cell viability and proliferation assays, real-time polymerase chain reaction, luciferase reporter assays, chromatin immunoprecipitation, docking and molecular dynamics simulations, X-ray crystallography, human UPR RT^2 PCR profiler arrays, live cell microscopic imaging and analysis, annexin V staining assays, immunoblotting, ERE DNA pull downs, and mass spectrometry were conducted in 11 biologically-different BC models, including those endocrine-resistant. Results were compared with the benchmark potent full oestrogen agonist E_2, less potent full oestrogen agonists E_1 and E_3, the benchmark partial agonist triphenylethylene bisphenol (BPTPE), the classical

antagonists (or SERMs) 4-hydroxyTAM (4OHT), endoxifen, and raloxifene, and the benchmark SERD ICI.

IO. Hypothesis of research

The first part of this research's hypothesis is that TTC-352 is classified as a weak full oestrogen agonist not a partial oestrogen agonist (as originally classified by the group of investigators that synthesized it). This stemmed from the observation that at least one BC patient developed occult endometrial hypertrophy after TTC-352 treatment (i.e., full oestrogen agonist AE). If TTC-352 was, indeed, a full oestrogen agonist, then the hypothesis would extend to include the following junctures: i) TTC-352 would improve helix 12 (H12)-to-Asp351 interaction of ERα, and the closure of H12 over the LBD; conferring an agonist conformation of the ligand-ERα complex (based on our earlier structural studies), and recruiting E_2-enriched coactivators; and ii) TTC-352 and E_4 would lead to a rapid activation of ERα-mediated UPR and apoptosis (based on our earlier biological studies of oestrogens in LTED BC), which, in turn, constitutes their molecular mechanisms of tumour regression in LTED endocrine-resistant MBC patients.

IP. Novelty and contribution of research

The novelty and contribution of this research lies in providing: (i) the first structural studies of ShERPAs including the X-ray crystallography of TTC-352:mutant ER with clinical implications given that the majority of MBC patients harbor ER mutations (Niu et al., 2015, Pejerrey et al., 2018, Toy et al., 2013b), (ii) the first report on the molecular mechanisms of TTC-352 and E_4's anti-cancer properties in LTED BC patients, (iii) the first comprehensive pharmacological studies of ShERPAs and E_4 in numerous patient-representative BC models, and (iv) the key interactions at the molecular and atomic levels of the benchmark partial agonist BPTPE:WT ER, involving Asp351 and H12, which explains the delayed ERα-

induced UPR and apoptosis compared to TTC-352. This sets the structure-function model of TTC-352 apart from BPTPE, and clearly demonstrates that TTC-352 is not a partial agonist, as originally classified by the group that synthesized it.

II. Materials and Methods

IIA. Reagents.

E_1, E_2, E_3, E_4, and 4OHT were purchased from Sigma-Aldrich (St. Louis, MO). Endoxifen (Endox) was purchased from Santa Cruz Biotechnology (Santa Cruz, CA), raloxifene (Ralox) from Sigma-Aldrich, and ICI from Tocris Bioscience/FisherScientific (Bristol, United Kingdom). BPTPE was originally synthesized at the Organic Synthesis Facility, Fox Chase Cancer Center (Philadelphia, PA) (Maximov et al., 2010). The ShERPAs BMI-135 and TTC-352 were a gift from Drs Debra Tonetti and Gregory R. J. Thatcher (University of Chicago, IL). The PERK inhibitor GSK G797800 was purchased from Toronto Research Chemicals (Toronto, Ontario, Canada). The IRE1α Inhibitor MKC-3946 was purchased from Calbiochem (San Diego, CA). Thioflavin T (ThT) was purchased from Sigma-Aldrich. For the ChIP assays, the antibodies used for pull-downs are: anti-ERα clone F-10X mouse monoclonal (2 μg/μl; 5 μg per reaction) (Santa Cruz Biotechnology), anti-SRC-3 clone AX15.3 mouse monoclonal (1 μg/μl; 5 μg per reaction) (Abcam, Cambridge, United Kingdom), and normal mouse IgG as IP negative control (2 μg/μl; 5 μg per reaction) (Santa Cruz Biotechnology). For Western blotting, anti-ERα (sc-544), anti-eIF2α (D-3), and anti-β-actin (C-4), were purchased from Santa Cruz Biotechnology. Anti-phospho-eIF2α (Ser51) (#9721), anti-ATF4 (D4B8), anti-CHOP (L63F7), and anti-cleaved PARP (Asp214) (19F4), were purchased from Cell Signaling Technology. Anti-XBP1 (isoforms non-spliced and spliced, ab37152) was purchased from Abcam.

IIB. Cell culture.

Wild type (WT) oestrogen-dependent BC cell line MCF-7:WS8 (Jiang et al., 1992); mutant p53 oestrogen-dependent BC cell line T47D:A18 (Murphy et al., 1990); the first *in vitro* cellular model recapitulating acquired-TAM resistance developed in athymic mice *in vivo* MCF-7:PF (Fan et al., 2014); oestrogen-responsive, ER-positive, progesterone receptor (PgR)-positive, and human epidermal growth factor receptor 2 (HER2)-positive luminal B BC cell line BT-474 (Kraus et al., 1987); oestrogen-responsive, ER-positive, PgR-positive, and androgen receptor-positive luminal A BC cell line ZR-75-1 (Engel et al., 1978); anti-hormone-resistant oestrogen-independent BC cell line MCF-7:5C (Lewis et al., 2005b); anti-hormone-sensitive oestrogen-independent BC cell line MCF-7:2A (Pink et al., 1995); and anti-hormone (Ralox)-resistant oestrogen-independent BC cell line MCF-7:RAL (Liu et al., 2003); TAM-sensitive, oestrogen-independent, ER-positive BC cell line LCC1 (Clarke et al., 1989, Brunner et al., 1993a); TAM-resistant and ICI-sensitive, oestrogen-independent, ER-positive BC cell line LCC2 (Brunner et al., 1993b); and TAM-and-ICI-cross resistant, ER-positive BC cell line LCC9 (Brunner et al., 1997), were cultured as described previously. Human endometrial adenocarcinoma cell line Ishikawa was cultured as described previously (Nishida et al., 1985). All cell cultures were done in T75 and T175 culture flasks (Thermo Fisher Scientific, Waltham, MA), passaged twice a week at 1:3 ratio, and grown in 5% CO_2 at 37°C. All cell lines were validated according to their short tandem repeat (STR) profiles at The University of Texas MD Anderson Cancer Center Characterized Cell Line Core (CCLC). The STR patterns of all cell lines were consistent with those from the CCLC standard cells (Supplementary Table. S1 *PAP1*, and Supplementary Table. S1 *PAP2*).

IIC. Cell viability and proliferation assays.

The biological properties of compounds (E_1, E_2, E_3, E_4, BMI-135, TTC-352, BPTPE, 4OHT, endoxifen, raloxifene, and ICI) in cells lines (MCF-7:WS8, T47D:A18, BT-474, ZR-75-1, MCF-7:PF, MCF-7:5C, MCF-7:2A, and MCF-7:RAL), were evaluated by assessing the DNA content of the cells, as a measure of cell viability and proliferation. MCF-7:WS8 and T47D:A18 cells were starved in oestrogen-free medium for 3 days, and then seeded into 24-well plates at a density of 8,000 cells/well for one-week treatment. MCF-7:PF, BT-474, and ZR-75-1 cells were starved in oestrogen-free medium for 3 days, and seeded into 24-well plates at a density of 10,000 cells/well for one-week treatment. MCF-7:5C cells were seeded into 24-well plates at a density of 10,000 cells/well for one-week treatment. MCF-7:2A cells were seeded into 24-well plates at a density of 3,000 cells/well for two-week treatment. MCF-7:RAL cells were seeded into 24-well plates at a density of 4,000 cells/well for three-week treatment. After 24 hours, cells were treated with compounds over the aforementioned periods of time, in oestrogen-free medium (MCF-7:WS8, T47D:A18, MCF-7:PF, BT-474, and ZR-75-1, MCF-7:5C, and MCF-7:2A), and in oestrogen-and-raloxifene-free medium (MCF-7:RAL). The medium was changed every 48 hours. On the last day of treatment, cells were harvested by medium aspiration, washed once with ice-cold Dulbecco's PBS (DPBS) (Life Technologies, Carlsbad, CA), and analyzed using the DNA Quantification Kit (Bio-Rad, Hercules, CA) according to manufacturer's instructions. Samples were then quantitated on a Synergy H1 plate reader (BioTek Instruments Inc., Winooski, VT) in black wall 96-well plates (Nalge Nunc International, Rochester, NY). All treatments were performed in triplicate. The calculated half maximal effective concentrations (EC50)s of all compounds in different human BC and human endometrial cancer cell lines are summarized (Table. 1 *PAP1*, and Supplementary Table. S2 *PAP2*).

IID. Quantitative real-time reverse transcription-polymerase chain reaction (RT-PCR).

MCF-7:WS8 (after 3-day starvation in oestrogen-free medium) and MCF-7:5C cells were seeded into 24-well plates at a density of 100,000 cells/well. After 24 hours, cells were treated with E_2 [1 nM], BMI-135 [1 µM], TTC-352 [1 µM], BPTPE [1 µM], and endoxifen [1 µM]. After 24-hour-treatment, cells were harvested, RNA was isolated using MagMAX-96 Total RNA Isolation Kit (Applied Biosystems, Carlsbad, CA), and processed using Kingfisher Duo Prime magnetic particle processor (Thermo Fisher Scientific) according to manufacturer's instructions. The cDNA was synthesized, utilizing 1µg of purified RNA, and using High Capacity cDNA Reverse transcription kit (Applied Bioscience) according to manufacturer's instructions. Synthesized cDNA diluted in nuclease-free water and Power SYBR green PCR master mix, was used for RT-PCR (Applied Bioscience) according to manufacturer's instructions. The RT-PCR was run using a QuantStudio 6 Flex Real Time PCR thermocycler (Applied Bioscience). All primers were obtained from Integrated DNA Technologies Inc. (IDT, Coralville, IA), and validated by melt curve analysis that revealed single peaks for all primer pairs. The primer sequences used for human TFF1 cDNA amplification are: 5'-CATCGACGTCCCTCCAGAAGA-3' sense, 5'-CTCTGGGACTAATCACCGTGCTG-3' anti-sense; human GREB1 gene: 5'-CAAAGAATAACCTGTTGGCCCTGC-3'sense, 5'-GACATGCCTGCGCTCTCATACTTA-3' anti-sense; and the reference gene 36B4: 5'-GTGTCCGACAATGGCAGCAT-3' sense, 5'-GACACCCTCCAGGAAGCGA-3' anti-sense. The fold changes of mRNA after treatment with compounds vs. vehicle control were calculated using the ΔΔCt method. All treatments were performed in triplicate.

IIE. Transient transfection and dual luciferase reporter assays.

Ishikawa cells were seeded into 24-well plates at a density of 100,000 cells/well. After 24 hours, cells were transfected with 28.8 µg of pERE(5X)TA-ffLuc, and 9.6 µg of pTA-srLuc reporter plasmids, using 3 µl of TransIT-LT1 transfection reagent (Mirus Biolabs, Madison, WI) per 1 µg of plasmid DNA, in 52.5 mL of OPTI-MEM serum-free media (Invitrogen, Carlsbad, CA). Transfection mix was added to cells in growth media to a final concentration of 0.3 µg pERE(5X)TA-ffLuc, and 0.1 µg of pTA-srLuc reporter plasmids per well. After 18 hours, transfection mix was removed and fresh media was added instead. After 24 hours post transfection, cells were treated with compounds (E_2, E_4, BMI-135, BPTPE, and endoxifen) for 24 hours. After 24-hour-treatment, cells were washed once with cold DPBS (Invitrogen), lysed, and the ERE luciferase activity was determined using Dual-Luciferase Reporter Assay System (Promega, Madison, WI) according to manufacturer's instructions. Samples were quantitated on a Synergy H1 plate reader (BioTek Instruments Inc.) in white wall 96-well plates (Nalge Nunc International). All treatments were performed in triplicate.

IIF. Chromatin immunoprecipitation (ChIP) assays.

The ChIP assay was performed as described previously (Sengupta et al., 2010, Obiorah et al., 2014). MCF-7:5C cells were grown in 15-cm Petri dishes to approximately 80% confluency, and treated for 45 minutes with compounds (E_2 [1 nM], E_4 [1 µM], BMI-135 [1 µM], BPTPE [1 µM], 4OHT [1 µM], and endoxifen [1 µM]) in growth media. After 45-minute-treatment, cells were washed once with warm DPBS, and then crosslinked with 1% formaldehyde in DPBS for 10 minutes at room temperature (73.4° F, or 23 °C). The crosslinking reactions were quenched with 0.125 M glycine, and cells were, subsequently, washed twice with ice-cold DPBS. Cells were scraped and collected into DPBS with Halt protease and phosphatase inhibitor cocktail (Thermo Fisher Scientific). Cells were pelleted by

centrifugation, and chromatin was isolated using Pierce Magnetic ChIP Kit (Thermo Fisher Scientific) according to manufacturer's instructions. The washing of the magnetic beads used for the pull-downs was processed using Kingfisher Duo Prime Magnetic Particle Processor (Thermo Fisher Scientific) according to manufacturer's instructions. The DNA fragments were purified using Qiaquick PCR purification kit (Qiagen, Germantown, MD). Then, 2 µl of eluted DNA was used for RT-PCR analysis. The sequences of used primer are: GREB1 proximal ERE enhancer site amplification: 5'-GTGGCAACTGGGTCATTCTGA-3' sense, 5'-CGACCCACAGAAATGAAAAGG-3' anti-sense (Integrated DNA Technologies). The data are expressed as percent input of starting chromatin material, after subtracting the percent input pull down of the IP negative control. The assays were performed in triplicate.

IIG. Immunoblotting.

MCF-7:WS8, MCF-7 ATCC, T47D:A18, BT-474, and ZR-75-1, were starved for 3 days in oestrogen-free medium. MCF-7:WS8, MCF-7 ATCC, T47D:A18, BT-474, ZR-75-1, MCF-7:5C, MCF-7:2A, MCF-7:RAL, LCC1, LCC2, and LCC9 BC cells, were seeded into 5-cm Petri dishes at a density of 2 million cells/dish for the 24-and-48-hour-time points, and at a density of 1.5 million cells/dish for the 72-hour-time point. After 24 hours, cells were treated with compounds (E_2 [1 nM], E_4 [1 µM], BMI-135 [1 µM], TTC-352 [1 µM], BPTPE [1 µM], 4OHT [1 µM], endoxifen [1 µM], raloxifene [1 µM], ICI [1 µM], thapsigargin [1 µM], GSK G797800 [10 µM], and MKC-3946 [20 µM]) for different periods. After treatments, cells were harvested in cell lysis buffer (Cell Signaling Technology, Danvers, MA) supplemented with Protease Inhibitor Cocktail Set I and Phosphatase Inhibitor Cocktail Set II (Calbiochem). Total protein content of the lysate was determined by a standard BCA assay (Bio-Rad Laboratories). Fifty micrograms of total protein were separated on 10% SDS polyacrylamide gel, and transferred to a nitrocellulose membrane. The membranes were probed overnight at 4°C with primary antibodies; diluted in 5% dry nonfat milk in Tris-

buffered saline/Tween 20 blocking buffer at ratios recommended by the supplier. This was followed by 1-hour incubation at room temperature with secondary antibodies conjugated with HRP. The signals were visualized using Western Lighting™ plus-ECL enhanced chemiluminescent substrate (PerkinElmer Inc., Waltham MA), and exposure of membranes to X-ray film. All treatments were performed in triplicate. Analysis was validated by densitometry using Image J (National Institutes of Health, Bethesda, MD). Densitometry data is presented in Supplementary Tables. S3-4 *PAP2*.

IIH. Human UPR RT^2 PCR Profiler PCR Arrays (Real-Time Profiler Assays).

MCF-7:5C cells were seeded into 6-well plates at a density of 200,000 cells/well for the 48-and-72-hour-time points, and 45,000 cells/well for day 7-time point. After 24 hours, cells were treated with compounds (E$_2$ [1 nM], E$_4$ [1 μM], BMI-135 [1 μM], and BPTPE [1 μM]). Cells were harvested using Qiazol reagent (Qiagen), and total RNA was isolated using an miRNeasy Mini Kit (Qiagen) according to manufacturer's instructions. During the RNA purification process, samples were treated with DNAse using the RNase-Free DNase Set (Qiagen) according to manufacturer's instructions. The cDNA was reverse transcribed using 2 μg of isolated RNA and the High Capacity cDNA Reverse Transcription Kit (Applied Bioscience) according to manufacturer's instructions. The cDNA was diluted 1:50, and a 2x RT^2 SYBR Green Mastermix (Qiagen) was used to prepare the reactions. The plates were loaded and run on a QuantStudio 6 Flex Real Time PCR thermocycler (Applied Bioscience) according to manufacturer's instructions. The Ct values were exported at the end of each run, compiled, and uploaded to the Qiagen's Data Analysis Center, for analysis. All treatments were performed in triplicate.

III. Live cell microscopic imaging and analysis.

MCF-7:5C cells were seeded into 15 μ-slide 2-well chambered coverslip slides (Ibidi, Martinsried, Germany) at a density of 300,000 cells/well for the 48-hour-time point, and at 200,000 cells/well for the 72-hour-time point. After 24 hours, cells were treated with compounds (E_2 [1 nM], E_4 [1 μM], BMI-135 [1 μM], TTC-352 [1 μM], 4OHT [1 μM], control [0.1% DMSO], and positive control thapsigargin [1 μM]). On the day of live cell imaging, the green fluorescent dye ThT (UPR-indicative dye) (Sigma-Aldrich) was freshly prepared at a final concertation of 5 μM as described previously (Beriault and Werstuck, 2013), and the blue fluorescent live cell nuclear dye Hoechst 33342 (counterstaining dye) (Thermo Fisher Scientific) was freshly prepared at a final concertation of 5 μg/mL. Thioflavin T solution was prepared by dissolving ThT in 70% ethanol, then diluting it in culture media to a concentration of 5 mM, and finally adding it to culture media containing test compounds; reaching a final concentration of 5 μM. The staining with ThT was for 1 hour, followed by substituting the culture media (containing test compounds and ThT) with PBS containing Hoechst 33342 for 15 minutes in a CO_2 incubator. Fluorescent images of MCF-7:5C live cells were taken at a 38 ms exposure under a 20X/0.7 objective with ZEISS Celldiscoverer 7 (Carl Zeiss AG, Oberkochen, Germany). Images were converted to 12-bit before being quantified by the ZEISS Zen Software Module-Image Analysis. Cells from each image were manually counted to normalize the fluorescent data per cell. Relative intensity per cell =ThT intensity/cell count, was generated for each treatment per image. An mean of the relative intensity per cell (using 3 images per treatment) was then calculated to give a final quantification alongside the standard deviation (SD). The excitation and emission settings were: Hoechst 33342 (Ex. 348 nm, Em. 455 nm), and ThT (Ex. 433 nm, Em. 475 nm). The relative intensity per cell data is represented in Table 2 *PAP1*.

IIJ. Annexin V staining assays.

MCF-7:5C cells were seeded into 10-cm Petri dishes at a density of 800,000 cells/dish for the 72-and-96-hour-time points. MCF-7:2A cells were seeded into 10-cm Petri dishes at a density of 400,000 cells/dish for day 9-time point, and at 100,000 cells/dish for day 13-time point. MCF-7:RAL cells were seeded into 10-cm Petri dishes at a density of 150,000 cells/dish for the day 14, day 17, and day 21-time points. After 24 hours, cells were treated with compounds (E$_2$ [1 nM], E$_4$ [1 μM], BMI-135 [1 μM], TTC-352 [1 μM], 4OHT [1 μM], raloxifene [1 μM] (with MCF7:RAL), ICI [1 μM] (with MCF7:RAL), GSK G797800 [10 μM] (with MCF7:5C), and MKC-3946 [20 μM] (with MCF7:5C), over the aforementioned time points. Cells were harvested by aspirating the media, washing them twice with warm DPBS, and treating them with accutase (Sigma-Aldrich), or trypsin solution (Life Technologies), at 5% CO$_2$ 37°C incubator. After the addition of warm DPBS to either accutase or trypsin, cells were harvested by pipetting, transferred to centrifuge tubes, and precipitated. Harvested cells were suspended in 1x binding buffer, and $1*10^5$ cells were simultaneously stained with FITC-labeled Annexin V and propidium iodide (PI) for 15 minutes at 37°C, using the FITC Annexin V Apoptosis Detection Kit I (BD Pharmingen, San Diego, CA) according to the manufacturer's instructions. The cells were analyzed using a BD Accuri C6 plus flow cytometer. The assay was performed in triplicates.

IIK. Statistical analyses.

All data are mean ± SD of three different fields, for each condition, from three independent biological experiments performed in technical duplicates. One-way ANOVA was used with a follow-up Tukey's test to determine the statistical significance of the treatments. For the cell viability and proliferation assays, EC$_{50}$ was calculated using the formula: Y=Bottom + (Top-Bottom)/(1+10^((LogEC50-X)*HillSlope)). For the volcano

plots, the fold-Change ($2^{\wedge}$ (- Delta Delta CT)) is the normalized gene expression ($2^{\wedge}$(- Delta CT)) in the Test Sample divided the normalized gene expression ($2^{\wedge}$ (- Delta CT)) in the Control Sample. Fold-Regulation represents fold-change results. Fold-change values greater than one indicates a positive- or an up-regulation, and the fold-regulation is equal to the fold-change. Fold-change values less than one indicate a negative or down-regulation, and the fold-regulation is the negative inverse of the fold-change. The p values of the volcano plots were calculated using a Student's t-test of the replicate $2^{\wedge}$ (- Delta CT) values, for each gene in the control group and treatment groups.

III. Results

IIIA. Effects of ShERPAs and E$_4$ on cell viability in numerous BC models.

Cell viability assays were used to test the biological properties of compounds. TTC-352, BMI-135, and E$_4$ exhibit a full agonist action, similar to E$_2$, across eight BC cell lines that are oestrogen-dependent (MCF-7:WS8, T47D:A18, BT-474, ZR-75-1, and MCF-7:PF), oestrogen-independent (MCF-7:5C, MCF-7:2A, and MCF-7:RAL), endocrine-sensitive (MCF-7:2A), endocrine-resistant (MCF-7:PF, MCF-7:5C, and MCF-7:RAL), mutant p53 (T47D:A18), HER2-positive (BT-474), luminal A (ZR-75-1), and luminal B (BT-474).

The concentration 1 μM for TTC-352, BMI-135, and E$_4$ achieved either the maximal cellular growth (P-value < 0.05 compared to vehicle control) (Fig. 2A-E, and Supplementary Fig. 1A-C *PAP1*, and Supplementary Fig. S1A-E *PAP2*), or the maximal cellular death (P < 0.05 compared to vehicle control) (Fig. 2F-H, and Supplementary Fig. 1D-F *PAP1*, and Supplementary Fig. S1F-H *PAP2*). TTC-352, BMI-135, and E$_4$ were shown to be a less potent full agonist compared to E$_2$ (Fig. 2 and Table 1 *PAP1*, and Supplementary Fig. S1 and Supplementary Table S2 *PAP2*). The calculated EC50s are summarized in Table 1 (*PAP1*) and Supplementary Table S2 (*PAP2*).

In MCF-7:5C, E_4 and BMI-135 completely reduced the amount of viable MCF-7:5C cells after one week of treatment, in a dose-dependent manner, with a maximum reduction of cells by an average of 58% for E_4 and 46% for BMI-135, at their highest concentration of 10^{-6} M ($P < 0.05$ compared to vehicle) (Fig. 2F *PAP1*). Reduction in the amount of viable MCF-7:5C cells by E_2 at 10^{-9} M was by an average of 58% (Fig. 2F *PAP1*). TTC-352 completely reduced the amount of viable MCF-7:5C cells after one-week of treatment, in a dose-dependent manner, with a maximum reduction of cells by an average of 50.12% at its highest concentration of 10^{-6} M (p-value < 0.05 compared to vehicle control) (Supplementary Fig. S1F *PAP2*). Reduction in the amount of viable MCF-7:5C cells by E_2 at 10^{-9} M was by an average of 76.93% (Supplementary Fig. S1F *PAP2*).

In MCF-7:2A, E_4 and BMI-135 completely reduced the amount of viable MCF-7:2A cells after a 2-week treatment, in a dose-dependent manner, with a maximum reduction of cells by an average of 57% for E_4 and 50% for BMI-135, at their highest concentration of 10^{-6} M ($P < 0.05$ compared to vehicle) (Fig. 2G *PAP1*). Reduction in the amount of viable MCF-7:2A cells by E_2 at 10^{-9} M was by an average of 67% (Fig. 2G *PAP1*). TTC-352 completely reduced the amount of viable MCF-7:2A cells after a 2-week treatment, in a dose-dependent manner, with a maximum reduction of cells by an average of 40% at its highest concentration of 10^{-6} M (p-value < 0.05 compared to vehicle control) (Supplementary Fig. S1G *PAP2*). Reduction in the amount of viable MCF-7:2A cells by E_2 at 10^{-9} M was by an average of 50.18% (Supplementary Fig. S1G *PAP2*).

In MCF-7:RAL, E_4 and BMI-135 completely reduced the amount of viable MCF-7:RAL cells after a 3-week treatment, in a dose-dependent manner, with a maximum reduction of cells by an average of 45% for E_4 and 43% for BMI-135, at their highest concentration of 10^{-6} M ($P < 0.05$ compared to vehicle) (Fig. 2H *PAP1*). Reduction in the amount of viable MCF-7:RAL cells by E_2 at 10^{-9} M was by an average of 45% (Fig. 2H

PAP1). TTC-352 completely reduced the amount of viable MCF-7:RAL cells after a 3-week treatment, in a dose-dependent manner, with a maximum reduction of cells by an average of 45% at its highest concentration of 10^{-6} M (p-value < 0.05 compared to vehicle control) (Supplementary Fig. S1H *PAP2*). Reduction in the amount of viable MCF-7:RAL cells by E_2 at 10^{-9} M was by an average of 45.32% (Supplementary Fig. S1H *PAP2*).

IIIB. ShERPAs TTC-352 and BMI-135 induce the transcriptional activity of ER similar to E_2 in WT BC MCF-7:WS8 and apoptotic-type BC MCF-7:5C.

qRT-PCR was used to assess the transcriptional activity of ERα on oestrogen-responsive genes (*TFF1* and *GREB1*) with TTC-352 and BMI-135. After 24-hour-treatment in MCF-7:WS8, TTC-352 and BMI-135 significantly ($P < 0.05$) increased the levels of *TFF1* and *GREB1* mRNAs compared to vehicle controls (Fig. 3A-B *PAP1*, and Fig. 2A-B *PAP2*). On the other hand, BPTPE induced a partial increase in the levels of *TFF1* and *GREB1* mRNAs, significantly ($P < 0.05$) less than that of E_2, TTC-352 and BMI-135 (Fig. 3A-B *PAP1*, and Fig. 2A-B *PAP2*). The minimal concentration that produced a complete increase in the levels of *TFF1* and *GREB1* was at 10^{-6} M for TTC-352 and BMI-135 ($P < 0.05$ compared to vehicle control).

After 24-hour-treatment in MCF-7:5C, TTC-352 and BMI-135 significantly ($P < 0.05$) increased the levels of *TFF1* and *GREB1* mRNAs compared to vehicle controls (Fig. 3C-D *PAP1*, and Fig. 2C-D *PAP2*). On the other hand, BPTPE induced a partial increase in the levels of *TFF1* and *GREB1* mRNAs, significantly ($P < 0.05$) less than that of E_2, TTC-352, and BMI-135 (Fig. 3C-D *PAP1*, and Fig. 2C-D *PAP2*). The minimal concentration that produced a complete increase in the levels of *TFF1* and *GREB1* was at 10^{-6} M for TTC-352 and BMI-135 ($P < 0.05$ compared to vehicle control).

The ERE-dependent transcriptional activity with E_4 was done by Abot and colleagues (Abot et al., 2014), and showed an induction similar to E_2, only with a lower potency.

Overall, the induction of the levels of *TFF1* and *GREB1* mRNAs by TTC-352 and BMI-135 in MCF-7:WS8 and MCF-7:5C is similar to that by full agonist E_2, only at a higher concentration.

IIIC. Effects of ShERPAs and E_4 are mediated via ERα.

MCF-7:5C, MCF-7:2A, and MCF-7:RAL representing LTED oestrogen-independent BC, were treated with 1 μM E_4, 1 μM BMI-135, and a combination of these with 1 μM 4OHT and 1 μM endoxifen, to investigate if E_4 and BMI-135 exert their function via ERα. In MCF-7:5C, full oestrogen agonists should cause cellular death within 1 week, antagonists should not (i.e., MCF-7:5C is endocrine-resistant), and the agonists' pairing with the antagonists should block the death effect. Indeed, E_2, E_4, and BMI-135 killed the cells within 1 week ($P < 0.05$ compared to vehicle) (Supplementary Fig. 2A *PAP1*), whereas, 4OHT and endoxifen did not ($P < 0.05$ compared to vehicle) (Supplementary Fig. 2A *PAP1*). The combination of E_2, E_4, and BMI-135 with 4OHT and endoxifen blocked the death effect (Supplementary Fig. 2A *PAP1*).

In MCF-7:2A, full agonists should cause cellular death within 2 weeks, antagonists should cause growth inhibition (i.e., MCF-7:2A is endocrine-sensitive), and the agonists' pairing with the antagonists should block the death effect. Indeed, E_2, E_4, and BMI-135 killed the cells within 2 weeks ($P < 0.05$ compared to vehicle) (Supplementary Fig. 2B *PAP1*), whereas, 4OHT and endoxifen caused growth inhibition ($P < 0.05$ compared to vehicle) (Supplementary Fig. 2B *PAP1*). The combination of E_2, E_4, and BMI-135 with 4OHT and endoxifen blocked the death effect (Supplementary Fig. 2B *PAP1*).

In MCF-7:RAL cells, full agonists should cause cellular death within 2-3 weeks *in vitro*, antagonists, especially the SERM raloxifene (positive control), should cause cellular growth, and the agonists' pairing with antagonists should block the death effect. Indeed, E_2, E_4, and BMI-135 killed the cells within 3 weeks ($P < 0.05$ compared to vehicle) (Supplementary Fig. 2C *PAP1*), whereas, the SERMs 4OHT, endoxifen and especially raloxifene, caused cellular growth ($P < 0.05$ compared to vehicle) (Supplementary Fig. 2C *PAP1*). The combination of E_2, E_4, and BMI-135 with 4OHT and endoxifen blocked the death effect (Supplementary Fig. 2C *PAP1*). Interestingly, the SERD ICI caused a decrease in cell DNA amount in MCF-7:RAL cells after a 3-week treatment ($P < 0.05$ compared to vehicle) (Supplementary Fig. 1F, and Supplementary Fig. 2C *PAP1*).

Endoxifen, the major biologically-active metabolite of TAM, was used as an anti-oestrogenic control alongside 4OHT, and neither induced a significant increase or decrease in viable cells, compared to vehicle control (Supplementary Fig. 2A *PAP1*). Only in MCF-7:2A cells, 4OHT and endoxifen caused growth inhibition (Supplementary Fig. 2B *PAP1*), and in MCF-7:RAL cells, both caused growth stimulation (Supplementary Fig. 2C *PAP1*), as predicted.

The transcriptional-translational, UPR, and apoptotic effects of TTC-352 were shown to be mediated via ERα. The combination of TTC-352 and 4OHT blocked SRC-3 recruitment compared to TTC-352 alone treatment (Fig. 9A *PAP2*); inhibited ERE activation compared to TTC-352 alone treatment (Fig. 9B *PAP2*); blocked the anti-proliferative effects of TTC-352 alone treatment (Supplementary Fig. S8A-C *PAP2*); inhibited the PERK UPR pathway activation (Fig. 9C-D *PAP2*); and prevented apoptosis (Fig. 9C, and E-G *PAP2*).

IIID. Effects of ShERPAs and E$_4$ on ERα regulation in numerous BC models.

Western blotting and densitometry were used to assess the regulation of ERα protein levels with compounds. In MCF-7:WS8, TTC-352 was able to down-regulate the protein levels of ERα after 72-hour-treatment, compared to vehicle control, and similar to E$_2$ and E$_4$ (Model I) (Fig. 3A and Supplementary Table. S3 *PAP2*). Whereas, BMI-135 seems to have a different effect by slightly downregulating ERα's protein levels by 72 hours, compared to vehicle control (Supplementary Fig. S2A and Supplementary Table. S4 *PAP2*). This down-regulation is less than that with BPTPE, nonetheless, BMI-135 does not accumulate the receptor compared to 4OHT and endoxifen (Supplementary Fig. S2A and Supplementary Table. S4 *PAP2*). This regulation trend with TTC-352, BMI-135, and E$_4$ in MCF-7:WS8 is replicated in MCF-7 ATCC (Supplementary Fig. S2B and Supplementary Table. S3 *PAP2*).

In T47D:A18, TTC-352 and BMI-135 maintain the protein levels of ERα (Model II), compared to vehicle control, and similar to E$_2$ and E$_4$ (Fig. 3B, Supplementary Fig. S2C and Supplementary Tables. S3-S4 *PAP2*). BPTPE, 4OHT, and endoxifen accumulate the receptor by 72 hours (Supplementary Fig. S2C and Supplementary Table. S4 *PAP2*).

In BT474, TTC-352 down-regulates the protein levels of ERα by 72 hours, compared to vehicle control, and similar to E$_2$ and E$_4$ (Model I) (Fig. 3C, Supplementary Fig. S2E, and Supplementary Tables. S3-S4 *PAP2*). Whereas, BMI-135 seems to have a similar trend except that the protein levels by 72 hours are similar to vehicle control (Supplementary Fig. S2E and Supplementary Table. S4 *PAP2*). The protein levels are up-regulated by 72 hours with BPTPE, and more so with endoxifen and 4OHT (Supplementary Fig. S2E and Supplementary Table. S4 *PAP2*).

In ZR-75-1, TTC-352 slightly down-regulates the protein levels of ERα after 72-hour-treatment, compared to vehicle control, and similar to E$_2$ and E4 (Model I) (Fig. 3D,

Supplementary Fig. S2D, and Supplementary Tables. S3-S4 *PAP2*). Whereas, BMI-135 seems to have a different trend whereby by 72 hours the protein levels become similar to vehicle control (Supplementary Fig. S2D and Supplementary Table. S4 *PAP2*). The protein levels are maintained by 72 hours with BPTPE, 4OHT, and endoxifen, compared to vehicle control (Supplementary Fig. S2D and Supplementary Table. S4 *PAP2*).

In MCF-7:5C, MCF-7:2A, and MCF-7:RAL, TTC-352, BMI-135, and E_4 down-regulate the protein levels of ERα by 72 hours, compared to vehicle control, and similar to E_2 (Model I) (Fig. 3E-G, and Supplementary Fig. S3D-F *PAP2*). In MCF-7:2A, ER[66] and ER[77] proteins levels with BMI-135, TTC-352, and E_4 are similarly regulated over time (Model I) (Fig. 3F, and Supplementary Fig. S3E *PAP2*) (Pink et al., 1995). In these cell lines, the protein levels are slightly down-regulated with BPTPE, and maintained or accumulated with endoxifen, 4OHT, and raloxifene (in MCF-7:RAL) (Supplementary Fig. S3D-F *PAP2*).

In LCC1, LCC2 and LCC9, TTC-352, BMI-135, and E_4 down-regulate the protein levels of ERα by 72 hours, compared to vehicle control, and similar to E_2 (Model I) (Fig. 3H-J, Supplementary Fig. S3A-C, and Supplementary Table. S3 *PAP2*). In these cell lines, the protein levels are down-regulated with BPTPE, and maintained or accumulated with endoxifen and 4OHT (Supplementary Fig. S3A-C, and Supplementary Table. S3 *PAP2*).

In eleven BC cell lines, TTC-352 regulated the protein levels of ERα in a similar manner to E_2 (Fig. 3 and Supplementary Table. S3 *PAP2*), and different from that with BPTPE (Supplementary Figs. S2-3, and Supplementary Table. S4 *PAP2*), and ICI significantly down-regulated the protein levels of ERα (Fig. 3, and Supplementary Figs. S2-S3 *PAP2*).

IIIE. ShERPAs and E$_4$ induce the transcriptional activity of ERα similar to E$_2$ in human endometrial cancer model Ishikawa.

Transient transfection and luciferase activity assays were used to determine the transcriptional activity of ERα on oestrogen-responsive genes (*5xERE*) with compounds, as ERE dual luciferase activity. After 24-hour-treatment of Ishikawa cells, E$_4$ and BMI-135 increased the levels of 5x-ERE luciferase activity compared to vehicle controls ($P < 0.05$) (Fig. 4A *PAP1*). On the other hand, the partial agonist BPTPE induced a partial increase in the levels of 5x-ERE luciferase activity, and less than that of full agonist E$_2$, E$_4$, and BMI-135 ($P < 0.05$), at concentration range of 10^{-8}-10^{-6} M (Fig. 4A *PAP1*). The minimal concentration that produced a complete increase in the levels of 5x-ERE luciferase activity was at 10^{-7} M for E$_4$ and BMI-135 ($P < 0.05$ compared to vehicle) (Fig. 4A *PAP1*).

To determine if the effects of E$_4$ and BMI-135 are mediated via ERα in Ishikawa cells, transiently-transfected Ishikawa cells were treated with test compounds in combination with antagonist endoxifen for 24 hours, and luciferase activity assays were conducted (Fig. 4B *PAP1*). The increase in the levels of 5x-ERE luciferase activity with E$_4$ and BMI-135 was blocked with endoxifen treatment at 10^{-6} M ($P < 0.05$ compared to vehicle) (Fig. 4B *PAP1*). This confirms that E$_4$ and BMI-135 exert their function via Ishikawa's ERα. In addition, endoxifen alone does not increase the levels of 5x-ERE luciferase activity in Ishikawa cells, acting as an antagonist in this uterine model (Fig. 4B *PAP1*).

Overall, the induction of the levels of 5x-ERE luciferase activity by E$_4$ and BMI-135 in Ishikawa cells is similar to that by full agonist E$_2$, only at a lower potency (Table 1 *PAP1*).

IIIF. ShERPAs and E$_4$ recruit ERα and SRC-3 to the *GREB1* proximal enhancer region similar to E$_2$ in MCF-7:5C BC model.

ChIP assays were used to assess the recruitment of ERα and SRC-3 to the *GREB1* proximal enhancer region with test compounds. Oestetrol and BMI-135 treatments resulted in a very strong recruitment of ERα to the *GREB1* proximal enhancer region similar to E$_2$, and higher than that with the partial agonist BPTPE ($P < 0.05$) (Fig. 5A *PAP1*).

Whereas, the recruitments of the coactivator SRC-3 to the *GREB1* proximal enhancer region with E$_4$ and BMI-135 treatments were higher than that with BPTPE ($P < 0.05$) (Fig. 5B *PAP1*). SRC-3 recruitment with E$_2$ was the highest. With E$_4$, there was an 18.72% recruitment reduction compared to E$_2$; with BMI-135, there was a 51.17% recruitment reduction compared to E$_2$; with BPTPE, there was a 65.47% recruitment reduction compared to E$_2$; and with endoxifen, there was a 98.14% recruitment reduction compared to E$_2$ (Fig. 5B *PAP1*).

Overall, the recruitment of ERα to the *GREB1* proximal enhancer region with E$_4$ and BMI-135 in MCF-7:5C cells is similar to that by full agonist E$_2$, and the recruitment of SRC-3 to the *GREB1* proximal enhancer region with E$_4$ and BMI-135 in MCF-7:5C cells is higher than that with the partial agonist BPTPE. Although SRC-3 recruitment with BMI-135 treatment is lower than that with E$_2$ ($P < 0.05$), it is higher than that with BPTPE ($P < 0.05$). TTC-352 treatment resulted in a very strong recruitment of SRC-3 to the *GREB1* proximal enhancer region (Fig. 9A *PAP2*).

IIIG. ShERPAs and E$_4$ activate the UPR.

Human UPR real-time profiler assays were used to assess the regulation of UPR genes with test compounds. Cell viability and proliferation assays showed a decline in MCF-7:5C cell DNA amount with E$_2$ and E$_4$ treatments at 72 hours (Fig. 7D *PAP1*). Furthermore, flow

cytometry showed apoptosis at 72 hours (annexin staining 14.8% with E_2 and 12.6% with E_4 versus vehicle control 4.5%) (Fig. 7E *PAP1*). The time point 48 hours, was chosen to investigate the terminal (or pro-apoptotic) UPR gene regulation with E_2 and E_4 treatments in MCF-7:5C cells, which precedes apoptosis by 72 hours.

After 48-hour-treatment with 1 nM E_2 and 1 μM E_4 (i.e., these concentrations were shown earlier to trigger maximal cellular death (Fig. 2 and Table 1 *PAP1*)), the endoplasmic reticulum associated degradation (ERAD) genes (downstream IRE1α/XBP1s and ATF6 p50): HTRA4 ($p < 0.001$), SYVN1 ($p < 0.001$), and HERPUD1 ($p < 0.001$), were down-regulated (Fig. 7B-C, and Supplementary Fig. 5A-B *PAP1*). The lipid or cholesterol metabolism genes (downstream IRE1α/XBP1s and ATF6 p50): MBTPS1 ($p < 0.001$) and SERP1 ($p < 0.001$), were down-regulated with E_2 treatment, whereas, only MBTPS1 ($p < 0.001$) with E_4 (Fig. 7B-C, and Supplementary Fig. 5A-B *PAP1*). The chaperone (chaperones are usually downstream IRE1α/XBP1s, PERK/P-eIF2α:ATF4 and ATF6 p50) gene SIL1 ($p < 0.001$) was down-regulated with E_4 treatment (Fig. 7C, and Supplementary Fig. 5B *PAP1*). By contrast, the genes CEBPB ($p < 0.001$) and INHBE ($p < 0.001$), which reflect high UPR stress, were up-regulated (Fig. 7B-C, and Supplementary Fig. 5A-B *PAP1*).

The heat map of MCF-7:5C cells with E_2 and E_4 treatments at 48 hours displays a general UPR gene downregulation (situated on the right side of the heat map) compared to vehicle control (situated on the left) (Fig. 7A *PAP1*). The majority of the profiler assays' genes belong to the lipid metabolism, ERAD, and chaperone gene groups, which are considered pro-survival mechanisms that help the cells cope with extrinsic or intrinsic cellular stress (Fig. 9 *PAP1*). This general downregulation by 48 hours (Fig. 7B-C, and Supplementary Fig. 5A-B *PAP1*) highlights MCF-7:5C cells' pro-apoptotic UPR phase and programming to undergo apoptosis by 72 hours (Fig. 7E *PAP1*).

Cell viability and proliferation assays showed a decline in MCF-7:5C cell DNA amount with BMI-135 treatment by 96 hours (Fig. 8D *PAP1*). Furthermore, flow cytometry showed apoptosis by 96 hours (annexin staining 17.1% with BMI-135 versus vehicle control 5.7%) (Fig. 8E *PAP1*). The time point 72 hours, was chosen to investigate the pro-apoptotic UPR gene regulation with BMI-135 treatment in MCF-7:5C cells, which precedes apoptosis by 96 hours. Another time point 48 hours, was chosen to compare and contrast the UPR gene regulation with that by 72 hours, and show how this regulation is dynamic and culminates over time.

After 48-hour-treatment with 1 μM BMI-135, the ERAD genes: EDEM1 ($p < 0.001$), HTRA4 ($p < 0.001$), SYVN1 ($p < 0.001$), and HERPUD1 ($p < 0.001$), were down-regulated (Fig. 8C, and Supplementary Fig. 5C *PAP1*). The lipid metabolism genes: MBTPS1 ($p < 0.001$) and SERP1 ($p < 0.001$), were down-regulated (Fig. 8C, and Supplementary Fig. 5C *PAP1*). By contrast, the genes CEBPB ($p < 0.001$) and INHBE ($p < 0.001$), were up-regulated (Fig. 8C, and Supplementary Fig. 5C *PAP1*). Interestingly, there was a 9.46 fold ($p < 0.05$) down-regulation of EIF2AK3 (PERK) (Supplementary Fig. 5C *PAP1*), which might play a role in MCF-7:5C cells' delayed course of apoptosis with BMI-135 treatment compared to E_2 and E_4. After a 72-hour-treatment with 1 μM BMI-135, there is an intensified (or terminal) UPR gene regulation compared to 48 hours, with an up-regulation of CEBPB ($p < 0.001$), INHBE ($p < 0.001$), PPP1R15A (GADD34, $p < 0.001$), DDIT3 (CHOP, $p < 0.001$), and ERN1 (IRE1α, $p < 0.001$). This is coupled with a down-regulation of the ERAD genes: HTRA4 ($p < 0.001$), SEL1L ($p < 0.01$), and HERPUD1 ($p < 0.001$), the chaperone gene HSPA2 ($p < 0.001$), and the lipid metabolism gene MBTPS1 ($p < 0.001$) (Fig. 8B, and Supplementary Fig. 5D *PAP1*).

The heat map of MCF-7:5C cells with BMI-135 treatment at 72 hours (Fig. 8A *PAP1*) displays a general UPR gene downregulation (situated on the right side of the heat map) compared to vehicle control (situated on the left). This general downregulation by 72 hours

(Fig. 8B, and Supplementary Fig. 5D *PAP1*) highlights MCF-7:5C cells' trajectory to undergo apoptosis by 96 hours (Fig. 8E *PAP1*).

Cell viability and proliferation assays showed a decline in MCF-7:5C cell DNA amount with BPTPE treatment by day 8 (Supplementary Fig. 4D *PAP1*). Furthermore, flow cytometry showed apoptosis by day 8 (annexin staining 31.5% with BPTPE versus vehicle control 9.4%) (Supplementary Fig. 4E *PAP1*). The time point day 7, was chosen to investigate the pro-apoptotic UPR gene regulation, which precedes apoptosis by day 8. Another time point day 3, was chosen to compare and contrast the UPR gene regulation with that by day 7, and show how this regulation is dynamic and culminates over time.

After a 3-day-treatment with 1 μM BPTPE, there was a relatively minor UPR gene activation compared to the one seen by day 7 (Supplementary Fig. 4B-C, and Supplementary Fig. 5E-F *PAP1*). Interestingly, there was a 2.15 fold ($p < 0.001$) down-regulation of EIF2AK3 with 3-day BPTPE treatment (Supplementary Fig. 5E *PAP1*), which might play a role in MCF-7:5C cells' delayed course of apoptosis with BPTPE treatment compared to E_2 and E_4. This is also observed with BMI-135's early treatment time point (Supplementary Fig. 5C *PAP1*). After a 7-day-treatment with BPTPE, there was a down-regulation of the ERAD gene HERPUD1 ($p < 0.001$), the lipid metabolism genes: INSIG2 ($p < 0.001$) and MBTPS1 ($p < 0.001$), and the chaperone genes: HSPA2 ($p < 0.001$) and DNAJB9 ($p < 0.001$) (Supplementary Fig. 4B, and Supplementary Fig. 5F *PAP1*).

The heat map of MCF-7:5C cells with BPTPE treatment at day 7 (Supplementary Fig. 4A *PAP1*) displays a general UPR gene downregulation (situated on the left side of the heat map) compared to vehicle control (situated on the right). This general downregulation by day 7 (Supplementary Fig. 4B, and Supplementary Fig. 5F *PAP1*) highlights MCF-7:5C cells' programming to undergo apoptosis by day 8 (Supplementary Fig. 4E *PAP1*).

The statistically-significant regulated UPR genes, with test compounds are stated and grouped, at select time points (Fig. 9 *PAP1*) to show the similar terminal UPR regulation preceding apoptosis.

PERK downstream targets p-eIF2α, ATF4, and CHOP, are up-regulated after 72-hour treatment with TTC-352 (Fig. 8B *PAP2*).

IIIH. ShERPAs and E$_4$ induce ThT fluorescence as a marker of UPR.

Thioflavin T was used to detect and quantify the EnR stress or UPR in living cells, as it interacts directly with the accumulated misfolded protein amyloid during the UPR (Beriault and Werstuck, 2013). The "blue" Hoechst 33342 fluorescent dye was used as a nuclear counterstaining dye in MCF-7:5C living cells (channel A), the "green" ThT fluorescent dye was used as a UPR-indicative dye (channel B), and a co-localization of ThT and Hoechst 33342 dyes is shown (channel C).

17β-oestradiol and E$_4$ were shown to induce ThT fluorescence by 48 hours, like the induction seen with positive control thapsigargin (i.e., triggers EnR stress by disrupting EnR Ca^{2+} homeostasis), and compared to vehicle control (Supplementary Fig. 6B *PAP1*). After 48-hour treatment, E$_4$ had the highest ThT relative intensity/cell of 1.244892, followed by thapsigargin of 0.875072; E$_2$ of 0.741126; and BMI-135 of 0.497225, compared to vehicle control of 0.27594 (Table 2A *PAP1*).

BMI-135 induces a stronger delayed ThT fluorescence by 72 hours (Fig. 10B and Table. 2B), compared to that seen by 48 hours (Supplementary Fig. 6B and Table 2A *PAP1*). The relative intensity/cell with 48-hour BMI-135 treatment was 0.497225, compared to vehicle control 0.27594 (Table 2A *PAP1*). Whereas, the relative intensity/cell with 72-hour BMI-135 treatment was 4.878173, compared to vehicle control 0.29573 (Table 2B *PAP1*). The relative intensity/cell over time is represented in Table 2 (*PAP1*).

TTC-352 induced ThT fluorescence by 72 hours compared to vehicle control, and somewhat similar to the induction seen with thapsigargin (Fig. 7B *PAP2*). ThT relative intensity/cell for thapsigargin was 3.320555, and 2.025762 for TTC-352, compared to 0.4725 for vehicle control.

IIII. ShERPAs and E_4 trigger apoptosis in multiple oestrogen-independent and endocrine-resistant BC models.

Flow cytometry was used to assess if the type of stress-induced cell death was actually apoptosis, when treated with 1 µM TTC-352, 1 µM BMI-135, and 1 µM E_4.

In MCF-7:5C, 1 µM E_4 induces apoptosis (annexin staining 12.6% versus vehicle control 4.5%) similar to the time course of 1 nM E_2 (annexin staining 14.8% versus vehicle control 4.5%) (Fig. 7E *PAP1*), which is by 72 hours. Whereas, MCF-7:5C's apoptosis with BMI-135 treatment (annexin staining 17.1% versus vehicle control 5.7%) is delayed, by 96 hours (Fig. 8E representing 96 hours, and Supplementary Fig. 8D representing 72 hours *PAP1*). The antagonist 4OHT (as a negative control), and its pairing with E_2, E_4 and BMI-135, do not induce apoptosis by 72 or 96 hours, as predicted (data not shown). TTC-352 induces apoptosis (annexin staining 22.9% versus vehicle control 6.9%) (Fig. 8A *PAP2*), similar to the time course of 1 nM E_2 (annexin staining 23.4% versus control 6.7%) (Supplementary Fig. S7A *PAP2*), which is in 3 days.

In MCF-7:2A, E_4 induces apoptosis (annexin staining 6.7% versus vehicle control 0.8%) similar to the time course of E_2 (annexin staining 8% versus vehicle control 0.8%) (Supplementary Fig. 8A *PAP1*), which is by day 9. Whereas, MCF-7:2A's apoptosis with BMI-135 treatment (annexin staining 7.3% versus vehicle control 2.2%) is delayed, by day 13 (Supplementary Fig. 8B representing day 13, and Supplementary Fig. 8C representing day 9 *PAP1*). The antagonist 4OHT (as a negative control), and its pairing with E_2, E_4, and BMI-

135, do not induce apoptosis by day 9 or 13, as predicted (data not shown). TTC-352 induces apoptosis (annexin staining 21.2% versus control 2.7%), similar to the time course of E_2 (annexin staining 20.4% versus control 2.7%) (Supplementary Fig. S7B *PAP2*), which is in 9 days.

In MCF-7:RAL, E_4 induces apoptosis (annexin staining 7.6% versus vehicle control 5.3%) similar to the time course of E_2 (annexin staining 9% versus control 5.3%) (Supplementary Fig. 9A *PAP1*), which is by day 14. Whereas, MCF-7:RAL's apoptosis with BMI-135 (annexin staining 8% versus control 0.8%) is delayed, until day 17 (Supplementary Fig. 9B representing day 17, and Supplementary Fig. 9C representing day 14 *PAP1*). The antagonists 4OHT and raloxifene, and their pairing with E_2, E_4, and BMI-135, do not induce apoptosis by day 14 or 17, as predicted (Supplementary Fig. 9A *PAP1*). Interestingly, treatment of MCF-7:RAL cells with ICI for 3 weeks caused a significant decline in cell DNA amount (Supplementary Fig. 2C *PAP1*), however, this is not due to apoptosis (Supplementary Fig. 9D *PAP1*). Such observed effect of ICI in MCF-7:RAL could be attributed to growth inhibition by preventing cell replication. TTC-352 induces apoptosis (annexin staining 8.4% versus control 1.5%), similar to the time course of E_2 (annexin staining 9.1% versus control 1.5%) (Supplementary Fig. S7C *PAP2*), which is in 14 days.

IIIJ. Inhibition of UPR PERK pathway blocks apoptosis in MCF-7:5C with ShERPAs and E_4 treatments.

Blocking the UPR transducer PERK with 10 μM GSK G797800 in combination with 1 nM E_2, and in combination with 1 μM E_4 by 72 hours, inhibited apoptosis (annexin staining 7.8% and 7.9%, respectively, versus vehicle control 7%) (Supplementary Fig. 7A *PAP1*), compared to E_2 and E_4 alone treatments that trigger apoptosis (Fig. 7E *PAP1*), and compared to the negative control GSK G797800 alone treatment that does not trigger apoptosis (annexin staining 5.7% versus vehicle control 7%) (Supplementary Fig. 7A *PAP1*).

Blocking PERK with 10 μM GSK G797800 in combination with 1 μM BMI-135 by 96 hours, inhibited apoptosis (annexin staining 4% versus vehicle control 5.7%) (Fig. 11A *PAP1*), compared to BMI-135 alone treatment that triggers apoptosis (Fig. 11A *PAP1*), and compared to GSK G797800 alone treatment (annexin staining 5.5% versus control 5.7%) (Fig. 11A *PAP1*).

Blocking PERK with 10 μM GSK G797800 in combination 1 μM TTC-352 by 72 hours, inhibited apoptosis (annexin staining 6.9% versus control 6.9%) (Fig. 8A *PAP2*), compared to TTC-352 alone treatment (Fig. 8A *PAP2*) (annexin staining 22.9% versus vehicle control 6.9%), and compared to 10 μM GSK G797800 alone treatment (annexin staining 8.3% versus control 6.9%) (Fig. 8A *PAP2*).

PERK downstream targets p-eIF2α, ATF4, and CHOP as well as apoptosis target cleaved PARP, are up-regulated after 72-hour treatment with TTC-352, whereas, the addition of GSK 797800 completely inhibits this UPR/apoptosis effect (Fig. 8B *PAP2*).

IIIK. Inhibition of UPR IRE1α:XBP1s pathway enhances apoptosis in MCF-7:5C with ShERPAs and E$_4$ treatments.

Inhibiting the UPR transducer IRE1α, by inhibiting basal XBP1 splicing, with 20 μM MKC-3946 in combination with 1 μM E$_4$ by 72 hours, induces more apoptosis (annexin staining 34.1% versus control 1.4%) (Supplementary Fig. 7B *PAP1*), compared to E$_4$ alone treatment that triggers apoptosis (annexin staining 18.6% versus control 1.4%) (Supplementary Fig. 7B *PAP1*), and compared to MKC-3946 alone treatment that triggers apoptosis (annexin staining 8.8% versus control 1.4%) (Supplementary Fig. 7B *PAP1*).

Blocking IRE1α with 20 μM MKC-3946 in combination with 1 μM BMI-135 by 96 hours, induces more apoptosis (annexin staining 33.3% versus control 1.4%) (Fig. 11B *PAP1*), compared to BMI-135 alone treatment (annexin staining 26.5% versus control 1.4%)

(Fig. 11B *PAP1*), and compared to MKC-3946 alone treatment (annexin staining 8.8% versus control 1.4%) (Fig. 11B *PAP1*).

Blocking IRE1α with 20 μM MKC-3946 in combination with 1 μM TTC-352 by 72 hours, enhanced apoptosis (annexin staining 35.5% versus vehicle control 1.4%) (Fig. 8C *PAP2*), compared to TTC-352 alone treatment (annexin staining 27.9% versus vehicle control 1.4%) (Fig. 8C *PAP2*), and compared to 20 μM MKC-3946 alone treatment (annexin staining 8.8% versus vehicle control 1.4%) (Fig. 8C *PAP2*).

IRE1α downstream target XBP1s (or spliced XBP1) is up-regulated after 72-hour treatment with TTC-352, whereas, the addition of MKC-3946 inhibits this splicing effect (Fig. 8D *PAP2*).

IV. Discussion

Oestetrol is a naturally-occurring fetal oestrogen, which is associated with a low risk of drug-drug interactions (CYP450 family), and a neutral impact on risk markers of venous thromboembolism unlike E_2 (Bennink et al., 2017, Singer et al., 2014, Verhoeven et al., 2018). TTC-352 and BMI-135 are members of a new class of oestrogen mimics, which did not cause significant uterine proliferation (Molloy et al., 2014, Xiong et al., 2016). Oestetrol and the ShERPA TTC-352 are currently being evaluated in endocrine-resistant MBC clinical trials (Dudek et al., 2020, Schmidt, 2020). This work reports: (i) the structural studies of E_4 and ShERPAs (Fig. 6 *PAP1*, and Figs. 5-6 *PAP2*), including the X-ray crystallography of TTC-352:mutant ER with clinical implications given that the majority of MBC patients harbor ER mutations (Fig. 5G-I *PAP2*) (Niu et al., 2015, Pejerrey et al., 2018, Toy et al., 2013b); (ii) the molecular mechanisms of E_4 and TTC-352's BC regression in LTED patients (Figs. 7-12, Supplementary Fig. 5B and 5D, and Supplementary Figs. 6-9 *PAP1*, and Figs. 7-10 *PAP2*); and (iii) the key interactions at the molecular and atomic levels of the benchmark

partial agonist BPTPE:WT ER, involving Asp351 and H12 (Fig.6B-C *PAP2*), which explains the reduced E_2-enriched coactivator binding (Fig. 5B *PAP1*, and Fig. 4A *PAP2*), and delayed ERα-induced UPR and apoptosis compared to TTC-352 (Supplementary Fig. 4 *PAP1*, and Figs. 7-8 *PAP2*).

Our earlier pharmacological studies classified ER binding ligands into agonists, partial agonists, and antagonists (Jordan and Lieberman, 1984), and complimented the subsequent X-ray crystallography studies of the agonist and antagonist ER complexes of the LBD (Brzozowski et al., 1997, Shiau et al., 1998b). Our earlier biological studies described E_2-induced apoptosis (Jordan, 2015b). Current studies, in a wide range of biologically-different human BC cell models as well as a human endometrial cancer cell model, shows TTC-352, BMI-135, and E_4 to be weak full oestrogen agonists (Figs. 2-6, Supplementary Fig. S1, and Supplementary Table. S2 *PAP2*, and Figs. 2-5, and Fig. 6B and 6F *PAP1*), with the induction of terminal UPR and apoptosis as their anti-tumour mechanism of action (Figs. 7-10, and Supplementary Fig. S7B-C *PAP2*, and Figs. 7-12, and Supplementary Figs. 5-9 *PAP1*). Although BMI-135 exhibits a slightly delayed UPR-and-apoptosis biology compared to E_2 and E_4 (Figs. 7-8, Figs. 9-11, and Supplementary Figs. 6-9 *PAP1*), it is still distinct from the much delayed UPR-and-apoptosis biology of the benchmark partial agonist BPTPE (Supplementary Fig. 4 *PAP1*).

This research area is of particular importance given that BC is projected to double by 2030 than it was in 2011 (Rosenberg et al., 2015). The majority will be ER-positive with a high risk of recurrence, even with clinically low-risk disease (T1N0) (Schroeder et al., 2017). Moreover, treated metastases often harbor private 'driver' mutations, compared to untreated metastases (Hu et al., 2020). In the case of ER-positive HER2-negative BC, metastases treated with endocrine therapy, acquire somatic single-nucleotide variants (Toy et al., 2013b). This highlights the need to evaluate and develop new rapidly-acting BC therapeutics such as

oestrogens. The recent long-term follow-up results of the WHI Trials (Jordan, 2020) reaffirm the clinical potential of novel and safe oestrogenic therapy in significantly reducing BC incidence and mortality in LTED patients.

The application of long-term adjuvant endocrine therapy (Jordan et al., 1979), to treat ER-positive BC, is invaluable for patient care. As a result, women's lives are extended or saved (Early Breast Cancer Trialists' Collaborative Group, 1998, Goss et al., 2003a, Goss et al., 2005). Nonetheless, recurrence of endocrine-resistant stage IV BC is common (Pisani et al., 2002), hence the discovery of new therapeutic options remains a clinical priority.

Cell models (Liu et al., 2003, Pink et al., 1995, Ariazi et al., 2011, Fan et al., 2014, Lewis et al., 2005b), and athymic mice models (Gottardis and Jordan, 1988, Gottardis et al., 1989b, Yao et al., 2000, Gottardis et al., 1989a), deciphered the evolution of acquired TAM resistance over years to eventually give rise to a vulnerability in BC: E_2-induced apoptosis (Jordan, 2008, Jordan, 2015b). Although oestrogen is approved to treat BC, there is a reluctance to use oestradiol as a salvage therapy (in stage IV BC), because of AEs. As a result, safer oestrogenic alternatives are being considered.

First, the actions of E_4 and BMI-135 were compared and contrasted with those of the well-characterized partial agonist BPTPE. Current study shows that E_4, and BMI-135:ERα complexes initiate and modulate the UPR (Figs. 7-12, and Supplementary Figs. 5-7 *PAP1*). This is an ERα-mediated (Supplementary Fig. 2 *PAP1*) activation of the unfolded proteins' synthesis, and thus of cellular stress.

The intrinsic activity of the ER complex was evaluated by comparing and contrasting TFF1 and GREB1 oestrogen-regulated gene activation with E_2, BMI-135, BPTPE, and endoxifen treatments in WT MCF-7 and LTED MCF-7:5C cells (Fig. 3 *PAP1*). The pharmacology of each ligand as a full agonist (E_2, E_4, and BMI-135), or a partial agonist

(BPTPE), or an antagonist with no intrinsic activity (endoxifen), mirrored the pharmacology in cells (Fig. 2 *PAP1*).

Molecular modeling studies demonstrated that E_4, BMI-135, and BPTPE bind to the classical agonist conformation of ERα, similar to E_2 (Fig. 6A, 6C, and 6E *PAP1*). The flexible docking and MD simulations, performed for BMI-135:ERα complex, show the dynamic profile of the system to be similar to E_2 (Supplementary Fig. 3A *PAP1*); with the ligand firmly bound to the active site (Supplementary Fig. 3B *PAP1*). Although BMI-135 is larger than E_2, the same contacts have been observed, with the notable exception of the H-bond to His524 (Fig. 6B *PAP1*). These H-bonds and hydrophobic contacts are stable for both ligands, with slightly larger frequencies of occurrence with E_2 (Supplementary Fig. 11A-B *PAP1*), which indicates a stronger binding mode of E_2. BPTPE exhibits equivalent binding contacts to E_2 (Fig. 6C-D *PAP1*), but forms a distinctive robust H-bond with Thr347 (Supplementary Fig. 11C *PAP1*), which induces the stability of the ligand binding, but increases the mobility of H12 and the loop connecting H11 and H12, which affects the overall stability of the system. This is most likely responsible for the partial agonist profile of BPTPE. These data support the molecular classification of E_4 and BMI-135 as full agonists, and further explain their observed biological behavior.

A comparison of E_4, BMI-135, and BPTPE in multiple WT and LTED BC cell lines (Fig.2 and Supplementary Fig. 1 *PAP1*) demonstrates the partial agonist actions of BPTPE on both growth (Fig. 2A-E, Fig. 3A-B, and Supplementary Fig. 1A-C and 1F *PAP1*) and E_2-induced apoptosis (Fig. 2F-H, Fig. 3C-D, and Supplementary Fig. 4D-E *PAP1*). All experiments used BPTPE as a well-characterized partial agonist (Jordan and Lieberman, 1984), which triggers delayed E_2-induced apoptosis in LTED BC cells, compared to E_2 (Obiorah et al., 2014, Obiorah and Jordan, 2014) (Supplementary Fig. 4E *PAP1*). The

mechanism is shown here to be through a delay in the induction of the pro-apoptotic UPR signaling (Supplementary Fig. 4B-C, and Supplementary Fig. 5E-F *PAP1*).

Delayed apoptosis with BPTPE (contains a free para-hydroxyl on the phenyl ring) mirrors the delayed apoptosis with the synthesized angular triphenylethylene (TPE) derivative 3OH**TPE** (contains the free para-hydroxyl) (Maximov et al., 2020). The other synthesized TPE derivative Z2OH**TPE**, does not contain the free para-hydroxyl, and causes early apoptosis, similar to E_2 (Maximov et al., 2020). This free para-hydroxyl in BPTPE and 3OHTPE, is part of the anti-oestrogenic side chain of endoxifen, which prevents the complete closure of ERα's H12 over the ligand:LBD (Supplementary Fig. 11C *PAP1*). This delays the coactivators' recruitment to the ER to form a transcriptionally-active complex (Fig. 5B *PAP1*), which delays the ligand:ERα–induced transcription and translation of the unfolded proteins, resulting in delayed apoptosis (Supplementary Fig. 4 *PAP1*).

Although BMI-135 does not exhibit the pharmacology of BPTPE (Figs. 2-5, Fig. 6A-B, and Table 1 *PAP1*), there is still a slight delay in the induction of the terminal UPR signaling and apoptosis, which is mediated by the BMI-135:ERα complex (Fig. 8B-C and 8E versus Supplementary Fig. 8D, Fig. 10B versus Supplementary Fig. 6B, Supplementary Fig. 5C-D, and Table. 2 *PAP1*).
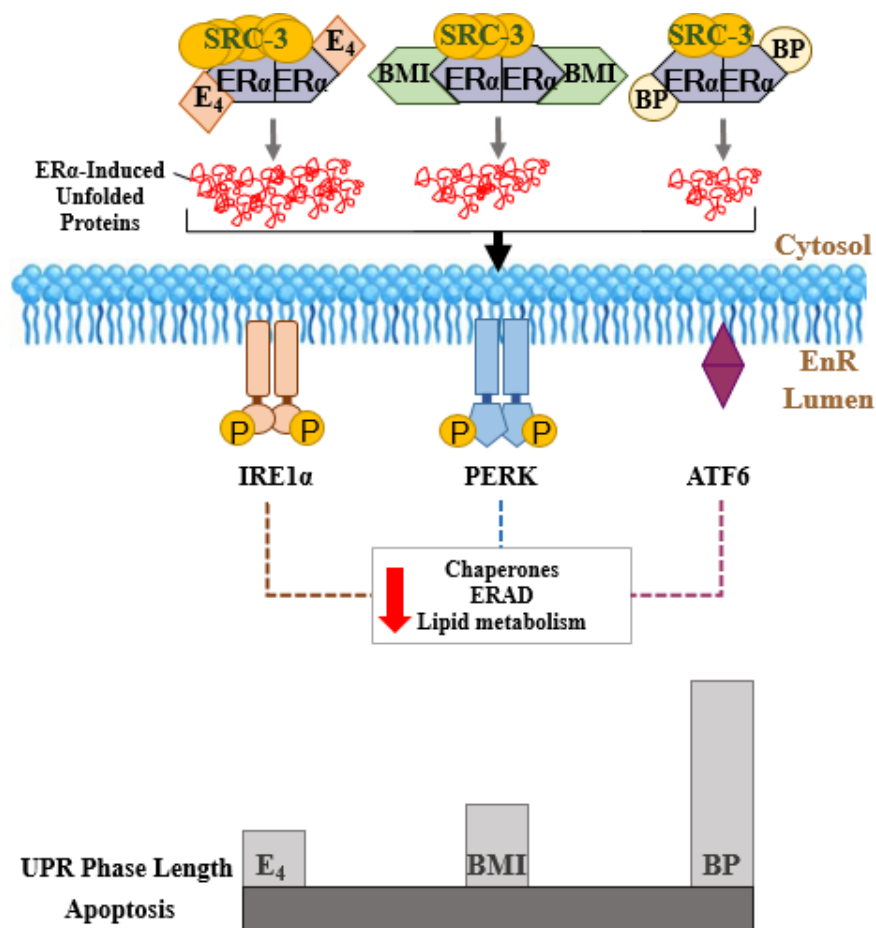
Figure 17 | **Schematic representation of the first paper's concluded anti-tumour molecular mechanisms of E₄, BMI-135, and BPTPE in LTED endocrine-resistant BC MCF-7:5C.**
Oestetrol:ERα complex recruits the most co-activator SRC-3 and thus induces the most accumulation of unfolded proteins (highest threshold of stress), followed by BMI-135:ERα (BMI-135 is referred to as BMI in the illustration), and BPTPE:ERα (BPTPE is referred to as BP in the illustration). This differential ligand:ERα:coactivator-induced endoplasmic reticulum stress activates the transducers of the UPR, with a down-regulation of chaperons, ERAD, and lipid metabolism genes and proteins ($P < 0.05$), which are considered pro-survival mechanisms. This down-regulation state constitutes the pro-apoptotic UPR phase, which is reached quickly with E₄, followed by BMI-135, and BPTPE, and eventually induces apoptosis.

The ChIP assay (Fig. 5 *PAP1*) is valuable to understand the delayed apoptotic biology with BMI-135 and BPTPE. Earlier studies (Obiorah et al., 2014, Sengupta et al., 2013) demonstrated a reduction in the binding of the BPTPE:ERα:SRC-3 complex, using the ChIP

assay in MCF-7 cells, which is reproduced here (Fig. 5A-B *PAP1*). A reduced DNA binding of the partial agonist complex occurs, which correlates with a reduction in the efficacy of the complex to synthesize misfolded or unfolded proteins, hence with a delay in the induction of the terminal UPR and apoptosis, compared to E_2 (Supplementary Fig. 4 *PAP1*). Although BMI-135 recruits equivalent quantities of ERα (Fig. 5A *PAP1*), there is a reduced recruitment of the coactivator SRC-3, compared to E_2 and E_4. Nonetheless, BMI-135:ERα's recruitment of SRC-3 is significantly higher than that with BPTPE (Fig. 5B *PAP1*). This correlates with BMI-135's slightly delayed induction of the terminal UPR and apoptosis (Fig. 8 *PAP1*).

The significant down-regulation of the pro-survival mechanisms: chaperones, ERAD, and lipid metabolism genes, alongside the significant up-regulation of marker UPR stress proteins (INHBE and CEBPB), constitute the terminal/pro-apoptotic UPR phase, and underscores the anti-tumour mechanism of E_2, E_4, BMI-135, and BPTPE (Figs. 7-9, Fig.12, and Supplementary Figs. 4-5 *PAP1*).

Apoptosis with E_4 and BMI-135 treatments was prevented by blocking the PERK pathway (Fig. 11A and Supplementary Fig. 7A *PAP1*). By contrast, blocking the IRE1α:XBP1s pathway, following E_4 and BMI-135 treatments, enhanced apoptosis (Fig. 11B and Supplementary Fig. 7B *PAP1*). These data demonstrate the modulation of apoptosis with E_4 and BMI-135 through the modulation of UPR's subcellular sensors.

The timing of UPR-indicative ThT fluorescence with E_4 and BMI-135 is synchronic with that of their significant pro-apoptotic UPR gene regulation. The ThT fluorescence and terminal UPR gene regulation were shown to be by 48 hours with E_2 and E_4 (before apoptosis by 72 hours); by 72 hours with BMI-135 (before apoptosis by 96 hours), and by day 7 with BPTPE (before apoptosis by day 8) (Figs. 7-8, Fig. 10B, Supplementary Figs. 4-5, Supplementary Fig. 6B, and Table 2 *PAP1*).

Our earlier translational research (Gottardis et al., 1988) identified a potential link between TAM treatment and the occurrence of endometrial cancer in patients (Jordan and Assikis, 1995). Raloxifene does not have an increased risk of endometrial cancer in clinical trials (Cummings et al., 1999, Vogel et al., 2006). BMI-135 is a raloxifene derivative (Fig. 1 *PAP1*) (Xiong et al., 2016), and was tested to determine whether the ShERPA BMI-135:ER:coregulators complex is an agonist, in the human endometrial cancer cell line Ishikawa transfected with 5x-ERE (Fig. 4 *PAP1*). BPTPE exhibited a partial agonist activity (Fig. 4A *PAP1*), but both E_4 and BMI-135 exhibited a weak full agonist activity compared to E_2 (Fig. 4A *PAP1*). This effect is mediated via the Ishikawa ERα (Fig. 4B *PAP1*). Although BMI-135 was shown not induce uterine growth in a mouse xenograft model (Xiong et al., 2016), based on this study's observations, it would be wise to require an endometrial screening for BC patients receiving E_4 or BMI-135.

Raloxifene induces acquired resistance as evidenced by SERM-stimulated BC cell growth (Liu et al., 2003, Balaburski et al., 2010) (Fig. 2H, Supplementary Fig. 1F and Supplementary Fig. 2C *PAP1*). Such laboratory data has clinical significance, as a case report of an anti-oestrogen withdrawal effect with raloxifene, was reported (Lemmo, 2016). Raloxifene-resistant BC-stimulated growth has not been widely-reported during the decades of treatment in patients with osteoporosis. This is surprising, but perhaps clinicians have not been aware of this form of SERM resistance. Nevertheless, our findings here (Supplementary Fig. 9A-B *PAP1*) suggest that E_4 or a ShERPA could be deployed, after raloxifene discontinuation, to induce tumour regression; through apoptosis in raloxifene-resistant BC. Furthermore, ICI could be deployed, as we have shown here that it has a growth inhibitory effect (Supplementary Fig. 1F, Supplementary Fig. 2C, and Supplementary Fig. 9D *PAP1*).

Second, the actions of TTC-352 were compared and contrasted with those of the well-characterized partial agonist BPTPE. MD simulations and MM-GBSA calculations for WT

ERα in complex with TTC-352, E_2, and BPTPE are valuable methodologies to discover key ligand-receptor interactions, which aids the pharmacological classification of TTC-352. Most importantly, they identify key structural components of oestrogenic therapeutics that ensure the appropriate closure of the ERα LBD by H12 in LTED BC. This closure is a prerequisite for the activation of ERE-mediated UPR and apoptosis, which is the basis of their anti-tumour properties.

The H-bond of TTC-352's benzothiophene scaffold to Glu353, followed by the H-bond to His524, are the most stable contacts contributing to the binding mechanism of TTC-352, which are also the two binding features specific for the oestrogenic activity of E_2 (E_2's A ring to Glu353) (Fig. 6A-B *PAP2*). Such strong H-bond between TTC-352 and Glu353, induces stability in the LBD and, consequently, to H3. This supports the formation of the H-bonds between the side-chain of Asp351 (H3) to the backbone of Leu539 and Leu540 (H12), which stabilizes H12 in the full-agonist conformation (Fig. 5C *PAP2*). Such LBD-stabilizing network of H-bonds is preserved with TTC-352, but more so with E_2, which explains the altered potency of TTC-352:ERα compared to E_2:ERα. By contrast, BPTPE's binding mechanism is governed by the H-bond of BPTPE's angular phenolic OH to Thr347, followed by the hydrophobic contacts, and a significantly weaker H-bond to Glu353 (Fig. 5E and Fig. 6C *PAP2*). Although the H-bond between BPTPE's angular phenolic group and Thr347 stabilizes its binding, it disturbs the H-bond network within H3 and the stabilizing H-bonds to H12 (i.e., Asp351 to Leu 539 and Leu540). As a result, H12 is prevented from adopting the proper orientation specific for the ER full-agonist conformation (Fig. 5F *PAP2*). This is consistent with BPTPE's reduced recruitment of coactivators (Fig. 4A *PAP2*), and our previous reports of its delayed activation of ERα-induced UPR and apoptosis as well as its functional modulation from a partial agonist (**3OH**TPE) to a full agonist (**Z2OH**TPE) by the removal of the para-phenol substitution (Maximov et al., 2020).

Both, Asp351 and H12, play a critical role in modulating the oestrogenic and anti-oestrogenic intrinsic efficacy of the ligand-ER complex. The natural mutation Asp351Tyr was discovered; overexpressed in TAM-stimulated MCF-7 tumours grown in athymic mice (Wolf and Jordan, 1994). The molecular pharmacology of the WT ER (Jiang and Jordan, 1992) and Asp351Tyr ER (Catherino et al., 1995) was established by stable transfection into ER-negative MDA-MB-231 BC. Unexpectedly, Asp351Try ER converted the raloxifene:WT Asp351 ER complex from anti-oestrogenic to oestrogenic (Levenson et al., 1997). Subsequent X-ray crystallography of the raloxifene:ER LBD (Brzozowski et al., 1997), demonstrated the critical role of the anti-oestrogenic side chain containing a piperidine ring N to shield and neutralize Asp351, which prevented the closure of H12, and the subsequent ERE activation. Subsequent interrogation of the structural modulation of raloxifene and its interactions with Asp351, demonstrated how Asp351 modulates the oestrogenic and anti-oestrogenic efficacy of the ligand-ER complex (Liu et al., 2002).

ESR1 somatic mutations, Y537S and D538G, stabilize ERα in the agonist state, and are linked to acquired resistance to endocrine therapies (Fanning et al., 2016). Mutations Tyr537Ser and Asp538Gly were most prevalent in BC metastases (Toy et al., 2013b), especially AI-resistant BC patients. These mutations improve the closure of H12 over ERα's LBD, through interacting with Asp351, and recruiting coactivators in the absence of oestrogen, which increases the oestrogen-like properties of the complex (Toy et al., 2013b).

ERE DNA pull downs and MS are valuable methodologies to determine if TTC-352 has an ERα:coactivators' binding profile of a full or partial agonist, and better understand why the TTC-352:ERα:coactivators' complex in the LTED endocrine-resistant MCF-7:5C is phenotypically apoptosis-promoting, whereas, such complex in WT MCF-7 is phenotypically growth-promoting.

In MCF-7:WS8 BC, TTC-352 and BMI-135 are different from BPTPE in terms of NCOA1-2 (or SRC1-2) and MED subunit recruitments, with NCOA3 (or SRC-3) not being readily-enriched with either ShERPAs compared to E_2 and E_4 (Fig. 4A *PAP2*). BPTPE did not recruit many of the E_2-enriched coactivators, and only a subset of endoxifen-enriched coregulators (Fig. 4A *PAP2*). In MCF-7:5C BC, TTC-352 and BMI-135 recruited NCOA3 and KMT2D at much lower levels than E_2 and E_4, with TTC-352 recruiting more MED subunits than E_2, while BMI-135 displaying shared MED subunit recruitment with E_4 (Fig. 4A *PAP2*). BPTPE did not have much of coactivator binding (Fig. 4A *PAP2*).

TTC-352's differential recruitment of MED subunit types alongside their differential enrichment levels, could explain its ability to cause a higher threshold of stress of ER-mediated unfolded proteins (Fig. 9 *PAP2*) followed by earlier apoptosis, compared to that with BMI-135 (Fig. 10A *PAP2*). In MCF-7:5C, NCOA3, KMT2D, and many MEDs (especially MED12-16 and MED23) are recruited to ERα with TTC-352, compared to E_2, but these coactivators are reduced upon the treatment of MCF-7:WS8 with TTC-352 (Supplementary Table. S5 *PAP2*). TTC-352's higher recruitment of major ER coactivators in MCF-7:5C, compared to MCF-7:WS8, can explain its ability to cause a high threshold of stress of ER-mediated unfolded proteins followed by apoptosis; making it phenotypically apoptosis-promoting, versus the growth-promoting MCF-7:WS8 (Fig. 10B *PAP2*). The altered recruitment patterns of major ER coactivators for transcriptional activation, with TTC-352, BMI-135, and E_4, in comparison to the levels promoted by E_2 or BPTPE, can better explain the observed differences in their potency and ERα-mediated UPR.
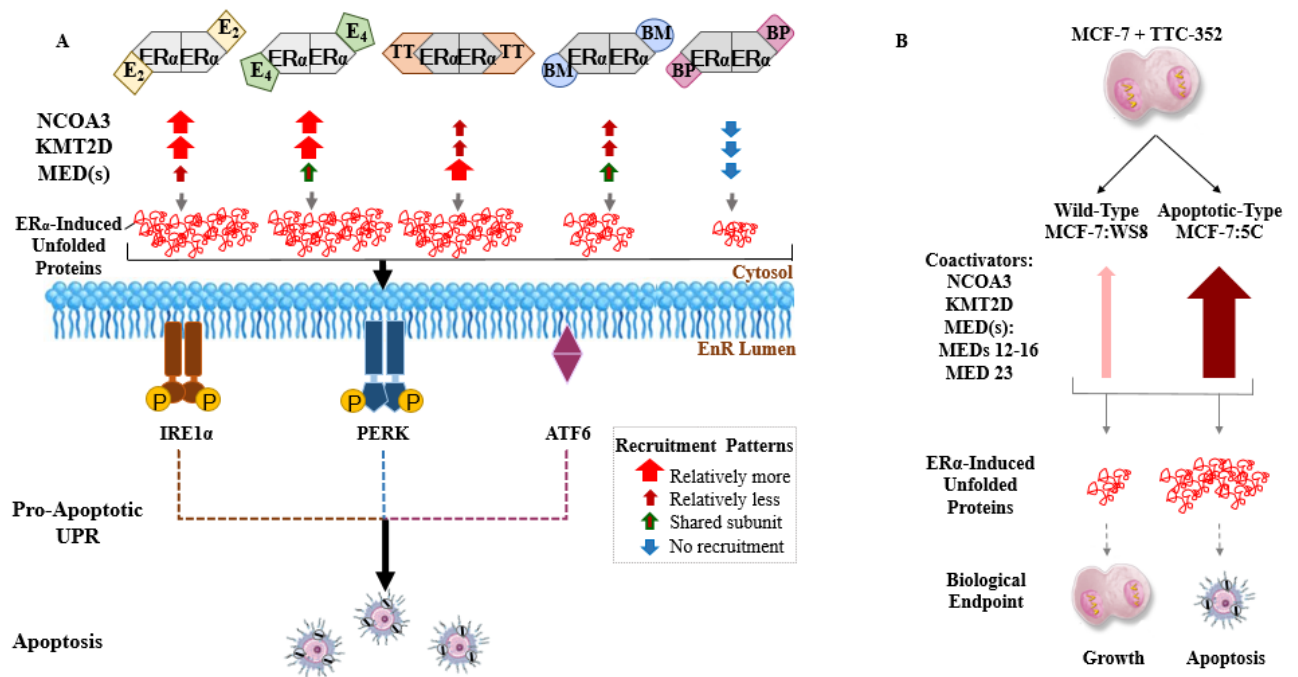
Figure 18 | **Schematic representation of the second paper's conclusions highlighting major ER coactivator-binding differences in MCF-7:5C between E$_2$, E$_4$, ShERPAs, and BPTPE, and with ShERPA TTC-352 between WT MCF-7:WS8 and LTED endocrine-resistant MCF-7:5C BC**. A) E$_2$, E$_4$, ShERPA BMI-135, ShERPA TTC-352, and BPTPE major ER coactivators' recruitment, and anti-tumour molecular mechanism in MCF-7:5C. E$_2$:ERα and E$_4$:ERα complexes mainly recruit NCOA3, KMT2D, and many of the same MEDs, and induce a high threshold of stress; through the synthesis of unfolded and/ or misfolded proteins, leading to rapid apoptosis. TTC-352 (referred to as TT in the illustration) recruited more MED subunits than E$_2$, but less NCOA3 and KMT2D than E$_2$ and E$_4$, with a similar threshold of stress and timing of apoptosis to E$_2$ and E$_4$. BMI-135 (referred to as BM in the illustration) recruited less NCOA3 and KMT2D than E$_2$ and E$_4$, and shared MED subunit recruitment with E$_4$, which generated a lower threshold of stress and delayed apoptosis (Abderrahman et al., 2020) compared to E$_2$, E$_4$, and TTC-352. BPTPE (referred to as BP in the illustration) did not have much of a coactivator-recruitment, which generates a very low threshold of stress and a much more delayed course of apoptosis (Abderrahman et al., 2020) compared to E$_2$, E$_4$, TTC-352, and BMI-135. This differential ligand:ERα:coactivator-reucitment-and-induced EnR stress, sets the therapeutics apart, in terms of the timing of activating the UPR, followed by inducing apoptosis. The box (in gray) highlights the observed recruitment patterns: thick arrow (in red) represents relatively more

recruitment, thin arrow (in burgundy) is relatively less recruitment, thin arrow (in burgundy with green border) is shared subunit recruitment, and thin arrow (in blue) is no recruitment. **B)** TTC-352's paradoxical effect in WT growth-inducing BC MCF-7:WS8 versus LTED apoptosis-inducing BC MCF-7:5C. NCOA3, KMT2D, and many MEDs (especially MED12-16 and MED23) are recruited to ER, in MCF-7:5C treated with TTC-352 (thick arrow in maroon), compared to E_2, but these same coactivators are reduced upon the treatment of MCF-7:WS8 with TTC-352 (thin arrow in rose). This differential ligand:ERα:coactivator-reucitment-and-induced EnR stress, phenotypically sets the two BC models apart.

Our MD simulations data complements the MS data whereby the dynamics of H12 orchestrate ER's coactivator-mediated transcriptional activity. In the agonist complex structure, H12 forms one side of a hydrophobic coactivator binding pocket, which allows the recruitment of an LXXLL motif present in many transcriptional cofactors (Shiau et al., 2002). This is, especially, true with SRC1-3 that possess three LXXLL motifs, two of which bridge across the ER dimer (at least for an extended polypeptide containing all three motifs), which accounts for the 100-fold higher affinity relative to the single LXXLL-containing peptide (Nolte et al., 1998). The overexpression of SRC-3 is observed in over 50% of BCs, and leads to constitutive ER-mediated transcriptional activity in the agonist conformation, conferring endocrine-resistance in preclinical models and in patients treated with TAM (Osborne et al., 2003b). E_2, E_4, TTC-352, and BMI-135 in complex with ERα, yield an agonist conformation of the ligand-ER complex (Figs. 5-6 *PAP2*), and, subsequently, recruit more coactivators (Fig. 4A *PAP2*), opposite to BPTPE. H12 acts as a molecular switch with the contribution of those H-Bond networks (Fig. 6 *PAP2*) and such coactivators (Fig. 4A *PAP2*).

Current study demonstrates that the structure-function model of the synthetic oestrogen mimic TTC-352 is a less potent full oestrogen agonist compared to E_2, allowing H12 to seal the LBD, which recruits many E_2-enriched coactivators, and induces rapid ERα-

mediated UPR and apoptosis. This contradicts the model of the benchmark partial agonist BPTPE, not allowing H12 to seal the LBD properly, which does not recruit many E_2-enriched coactivators, and induces delayed ERα-mediated UPR and apoptosis. These data suggest that BC patients would potentially benefit more from full agonists like TTC-352 rather than partial agonists, because of BPTPE's delayed UPR-apoptotic effect. A partial agonist with delayed apoptosis might create a higher probability of tumour clonal evolution and acquired-resistance (Rodriguez-Brenes and Wodarz, 2015).

Overall, the results of current studies support the continuation of future clinical trials with the new agents TTC-352 and E_4, and, most importantly, provide a structural, pharmacological, and mechanistic guide for the future design of effective oestrogenic agents to treat advanced BC –that is, BC ERα-targeted full oestrogen agonist molecules whose structure facilitates Asp351-to-H12 interaction; ensuring the closure of H12 over the LBD, recruiting E_2-enriched coactivators, and triggering a rapid UPR and apoptosis, to kill off the tumour cells.

V. Progress and Promise

Based on the findings of this body of work, the design of a future safer and effective new generation of oestrogenic agents, should be geared towards using a full oestrogen agonist (i.e., E_4 and TTC-352), not a partial oestrogen agonist (i.e., BPTPE) (Figure. 19). This is based upon the findings of my thesis that a partial agonist is associated with a delayed ERα-mediated UPR and apoptosis in LTED BC, compared to full agonists. This, in turn, increases the risk of clonal evolution, endocrine resistance, and metastasis formation.
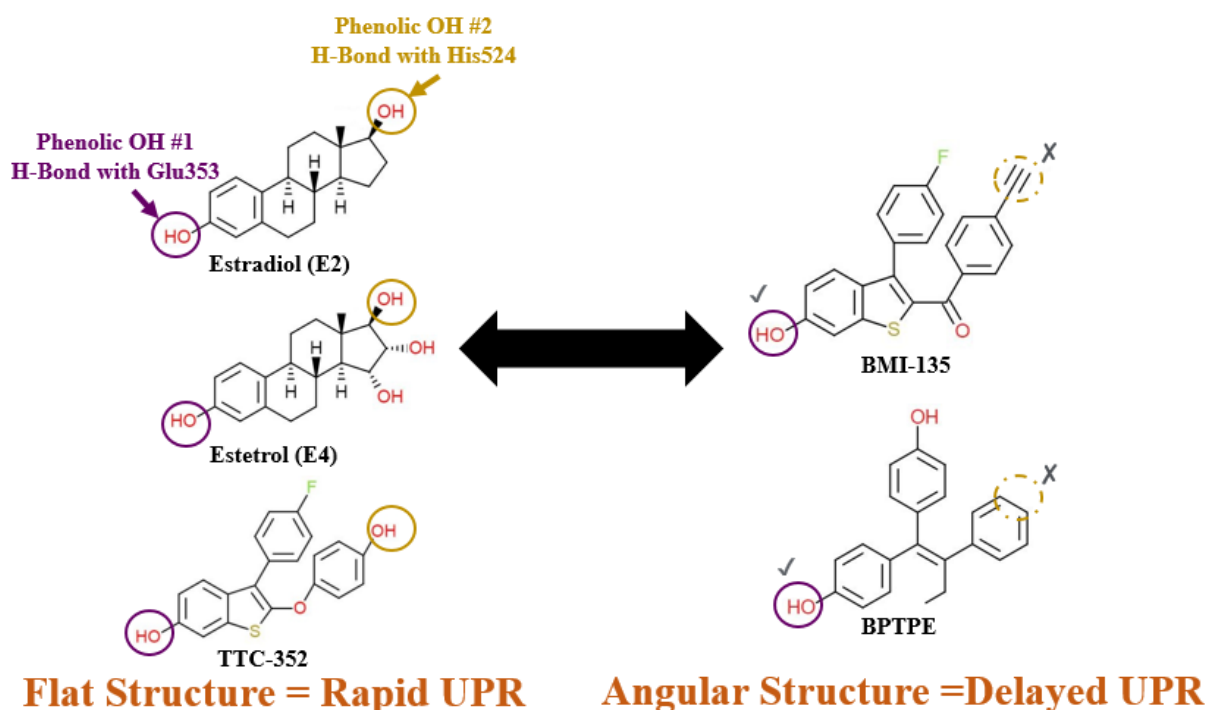
Figure 19 | **Schematic representation of the structural nuances between the test ligands, and how that influence the Asp351-to-H12 interaction, and subsequently coactivator recruitment, and UPR and apoptosis induction.**

Second, future oestrogenic agents should be planar (not angular) in their structural design, with the preservation of the active phenolic hydroxyl (on the A ring of the steroid structure of E_2 and E_4, or the benzothiophene scaffold of BMI-135 and TTC-352). Such active phenolic hydroxyl guarantees the H-bond with Glu353 that allows for the Asp351-to-H12 interaction. In addition, the preservation of another active phenolic hydroxyl (on the D ring of the steroid structures of E_2 and E_4, or the benzene ring of TTC-352 [compared to its absence in BMI-135 and BPTPE]) would guarantee yet another stabilizing H-bond to His524 that allows for the Asp351-to-H12 interaction. These two H-bonds that ensure the Asp-351-to-H12 interaction, result in the recruitment of E_2-enriched coactivators, and thus the rapid induction of the UPR and apoptosis aimed at tumour regression (compared to their delay with BMI-135 and BPTPE).

Third, future oestrogenic agents should be designed to target the nuclear ERα (not membrane ERα), as E_4 does. This allows for the avoidance of venous thromboembolism-related AEs.

Fourth, future oestrogenic agents (with a structural design similar to E_4 or TTC-352), can potentially be effective for the treatment of endocrine-resistant MBC patients with both WT, and mutant-type ERα. This is based on my papers' findings upon modeling my test ligands with WT and mutant ERα, which would yield an Asp351-to-H12 interaction that results in the induction of the UPR and apoptosis in LTED BC. In the case of the mutant-type ERα, oestrogenic agents (similar to E_4 or TTC-352) would introduce an additional H-bond with Glu353 and/ or His524 that facilities the Asp351-to-H12 interaction (other than the H-bond between 537S/G and Asp351). The presence of the ligand and the associated additional stabilizing H-bond network, hypothetically allows for the recruitment of numerous E_2-enriched coactivators. This, in turn, leads to the massive translation of unfolded proteins, and the subsequent induction of the UPR and apoptosis in LTED BC. This effect is unlike the presence of a single H-bond between 537S/G and Asp351, which although it facilitates the Asp351-to-H12 interaction, it doesn't necessarily allow for the recruitment of many E_2-enriched coactivators and, as a result, would induce a translational-directed growth, instead of a translational-directed apoptosis (via the UPR). Overall, such agents could potentially be effective in converting the growth-promoting mutant ER BC phenotype into an apoptosis-promoting mutant ER BC phenotype, other than already being apoptosis-promoting in WT ER BC phenotype.

Lastly, resistance to AIs is associated with ER point mutations, while resistance to tamoxifen is associated with SRC3 overexpression. Based on that fact and the fourth point above, one could speculate that SRC3-overexpressing, growth-promoting, endocrine-resistant BC phenotype could be converted to an SRC3-overexpressing, apoptosis-promoting BC

phenotype with the addition of an oestrogenic ligand (such as those of E_4 and TTC-352). In the case of SRC3-overexpressing BC phenotype (i.e., SRC3 overexpression contributes to its oestrogen-independent growth and endocrine-resistance) (Osborne et al., 2003a), a modest buildup of the unfolded proteins happens during tumour growth. However, the use of an oestrogenic ligand, and the associated additional stabilizing H-bond network, hypothetically allows for the recruitment of numerous E_2-enriched coactivators that leads to the massive translation of unfolded proteins, and the subsequent induction of the UPR and apoptosis in LTED BC. The SRC-3 overexpression with tamoxifen treatment, combined with LTED, and in the presence of a postmenopausal woman's oestrogen (i.e., E_1), might as well explain the survival advantage seen only with tamoxifen (not AIs) for up to 10 years after the initiation of tamoxifen treatment, even after the discontinuation of 5 years of tamoxifen treatment (Fisher et al., 2004). A closer examination of the Osborne and colleagues study (Osborne et al., 2003a) shows that the frozen tumour specimens (used for evaluating the role of SRC-3 overexpression in conferring endocrine resistance), were obtained from 316 BC patients with positive axillary lymph nodes at the time of initial surgery. This means that the SRC3-overexpressing BC phenotype was not LTED, to create the suitable environment for its conversion to an apoptosis-promoting BC phenotype, upon the addition of oestrogen. In such case, longer oestrogenic deprivation can be achieved with AIs upon the failure of tamoxifen. In fact, the standard of care tends to use a combination of 2 years of tamoxifen, followed by 2-3 years of AIs.

Overall, E_4 and TTC-352 were previously shown to be effective in women with endocrine-resistant BC, after the failure of several lines of endocrine treatments (including CDK4/6 inhibitors in the case of TTC-352).

VI. Reflections

The strength of this body of work lies in the fact that it uses 11 biologically-different patient-derived BC models. The results were also compared within a wide range of ERα ligands, including: the potent full agonist E_2, the less potent full agonists E_1 and E_3, the benchmark partial agonist triphenylethylene bisphenol (BPTPE), antagonists 4-hydroxytamoxifen, endoxifen, and raloxifene, and the SERD ICI. Additionally, the test ligands were evaluated in a wide range of cell-based assays, including: cell viability assays, real-time polymerase chain reaction, luciferase reporter assays, chromatin immunoprecipitation, human unfolded protein response (UPR) RT^2 PCR profiler arrays, immunoblotting, ERE DNA pull downs, mass spectrometry, X-ray crystallography, docking and molecular dynamic simulations, live cell imaging, and annexin V staining. Such techniques covered the trail of what happens starting from the moment the ligand binds to the ER, and ending with the biological endpoint of apoptosis.

What could have been done differently, if one possessed more financial resources, is the evaluation of the corepressors' recruitment with the test ligands in WT MCF-7:WS8 and apoptotic-type MCF-7:5C, and the evaluation of the dynamic UPR gene regulation over more than two time points. The natural progression of my *in vitro* studies would have been to proceed towards *in vivo* studies, however, this had already been completed by the original investigators of E_4 and SEMs.

Breast cancer is projected to double by 2030 than it was in 2011 (Rosenberg et al., 2015), the majority of which will be ER-positive with a high risk of recurrence Moreover, treated ER-positive BC metastases often harbor private 'driver' mutations, compared to untreated metastases (Hu et al., 2020). This highlights the need to leverage new rapidly-acting BC therapeutics such as oestrogens, which could become one treatment modality to

offer to women with endocrine-resistant MBC, after the failure of their treatments (i.e.,

tamoxifen, AIs, fulvestrant, mTOR inhibitors, and CDK4/6 inhibitors). The recent long-term

follow-up results of the WHI Trials (Jordan, 2020) reaffirm the clinical potential of novel and

safe oestrogenic therapy, in significantly reducing BC incidence and mortality, in LTED

patients. The WHI trials (i.e., 27,347 postmenopausal women, from 40 U.S. centers)

described oestrogen therapy as the following: "Prior use of CEE alone is the first

pharmacologic intervention demonstrated to be associated with a statistically significantly

reduction in deaths from breast cancer." Furthermore, the clinical trial of E_4 (Schmidt, 2020)

goes to show that while oestrogen therapy can be safe and effective in treating endocrine-

resistant MBC, it can also yield favorable effects on the patients' well-being (i.e.,

ameliorating the symptoms of oestrogen deficiency, such as: hot flashes, vaginal dryness,

sleep disturbances, mood changes, bone osteoporotic changes, and arthralgia). This positions

oestrogen treatment among the few if any of the treatment modalities, which not only treat

the disease, but also improve the patients' quality of life. Other than using oestrogenic agents

to treat advanced or resistant BC, the biology of oestrogen-induced apoptosis can be used as a

treasure hunting grounds to identify novel anti-cancer targets, which can be targeted to

potentially treat different cancers.

What can be achieved to personalize treatments to our BC patients, based on the

findings and areas of investigation of my thesis, can be summarized as the following:

I. The development of assays to measure circulating *ESR1* mutations, in patients treated

   with AIs. These levels can serve an independent risk factor for poor outcome after AI

   failure, and to indicate that it could then be appropriate to use an oestrogenic agent to

   convert the mutant ER growth-promoting BC phenotype to that of apoptosis-

   promoting.

II. The development of assays to measure SRC-3 overexpression in BC tumours, in patients treated with tamoxifen. These levels can serve as a diagnostic tool, to indicate when it's appropriate to continue with the LTED using AIs instead, and to indicate that it could then be appropriate to use an oestrogenic agent to convert the SRC-3-overexpresisng growth-promoting BC phenotype to that of apoptosis-promoting (as long as LTED had taken place).

III. The development of assays to measure the ratio of circulating oestrogens that are indicative of the woman's dynamic metabolism, in terms of the balance between oestrogen synthesis and deactivation. This can help identify which postmenopausal women have higher levels of oestrogens that could be causing tumour regression in association with any observed BC regression, or significant decreases in BC incidence and mortality.

IV. The development of a mathematical model for the UPR activation and dynamics over time, using patient-derived tissues treated with E_2. This can help identify the rate and anti-cancer kinetics of this biology in real time.

VII. References:

1996. Randomized trial of two versus five years of adjuvant tamoxifen for postmenopausal early stage breast cancer. Swedish Breast Cancer Cooperative Group. *J Natl Cancer Inst,* 88**,** 1543-9.

2019a. *Prostate Cancer: Facts and Statistics* [Online]. Zero Cancer Available: https://zerocancer.org/learn/about-prostate-cancer/facts-statistics/ [Accessed Jan 20 2020].

2019b. *U.S. Breast Cancer Statistics* [Online]. BREASTCANCER.ORG. Available: https://www.breastcancer.org/symptoms/understand_bc/statistics [Accessed Jan 20 2020].

ABDERRAHMAN, B. 2017a. Health Literacy, Medication Adherence and Thriving Health Care Systems: Connecting the Dots *Clinical Pharmacist,* 9**,** 322-324.

ABDERRAHMAN, B. 2017b. Medication Non-Adherence in Breast Cancer Prevention and Treatment Settings: A Substantial Clinical Problem. *Pharm J.*

ABDERRAHMAN, B. & JORDAN, V. C. 2015. Cancer chemoprevention at the crossroads? *Breast Cancer Manag,* 4**,** 285-288.

ABDERRAHMAN, B. & JORDAN, V. C. 2016a. Breast cancer prevention trumps cure. *Clinical Pharmacist* 9.

ABDERRAHMAN, B. & JORDAN, V. C. 2016b. Estrogen Deprivation Therapy in Ovarian Cancer: An Opportunity. *J Clin Oncol,* 34**,** 2675-6.

ABDERRAHMAN, B. & JORDAN, V. C. 2016c. long-term adjuvant tamoxifen therapy and decreases in contralateral breast cancer. *JAMA Oncol,* 3**,** 163-164.

ABDERRAHMAN, B. & JORDAN, V. C. 2016d. The modulation of estrogen-induced apoptosis as an interpretation of the women's health initiative trials. *Expert Rev Endocrinol Metab,* 11**,** 81-86.

ABDERRAHMAN, B. & JORDAN, V. C. 2016e. Steroid Receptors in Breast Cancer. *In:* BLAND, I. B., KLIMBERG, V. S., COPELAND III, E. M. & GRADISHAR, W. J. (eds.) *The Breast: Comprehensive Management of Benign and Malignant Diseases.* 5th ed.: Elsevier.

ABDERRAHMAN, B. & JORDAN, V. C. 2018. Telling details of breast-cancer recurrence. *Nature,* 553**,** 155.

ABDERRAHMAN, B., MAXIMOV, P. Y., CURPAN, R. F., HANSPAL, J. S., FAN, P., XIONG, R., TONETTI, D. A., THATCHER, G. R. J. & JORDAN, V. C. 2020. Pharmacology and Molecular Mechanisms of Clinically-Relevant Estrogen Estetrol and Estrogen Mimic BMI-135 for the Treatment of Endocrine-Resistant Breast Cancer *Molecular Pharmacology*

ABOT, A., FONTAINE, C., BUSCATO, M., SOLINHAC, R., FLOURIOT, G., FABRE, A., DROUGARD, A., RAJAN, S., LAINE, M., MILON, A., MULLER, I., HENRION, D., ADLANMERINI, M., VALERA, M. C., GOMPEL, A., GERARD, C., PEQUEUX, C., MESTDAGT, M., RAYMOND-LETRON, I., KNAUF, C., FERRIERE, F., VALET, P., GOURDY, P., KATZENELLENBOGEN, B. S., KATZENELLENBOGEN, J. A., LENFANT, F., GREENE, G. L., FOIDART, J. M. & ARNAL, J. F. 2014. The uterine and vascular actions of estetrol delineate a distinctive profile of estrogen receptor alpha modulation, uncoupling nuclear and membrane activation. *Embo Molecular Medicine,* 6**,** 1328-1346.

AMERICAN CANCER SOCIETY. *Key Statistics for Prostate Cancer* [Online]. Available: https://www.cancer.org/cancer/prostate-cancer/about/key-statistics.html [Accessed July 8 2019].

ANDERSON, G. L., LIMACHER, M., ASSAF, A. R., BASSFORD, T., BERESFORD, S. A., BLACK, H., BONDS, D., BRUNNER, R., BRZYSKI, R., CAAN, B., CHLEBOWSKI, R., CURB, D., GASS, M., HAYS, J., HEISS, G., HENDRIX, S., HOWARD, B. V., HSIA, J., HUBBELL, A., JACKSON, R., JOHNSON, K. C., JUDD, H., KOTCHEN, J. M., KULLER, L., LACROIX, A. Z., LANE, D., LANGER, R. D., LASSER, N., LEWIS, C. E., MANSON, J., MARGOLIS, K., OCKENE, J., O'SULLIVAN, M. J., PHILLIPS, L., PRENTICE, R. L., RITENBAUGH, C., ROBBINS, J., ROSSOUW, J. E., SARTO, G., STEFANICK, M. L., VAN HORN, L., WACTAWSKI-WENDE, J., WALLACE, R., WASSERTHEIL-SMOLLER, S. & WOMEN'S HEALTH INITIATIVE STEERING, C. 2004. Effects of conjugated equine estrogen in postmenopausal women with hysterectomy: the Women's Health Initiative randomized controlled trial. *JAMA,* 291**,** 1701-12.

APTER, D., ZIMMERMAN, Y., BEEKMAN, L., MAWET, M., MAILLARD, C., FOIDART, J. M. & BENNINK, H. J. T. C. 2017. Estetrol combined with drospirenone: an oral contraceptive with high acceptability, user satisfaction, well-being and favourable body weight control. *European Journal of Contraception and Reproductive Health Care,* 22**,** 260-267.

ARIAZI, E. A., CUNLIFFE, H. E., LEWIS-WAMBI, J. S., SLIFKER, M. J., WILLIS, A. L., RAMOS, P., TAPIA, C., KIM, H. R., YERRUM, S., SHARMA, C. G., NICOLAS, E., BALAGURUNATHAN, Y., ROSS, E. A. & JORDAN, V. C. 2011. Estrogen induces apoptosis in estrogen deprivation-resistant breast cancer through stress responses as identified by global gene expression across time. *Proc Natl Acad Sci U S A,* 108**,** 18879-86.

ATTARD, G., RICHARDS, J. & DE BONO, J. S. 2011. New strategies in metastatic prostate cancer: targeting the androgen receptor signaling pathway. *Clin Cancer Res,* 17**,** 1649-57.

BALABURSKI, G. M., DARDES, R. C., JOHNSON, M., HADDAD, B., ZHU, F., ROSS, E. A., SENGUPTA, S., KLEIN-SZANTO, A., LIU, H., LEE, E. S., KIM, H. & JORDAN, V. C. 2010. Raloxifene-stimulated experimental breast cancer with the paradoxical actions of estrogen to promote or prevent tumor growth: A unifying concept in anti-hormone resistance. *International Journal of Oncology,* 37**,** 387-398.

BAUM, M., BUDZAR, A. U., CUZICK, J., FORBES, J., HOUGHTON, J. H., KLIJN, J. G., SAHMOUD, T. & GROUP, A. T. 2002. Anastrozole alone or in combination with tamoxifen versus tamoxifen alone for adjuvant treatment of postmenopausal women with early breast cancer: first results of the ATAC randomised trial. *Lancet,* 359**,** 2131-9.

BENNINK, H. J. T. C., VERHOEVEN, C., DUTMAN, A. E. & THIJSSEN, J. 2017. The use of high-dose estrogens for the treatment of breast cancer. *Maturitas,* 95**,** 11-23.

BERIAULT, D. R. & WERSTUCK, G. H. 2013. Detection and quantification of endoplasmic reticulum stress in living cells using the fluorescent compound, Thioflavin T. *Biochimica Et Biophysica Acta-Molecular Cell Research,* 1833**,** 2293-2301.

BHATTACHARYA, P., ABDERRAHMAN, B. & JORDAN, V. C. 2017. Tamoxifen Decreases Mortality, but How? *J Clin Oncol,* 35**,** 379.

BLACKARD, C. E., DOE, R. P., MELLINGER, G. T. & BYAR, D. P. 1970. Incidence of cardiovascular disease and death in patients receiving diethylstilbestrol for carcinoma of the prostate. *Cancer,* 26**,** 249-56.

BOCCARDO, F., RUBAGOTTI, A., PUNTONI, M., GUGLIELMINI, P., AMOROSO, D., FINI, A., PALADINI, G., MESITI, M., ROMEO, D., RINALDINI, M., SCALI, S., PORPIGLIA, M., BENEDETTO, C., RESTUCCIA, N., BUZZI, F., FRANCHI, R., MASSIDDA, B., DISTANTE, V., AMADORI, D. & SISMONDI, P. 2005. Switching to anastrozole versus continued tamoxifen treatment of early breast cancer: Preliminary results of the Italian Tamoxifen Anastrozole trial. *Journal of Clinical Oncology,* 23**,** 5138-5147.

BREAST INTERNATIONAL GROUP 1-98 COLLABORATIVE, G., THURLIMANN, B., KESHAVIAH, A., COATES, A. S., MOURIDSEN, H., MAURIAC, L., FORBES, J. F., PARIDAENS, R., CASTIGLIONE-GERTSCH, M., GELBER, R. D., RABAGLIO, M., SMITH, I., WARDLEY, A., PRICE, K. N. & GOLDHIRSCH, A. 2005. A comparison of letrozole and tamoxifen in postmenopausal women with early breast cancer. *N Engl J Med,* 353**,** 2747-57.

BRUNNER, N., BOULAY, V., FOJO, A., FRETER, C. E., LIPPMAN, M. E. & CLARKE, R. 1993a. Acquisition of hormone-independent growth in MCF-7 cells is accompanied by increased expression of estrogen-regulated genes but without detectable DNA amplifications. *Cancer Res,* 53**,** 283-90.

BRUNNER, N., BOYSEN, B., JIRUS, S., SKAAR, T. C., HOLSTHANSEN, C., LIPPMAN, J., FRANDSEN, T., SPANGTHOMSEN, M., FUQUA, S. A. W. & CLARKE, R. 1997. MCF7/LCC9: An antiestrogen-resistant MCF-7 variant in which acquired resistance to the steroidal antiestrogen ICI 182,780 confers an early cross-resistance to the nonsteroidal antiestrogen tamoxifen. *Cancer Research,* 57**,** 3486-3493.

BRUNNER, N., FRANDSEN, T. L., HOLSTHANSEN, C., BEI, M., THOMPSON, E. W., WAKELING, A. E., LIPPMAN, M. E. & CLARKE, R. 1993b. Mcf7/Lcc2 - a 4-Hydroxytamoxifen Resistant Human Breast-Cancer Variant That Retains Sensitivity to the Steroidal Antiestrogen Ici-182,780. *Cancer Research,* 53**,** 3229-3232.

BRZOZOWSKI, A. M., PIKE, A. C., DAUTER, Z., HUBBARD, R. E., BONN, T., ENGSTROM, O., OHMAN, L., GREENE, G. L., GUSTAFSSON, J. A. & CARLQUIST, M. 1997. Molecular basis of agonism and antagonism in the oestrogen receptor. *Nature,* 389**,** 753-8.

CANCER RESEARCH UK. *Prostate cancer statistics* [Online]. Available: https://www.cancerresearchuk.org/health-professional/cancer-statistics/statistics-by-cancer-type/prostate-cancer#heading-One [Accessed July 8 2019].

CANCER RESEARCH UK. 2014. *Breast cancer statistics* [Online]. Cancer Research UK Available: https://goo.gl/KFWN7e [Accessed August 14 2017].

CATHERINO, W. H., WOLF, D. M. & JORDAN, V. C. 1995. A Naturally-Occurring Estrogen-Receptor Mutation Results in Increased Estrogenicity of a Tamoxifen Analog. *Molecular Endocrinology,* 9**,** 1053-1063.

CHALASANI, P., STOPECK, A., CLARKE, K. & LIVINGSTON, R. 2014. A pilot study of estradiol followed by exemestane for reversing endocrine resistance in postmenopausal women with hormone receptor-positive metastatic breast cancer. *Oncologist,* 19**,** 1127-8.

CHEN, Y., CLEGG, N. J. & SCHER, H. I. 2009. Anti-androgens and androgen-depleting therapies in prostate cancer: new agents for an established target. *Lancet Oncol,* 10**,** 981-91.

CHLEBOWSKI, R. T., ANDERS, G. L., ARAGAKI, A. K., MANSON, J. E., STEFANICK, M., PAN, K., BARRINGTON, W., KULLER, L. H., SIMON, M. S. L., D. , JOHNSON, K. C., ROHAN, T. E., GASS, M. L. S., CAULEY, J. A., PASKETT, E. D., SATTARI, M. & PRENTICE, R. L. 2019. Abstract nr GS5-00: Long-term influence of estrogen plus progestin and estrogen alone use on breast cancer incidence: The Women's Health Initiative randomized trials

SABCS.

CHUU, C. P., KOKONTIS, J. M., HIIPAKKA, R. A., FUKUCHI, J., LIN, H. P., LIN, C. Y., HUO, C. & SU, L. C. 2011. Androgens as therapy for androgen receptor-positive castration-resistant prostate cancer. *J Biomed Sci,* 18**,** 63.

CLARK, G. M., OSBORNE, C. K. & MCGUIRE, W. L. 1984. Correlations between Estrogen-Receptor, Progesterone-Receptor, and Patient Characteristics in Human-Breast Cancer. *Journal of Clinical Oncology,* 2**,** 1102-1109.

CLARKE, R., BRUNNER, N., KATZENELLENBOGEN, B. S., THOMPSON, E. W., NORMAN, M. J., KOPPI, C., PAIK, S., LIPPMAN, M. E. & DICKSON, R. B. 1989. Progression of human breast cancer cells from hormone-dependent to hormone-independent growth both in vitro and in vivo. *Proc Natl Acad Sci U S A,* 86**,** 3649-53.

CLATOT, F., PERDRIX, A., AUGUSTO, L., BEAUSSIRE, L., DELACOUR, J., CALBRIX, C., SEFRIOUI, D., VIAILLY, P. J., BUBENHEIM, M., MOLDOVAN, C., ALEXANDRU, C., TENNEVET, I., RIGAL, O., GUILLEMET, C., LEHEURTEUR, M., GOUERANT, S., PETRAU, C., THERY, J. C., PICQUENOT, J. M., VEYRET, C., FREBOURG, T., JARDIN, F., SARAFAN-VASSEUR, N. & DI FIORE, F. 2016. Kinetics, prognostic and predictive values of ESR1 circulating mutations in metastatic breast cancer patients progressing on aromatase inhibitor. *Oncotarget,* 7**,** 74448-74459.

COATES, A. S., KESHAVIAH, A., THURLIMANN, B., MOURIDSEN, H., MAURIAC, L., FORBES, J. F., PARIDAENS, R., CASTIGLIONE-GERTSCH, M., GELBER, R. D., COLLEONI, M., LANG, I., DEL MASTRO, L., SMITH, I., CHIRGWIN, J., NOGARET, J. M., PIENKOWSKI, T., WARDLEY, A., JAKOBSEN, E. H., PRICE, K. N. & GOLDHIRSCH, A. 2007. Five years of letrozole compared with tamoxifen as initial adjuvant therapy for postmenopausal women with endocrine-responsive early breast cancer: Update of study BIG 1-98. *Journal of Clinical Oncology,* 25**,** 486-492.

COELINGH BENNINK, H. J., VERHOEVEN, C., ZIMMERMAN, Y., VISSER, M., FOIDART, J. M. & GEMZELL-DANIELSSON, K. 2016. Clinical effects of the fetal estrogen estetrol in a multiple-rising-dose study in postmenopausal women. *Maturitas,* 91**,** 93-100.

COLE, M. P., JONES, C. T. & TODD, I. D. 1971. A new anti-oestrogenic agent in late breast cancer. An early clinical appraisal of ICI46474. *Br J Cancer,* 25**,** 270-5.

COOMBES, R. C. 2004. A randomized trial of exemestane after two to three years of tamoxifen therapy in postmenopausal women with primary breast cancer (vol 350, pg 1081, 2004). *New England Journal of Medicine,* 351**,** 2461-2461.

COX, R. L. & CRAWFORD, E. D. 1995. Estrogens in the Treatment of Prostate-Cancer. *Journal of Urology,* 154**,** 1991-1998.

CUI, J., SHEN, Y. & LI, R. 2013. Estrogen synthesis and signaling pathways during aging: from periphery to brain. *Trends Mol Med,* 19**,** 197-209.

CUMMINGS, S. R., ECKERT, S., KRUEGER, K. A., GRADY, D., POWLES, T. J., CAULEY, J. A., NORTON, L., NICKELSEN, T., BJARNASON, N. H., MORROW, M., LIPPMAN, M. E., BLACK, D., GLUSMAN, J. E., COSTA, A. & JORDAN, V. C. 1999. The effect of raloxifene on risk of breast cancer in postmenopausal women: results from the MORE randomized trial. Multiple Outcomes of Raloxifene Evaluation. *JAMA,* 281**,** 2189-97.

CYBULSKY, A. V. 2017. Endoplasmic reticulum stress, the unfolded protein response and autophagy in kidney diseases. *Nat Rev Nephrol,* 13**,** 681-696.

DAVIES, C., PAN, H., GODWIN, J., GRAY, R., ARRIAGADA, R., RAINA, V., ABRAHAM, M., MEDEIROS ALENCAR, V. H., BADRAN, A., BONFILL, X., BRADBURY, J., CLARKE, M., COLLINS, R., DAVIS, S. R., DELMESTRI, A., FORBES, J. F., HADDAD, P., HOU, M. F., INBAR, M., KHALED, H., KIELANOWSKA, J., KWAN, W. H., MATHEW, B. S., MITTRA, I., MULLER, B., NICOLUCCI, A., PERALTA, O., PERNAS, F., PETRUZELKA, L., PIENKOWSKI, T., RADHIKA, R., RAJAN, B., RUBACH, M. T., TORT, S., URRUTIA, G., VALENTINI, M., WANG, Y., PETO, R. & ADJUVANT TAMOXIFEN: LONGER AGAINST SHORTER COLLABORATIVE, G. 2013. Long-term effects of continuing adjuvant tamoxifen to 10 years versus stopping at 5 years after diagnosis of oestrogen receptor-positive breast cancer: ATLAS, a randomised trial. *Lancet,* 381**,** 805-16.

DE BONO, J. S., LOGOTHETIS, C. J., MOLINA, A., FIZAZI, K., NORTH, S., CHU, L., CHI, K. N., JONES, R. J., GOODMAN, O. B., JR., SAAD, F., STAFFURTH, J. N., MAINWARING, P., HARLAND, S., FLAIG, T. W., HUTSON, T. E., CHENG, T., PATTERSON, H., HAINSWORTH, J. D., RYAN, C. J., STERNBERG, C. N., ELLARD, S. L., FLECHON, A., SALEH, M., SCHOLZ, M., EFSTATHIOU, E., ZIVI, A., BIANCHINI, D., LORIOT, Y., CHIEFFO, N., KHEOH, T., HAQQ, C. M., SCHER, H. I. & INVESTIGATORS, C.-A.-. 2011. Abiraterone and increased survival in metastatic prostate cancer. *N Engl J Med,* 364**,** 1995-2005.

DO, Y., RYU, S., NAGARKATTI, M. & NAGARKATTI, P. S. 2002. Role of death receptor pathway in estradiol-induced T-cell apoptosis in vivo. *Toxicol Sci,* 70**,** 63-72.

DONESTA BIOSCIENCE. 2016. *E4Relief (Response to Estetrol in Life Improvement for MEnopausal-associated Hot Flushes) (ClinicalTrials.gov Identifier: NCT02834312)* [Online]. ClinicalTrials.gov. Available: https://clinicaltrials.gov/ct2/show/NCT02834312 [Accessed].

DUDEK, A. Z., LIU, L. C., FISCHER, J. H., WILEY, E. L., SACHDEV, J. C., BLEEKER, J., HURLEY, R. W., TONETTI, D. A., THATCHER, G. R. J., VENUTI, R. P. & O'REGAN, R. 2020. Phase 1 study of TTC-352 in patients with metastatic breast cancer progressing on endocrine and CDK4/6 inhibitor therapy. *Breast Cancer Res Treat*.

DUTMAN, E., ZIMMERMAN, Y. & COELINGH-BENNINK, H. 2017. The effects of the human fetal estrogen estetrol (E4) in healthy men to estimate its potential use for the treatment of prostate cancer. *Eur Urol Suppl,* 16**,** e362-e364.

EARLY BREAST CANCER TRIALISTS' COLLABORATIVE, G., DAVIES, C., GODWIN, J., GRAY, R., CLARKE, M., CUTTER, D., DARBY, S., MCGALE, P., PAN, H. C., TAYLOR, C., WANG, Y. C., DOWSETT, M., INGLE, J. & PETO, R. 2011. Relevance of breast cancer hormone receptors and other factors to the efficacy of adjuvant tamoxifen: patient-level meta-analysis of randomised trials. *Lancet,* 378**,** 771-84.

EARLY BREAST CANCER TRIALISTS' COLLABORATIVE GROUP 1998. Tamoxifen for early breast cancer: an overview of the randomised trials. Early Breast Cancer Trialists' Collaborative Group. *Lancet,* 351**,** 1451-67.

EARLY BREAST CANCER TRIALISTS' COLLABORATIVE GROUP, T. 1998. Tamoxifen for early breast cancer: an overview of the randomised trials. Early Breast Cancer Trialists' Collaborative Group. *Lancet,* 351**,** 1451-67.

EDWARDS, J. & BARTLETT, J. M. 2005. The androgen receptor and signal-transduction pathways in hormone-refractory prostate cancer. Part 1: Modifications to the androgen receptor. *BJU Int,* 95**,** 1320-6.

EELES, R. A., MORDEN, J. P., GORE, M., MANSI, J., GLEES, J., WENCZL, M., WILLIAMS, C., KITCHENER, H., OSBORNE, R., GUTHRIE, D., HARPER, P. & BLISS, J. M. 2015. Adjuvant Hormone Therapy May Improve Survival in Epithelial Ovarian Cancer: Results of the AHT Randomized Trial. *Journal of Clinical Oncology,* 33**,** 4138-+.

ELLIS, M. J., GAO, F., DEHDASHTI, F., JEFFE, D. B., MARCOM, P. K., CAREY, L. A., DICKLER, M. N., SILVERMAN, P., FLEMING, G. F., KOMMAREDDY, A., JAMALABADI-MAJIDI, S., CROWDER, R. & SIEGEL, B. A. 2009. Lower-dose vs high-dose oral estradiol therapy of hormone receptor-

positive, aromatase inhibitor-resistant advanced breast cancer: a phase 2 randomized study. *JAMA,* 302**,** 774-80.

ELLIS, M. J., LLOMBART-CUSSAC, A., FELTL, D., DEWAR, J. A., JASIOWKA, M., HEWSON, N., RUKAZENKOV, Y. & ROBERTSON, J. F. 2015. Fulvestrant 500 mg Versus Anastrozole 1 mg for the First-Line Treatment of Advanced Breast Cancer: Overall Survival Analysis From the Phase II FIRST Study. *J Clin Oncol,* 33**,** 3781-7.

ENGEL, L. W., YOUNG, N. A., TRALKA, T. S., LIPPMAN, M. E., O'BRIEN, S. J. & JOYCE, M. J. 1978. Establishment and characterization of three new continuous cell lines derived from human breast carcinomas. *Cancer Res,* 38**,** 3352-64.

FAN, P., AGBOKE, F. A., CUNLIFFE, H. E., RAMOS, P. & JORDAN, V. C. 2014. A molecular model for the mechanism of acquired tamoxifen resistance in breast cancer. *Eur J Cancer,* 50**,** 2866-76.

FANNING, S. W., MAYNE, C. G., DHARMARAJAN, V., CARLSON, K. E., MARTIN, T. A., NOVICK, S. J., TOY, W., GREEN, B., PANCHAMUKHI, S., KATZENELLENBOGEN, B. S., TAJKHORSHID, E., GRIFFIN, P. R., SHEN, Y., CHANDARLAPATY, S., KATZENELLENBOGEN, J. A. & GREENE, G. L. 2016. Estrogen receptor alpha somatic mutations Y537S and D538G confer breast cancer endocrine resistance by stabilizing the activating function-2 binding conformation. *Elife,* 5.

FENG, Q. & O'MALLEY, B. W. 2014. Nuclear receptor modulation--role of coregulators in selective estrogen receptor modulator (SERM) actions. *Steroids,* 90**,** 39-43.

FERLAY, J., SOERJOMATARAM, I., DIKSHIT, R., ESER, S., MATHERS, C., REBELO, M., PARKIN, D. M., FORMAN, D. & BRAY, F. 2015. Cancer incidence and mortality worldwide: sources, methods and major patterns in GLOBOCAN 2012. *Int J Cancer,* 136**,** E359-86.

FINN, R. S., ALESHIN, A. & SLAMON, D. J. 2016. Targeting the cyclin-dependent kinases (CDK) 4/6 in estrogen receptor-positive breast cancers. *Breast Cancer Res,* 18**,** 17.

FISHER, B., DIGNAM, J., BRYANT, J., DECILLIS, A., WICKERHAM, D. L., WOLMARK, N., COSTANTINO, J., REDMOND, C., FISHER, E. R., BOWMAN, D. M., DESCHENES, L., DIMITROV, N. V., MARGOLESE, R. G., ROBIDOUX, A., SHIBATA, H., TERZ, J., PATERSON, A. H., FELDMAN, M. I., FARRAR, W., EVANS, J. & LICKLEY, H. L. 1996. Five versus more than five years of tamoxifen therapy for breast cancer patients with negative lymph nodes and estrogen receptor-positive tumors. *J Natl Cancer Inst,* 88**,** 1529-42.

FISHER, B., JEONG, J. H., BRYANT, J., ANDERSON, S., DIGNAM, J., FISHER, E. R., WOLMARK, N., NATIONAL SURGICAL ADJUVANT, B. & BOWEL PROJECT RANDOMISED CLINICAL, T. 2004. Treatment of lymph-node-negative, oestrogen-receptor-positive breast cancer: long-term findings from National Surgical Adjuvant Breast and Bowel Project randomised clinical trials. *Lancet,* 364**,** 858-68.

FULDA, S., GORMAN, A. M., HORI, O. & SAMALI, A. 2010. Cellular stress responses: cell survival and cell death. *Int J Cell Biol,* 2010**,** 214074.

GARNICK, M. B. 1984. Leuprolide Versus Diethylstilbestrol for Metastatic Prostate-Cancer. *New England Journal of Medicine,* 311**,** 1281-1286.

GERARD, C., MESTDAGT, M., TSKITISHVILI, E., COMMUNAL, L., GOMPEL, A., SILVA, E., ARNAL, J. F., LENFANT, F., NOEL, A., FOIDART, J. M. & PEQUEUX, C. 2015. Combined estrogenic and anti-estrogenic properties of estetrol on breast cancer may provide a safe therapeutic window for the treatment of menopausal symptoms. *Oncotarget,* 6**,** 17621-17636.

GOSS, P. E., INGLE, J. N., MARTINO, S., ROBERT, N. J., MUSS, H. B., PICCART, M. J., CASTIGLIONE, M., TU, D., SHEPHERD, L. E., PRITCHARD, K. I., LIVINGSTON, R. B., DAVIDSON, N. E., NORTON, L., PEREZ, E. A., ABRAMS, J. S., CAMERON, D. A., PALMER, M. J. & PATER, J. L. 2005. Randomized trial of letrozole following tamoxifen as extended adjuvant therapy in receptor-positive breast cancer: updated findings from NCIC CTG MA.17. *J Natl Cancer Inst,* 97**,** 1262-71.

GOSS, P. E., INGLE, J. N., MARTINO, S., ROBERT, N. J., MUSS, H. B., PICCART, M. J., CASTIGLIONE, M., TU, D., SHEPHERD, L. E., PRITCHARD, K. I., LIVINGSTON, R. B., DAVIDSON, N. E., NORTON, L., PEREZ, E. A., ABRAMS, J. S., THERASSE, P., PALMER, M. J. & PATER, J. L. 2003a. A randomized

trial of letrozole in postmenopausal women after five years of tamoxifen therapy for early-stage breast cancer. *N Engl J Med,* 349**,** 1793-802.

GOSS, P. E., INGLE, J. N., MARTINO, S., ROBERT, N. J., MUSS, H. B., PICCART, M. J., CASTIGLIONE, M., TU, D., SHEPHERD, L. E., PRITCHARD, K. I., LIVINGSTON, R. B., DAVIDSON, N. E., NORTON, L., PEREZ, E. A., ABRAMS, J. S., THERASSE, P., PALMER, M. J. & PATER, J. L. 2003b. A randomized trial of letrozole in postmenopausal women after five years of tamoxifen therapy for early-stage breast cancer. *New England Journal of Medicine,* 349**,** 1793-1802.

GOTTARDIS, M. M., JIANG, S. Y., JENG, M. H. & JORDAN, V. C. 1989a. Inhibition of tamoxifen-stimulated growth of an MCF-7 tumor variant in athymic mice by novel steroidal antiestrogens. *Cancer Res,* 49**,** 4090-3.

GOTTARDIS, M. M. & JORDAN, V. C. 1988. Development of tamoxifen-stimulated growth of MCF-7 tumors in athymic mice after long-term antiestrogen administration. *Cancer Res,* 48**,** 5183-7.

GOTTARDIS, M. M., ROBINSON, S. P., SATYASWAROOP, P. G. & JORDAN, V. C. 1988. Contrasting actions of tamoxifen on endometrial and breast tumor growth in the athymic mouse. *Cancer Res,* 48**,** 812-5.

GOTTARDIS, M. M., WAGNER, R. J., BORDEN, E. C. & JORDAN, V. C. 1989b. Differential ability of antiestrogens to stimulate breast cancer cell (MCF-7) growth in vivo and in vitro. *Cancer Res,* 49**,** 4765-9.

GRAY, R. G., REA, D., HANDLEY, K., BOWDEN, S. J., PERRY, P., EARL, H. M., POOLE, C. J., BATES, T., CHETIYAWARDANA, S., DEWAR, J. A., FERNANDO, I. N., GRIEVE, R., NICOLL, J., RAYTER, Z., ROBINSON, A., SALMAN, A., YARNOLD, J., BATHERS, S., MARSHALL, A., LEE, M. & GRP, A. C. 2013. aTTom: Long-term effects of continuing adjuvant tamoxifen to 10 years versus stopping at 5 years in 6,953 women with early breast cancer. *Journal of Clinical Oncology,* 31.

GROOTJANS, J., KASER, A., KAUFMAN, R. J. & BLUMBERG, R. S. 2016. The unfolded protein response in immunity and inflammation. *Nat Rev Immunol,* 16**,** 469-84.

HADDOW, A. 1970. David A. Karnofsky memorial lecture. Thoughts on chemical therapy. *Cancer,* 26**,** 737-54.

HADDOW, A., WATKINSON, J. M., PATERSON, E. & KOLLER, P. C. 1944. Influence of synthetic oestrogens upon advanced malignant disease. *British Medical Journal,* 1944**,** 393-398.

HADJI, P., AAPRO, M. S., BODY, J. J., GNANT, M., BRANDI, M. L., REGINSTER, J. Y., ZILLIKENS, M. C., GLUER, C. C., DE VILLIERS, T., BABER, R., ROODMAN, G. D., COOPER, C., LANGDAHL, B., PALACIOS, S., KANIS, J., AL-DAGHRI, N., NOGUES, X., ERIKSEN, E. F., KURTH, A., RIZZOLI, R. & COLEMAN, R. E. 2017. Management of Aromatase Inhibitor-Associated Bone Loss (AIBL) in postmenopausal women with hormone sensitive breast cancer: Joint position statement of the IOF, CABS, ECTS, IEG, ESCEO IMS, and SIOG. *J Bone Oncol,* 7**,** 1-12.

HARRIS, R. M., WOOD, D. M., BOTTOMLEY, L., BLAGG, S., OWEN, K., HUGHES, P. J., WARING, R. H. & KIRK, C. J. 2004. Phytoestrogens are potent inhibitors of estrogen sulfation: implications for breast cancer risk and treatment. *J Clin Endocrinol Metab,* 89**,** 1779-87.

HEERY, D. M., KALKHOVEN, E., HOARE, S. & PARKER, M. G. 1997. A signature motif in transcriptional co-activators mediates binding to nuclear receptors. *Nature,* 387**,** 733-6.

HETZ, C. 2012. The unfolded protein response: controlling cell fate decisions under ER stress and beyond. *Nat Rev Mol Cell Biol,* 13**,** 89-102.

HETZ, C. & SAXENA, S. 2017a. ER stress and the unfolded protein response in neurodegeneration. *Nature Reviews Neurology,* 13**,** 477-491.

HETZ, C. & SAXENA, S. 2017b. ER stress and the unfolded protein response in neurodegeneration. *Nat Rev Neurol,* 13**,** 477-491.

HOLINKA, C. F., DICZFALUSY, E. & COELINGH BENNINK, H. J. 2008. Estetrol: a unique steroid in human pregnancy. *J Steroid Biochem Mol Biol,* 110**,** 138-43.

HOSFORD, S. R., SHEE, K., WELLS, J. D., TRAPHAGEN, N. A., FIELDS, J. L., HAMPSCH, R. A., KETTENBACH, A. N., DEMIDENKO, E. & MILLER, T. W. 2019. Estrogen therapy induces an

unfolded protein response to drive cell death in ER+ breast cancer. *Mol Oncol,* 13**,** 1778-1794.

HOWELL, A., CUZICK, J., BAUM, M., BUZDAR, A., DOWSETT, M., FORBES, J. F., HOCTIN-BOES, G., HOUGHTON, J., LOCKER, G. Y., TOBIAS, J. S. & GROUP, A. T. 2005. Results of the ATAC (Arimidex, Tamoxifen, Alone or in Combination) trial after completion of 5 years' adjuvant treatment for breast cancer. *Lancet,* 365**,** 60-2.

HU, Z., LI, Z., MA, Z. & CURTIS, C. 2020. Multi-cancer analysis of clonality and the timing of systemic spread in paired primary tumors and metastases. *Nat Genet*.

HUGGINS, C. & HODGES, C. V. 1941. Studies on prostatic cancer - I The effect of castration, of estrogen and of androgen injection on serum phosphatases in metastatic carcinoma of the prostate. *Cancer Res,* 1**,** 293-297.

HUGGINS, C. & HODGES, C. V. 1972. Studies on prostatic cancer. I. The effect of castration, of estrogen and androgen injection on serum phosphatases in metastatic carcinoma of the prostate. *CA Cancer J Clin,* 22**,** 232-40.

IMAI, Y., YOUN, M. Y., KONDOH, S., NAKAMURA, T., KOUZMENKO, A., MATSUMOTO, T., TAKADA, I., TAKAOKA, K. & KATO, S. 2009. Estrogens maintain bone mass by regulating expression of genes controlling function and life span in mature osteoclasts. *Ann N Y Acad Sci,* 1173 Suppl 1**,** E31-9.

INGLE, J. N., AHMANN, D. L., GREEN, S. J., EDMONSON, J. H., BISEL, H. F., KVOLS, L. K., NICHOLS, W. C., CREAGAN, E. T., HAHN, R. G., RUBIN, J. & FRYTAK, S. 1981. Randomized clinical trial of diethylstilbestrol versus tamoxifen in postmenopausal women with advanced breast cancer. *N Engl J Med,* 304**,** 16-21.

IWASE, H., YAMAMOTO, Y., YAMAMOTO-IBUSUKI, M., MURAKAMI, K. I., OKUMURA, Y., TOMITA, S., INAO, T., HONDA, Y., OMOTO, Y. & IYAMA, K. I. 2013. Ethinylestradiol is beneficial for postmenopausal patients with heavily pre-treated metastatic breast cancer after prior aromatase inhibitor treatment: a prospective study. *British Journal of Cancer,* 109**,** 1537-1542.

JESELSOHN, R., BUCHWALTER, G., DE ANGELIS, C., BROWN, M. & SCHIFF, R. 2015. ESR1 mutations-a mechanism for acquired endocrine resistance in breast cancer. *Nat Rev Clin Oncol,* 12**,** 573-83.

JIANG, S. Y. & JORDAN, V. C. 1992. Growth regulation of estrogen receptor-negative breast cancer cells transfected with complementary DNAs for estrogen receptor. *J Natl Cancer Inst,* 84**,** 580-91.

JIANG, S. Y., WOLF, D. M., YINGLING, J. M., CHANG, C. & JORDAN, V. C. 1992. An estrogen receptor positive MCF-7 clone that is resistant to antiestrogens and estradiol. *Mol Cell Endocrinol,* 90**,** 77-86.

JING, G., WANG, J. J. & ZHANG, S. X. 2012. ER stress and apoptosis: a new mechanism for retinal cell death. *Exp Diabetes Res,* 2012**,** 589589.

JORDAN, N. J., GEE, J. M., BARROW, D., WAKELING, A. E. & NICHOLSON, R. I. 2004. Increased constitutive activity of PKB/Akt in tamoxifen resistant breast cancer MCF-7 cells. *Breast Cancer Res Treat,* 87**,** 167-80.

JORDAN, V., C., DIX, C. J. & ALLEN, K. E. 1979. The effectiveness of long-term treatment in a laboratory model for adjuvant hormone therapy of breast cancer. *In:* SALMON, S. E. & JONES, S. E. (eds.) *Adjuvant Therpy of Cancer II.* New York Greene and Stratton.

JORDAN, V. C. 1976. Effect of Tamoxifen (Ici 46,474) on Initiation and Growth of Dmba - Induced Rat Mammary Carcinomata. *European Journal of Cancer,* 12**,** 419-424.

JORDAN, V. C. 1990. Long-term adjuvant tamoxifen therapy for breast cancer. *Breast Cancer Res Treat,* 15**,** 125-36.

JORDAN, V. C. 2003. Tamoxifen: a most unlikely pioneering medicine. *Nat Rev Drug Discov,* 2**,** 205-13.

JORDAN, V. C. 2008. The 38th David A. Karnofsky lecture: the paradoxical actions of estrogen in breast cancer--survival or death? *J Clin Oncol,* 26**,** 3073-82.

JORDAN, V. C. 2015a. The new biology of estrogen-induced apoptosis applied to treat and prevent breast cancer. *Endocrine-Related Cancer,* 22**,** R1-R31.

JORDAN, V. C. 2015b. The new biology of estrogen-induced apoptosis applied to treat and prevent breast cancer. *Endocr Relat Cancer,* 22**,** R1-31.

JORDAN, V. C. 2020. Molecular Mechanism for Breast Cancer Incidence in the Women's Health Initiative. *Cancer Prev Res (Phila).*

JORDAN, V. C. & ALLEN, K. E. 1980. Evaluation of the antitumour activity of the non-steroidal antioestrogen monohydroxytamoxifen in the DMBA-induced rat mammary carcinoma model. *Eur J Cancer,* 16**,** 239-51.

JORDAN, V. C. & ASSIKIS, V. J. 1995. Endometrial carcinoma and tamoxifen: clearing up a controversy. *Clin Cancer Res,* 1**,** 467-72.

JORDAN, V. C. & BRODIE, A. M. 2007. Development and evolution of therapies targeted to the estrogen receptor for the treatment and prevention of breast cancer. *Steroids,* 72**,** 7-25.

JORDAN, V. C., CURPAN, R. & MAXIMOV, P. Y. 2015. Estrogen Receptor Mutations Found in Breast Cancer Metastases Integrated With the Molecular Pharmacology of Selective ER Modulators. *Jnci-Journal of the National Cancer Institute,* 107.

JORDAN, V. C., LABABIDI, M. K. & LANGAN-FAHEY, S. 1991. Suppression of mouse mammary tumorigenesis by long-term tamoxifen therapy. *J Natl Cancer Inst,* 83**,** 492-6.

JORDAN, V. C. & LIEBERMAN, M. E. 1984. Estrogen-stimulated prolactin synthesis in vitro. Classification of agonist, partial agonist, and antagonist actions based on structure. *Mol Pharmacol,* 26**,** 279-85.

KAMEDA, T., MANO, H., YUASA, T., MORI, Y., MIYAZAWA, K., SHIOKAWA, M., NAKAMARU, Y., HIROI, E., HIURA, K., KAMEDA, A., YANG, N. N., HAKEDA, Y. & KUMEGAWA, M. 1997. Estrogen inhibits bone resorption by directly inducing apoptosis of the bone-resorbing osteoclasts. *J Exp Med,* 186**,** 489-95.

KHAN, Q. J., O'DEA, A. P. & SHARMA, P. 2010. Musculoskeletal adverse events associated with adjuvant aromatase inhibitors. *J Oncol,* 2010.

KOTOV, A., FALANY, J. L., WANG, J. & FALANY, C. N. 1999. Regulation of estrogen activity by sulfation in human Ishikawa endometrial adenocarcinoma cells. *J Steroid Biochem Mol Biol,* 68**,** 137-44.

KRAUS, M. H., POPESCU, N. C., AMSBAUGH, S. C. & KING, C. R. 1987. Overexpression of the EGF receptor-related proto-oncogene erbB-2 in human mammary tumor cell lines by different molecular mechanisms. *EMBO J,* 6**,** 605-10.

KRUM, S. A., MIRANDA-CARBONI, G. A., HAUSCHKA, P. V., CARROLL, J. S., LANE, T. F., FREEDMAN, L. P. & BROWN, M. 2008. Estrogen protects bone by inducing Fas ligand in osteoblasts to regulate osteoclast survival. *EMBO J,* 27**,** 535-45.

LAKHANI, N. J., VENITZ, J., FIGG, W. D. & SPARREBOOM, A. 2003. Pharmacogenetics of estrogen metabolism and transport in relation to cancer. *Curr Drug Metab,* 4**,** 505-13.

LANGDON, S. P., RITCHIE, A., YOUNG, K., CREW, A. J., SWEETING, V., BRAMLEY, T., HILLIER, S., HAWKINS, R. A., TESDALE, A. L., SMYTH, J. F. & ET AL. 1993. Contrasting effects of 17 beta-estradiol on the growth of human ovarian carcinoma cells in vitro and in vivo. *Int J Cancer,* 55**,** 459-64.

LEE, H., KIM, H., CHUNG, Y., KIM, J. & YANG, H. 2013. Thymocyte Differentiation is Regulated by a Change in Estradiol Levels during the Estrous Cycle in Mouse. *Dev Reprod,* 17**,** 441-9.

LEMMO, W. 2016. Anti-Estrogen Withdrawal Effect With Raloxifene? A Case Report. *Integr Cancer Ther,* 15**,** 245-9.

LEVENSON, A. S., CATHERINO, W. H. & JORDAN, V. C. 1997. Estrogenic activity is increased for an antiestrogen by a natural mutation of the estrogen receptor. *Journal of Steroid Biochemistry and Molecular Biology,* 60**,** 261-268.

LEWIS, J. S., MEEKE, K., OSIPO, C., ROSS, E. A., KIDAWI, N., LI, T., BELL, E., CHANDEL, N. S. & JORDAN, V. C. 2005a. Intrinsic mechanism of estradiol-induced apoptosis in breast cancer cells resistant to estrogen deprivation. *J Natl Cancer Inst,* 97**,** 1746-59.

LEWIS, J. S., OSIPO, C., MEEKE, K. & JORDAN, V. C. 2005b. Estrogen-induced apoptosis in a breast cancer model resistant to long-term estrogen withdrawal. *Journal of Steroid Biochemistry and Molecular Biology,* 94**,** 131-141.

LIN, J. H., LI, H., YASUMURA, D., COHEN, H. R., ZHANG, C., PANNING, B., SHOKAT, K. M., LAVAIL, M. M. & WALTER, P. 2007. IRE1 signaling affects cell fate during the unfolded protein response. *Science,* 318**,** 944-9.

LIU, H., LEE, E. S., GAJDOS, C., PEARCE, S. T., CHEN, B., OSIPO, C., LOWETH, J., MCKIAN, K., DE LOS REYES, A., WING, L. & JORDAN, V. C. 2003. Apoptotic action of 17beta-estradiol in raloxifene-resistant MCF-7 cells in vitro and in vivo. *J Natl Cancer Inst,* 95**,** 1586-97.

LIU, H., PARK, W. C., BENTREM, D. J., MCKIAN, K. P., REYES ADE, L., LOWETH, J. A., SCHAFER, J. M., ZAPF, J. W. & JORDAN, V. C. 2002. Structure-function relationships of the raloxifene-estrogen receptor-alpha complex for regulating transforming growth factor-alpha expression in breast cancer cells. *J Biol Chem,* 277**,** 9189-98.

LONNING, P. E., TAYLOR, P. D., ANKER, G., IDDON, J., WIE, L., JORGENSEN, L. M., MELLA, O. & HOWELL, A. 2001. High-dose estrogen treatment in postmenopausal breast cancer patients heavily exposed to endocrine therapy. *Breast Cancer Res Treat,* 67**,** 111-6.

MALY, D. J. & PAPA, F. R. 2014. Druggable sensors of the unfolded protein response. *Nat Chem Biol,* 10**,** 892-901.

MATSUURA, S., ITAKURA, A., OHNO, Y., NAKASHIMA, Y., MURATA, Y., TAKEUCHI, M., KOBAYASHI, M. & MIZUTANI, S. 2004. Effects of estradiol administration on feto-placental growth in rat. *Early Hum Dev,* 77**,** 47-56.

MAXIMOV, P. Y., ABDERRAHMAN, B., HAWSAWI, Y. M., CHEN, Y., FOULDS, C. E., JAIN, A., MALOVANNAYA, A., FAN, P., CURPAN, R. F., HAN, R., FANNING, S. W., BROOM, B. M., RINCON, D. M. Q., GREENLAND, J. A., GREENE, G. L. & JORDAN, V. C. 2020. The Structure-Function Relationship of Angular Estrogens and Estrogen Receptor Alpha to Initiate Estrogen-Induced Apoptosis in Breast Cancer Cells. *Mol Pharmacol,* 98**,** 24-37.

MAXIMOV, P. Y., LEE, T. M. & JORDAN, V. C. 2013. The discovery and development of selective estrogen receptor modulators (SERMs) for clinical practice. *Curr Clin Pharmacol,* 8**,** 135-55.

MAXIMOV, P. Y., MYERS, C. B., CURPAN, R. F., LEWIS-WAMBI, J. S. & JORDAN, V. C. 2010. Structure-function relationships of estrogenic triphenylethylenes related to endoxifen and 4-hydroxytamoxifen. *J Med Chem,* 53**,** 3273-83.

MCDONNELL, D. P., WARDELL, S. E. & NORRIS, J. D. 2015. Oral Selective Estrogen Receptor Downregulators (SERDs), a Breakthrough Endocrine Therapy for Breast Cancer. *J Med Chem,* 58**,** 4883-7.

MEDLOCK, K. L., LYTTLE, C. R., KELEPOURIS, N., NEWMAN, E. D. & SHEEHAN, D. M. 1991. Estradiol down-regulation of the rat uterine estrogen receptor. *Proc Soc Exp Biol Med,* 196**,** 293-300.

MELISKO, M. E., GOLDMAN, M. E., HWANG, J., DE LUCA, A., FANG, S., ESSERMAN, L. J., CHIEN, A. J., PARK, J. W. & RUGO, H. S. 2017. Vaginal Testosterone Cream vs Estradiol Vaginal Ring for Vaginal Dryness or Decreased Libido in Women Receiving Aromatase Inhibitors for Early-Stage Breast Cancer: A Randomized Clinical Trial. *JAMA Oncol,* 3**,** 313-319.

MICHAUD, J. E., BILLUPS, K. L. & PARTIN, A. W. 2015. Testosterone and prostate cancer: an evidence-based review of pathogenesis and oncologic risk. *Ther Adv Urol,* 7**,** 378-87.

MOLLOY, M. E., WHITE, B. E., GHEREZGHIHER, T., MICHALSEN, B. T., XIONG, R., PATEL, H., ZHAO, H., MAXIMOV, P. Y., JORDAN, V. C., THATCHER, G. R. & TONETTI, D. A. 2014. Novel selective estrogen mimics for the treatment of tamoxifen-resistant breast cancer. *Mol Cancer Ther,* 13**,** 2515-26.

MURPHY, C. S., PINK, J. J. & JORDAN, V. C. 1990. Characterization of a receptor-negative, hormone-nonresponsive clone derived from a T47D human breast cancer cell line kept under estrogen-free conditions. *Cancer Res,* 50**,** 7285-92.

MUSGROVE, E. A. & SUTHERLAND, R. L. 2009. Biological determinants of endocrine resistance in breast cancer. *Nat Rev Cancer,* 9**,** 631-43.

NAKAMURA, T., IMAI, Y., MATSUMOTO, T., SATO, S., TAKEUCHI, K., IGARASHI, K., HARADA, Y., AZUMA, Y., KRUST, A., YAMAMOTO, Y., NISHINA, H., TAKEDA, S., TAKAYANAGI, H., METZGER, D., KANNO, J., TAKAOKA, K., MARTIN, T. J., CHAMBON, P. & KATO, S. 2007. Estrogen prevents bone loss via estrogen receptor alpha and induction of Fas ligand in osteoclasts. *Cell,* 130**,** 811-23.

NISHIDA, M., KASAHARA, K., KANEKO, M., IWASAKI, H. & HAYASHI, K. 1985. [Establishment of a new human endometrial adenocarcinoma cell line, Ishikawa cells, containing estrogen and progesterone receptors]. *Nihon Sanka Fujinka Gakkai Zasshi,* 37, 1103-11.

NIU, J., ANDRES, G., KRAMER, K., KUNDRANDA, M. N., ALVAREZ, R. H., KLIMANT, E., PARIKH, A. R., TAN, B., STAREN, E. D. & MARKMAN, M. 2015. Incidence and clinical significance of ESR1 mutations in heavily pretreated metastatic breast cancer patients. *Onco Targets Ther,* 8**,** 3323-8.

NOLTE, R. T., WISELY, G. B., WESTIN, S., COBB, J. E., LAMBERT, M. H., KUROKAWA, R., ROSENFELD, M. G., WILLSON, T. M., GLASS, C. K. & MILBURN, M. V. 1998. Ligand binding and co-activator assembly of the peroxisome proliferator-activated receptor-gamma. *Nature,* 395**,** 137-43.

O'LEARY, B., FINN, R. S. & TURNER, N. C. 2016. Treating cancer with selective CDK4/6 inhibitors. *Nat Rev Clin Oncol,* 13**,** 417-30.

OBIORAH, I., SENGUPTA, S., CURPAN, R. & JORDAN, V. C. 2014. Defining the Conformation of the Estrogen Receptor Complex That Controls Estrogen-Induced Apoptosis in Breast Cancer. *Molecular Pharmacology,* 85**,** 789-799.

OBIORAH, I. E. & JORDAN, V. C. 2014. Differences in the rate of oestrogen-induced apoptosis in breast cancer by oestradiol and the triphenylethylene bisphenol. *Br J Pharmacol,* 171**,** 4062-72.

OSBORNE, C. K., BARDOU, V., HOPP, T. A., CHAMNESS, G. C., HILSENBECK, S. G., FUQUA, S. A., WONG, J., ALLRED, D. C., CLARK, G. M. & SCHIFF, R. 2003a. Role of the estrogen receptor coactivator AIB1 (SRC-3) and HER-2/neu in tamoxifen resistance in breast cancer. *J Natl Cancer Inst,* 95**,** 353-61.

OSBORNE, C. K., BARDOU, V., HOPP, T. A., CHAMNESS, G. C., HILSENBECK, S. G., FUQUA, S. A. W., WONG, J. M., ALLRED, D. C., CLARK, G. M. & SCHIFF, R. 2003b. Role of the estrogen receptor coactivator AIB1 (SRC-3) and HER-2/neu in tamoxifen resistance in breast cancer. *Journal of the National Cancer Institute,* 95**,** 353-361.

OSBORNE, C. K., BOLDT, D. H., CLARK, G. M. & TRENT, J. M. 1983. Effects of tamoxifen on human breast cancer cell cycle kinetics: accumulation of cells in early G1 phase. *Cancer Res,* 43**,** 3583-5.

OSTERBERG, L. & BLASCHKE, T. 2005. Adherence to medication. *N Engl J Med,* 353**,** 487-97.

PAKOS-ZEBRUCKA, K., KORYGA, I., MNICH, K., LJUJIC, M., SAMALI, A. & GORMAN, A. M. 2016. The integrated stress response. *EMBO Rep,* 17**,** 1374-1395.

PAPLOMATA, E. & O'REGAN, R. 2014. The PI3K/AKT/mTOR pathway in breast cancer: targets, trials and biomarkers. *Ther Adv Med Oncol,* 6**,** 154-66.

PATEL, S., KILBURN, B., IMUDIA, A., ARMANT, D. R. & SKAFAR, D. F. 2015. Estradiol Elicits Proapoptotic and Antiproliferative Effects in Human Trophoblast Cells. *Biol Reprod,* 93**,** 74.

PEJERREY, S. M., DUSTIN, D., KIM, J. A., GU, G., RECHOUM, Y. & FUQUA, S. A. W. 2018. The Impact of ESR1 Mutations on the Treatment of Metastatic Breast Cancer. *Horm Cancer,* 9**,** 215-228.

PIERRE, P. 2019. Integrating stress responses and immunity. *Science,* 365**,** 28-29.

PINK, J. J., JIANG, S. Y., FRITSCH, M. & JORDAN, V. C. 1995. An Estrogen-Independent Mcf-7 Breast-Cancer Cell-Line Which Contains a Novel 80-Kilodalton Estrogen Receptor-Related Protein. *Cancer Research,* 55**,** 2583-2590.

PINK, J. J. & JORDAN, V. C. 1996. Models of estrogen receptor regulation by estrogens and antiestrogens in breast cancer cell lines. *Cancer Research,* 56**,** 2321-2330.

PISANI, P., BRAY, F. & PARKIN, D. M. 2002. Estimates of the world-wide prevalence of cancer for 25 sites in the adult population. *Int J Cancer,* 97**,** 72-81.

REBELLO, G., RAMESAR, R., VORSTER, A., ROBERTS, L., EHRENREICH, L., OPPON, E., GAMA, D., BARDIEN, S., GREENBERG, J., BONAPACE, G., WAHEED, A., SHAH, G. N. & SLY, W. S. 2004. Apoptosis-inducing signal sequence mutation in carbonic anhydrase IV identified in patients with the RP17 form of retinitis pigmentosa. *Proc Natl Acad Sci U S A,* 101**,** 6617-22.

REID, A. H. M., ATTARD, G., BARRIE, E. & DE BONO, J. S. 2008. CYP17 inhibition as a hormonal strategy for prostate cancer. *Nature Clinical Practice Urology,* 5**,** 610-620.

RIJHSINGHANI, A. G., THOMPSON, K., BHATIA, S. K. & WALDSCHMIDT, T. J. 1996. Estrogen blocks early T cell development in the thymus. *Am J Reprod Immunol,* 36**,** 269-77.

ROBERTSON, J. F. R. 2007. Fulvestrant (Faslodex (R)) - How to make a good drug better. *Oncologist,* 12**,** 774-784.

ROBERTSON, J. F. R., BONDARENKO, I. M., TRISHKINA, E., DVORKIN, M., PANASCI, L., MANIKHAS, A., SHPARYK, Y., CARDONA-HUERTA, S., CHEUNG, K. L., PHILCO-SALAS, M. J., RUIZ-BORREGO, M., SHAO, Z., NOGUCHI, S., ROWBOTTOM, J., STUART, M., GRINSTED, L. M., FAZAL, M. & ELLIS, M. J. 2016. Fulvestrant 500 mg versus anastrozole 1 mg for hormone receptor-positive advanced breast cancer (FALCON): an international, randomised, double-blind, phase 3 trial. *Lancet,* 388**,** 2997-3005.

RODRIGUEZ-BRENES, I. A. & WODARZ, D. 2015. Preventing clonal evolutionary processes in cancer: Insights from mathematical models. *Proc Natl Acad Sci U S A,* 112**,** 8843-50.

ROEHM, E. 2015. A Reappraisal of Women's Health Initiative Estrogen-Alone Trial: Long-Term Outcomes in Women 50-59 Years of Age. *Obstet Gynecol Int,* 2015**,** 713295.

RON, D. & WALTER, P. 2007. Signal integration in the endoplasmic reticulum unfolded protein response. *Nat Rev Mol Cell Biol,* 8**,** 519-29.

ROODI, N., BAILEY, L. R., KAO, W. Y., VERRIER, C. S., YEE, C. J., DUPONT, W. D. & PARL, F. F. 1995. Estrogen receptor gene analysis in estrogen receptor-positive and receptor-negative primary breast cancer. *J Natl Cancer Inst,* 87**,** 446-51.

ROSENBERG, P. S., BARKER, K. A. & ANDERSON, W. F. 2015. Estrogen Receptor Status and the Future Burden of Invasive and In Situ Breast Cancers in the United States. *J Natl Cancer Inst,* 107.

RYAN, C. J., MOLINA, A. & GRIFFIN, T. 2013. Abiraterone in metastatic prostate cancer. *N Engl J Med,* 368**,** 1458-9.

RYAN, C. J. & TINDALL, D. J. 2011. Androgen receptor rediscovered: the new biology and targeting the androgen receptor therapeutically. *J Clin Oncol,* 29**,** 3651-8.

RYAN, K. J. 1959. Biological aromatization of steroids. *J Biol Chem,* 234**,** 268-72.

RYOO, H. D., DOMINGOS, P. M., KANG, M. J. & STELLER, H. 2007. Unfolded protein response in a Drosophila model for retinal degeneration. *EMBO J,* 26**,** 242-52.

SALONEN, A. J., VIITANEN, J., LUNDSTEDT, S., ALA-OPAS, M., TAARI, K., TAMMELA, T. L. & FINNPROSTATE, G. 2008. Finnish multicenter study comparing intermittent to continuous androgen deprivation for advanced prostate cancer: interim analysis of prognostic markers affecting initial response to androgen deprivation. *J Urol,* 180**,** 915-9; discussion 919-20.

SAMAVAT, H. & KURZER, M. S. 2015. Estrogen metabolism and breast cancer. *Cancer Letters,* 356**,** 231-243.

SCHIAVON, G. & SMITH, I. E. 2014. Status of adjuvant endocrine therapy for breast cancer. *Breast Cancer Res,* 16**,** 206.

SCHIFF, R., MASSARWEH, S. A., SHOU, J., BHARWANI, L., ARPINO, G., RIMAWI, M. & OSBORNE, C. K. 2005. Advanced concepts in estrogen receptor biology and breast cancer endocrine

resistance: implicated role of growth factor signaling and estrogen receptor coregulators. *Cancer Chemother Pharmacol,* 56 Suppl 1**,** 10-20.

SCHMIDT, M., HÖNIG, A, ZIMMERMAN Y, VERHOEVEN C, ALMSTEDT K, BATTISTA M, LENHARD HG, KRIJGH J, BENNINK HC 2020. Abstract P5-11-15: Estetrol for treatment of advanced ER+/HER2- breast cancer. *Cancer Research* 80.

SCHRODER, M. & KAUFMAN, R. J. 2005. The mammalian unfolded protein response. *Annu Rev Biochem,* 74**,** 739-89.

SCHROEDER, B., ZHANG, Y., STAL, O., FORNANDER, T., BRUFSKY, A., SGROI, D. C. & SCHNABEL, C. A. 2017. Risk stratification with Breast Cancer Index for late distant recurrence in patients with clinically low-risk (T1N0) estrogen receptor-positive breast cancer. *NPJ Breast Cancer,* 3**,** 28.

SCHWEIZER, M. T., ANTONARAKIS, E. S., WANG, H., AJIBOYE, A. S., SPITZ, A., CAO, H., LUO, J., HAFFNER, M. C., YEGNASUBRAMANIAN, S., CARDUCCI, M. A., EISENBERGER, M. A., ISAACS, J. T. & DENMEADE, S. R. 2015. Effect of bipolar androgen therapy for asymptomatic men with castration-resistant prostate cancer: results from a pilot clinical study. *Sci Transl Med,* 7**,** 269ra2.

SENGUPTA, S., OBIORAH, I., MAXIMOV, P. Y., CURPAN, R. & JORDAN, V. C. 2013. Molecular mechanism of action of bisphenol and bisphenol A mediated by oestrogen receptor alpha in growth and apoptosis of breast cancer cells. *British Journal of Pharmacology,* 169**,** 167-178.

SENGUPTA, S., SHARMA, C. G. & JORDAN, V. C. 2010. Estrogen regulation of X-box binding protein-1 and its role in estrogen induced growth of breast and endometrial cancer cells. *Horm Mol Biol Clin Investig,* 2**,** 235-243.

SGROI, D. C., SESTAK, I., CUZICK, J., ZHANG, Y., SCHNABEL, C. A., SCHROEDER, B., ERLANDER, M. G., DUNBIER, A., SIDHU, K., LOPEZ-KNOWLES, E., GOSS, P. E. & DOWSETT, M. 2013. Prediction of late distant recurrence in patients with oestrogen-receptor-positive breast cancer: a prospective comparison of the breast-cancer index (BCI) assay, 21-gene recurrence score, and IHC4 in the TransATAC study population. *Lancet Oncol,* 14**,** 1067-1076.

SHIAU, A. K., BARSTAD, D., LORIA, P. M., CHENG, L., KUSHNER, P. J., AGARD, D. A. & GREENE, G. L. 1998a. The structural basis of estrogen receptor/coactivator recognition and the antagonism of this interaction by tamoxifen. *Cell,* 95**,** 927-37.

SHIAU, A. K., BARSTAD, D., LORIA, P. M., CHENG, L., KUSHNER, P. J., AGARD, D. A. & GREENE, G. L. 1998b. The structural basis of estrogen receptor/coactivator recognition and the antagonism of this interaction by tamoxifen. *Cell,* 95**,** 927-937.

SHIAU, A. K., BARSTAD, D., RADEK, J. T., MEYERS, M. J., NETTLES, K. W., KATZENELLENBOGEN, B. S., KATZENELLENBOGEN, J. A., AGARD, D. A. & GREENE, G. L. 2002. Structural characterization of a subtype-selective ligand reveals a novel mode of estrogen receptor antagonism. *Nat Struct Biol,* 9**,** 359-64.

SHIMAZAWA, M., INOKUCHI, Y., ITO, Y., MURATA, H., AIHARA, M., MIURA, M., ARAIE, M. & HARA, H. 2007. Involvement of ER stress in retinal cell death. *Mol Vis,* 13**,** 578-87.

SHOU, J., LAI, Y., XU, J. & HUANG, J. 2016. Prognostic value of FOXA1 in breast cancer: A systematic review and meta-analysis. *Breast,* 27**,** 35-43.

SIEGEL, R. L., MILLER, K. D. & JEMAL, A. 2015. Cancer statistics, 2015. *CA Cancer J Clin,* 65**,** 5-29.

SIEGEL, R. L., MILLER, K. D. & JEMAL, A. 2020. Cancer statistics, 2020. *CA Cancer J Clin,* 70**,** 7-30.

SINGER, C. F., BENNINK, H. J., NATTER, C., STEURER, S., RUDAS, M., MOINFAR, F., APPELS, N., VISSER, M. & KUBISTA, E. 2014. Antiestrogenic effects of the fetal estrogen estetrol in women with estrogen-receptor positive early breast cancer. *Carcinogenesis,* 35**,** 2447-51.

SONG, J., RUTHERFORD, T., NAFTOLIN, F., BROWN, S. & MOR, G. 2002. Hormonal regulation of apoptosis and the Fas and Fas ligand system in human endometrial cells. *Mol Hum Reprod,* 8**,** 447-55.

SONG, R. X., MOR, G., NAFTOLIN, F., MCPHERSON, R. A., SONG, J., ZHANG, Z., YUE, W., WANG, J. & SANTEN, R. J. 2001. Effect of long-term estrogen deprivation on apoptotic responses of breast cancer cells to 17beta-estradiol. *J Natl Cancer Inst,* 93**,** 1714-23.

STAPLES, J. E., GASIEWICZ, T. A., FIORE, N. C., LUBAHN, D. B., KORACH, K. S. & SILVERSTONE, A. E. 1999. Estrogen receptor alpha is necessary in thymic development and estradiol-induced thymic alterations. *J Immunol,* 163**,** 4168-74.

SUTHERLAND, R. L., GREEN, M. D., HALL, R. E., REDDEL, R. R. & TAYLOR, I. W. 1983. Tamoxifen induces accumulation of MCF 7 human mammary carcinoma cells in the G0/G1 phase of the cell cycle. *Eur J Cancer Clin Oncol,* 19**,** 615-21.

SYED, V. & HO, S. M. 2003. Progesterone-induced apoptosis in immortalized normal and malignant human ovarian surface epithelial cells involves enhanced expression of FasL. *Oncogene,* 22**,** 6883-6890.

SZEGEZDI, E., LOGUE, S. E., GORMAN, A. M. & SAMALI, A. 2006. Mediators of endoplasmic reticulum stress-induced apoptosis. *EMBO Rep,* 7**,** 880-5.

THOMAS, C. & GUSTAFSSON, J. A. 2011. The different roles of ER subtypes in cancer biology and therapy. *Nat Rev Cancer,* 11**,** 597-608.

TONETTI, D. A., XIONG, R., ZHAO, J., GUTGESELL, L., DUDEK, A. Z. & THATCHER, G. R. 2017. (Abstract e14090) Efficacy, maximal tolerated dose, and toxicokinetics of TTC-352 in rats and dogs, a partial ER agonist for metastatic ER+ breast cancer. *J Clin Oncol*.

TOY, W., SHEN, Y., WON, H., GREEN, B., SAKR, R. A., WILL, M., LI, Z., GALA, K., FANNING, S., KING, T. A., HUDIS, C., CHEN, D., TARAN, T., HORTOBAGYI, G., GREENE, G., BERGER, M., BASELGA, J. & CHANDARLAPATY, S. 2013a. ESR1 ligand-binding domain mutations in hormone-resistant breast cancer. *Nat Genet,* 45**,** 1439-45.

TOY, W., SHEN, Y., WON, H., GREEN, B., SAKR, R. A., WILL, M., LI, Z. Q., GALA, K., FANNING, S., KING, T. A., HUDIS, C., CHEN, D., TARAN, T., HORTOBAGYI, G., GREENE, G., BERGER, M., BASELGA, J. & CHANDARLAPATY, S. 2013b. ESR1 ligand-binding domain mutations in hormone-resistant breast cancer. *Nature Genetics,* 45**,** 1439-U189.

TSUCHIYA, Y., NAKAJIMA, M. & YOKOI, T. 2005. Cytochrome P450-mediated metabolism of estrogens and its regulation in human. *Cancer Lett,* 227**,** 115-24.

VERHOEVEN, C., SCHMIDT, M., HÖNIG, A., DÜNNEBACKE, J., DUTMAN, E., KRIJGH, J. & COELINGH-BENNINK, H. 2018. *Abstract OT1-04-01: Estetrol for treatment of advanced ER+ breast cancer* [Online]. Available: http://cancerres.aacrjournals.org/content/78/4_Supplement/OT1-04-01 [Accessed].

VICIER, C., DIECI, M. V., ARNEDOS, M., DELALOGE, S., VIENS, P. & ANDRE, F. 2014. Clinical development of mTOR inhibitors in breast cancer. *Breast Cancer Res,* 16**,** 203.

VOGEL, V. G., COSTANTINO, J. P., WICKERHAM, D. L., CRONIN, W. M., CECCHINI, R. S., ATKINS, J. N., BEVERS, T. B., FEHRENBACHER, L., PAJON, E. R., JR., WADE, J. L., 3RD, ROBIDOUX, A., MARGOLESE, R. G., JAMES, J., LIPPMAN, S. M., RUNOWICZ, C. D., GANZ, P. A., REIS, S. E., MCCASKILL-STEVENS, W., FORD, L. G., JORDAN, V. C., WOLMARK, N., NATIONAL SURGICAL ADJUVANT, B. & BOWEL, P. 2006. Effects of tamoxifen vs raloxifene on the risk of developing invasive breast cancer and other disease outcomes: the NSABP Study of Tamoxifen and Raloxifene (STAR) P-2 trial. *JAMA,* 295**,** 2727-41.

VOGEL, V. G., COSTANTINO, J. P., WICKERHAM, D. L., CRONIN, W. M., CECCHINI, R. S., ATKINS, J. N., BEVERS, T. B., FEHRENBACHER, L., PAJON, E. R., WADE, J. L., 3RD, ROBIDOUX, A., MARGOLESE, R. G., JAMES, J., RUNOWICZ, C. D., GANZ, P. A., REIS, S. E., MCCASKILL-STEVENS, W., FORD, L. G., JORDAN, V. C., WOLMARK, N., NATIONAL SURGICAL ADJUVANT, B. & BOWEL, P. 2010. Update of the National Surgical Adjuvant Breast and Bowel Project Study of Tamoxifen and Raloxifene (STAR) P-2 Trial: Preventing breast cancer. *Cancer Prev Res (Phila),* 3**,** 696-706.

WALTER, P. & RON, D. 2011. The unfolded protein response: from stress pathway to homeostatic regulation. *Science,* 334**,** 1081-6.

WANG, L., LIU, S., ZHAO, Y., LIU, D., LIU, Y., CHEN, C., KARRAY, S., SHI, S. & JIN, Y. 2015. Osteoblast-induced osteoclast apoptosis by fas ligand/FAS pathway is required for maintenance of bone mass. *Cell Death and Differentiation,* 22**,** 1654-1664.

WANG, Q., LI, W., ZHANG, Y., YUAN, X., XU, K., YU, J., CHEN, Z., BEROUKHIM, R., WANG, H., LUPIEN, M., WU, T., REGAN, M. M., MEYER, C. A., CARROLL, J. S., MANRAI, A. K., JANNE, O. A., BALK, S. P., MEHRA, R., HAN, B., CHINNAIYAN, A. M., RUBIN, M. A., TRUE, L., FIORENTINO, M., FIORE, C., LODA, M., KANTOFF, P. W., LIU, X. S. & BROWN, M. 2009. Androgen receptor regulates a distinct transcription program in androgen-independent prostate cancer. *Cell,* 138**,** 245-56.

WANG, Z. Y. & YIN, L. 2015. Estrogen receptor alpha-36 (ER-alpha36): A new player in human breast cancer. *Mol Cell Endocrinol,* 418 Pt 3**,** 193-206.

WOLF, D. M. & JORDAN, V. C. 1993. A laboratory model to explain the survival advantage observed in patients taking adjuvant tamoxifen therapy. *Recent Results Cancer Res,* 127**,** 23-33.

WOLF, D. M. & JORDAN, V. C. 1994. The estrogen receptor from a tamoxifen stimulated MCF-7 tumor variant contains a point mutation in the ligand binding domain. *Breast Cancer Res Treat,* 31**,** 129-38.

WONG, Y. N., FERRALDESCHI, R., ATTARD, G. & DE BONO, J. 2014. Evolution of androgen receptor targeted therapy for advanced prostate cancer. *Nat Rev Clin Oncol,* 11**,** 365-76.

XING, L. P. & BOYCE, B. F. 2005. Regulation of apoptosis in osteoclasts and osteoblastic cells. *Biochemical and Biophysical Research Communications,* 328**,** 709-720.

XIONG, R., PATEL, H. K., GUTGESELL, L. M., ZHAO, J., DELGADO-RIVERA, L., PHAM, T. N. D., ZHAO, H., CARLSON, K., MARTIN, T., KATZENELLENBOGEN, J. A., MOORE, T. W., TONETTI, D. A. & THATCHER, G. R. J. 2016. Selective Human Estrogen Receptor Partial Agonists (ShERPAs) for Tamoxifen-Resistant Breast Cancer. *J Med Chem,* 59**,** 219-237.

XU, H., YU, S., LIU, Q., YUAN, X., MANI, S., PESTELL, R. G. & WU, K. 2017. Recent advances of highly selective CDK4/6 inhibitors in breast cancer. *J Hematol Oncol,* 10**,** 97.

YANG, L. P., WU, L. M., GUO, X. J., LI, Y. & TSO, M. O. M. 2008. Endoplasmic reticulum stress is activated in light-induced retinal degeneration. *Journal of Neuroscience Research,* 86**,** 910-919.

YANG, Y. A. & YU, J. 2015. Current perspectives on FOXA1 regulation of androgen receptor signaling and prostate cancer. *Genes Dis,* 2**,** 144-151.

YAO, K., LEE, E. S., BENTREM, D. J., ENGLAND, G., SCHAFER, J. I., O'REGAN, R. M. & JORDAN, V. C. 2000. Antitumor action of physiological estradiol on tamoxifen-stimulated breast tumors grown in athymic mice. *Clin Cancer Res,* 6**,** 2028-36.

YI, P., WANG, Z., FENG, Q., PINTILIE, G. D., FOULDS, C. E., LANZ, R. B., LUDTKE, S. J., SCHMID, M. F., CHIU, W. & O'MALLEY, B. W. 2015. Structure of a biologically active estrogen receptor-coactivator complex on DNA. *Mol Cell,* 57**,** 1047-1058.

Pharmacology and Molecular Mechanisms of Clinically Relevant Estrogen Estetrol and Estrogen Mimic BMI-135 for the Treatment of Endocrine-Resistant Breast Cancer [S]

Balkees Abderrahman, Philipp Y. Maximov, Ramona F. Curpan, Jay S. Hanspal, Ping Fan, Rui Xiong, Debra A. Tonetti, Gregory R.J. Thatcher, and V. Craig Jordan

Department of Breast Medical Oncology, University of Texas MD Anderson Cancer Center, Houston, Texas (B.A., P.Y.M., J.S.H., P.F., V.C.J.); Coriolan Dragulescu Institute of Chemistry, Romanian Academy, Timisoara, Romania (R.F.C.); and Department of Pharmaceutical Sciences, University of Illinois at Chicago, Chicago, Illinois (R.X., D.A.T., G.R.J.T.)

Received May 2, 2020; accepted July 28, 2020

ABSTRACT

Long-term estrogen deprivation (LTED) with tamoxifen (TAM) or aromatase inhibitors leads to endocrine-resistance, whereby physiologic levels of estrogen kill breast cancer (BC). Estrogen therapy is effective in treating patients with advanced BC after resistance to TAM and aromatase inhibitors develops. This therapeutic effect is attributed to estrogen-induced apoptosis via the estrogen receptor (ER). Estrogen therapy can have unpleasant gynecologic and nongynecologic adverse events. Here, we study estetrol (E_4) and a model Selective Human ER Partial Agonist (ShERPA) BMI-135. Estetrol and ShERPA TTC-352 are being evaluated in clinical trials. These agents are proposed as safer estrogenic candidates compared with 17β-estradiol (E_2) for the treatment of endocrine-resistant BC. Cell viability assays, real-time polymerase chain reaction, luciferase reporter assays, chromatin immunoprecipitation, docking and molecular dynamics simulations, human unfolded protein response (UPR) RT^2 PCR profiler arrays, live cell microscopic imaging and analysis, and annexin V staining assays were conducted. Our work was done in eight biologically different human BC cell lines and one human endometrial cancer cell line, and results were compared with full agonists estrone, E_2, and estriol, a benchmark partial agonist triphenylethylene bisphenol (BPTPE), and antagonists 4-hydroxytamoxifen and endoxifen. Our study shows the pharmacology of E_4 and BMI-135 as less-potent full-estrogen agonists as well as their molecular mechanisms of tumor regression in LTED BC through triggering a rapid UPR and apoptosis. Our work concludes that the use of a full agonist to treat BC is potentially superior to a partial agonist given BPTPE's delayed induction of UPR and apoptosis, with a higher probability of tumor clonal evolution and resistance.

SIGNIFICANCE STATEMENT

Given the unpleasant gynecologic and nongynecologic adverse effects of estrogen treatment, the development of safer estrogens for endocrine-resistant breast cancer (BC) treatment and hormone replacement therapy remains a priority. The naturally occurring estrogen estetrol and Selective Human Estrogen-Receptor Partial Agonists are being evaluated in endocrine-resistant BC clinical trials. This work provides a comprehensive evaluation of their pharmacology in numerous endocrine-resistant BC models and an endometrial cancer model and their molecular mechanisms of tumor regression through the unfolded protein response and apoptosis.

Introduction

In 1944, Sir Alexander Haddow used high-dose synthetic estrogen therapy to treat metastatic breast cancer (MBC) (Haddow et al., 1944) in patients who were long-term (≥5 years past menopause) estrogen-deprived (LTED) (Haddow, 1970). A 30% response rate was reported. High-dose estrogen therapy was used for 30 years prior to the introduction of tamoxifen (TAM) (Jordan, 2003). Tamoxifen was preferred because of

the lower incidence of adverse events (AEs) (Cole et al., 1971; Ingle et al., 1981). In the 1970s, the translational research proposal of long-term adjuvant antihormone TAM therapy was successfully advanced (Jordan et al., 1979; Jordan and Allen, 1980). This strategy established TAM as the agent of choice for adjuvant therapy (Early Breast Cancer Trialists' Collaborative Group, 1998).

Acquired resistance to TAM therapy in vivo initially involves the growth of breast cancer (BC) populations within 1 to 2 years that are TAM- and estrogen-dependent (Gottardis and Jordan, 1988; Gottardis et al., 1989b). Subsequent studies in vivo demonstrated that 5 years of TAM treatment (mimicking the standard of care period at the time) leads to new BC populations that grow with TAM but die with physiologic levels of estrogen (Wolf and Jordan, 1993; Yao et al., 2000). This discovery explained (Jordan, 2008) why high-dose estrogen therapy was only effective ≥5 years past menopause in Haddow's original clinical studies (Haddow, 1970).

Physiologic estrogen in LTED BC cells triggers a cellular stress response named the unfolded protein response (UPR) and induces apoptosis (Song et al., 2001; Lewis et al., 2005a; Ariazi et al., 2011). Hosford et al. (2019) confirmed the involvement of the UPR and apoptosis in patient-derived estrogen-deprived estrogen receptor (ER)-positive xenografts treated with 17β-estradiol (E_2). This UPR and apoptosis–paired biology underpinning estrogen-induced tumor regression not only explains the earlier observational clinical science (Haddow, 1970) but also reaffirms estrogen's therapeutic potential for the treatment of endocrine-resistant BC.

Lønning et al. (2001) used high-dose estrogen therapy in postmenopausal women with advanced endocrine-resistant BC (median deprivation of 4 years). The conjugated equine estrogen arm in the Women's Health Initiative trial and its long-term follow-up (Anderson *et al.*, 2004; Chlebowski *et al.*, 2020; Jordan, 2020) unintentionally illustrated the clinical relevance of estrogen-induced tumor regression (Abderrahman and Jordan, 2016). The Women's Health Initiative trial had more than 75% of the postmenopausal women LTED for 10 years past menopause. When given estrogen replacement therapy, there were significant decreases in BC incidence and mortality (Anderson *et al.*, 2004; Roehm, 2015; Chlebowski *et al.*, 2020). Ellis et al. (2009) demonstrated the antitumor actions of low-dose estrogen therapy in postmenopausal women with advanced adjuvant aromatase inhibitor–resistant BC (deprivation ≥2 years). Iwase et al. (2013), using ethinylestradiol in patients with MBC (median age 63 years), had a 56% clinical benefit rate. Chalasani et al. (2014), using E_2 during 3-month exemestane breaks in patients with MBC, had measurable clinical activity. These clinical studies reaffirm the earlier laboratory findings that estrogen treatment after LTED with TAM in vivo leads to BC regression (Yao et al., 2000).

These in vivo and in vitro studies and clinical trials support the clinical benefit of using estrogen alone or in combination with growth inhibitors and/or apoptosis promoters for the treatment of endocrine-resistant BC. Nonetheless, concerns regarding AEs require the development of safer estrogens.

There are four naturally occurring forms of estrogen (Fig. 1): estrone (E_1), E_2, estriol (E_3), and estetrol (E_4).

Estetrol (Fig. 1), produced by the fetal liver during pregnancy (Holinka et al., 2008), is proposed as a promising estrogen for the treatment of advanced BC (Singer et al., 2014; Coelingh Bennink et al., 2017; Verhoeven et al., 2018; Schmidt et al., 2020), advanced prostate cancer (Dutman et al., 2017), use in hormone replacement therapy (Gérard et al., 2015; Coelingh Bennink et al., 2016; https://clinicaltrials.gov/ct2/show/NCT02834312), and in contraception (Creinin et al., 2019). In preclinical models, E_4 selectively activates the nuclear ERα, which plays a prominent role in the vasculoprotective action of estrogens (Abot et al., 2014). An ongoing phase I/IIA clinical trial of E_4 (Schmidt et al., 2020) shows the majority of patients experience favorable effects on wellbeing, and one patient completed both phases with stable disease after 24 weeks of treatment.

Selective Human ER Partial Agonists (ShERPAs), also known as selective estrogen mimics (Fig. 1), are novel benzothiophene [raloxifene (Ralox) or arzoxifene] derivatives with nanomolar potency designed to treat endocrine-resistant BC (Molloy et al., 2014; Xiong et al., 2016). The ShERPAs BMI-135 and TTC-352 were shown to cause tumor regression in TAM-resistant BC xenograft models and not to cause significant estrogen-like uterine growth in these models (Molloy et al., 2014; Xiong et al., 2016). An ongoing phase I clinical trial of TTC-352 (O'Regan et al., 2019) shows manageable safety and early clinical evidence of activity in patients with MBC progressing on endocrine therapy.

Given the clinical relevance of E_4 and ShERPAs, here we expand the study of their pharmacology in a broad range of BC and endometrial cancer cell lines and delineate their antitumor molecular mechanisms through triggering the UPR and apoptosis in select LTED and endocrine-resistant BC models.

Materials and Methods

Cell Culture and Reagents. E_1, E_2, E_3, E_4, and 4-hydroxyTAM (4OHT) were purchased from Sigma-Aldrich (St. Louis, MO). Endoxifen was purchased from Santa Cruz Biotechnology (Santa Cruz, CA), Ralox was purchased from Sigma-Aldrich, and ICI 182,780 fulvestrant (ICI) was purchased from Tocris Bioscience (Bristol, UK). Triphenylethylene bisphenol (BPTPE) was originally synthesized at the Organic Synthesis Facility, Fox Chase Cancer Center (Philadelphia, PA) (Maximov et al., 2010). The ShERPA BMI-135 was a gift from Dr. Debra Tonetti and Dr. Gregory R.J. Thatcher (University of Chicago, IL). The protein kinase regulated by RNA-like EnR kinase (PERK) inhibitor GSK G797800 was purchased from Toronto Research Chemicals (Toronto, ON, Canada). The inositol-requiring enzyme 1 (IRE1α) Inhibitor MKC-3946 was purchased from Calbiochem (San Diego, CA). Thioflavin T (ThT) was purchased from Sigma-Aldrich. All compounds except BMI-135 and E_4 were dissolved in ethanol, stored at $-20°C$, and protected from light. Compounds BMI-135 and E_4 were dissolved in DMSO. Wild-type (WT) estrogen-dependent BC cell line MCF-7:WS8 (Jiang et al., 1992); mutant p53 estrogen-dependent BC cell line T47D:A18 (Murphy et al., 1990b); the first in vitro cellular model recapitulating acquired-TAM resistance developed in athymic mice in vivo MCF-7:PF (Fan et al., 2014); estrogen-responsive, ER-positive, progesterone receptor–positive, and human epidermal growth factor receptor 2–positive luminal B BC cell line BT-474 (Kraus et al., 1987); estrogen-responsive, ER-positive, progesterone receptor–positive, and androgen receptor–positive luminal A BC cell line ZR-75-1 (Engel et al., 1978); antihormone-resistant estrogen-independent BC cell line MCF-7:5C (Lewis et al., 2005b); antihormone-sensitive estrogen-independent BC cell line MCF-7:2A (Pink et al., 1995); and antihormone (Ralox)-resistant estrogen-independent BC cell line MCF-7:RAL (Liu et al., 2003) were cultured

ABBREVIATIONS: AE, adverse event; ATF, activating transcription factor; BC, breast cancer; BPTPE, triphenylethylene bisphenol; ChIP, chromatin immunoprecipitation; CT, cycle threshold; DBPS, Dulbecco's phosphate-buffered saline; E_1, estrone; E_2, 17β-estradiol; E_3, estriol; E_4, estetrol; EnR, endoplasmic reticulum; ER, estrogen receptor; ERAD, EnR-associated degradation; ERE, estrogen-responsive element; FITC, fluorescein isothiocyanate; GREB1, Growth Regulation by Estrogen in Breast Cancer 1; ICI, ICI 182,780 fulvestrant; IRE1α, inositol-requiring enzyme 1; LBD, ligand-binding domain; LTED, long-term estrogen deprivation; MBC, metastatic BC; MBTPS1, Membrane Bound Transcription Factor Peptidase, Site 1; MD, molecular dynamics; 4OHT, 4-hydroxyTAM; PCR, polymerase chain reaction; PERK, protein kinase regulated by RNA-like EnR kinase; PI, propidium iodide; Ralox, raloxifene; RMSD, root-mean-square deviation; RMSF, root-mean-square fluctuation; RT-PCR, real-time PCR; SERM, Selective Estrogen Receptor Modulator; ShERPA, Selective Human Estrogen Receptor Partial Agonist; SRC-3, steroid receptor coactivator 3; TAM, tamoxifen; TFF1, trefoil factor 1; ThT, Thioflavin T; TPE, triphenylethylene; UPR, unfolded protein response; WT, wild type.
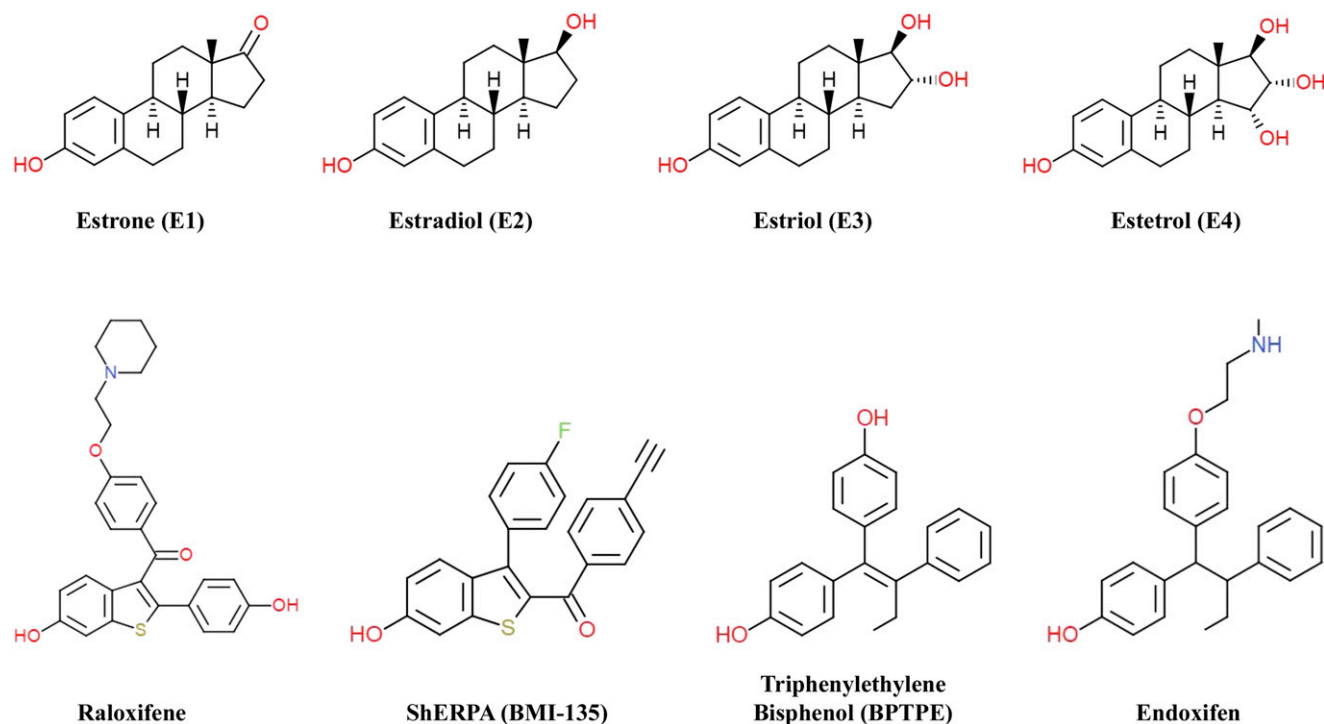
Fig. 1. Chemical structures of naturally occurring estrogens (E_1, E_2, E_3, and E_4), SERM raloxifene, synthesized ShERPA BMI-135 based on the benzothiophene scaffold of raloxifene, partial agonist BPTPE, and SERM endoxifen. The estrogen E_2 is the most potent estrogen. However, E_1 is generally 12 times less potent than E_2, and E_3 is generally 80 times less potent than E_2.

as previously described. Human endometrial adenocarcinoma cell line Ishikawa was cultured as previously described (Nishida et al., 1985). All cell cultures were done in T75 and T175 culture flasks (Thermo Fisher Scientific, Waltham, MA), passaged twice a week at 1:3 ratio, and grown in 5% CO_2 at 37°C. All cell lines were validated according to their short tandem repeat profiles at The University of Texas MD Anderson Cancer Center Characterized Cell Line Core. The short tandem repeat patterns of all cell lines were consistent with those from the Characterized Cell Line Core standard cells (Supplemental Table 1).

Cell Viability and Proliferation Assays. The biologic properties of test compounds (E_1, E_2, E_3, E_4, BMI-135, BPTPE, 4OHT, endoxifen, raloxifene, and ICI) in cells lines (MCF-7:WS8, T47D:A18, MCF-7:PF, BT-474, ZR-75-1, MCF-7:5C, MCF-7:2A, and MCF-7:RAL) were evaluated by assessing the DNA content of the cells as a measure of cell viability and proliferation using a DNA fluorescence Quantitation kit (Bio-Rad Laboratories, Hercules, CA) as previously described (Fan et al., 2013). The EC_{50} of all test compounds in different human BC and human endometrial cancer cell lines are summarized in

Table 1. EC_{50} was calculated using the formula: Y = Bottom + (Top-Bottom)/(1 + 10^(($LogEC_{50}$-X)*HillSlope)).

Real-Time Polymerase Chain Reaction. MCF-7:WS8 and MCF-7:5C cells were seeded into six-well plates at a density of 100,000 cells/well. Cells were treated the next day with test compounds (E_2, BMI-135, BPTPE, and endoxifen) for 24 hours. RNA isolation, cDNA synthesis, and real-time polymerase chain reaction (RT-PCR) were performed as previously described (Obiorah et al., 2014). All primers were obtained from Integrated DNA Technologies Inc. (IDT, Coralville, IA) and validated by melt-curve analysis that revealed single peaks for all primer pairs. The primer sequences used for human trefoil factor 1 (TFF1) cDNA amplification were: 5′-CAT CGACGTCCCTCCAGAAGA-3′ sense, 5′-CTCTGGGACTAATCACCG TGCTG-3′ antisense; human Growth Regulation by Estrogen in Breast Cancer 1 (GREB1) gene: 5′-CAAAGAATAACCTGTTGGCCC-TGC-3′sense, 5′-GACATGCCTGCGCTCTCATACTTA-3′ antisense; and the reference gene 36B4: 5′-GTGTCCGACAATGGCAGCAT-3′ sense, 5′-GACACCCTCCAGGAAGCGA-3′ antisense.

TABLE 1

EC_{50} of test compounds in different human BC and human endometrial cancer cell lines

The EC_{50} was calculated to indicate potency differences between test compounds used in treating these cell lines over a specific period of time (Figs. 2 and 4), as indicated in the table.

Cell Line	Time Frame	Compound	E_1	E_2	E_3	E_4	BMI-135
MCF-7:5C	1 wk	EC_{50} (−log [M])	−9.19	−10.89	−10.04	−8.73	−8.39
MCF-7:5C	2 wk		−10.00	-	−10.31	−9.30	−8.98
MCF-7:2A	2 wk		−8.99	−10.74	−9.14	−8.50	−8.29
MCF-7:RAL	1 wk		−11.11	−12.99	−9.13	−10.07	−9.97
MCF-7:RAL	2 wk		−8.93	−11.06	−9.04	−7.22	−9.24
MCF-7:RAL	3 wk		−9.53	−10.89	−9.75	−8.38	−7.47
MCF-7:PF	1 wk		−8.68	−10.67	−9.43	−8.52	−8.87
MCF-7:WS8	1 wk		−10.01	−11.92	−10.81	−9.80	−9.01
T47D:A18	1 wk		−9.33	−11.25	−10.01	−8.98	−8.87
BT-474	1 wk		-	−11.31	-	-	−8.71
ZR-75-1	1 wk		-	−11.39	-	-	−8.21
Ishikawa	1 wk		-	−10.97	-	−8.26	−8.57

Transient Transfection and Dual Luciferase Reporter Assays. Ishikawa cells were seeded into 24-well plates at a density of 100,000 cells/well. After 24 hours, cells were transfected with 28.8 μg of pERE(5X)TA-ffLuc and 9.6 μg of pTA-srLuc reporter plasmids using 3 μl of TransIT-LT1 transfection reagent (Mirus Biolabs, Madison, WI) per 1 μg of plasmid DNA in 52.5 ml of OPTI-MEM serum-free media (Invitrogen, Carlsbad, CA). Transfection mix containing the transfection complexes was added to cells in growth media to a final concentration of 0.3 μg pERE(5X)TA-ffLuc and 0.1 μg of pTA-srLuc reporter plasmids per well. After 18 hours, transfection reagents were removed, and fresh media were added instead. After 24 hours post-transfection, cells were treated with test compounds (E_2, E_4, BMI-135, BPTPE, and endoxifen) for 24 hours. After 24-hour treatment, cells were washed once with cold Dulbecco's phosphate-buffered saline (DPBS) (Invitrogen) and lysed, and the estrogen-responsive element (ERE) luciferase activity was determined using Dual-Luciferase Reporter Assay System (Promega, Madison, WI) according to manufacturer's instructions. Samples were quantitated on a Synergy H1 plate reader (BioTek Instruments Inc., Winooski, VT) in white-wall 96-well plates (Nalge Nunc International, Rochester, NY).

Chromatin Immunoprecipitation Assays. The chromatin immunoprecipitation (ChIP) assay was performed as previously described (Sengupta et al., 2010; Obiorah et al., 2014). The antibodies used for the pull-downs were anti-ERα clone F-10X mouse monoclonal (2 μg/μl; 5 μg per reaction) (Santa Cruz Biotechnology), anti–steroid receptor coactivator 3 (SRC-3) clone AX15.3 mouse monoclonal (1 μg/μl; 5 μg per reaction) (Abcam, Cambridge, UK), and normal mouse IgG as intraperitoneal negative control (2 μg/μl; 5 μg per reaction) (Santa Cruz Biotechnology). The DNA fragments were purified using Qiaquick polymerase chain reaction (PCR) purification kit (Qiagen, Germantown, MD). Then, 2 μl of eluted DNA was used for RT-PCR analysis. The primer sequences used were GREB1 proximal ERE enhancer site amplification: 5′-GTGGCAACTGGG TCATTCTGA-3′ sense and 5′-CGACCCACAGAAATGAAAAGG-3′ antisense (Integrated DNA Technologies). The data are expressed as percent input of starting chromatin material after subtracting the percent input pull-down of the intraperitoneal negative control.

Docking of BMI-135 to ERα. The experimental complex structure of TTC-352:ERα was employed for docking BMI-135:ERα because BMI-135 could not crystallize with the ER ligand-binding domain (LBD). The structure was prepared using Maestro software (Schrödinger Release 2019-3; Schrödinger, LLC, New York, NY, 2019) and Protein Preparation Wizard (Schrödinger Release 2019-3: Epik, Impact, Prime; Schrödinger, LLC, 2019). Briefly, the workflow involves the following steps: addition of hydrogen atoms, correction of bonds and bond order assignments, deletion of water molecules beyond 5 Å of a heteroatom, generation of ionization states at pH 7.4, and, finally, the restrained refinement of the ligand-receptor complex. The polar amino acids Asp, Glu, Arg, and Lys were modeled as charged and all Tyr were modeled as neutrals. The ligand was prepared for simulation using the LigPrep module (Schrödinger Release 2019-3; Schrödinger, LLC, 2019) in default settings. The experimental structure of ERα in complex with E_2 was resolved with Tyr537 mutated to Ser. Since all biologic experiments were performed against the WT receptor, we modeled the experimental structure by mutating Ser537 to Tyr using the Maestro software. Then, the residues within a range of 5 Å of Tyr537 were refined while the remaining protein-ligand complex was kept frozen. The ligand was docked to the active site of WT ERα using Induced Fit Docking (Schrödinger Release 2019-3: Glide, Prime; Schrödinger, LLC, 2019) based on Prime and Glide docking (Sherman et al., 2006a,b). This methodology takes into account the receptor's flexibility, allowing the side-chain and backbone movements in the binding site to better adjust to the shape and binding mode of the ligand. The grid was centered on the cocrystallized ligand, and the receptor van der Waals radii of the heavy atoms were scaled down to 0.5. The residues within 5 Å

of ligand poses were selected to be refined. The extraprecision option was selected for docking. The top 20–ranked ligand-receptor structures were retained, and the best docking solution was selected based on the Induced Fit Docking score and visual inspection.

Molecular Dynamics Simulations. Molecular dynamics (MD) simulations for the selected BMI-135:ERα complex were carried out with Desmond software (Schrödinger Release 2019-3, Schrödinger, LLC, 2019), utilizing the methodology previously described (Maximov et al., 2020). Briefly, the System Builder module of Desmond was used to solvate the ligand:receptor complex in a periodic orthorhombic water box based on the transferable intermolecular potential with 3 points (TIP3P) model. The charge neutrality of the system was guaranteed by adding sodium and chloride ions. To relax and equilibrate the system, Desmond's default relaxation protocol was employed. Minimization was followed by 50-nanosecond MD production run performed in periodic boundary conditions in the isothermal–isobaric (NPT) ensemble at constant pressure and temperature of 1 atm and 300 K, respectively. The integration time step and the recording interval of coordinates were set to 2 femtoseconds and 2 picoseconds, respectively. Trajectory analysis was carried out using the analysis tool Simulation Integration Diagram of Maestro. The root-mean-square deviation (RMSD) and root-mean-square fluctuation (RMSF) of the receptor backbone atoms relative to the reference structure were calculated and compared with the same metrics computed for the trajectories of ERα bound to E_2 and BPTPE, respectively [previously published (Maximov et al., 2020)]. The clustering algorithm of Desmond was used to extract the most representative frames of trajectory in terms of the conformational space sampling. The trajectory was clustered, the top 10 most-populated clusters were retained, and the representative structure of each cluster was extracted. Then, free binding energy calculations were performed with the Molecular Mechanics/Generalized Born Surface Area (MM-GBSA) method implemented in Schrödinger 2019-3 to select the best structure for analysis and comparison with the E_2 complex. Moreover, protein-ligand interactions (e.g., H-bonds and hydrophobic contacts) were monitored throughout the simulation. All graphs were prepared using the ggplot package of R software (R, version 3.2.3; The R Foundation, Vienna, Austria, 2015), and the figures were generated using PyMol 2.0 (Schrödinger, LLC, 2019).

Human Unfolded Protein Response RT[2] PCR Profiler PCR Arrays (Real-Time Profiler Assay). MCF-7:5C cells were seeded into six-well plates at a density of 200,000 cells/well for the 48- and 72-hour time points and 45,000 cells/well for day-7 time point. After 24 hours, cells were treated with test compounds (E_2, E_4, BMI-135, and BPTPE). Cells were harvested using Qiazol reagent (Qiagen, Hilden, Germany), and total RNA was isolated using an miRNeasy Mini Kit (Qiagen) according to manufacturer's instructions. During the RNA purification process, samples were treated with DNase using the RNase-Free DNase Set (Qiagen) according to manufacturer's instructions. The cDNA was reverse-transcribed using 2 μg of isolated RNA and the High Capacity cDNA Reverse Transcription Kit (Applied Bioscience, Carlsbad, CA) according to manufacturer's instructions. The cDNA was diluted 1:50, and a 2x RT[2] SYBR Green Mastermix (Qiagen) was used to prepare the reactions. The plates were loaded and run on a QuantStudio 6 Flex Real-Time PCR thermocycler (Applied Bioscience) according to manufacturer's instructions. The Ct values were exported at the end of each run, compiled, and uploaded to Qiagen's Data Analysis Center for analysis. For the volcano plots, the fold change [$2^{(-\Delta\Delta CT)}$] in the normalized gene expression [$2^{(-\Delta CT)}$] in the test sample divided the normalized gene expression [$2^{(-\Delta CT)}$] in the control sample. Fold regulation represents fold-change results in a biologically meaningful way. Fold-change values greater than one indicate a positive regulation or an upregulation, and the fold regulation is equal to the fold change. Fold-change values less than one indicate a negative regulation or down-regulation, and the fold regulation is the negative inverse of the fold

change. The P values of the volcano plots were calculated using a Student's t test of the replicate $2^{\wedge}(-\Delta CT)$ values for each gene in the control group and treatment groups.

Live Cell Imaging and Analysis. MCF-7:5C cells were seeded into 15 μ-slide two-well chambered coverslip slides (Ibidi, Martinsried, Germany) at a density of 300,000 cells/well for the 48-hour time point and at 200,000 cells/well for the 72-hour time point. After 24 hours, cells were treated with test compounds (E_2, E_4, BMI-135, and thapsigargin). On the day of live cell imaging, the green fluorescent dye ThT (UPR-indicative dye) (Sigma-Aldrich) was freshly prepared as previously described (Beriault and Werstuck, 2013), and the blue fluorescent live cell nuclear dye Hoechst 33342 (counterstain dye) (Thermo Fisher Scientific) was freshly prepared at a final concertation of 5 μg/ml. The staining with ThT was for 1 hour, and this was followed by substituting the culture media (containing test compounds and ThT) with PBS containing Hoechst 33342 for 15 minutes in a CO_2 incubator. Fluorescent images of MCF-7:5C live cells were taken at a 38-millisecond exposure under a 20×/0.7 objective with ZEISS Celldiscoverer 7 (Carl Zeiss AG, Oberkochen, Germany). Images were converted to 12-bit before being quantified by the ZEISS Zen Software Module-Image Analysis. Cells from each image were manually counted to normalize the fluorescent data per cell. Relative intensity per cell = ThT intensity/cell count and was generated for each treatment per image. A mean of the relative intensity per cell (using three images per treatment) was then calculated to give a final quantification alongside the S.D. The relative intensity per cell data are represented in Table 2. The excitation and emission settings were Hoechst 33342 (Excitation: 348 nm, Emission: 455 nm) and ThT (Excitation: 433 nm, Emission: 475 nm).

Annexin V–Staining Assays. MCF-7:5C cells were seeded into 10-cm Petri dishes at a density of 800,000 cells/dish for the 72- and 96-hour time points. MCF-7:2A cells were seeded into 10-cm Petri dishes at a density of 400,000 cells/dish for day-9 time point and at 100,000 cells/dish for day-13 time point. MCF-7:RAL cells were seeded into 10-cm Petri dishes at a density of 150,000 cells/dish for day-14, day-17, and day-21 time points. After 24 hours, cells were treated with test compounds (E_2, E_4, BMI-135, BPTPE, 4OHT, endoxifen, raloxifene, ICI, GSK G797800, and MKC-3946). Harvested cells were suspended in 1× binding buffer, and 1×10^5 cells were stained simultaneously with FITC-labeled annexin V and propidium iodide (PI) for 15 minutes at 37°C using the FITC Annexin V Apoptosis Detection Kit I (BD Pharmingen, San Diego, CA) according to the manufacturer's instructions. The cells were analyzed using a BD Accuri C6 plus flow cytometer.

Statistical Analyses. All data are mean ± S.D. of three different fields for each condition from three independent biologic experiments performed in technical duplicates. One-way ANOVA was used with

TABLE 2
Quantification of the UPR in live MCF-7:5C cells through measuring ThT relative intensity/cell

(A) ThT relative intensity/cell (mean and S.D.) with test compounds after 48-hour treatments. (B) ThT relative intensity/cell (mean and S.D.s) after 72-hour treatments. This reflects the differential capacity of test compounds in inducing EnR stress over time. ThT relative intensity/cell per treatment is representative of three biologic repeats.

Compound	(A) Day 2 Relative Intensity/Cell (Mean)	S.D.
Veh	0.276	0.052
Thapsigargin	0.875	0.061
E_4	1.245	0.073
E_2	0.741	0.097
BMI-135	0.497	0.047
Compound	(B) Day 3 Relative Intensity/Cell (Mean)	S.D.
Veh	0.296	0.057
Thapsigargin	10.055	0.068
BMI-135	4.878	0.049

a follow-up Tukey's test to determine the statistical significance of the treatments.

Results

Effects of E_4 and BMI-135 on Cell Viability and Proliferation in Numerous BC Models. Cell viability and proliferation assays were used to investigate the biologic properties of test compounds. Estetrol and ShERPA BMI-135 display activity similar to E_2 but right shifted across eight BC cell lines that are estrogen-dependent (MCF-7:WS8, T47D: A18, MCF-7:PF, BT-474, and ZR-75-1), estrogen-independent (MCF-7:5C, MCF-7:2A, and MCF-7:RAL), endocrine-sensitive (MCF-7:2A), endocrine-resistant (MCF-7:PF, MCF-7:5C, and MCF-7:RAL), mutant p53 (T47D:A18), human epidermal growth factor receptor 2–positive (BT-474), luminal A (ZR-75-1), and luminal B (BT-474).

The concentration 1 μM for E_4 and BMI-135 achieved either the maximal cellular growth (Fig. 2, A–E; Supplemental Fig. 1, A–C), or the maximal cellular death (Fig. 2, F–H; Supplemental Fig. 1, D–F). Both were shown to be less potent full agonists compared with E_2, requiring higher concentrations to produce the same maximal effect of E_2. The EC_{50} for all test compounds used in treating these cell lines are summarized in Table 1.

In MCF-7:5C, E_4 and BMI-135 almost completely reduced the amount of viable MCF-7:5C cells after 1 week of treatment in a dose-dependent manner, with a maximum reduction of cells by an average of 58% for E_4 and 46% for BMI-135 at their highest concentration of 10^{-6} M ($P < 0.05$ compared with vehicle) (Fig. 2F). Reduction in the amount of viable MCF-7:5C cells by E_2 at 10^{-9} M was by an average of 58% (Fig. 2F). In MCF-7:2A, E_4 and BMI-135 almost completely reduced the amount of viable MCF-7:2A cells after a 2-week treatment in a dose-dependent manner, with a maximum reduction of cells by an average of 57% for E_4 and 50% for BMI-135 at their highest concentration of 10^{-6} M ($P < 0.05$ compared with vehicle) (Fig. 2G). Reduction in the amount of viable MCF-7: 2A cells by E_2 at 10^{-9} M was by an average of 67% (Fig. 2G). In MCF-7:RAL, E_4 and BMI-135 almost completely reduced the amount of viable MCF-7:RAL cells after a 3-week treatment in a dose-dependent manner, with a maximum reduction of cells by an average of 45% for E_4 and 43% for BMI-135 at their highest concentration of 10^{-6} M ($P < 0.05$ compared with vehicle) (Fig. 2H). Reduction in the amount of viable MCF-7: RAL cells by E_2 at 10^{-9} M was by an average of 45% (Fig. 2H).

Effects of E_4 and BMI-135 Are Mediated via ERα. MCF-7:5C, MCF-7:2A, and MCF-7:RAL representing LTED estrogen-independent BC were treated with 1 μM E_4, 1 μM BMI-135, and a combination of these with 1 μM 4OHT and 1 μM endoxifen to investigate whether E_4 and BMI-135 exert their function via ERα. In MCF-7:5C, full estrogen agonists should cause cellular death within 1 week, antagonists should not (i.e., MCF-7:5C is endocrine-resistant), and the agonists' pairing with the antagonists should block the death effect. Indeed, E_2, E_4, and BMI-135 killed the cells within 1 week ($P < 0.05$ compared with vehicle) (Supplemental Fig. 2A), whereas 4OHT and endoxifen did not ($P < 0.05$ compared with vehicle) (Supplemental Fig. 2A). The combination of E_2, E_4, and BMI-135 with 4OHT and endoxifen blocked the death effect (Supplemental Fig. 2A).

In MCF-7:2A, full agonists should cause cellular death within 2 weeks, antagonists should cause growth inhibition
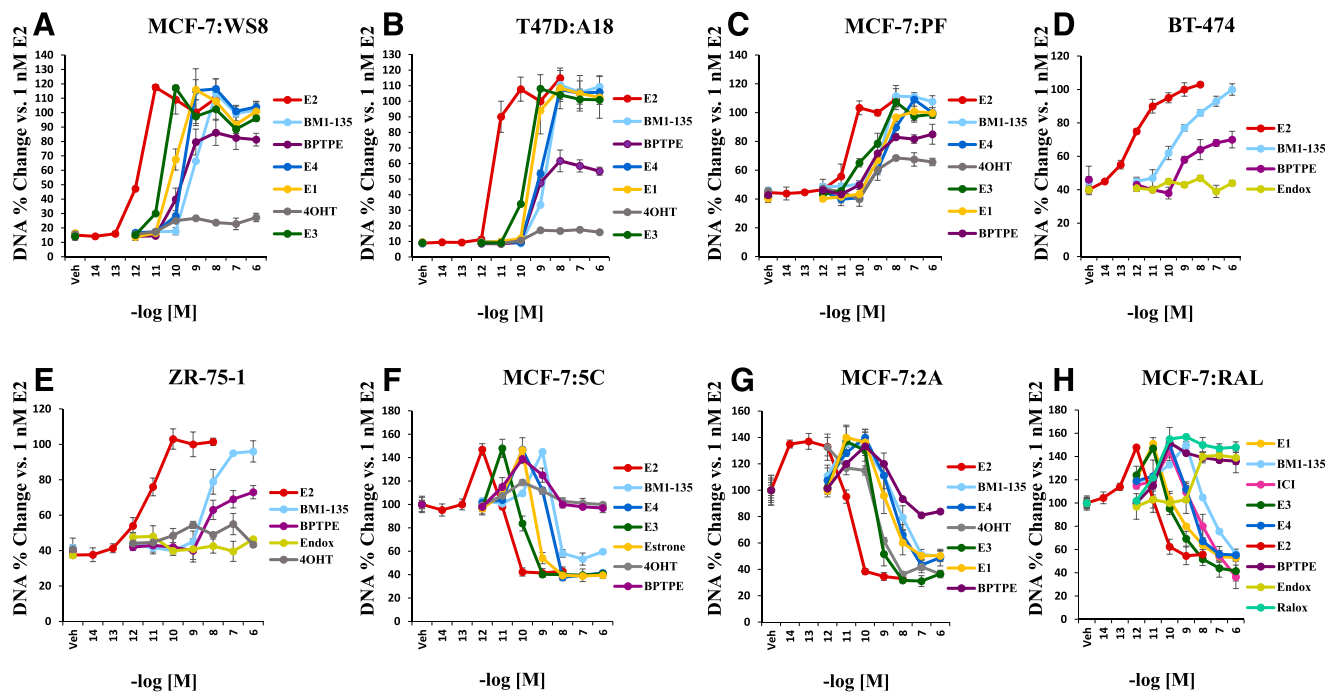
Fig. 2. Cell viability and proliferation assays in multiple BC cell lines with test compounds. (A) Effects of test compounds alone after 7 days of treatment (percent DNA of vehicle vs. test compounds' concertation) in MCF-7:WS8. (B) Effects of test compounds alone after 7 days of treatment in T47D:A18. (C) Effects of test compounds alone after 7 days of treatment in MCF-7:PF. (D) Effects of test compounds alone after 7 days of treatment in BT-474. (E) Effects of test compounds alone after 7 days of treatment in ZR-75-1. (F) Effects of test compounds alone after 7 days of treatment in MCF-7:5C. (G) Effects of test compounds alone after 14 days of treatment in MCF-7:2A. (H) Effects of test compounds alone after 21 days of treatment in MCF-7:RAL. Endox, endoxifen.

(i.e., MCF-7:2A is endocrine-sensitive), and the agonists' pairing with the antagonists should block the death effect. Indeed, E_2, E_4, and BMI-135 killed the cells within 2 weeks ($P < 0.05$ compared with vehicle) (Supplemental Fig. 2B), whereas 4OHT and endoxifen caused growth inhibition ($P < 0.05$ compared with vehicle) (Supplemental Fig. 2B). The combination of E_2, E_4, and BMI-135 with 4OHT and endoxifen blocked the death effect (Supplemental Fig. 2B).

In MCF-7:RAL cells, full agonists should cause cellular death within 2 to 3 weeks in vitro; antagonists, especially Selective ER Modulator (SERM) raloxifene (positive control), should cause cellular growth; and the agonists' pairing with antagonists should block the death effect. Indeed, E_2, E_4, and BMI-135 killed the cells within 3 weeks ($P < 0.05$ compared with vehicle) (Supplemental Fig. 2C), whereas the SERMs 4OHT, endoxifen, and especially raloxifene caused cellular growth ($P < 0.05$ compared with vehicle) (Supplemental Fig. 2C). The combination of E_2, E_4, and BMI-135 with 4OHT and endoxifen blocked the death effect (Supplemental Fig. 2C). Interestingly, ICI (a selective ER downregulator or "pure antiestrogen") caused a decrease in cell DNA amount in MCF-7:RAL cells after a 3-week treatment ($P < 0.05$ compared with vehicle) (Supplemental Figs. 1F and 2C).

Endoxifen, the major biologically active metabolite of TAM, was used as an antiestrogenic control alongside 4OHT and neither induced an increase or decrease in viable cells ($P < 0.05$ compared with vehicle controls) (Supplemental Fig. 2A). Only in MCF-7:2A cells did 4OHT and endoxifen cause growth inhibition (Supplemental Fig. 2B), and in MCF-7:RAL cells, both caused growth stimulation (Supplemental Fig. 2C), as predicted.

BMI-135 Induces the Transcriptional Activity of ERα Similar to E_2 in WT MCF-7:WS8 and Apoptotic-Type

MCF-7:5C BC Models. Quantitative RT-PCR was used to assess the transcriptional activity of ERα on ERE genes (*TFF1* and *GREB1*) with test compounds. After 24-hour treatment in MCF-7:WS8 cells, BMI-135 increased the levels of *TFF1* and *GREB1* mRNAs compared with vehicle controls ($P < 0.05$) (Fig. 3, A and B). On the other hand, the partial agonist BPTPE induced a partial increase in the levels of *TFF1* and *GREB1* mRNAs and less than that of full agonist E_2 ($P < 0.05$) and BMI-135 ($P < 0.05$) (Fig. 3, A and B). The minimal concentration that produced a complete increase in the levels of *TFF1* and *GREB1* was at 10^{-6} M for BMI-135 ($P < 0.05$ compared with vehicle) (Fig. 3, A and B).

After 24-hour treatment in MCF-7:5C cells, BMI-135 increased the levels of *TFF1* and *GREB1* mRNAs compared with vehicle controls ($P < 0.05$) (Fig. 3, C and D). On the other hand, BPTPE induced a partial increase in the levels of *TFF1* and *GREB1* mRNAs and less than that of E_2 ($P < 0.05$) and BMI-135 ($P < 0.05$) (Fig. 3, C and D). The minimal concentration that produced a complete increase in the levels of *TFF1* and *GREB1* was at 10^{-6} M for BMI-135 ($P < 0.05$ compared with vehicle) (Fig. 3, C and D).

The ERE-dependent transcriptional activity with E_4 was done by Abot et al. (2014) and showed an induction similar to E_2, only with a lower potency.

Overall, the induction of the mRNA levels of *TFF1* and *GREB1* by BMI-135 in MCF-7:WS8 and MCF-7:5C was similar to that by full agonist E_2, only at a lower potency.

Estetrol and BMI-135 Induce the Transcriptional Activity of ERα Similar to E_2 in Human Endometrial Cancer Model Ishikawa. Transient transfection and luciferase activity assays were used to determine the transcriptional activity of ERα on estrogen-responsive genes (*5xERE*) with test compounds as ERE dual luciferase activity. After
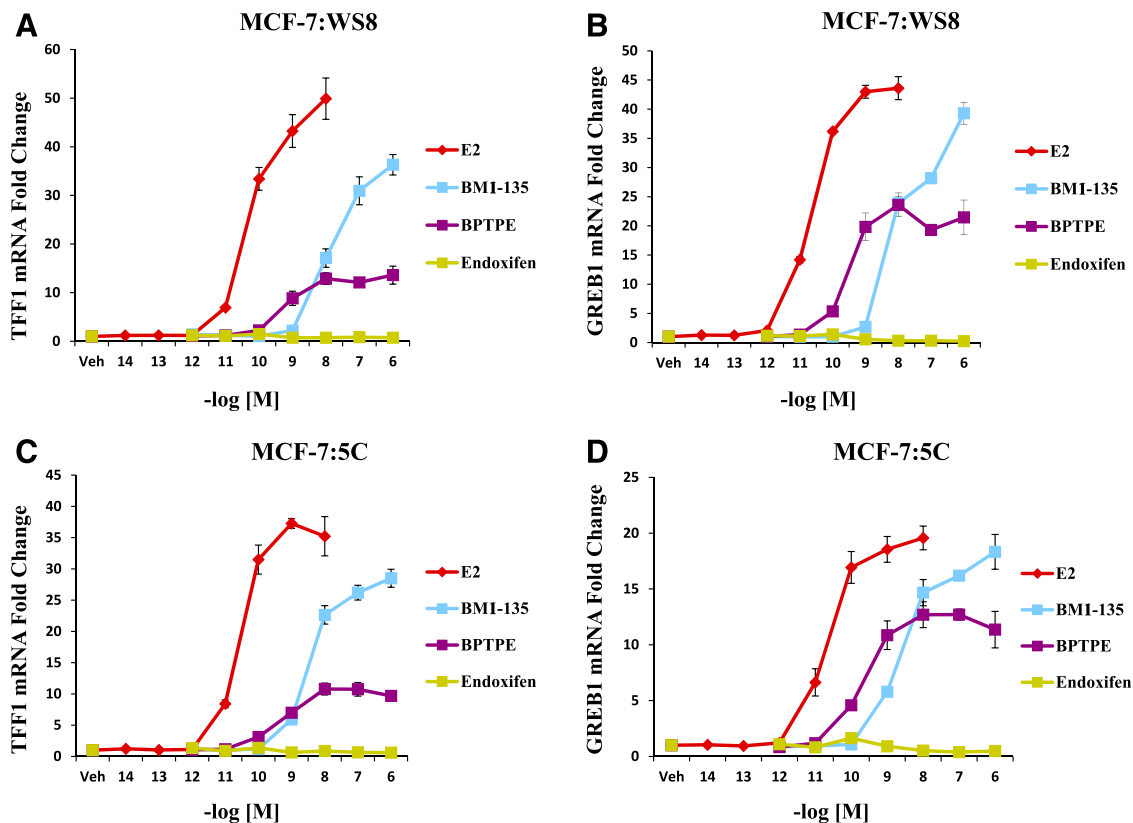
Fig. 3. Transcriptional activity of well characterized estrogen-responsive genes TFF1 (or pS2) and GREB1 in WT MCF-7:WS8 and LTED MCF-7:5C with test compounds. (A) mRNA expression of TFF1 in MCF-7:WS8 cells after 24-hour treatment with 1 nM E_2 and 1 μM for other test compounds. (B) mRNA expression of GREB1 in MCF-7:WS8 cells after 24-hour treatment with 1 nM E_2 and 1 μM for other test compounds. (C) mRNA expression of TFF1 in MCF-7:5C cells after 24-hour treatment with 1 nM E_2 and 1 μM for other test compounds. (D) mRNA expression of GREB1 in MCF-7:5C cells after 24-hour treatment with 1 nM E_2 and 1 μM for other test compounds. Data are mean ± S.D. from three independent experiments performed in triplicate analyzed by one-way ANOVA.

24-hour treatment of Ishikawa cells, E_4 and BMI-135 increased the levels of 5x-ERE luciferase activity compared with vehicle controls ($P < 0.05$) (Fig. 4A). On the other hand, the partial agonist BPTPE induced a partial increase in the levels of 5x-ERE luciferase activity and less than that of full agonist E_2, E_4, and BMI-135 ($P < 0.05$) at concentration range of 10^{-8}–10^{-6} M (Fig. 4A). The minimal concentration that produced a complete increase in the levels of 5x-ERE luciferase activity was at 10^{-7} M for E_4 and BMI-135 ($P < 0.05$ compared with vehicle) (Fig. 4A).

To determine whether the effects of E_4 and BMI-135 were mediated via ERα in Ishikawa cells, transiently transfected
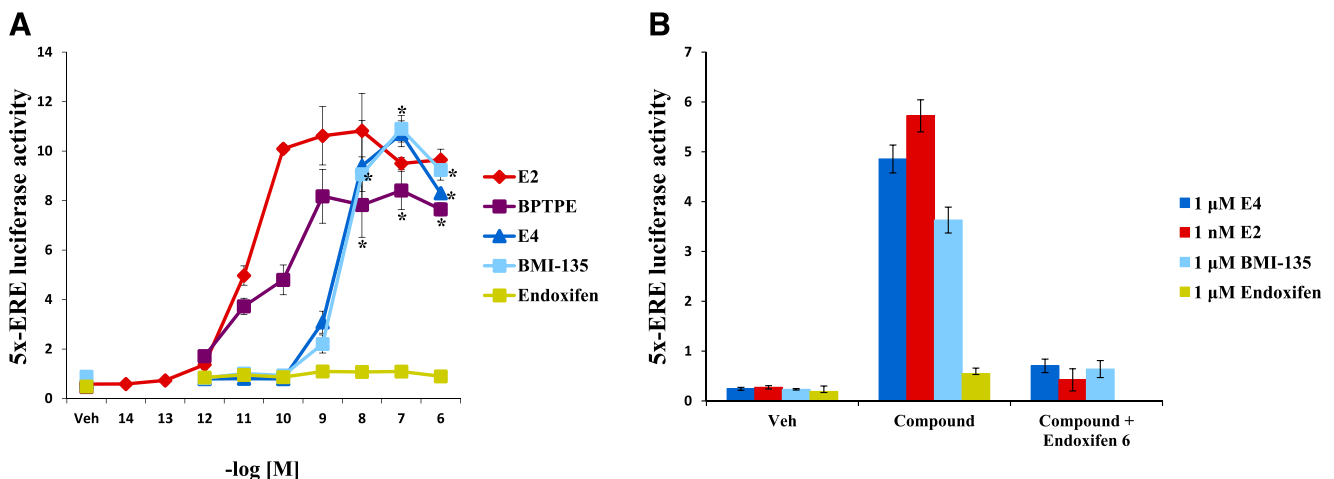
Fig. 4. Transient transfection of the human endometrial cancer cells Ishiskawa with 5x-ERE and dual luciferase activity assay. (A) Dose-response curve of test compounds vs. 5x-ERE luciferase activity (promoter activity = Firefly luciferase activity/*Renilla* luciferase activity). (B) 5x-ERE luciferase activity with indicated test compounds alone vs. in combination with 1 μM endoxifen. Data are mean ± S.D. from three independent experiments performed in triplicate analyzed by one-way ANOVA. *$P < 0.05$: statistical difference between E_4 or BMI-135 and BPTPE treatments over 10^{-8}–10^{-6} concentration range (*t* test). Veh, vehicle.

Ishikawa cells were treated with test compounds in combination with antagonist endoxifen for 24 hours, and luciferase activity assays were conducted (Fig. 4B). The increase in the levels of 5x-ERE luciferase activity with E_4 and BMI-135 was blocked with endoxifen treatment at 10^{-6} M ($P < 0.05$ compared with vehicle) (Fig. 4B). This confirms that E_4 and BMI-135 exert their function via Ishikawa's ERα. In addition, endoxifen alone did not increase the levels of 5x-ERE luciferase activity in Ishikawa cells, acting as an antagonist in this uterine model (Fig. 4B).

Overall, the induction of the levels of 5x-ERE luciferase activity by E_4 and BMI-135 in Ishikawa cells was similar to that by full agonist E_2, only at a lower potency (Table 1).

E_4 and BMI-135 Recruit ERα and SRC-3 to the *GREB1* Proximal Enhancer Region Similar to E_2 in MCF-7:5C BC Model. ChIP assays were used to assess the recruitment of ERα and SRC-3 to the *GREB1* proximal enhancer region with test compounds. Estetrol and BMI-135 treatments resulted in a very strong recruitment of ERα to the *GREB1* proximal enhancer region similar to E_2 and higher than that with the partial agonist BPTPE ($P < 0.05$) (Fig. 5A).

However, the recruitments of the coactivator SRC-3 to the *GREB1* proximal enhancer region with E_4 and BMI-135 treatments were higher than that with BPTPE ($P < 0.05$) (Fig. 5B). SRC-3 recruitment with E_2 was the highest. With E_4, there was an 18.72% recruitment reduction compared with E_2; with BMI-135, there was a 51.17% recruitment reduction compared with E_2; with BPTPE, there was a 65.47% recruitment reduction compared with E_2; and with endoxifen, there was a 98.14% recruitment reduction compared with E_2 (Fig. 5B).

Overall, the recruitment of ERα to the *GREB1* proximal enhancer region with E_4 and BMI-135 in MCF-7:5C cells was similar to that by full agonist E_2, and the recruitment of SRC-3 to the *GREB1* proximal enhancer region with E_4 and BMI-135 in MCF-7:5C cells was higher than that with the partial agonist BPTPE. Although SRC-3 recruitment with BMI-135 treatment was lower than that with E_2 ($P < 0.05$), it was higher than that with BPTPE ($P < 0.05$).

Analysis of E_4 and BMI-135's Binding Mode in Comparison with Full Agonist E_2 and Partial Agonist BPTPE. To outline the similarities and differences between BMI-135 and other investigated ligands (e.g., E_2, E_4, and BPTPE), their overall conformations and interactions with residues of the binding site were analyzed (Fig. 6; Supplemental Fig. 10, B–I). The BMI-135 ligand was docked into the experimental structure of the ERα:TTC-352 complex and adopted the canonical agonist conformation with helix 12 (H12) positioned over the binding pocket, sealing the ligand inside. We used the induced fit docking methodology because it allows flexibility for certain parts of the receptor (e.g., amino acids of the binding site). The top-ranked BMI-135–receptor pose and experimental structures of ERα bound to E_2, E_4, and BPTPE adopt the agonist conformation of ERα, with H12 sitting in a groove between H5 and H11 delineated by H3 and the ligands occupying the binding pocket composed of residues from helices H3, H6, H8, and H11 (Fig. 6, A, C, and E).

The predicted binding mode of BMI-135 shared, to some extent, the network of interactions specific to E_2, E_4, and BPTPE, as shown (Fig. 6, B, D, and F; Supplemental Fig. 10, F–I). The familiar H-bond network between a phenolic hydroxyl, Glu353, and Arg394 was common to ligands. The benzothiophene moiety of BMI-135 was implicated in π-π stacking interactions with Phe404 and made several additional contacts with Ala350 (H3), Leu387, Met388, and Leu391 (H6), similar to A and B rings of E_2. The two substituted phenyl rings were involved in hydrophobic contacts with Leu346 (H3), Ala350 (H3), Ile424 (H8), and Leu525 (H11), and the fluorine substituent was headed toward Thr347 (H3). The most apparent difference between BMI-135 and E_2 binding modes (also seen for BPTPE) was the absence of H-bond with the imidazole ring of His524. We noticed that the side chain of His524 was pushed toward the outer part of the protein by the bulkier ethinyl group of BMI-135, which hovered between helices H3, H8, and H11 in a space delineated by residues Met343 (H3), Val418 (H8), Met421 (H8), Leu525 (H11), and Met528 (H11) (Supplemental
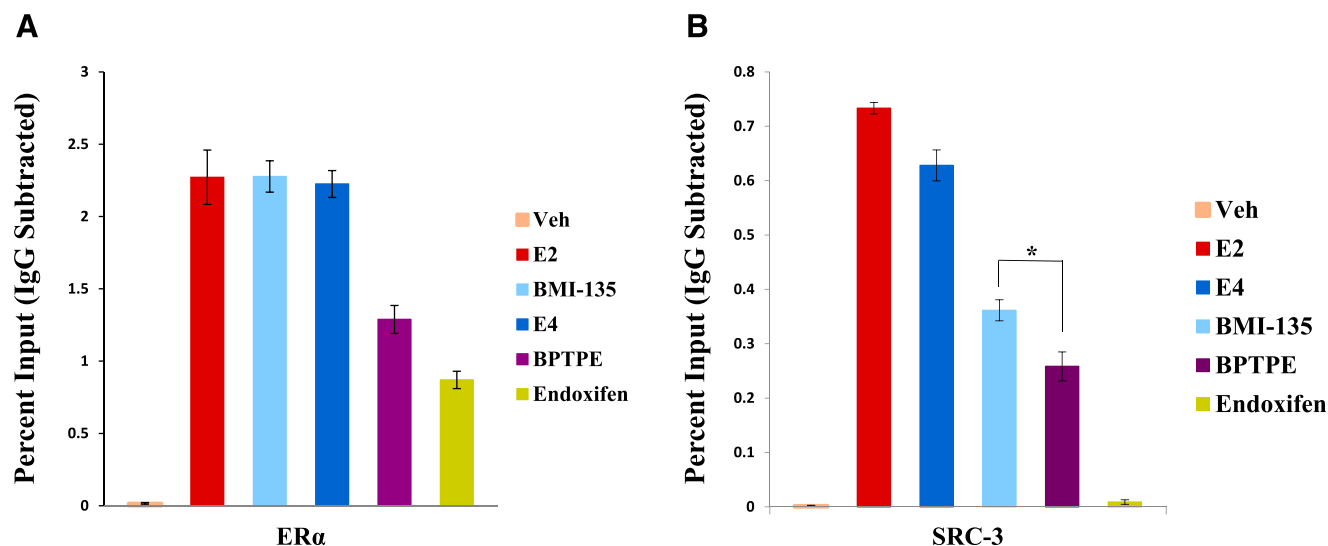
Fig. 5. ChIP assay in MCF-7:5C cells showing the recruitment of ERα and coactivator SRC-3 to TFF1 ERE promoter. Recruitment of ERα (A) and SRC-3 (B) after 45-minute treatment with indicated ligands; 1 nM E_2 and 1 μM for the rest of test compounds. Recruitment of ERα and SRC-3 was calculated as percentage of the total input after subtracting the IgG recruitment. All treatments were performed in triplicate; data represent the average of these replicates. *$P < 0.05$: statistical difference between BMI-135 and BPTPE treatments with SRC-3 recruitment. Veh, vehicle.
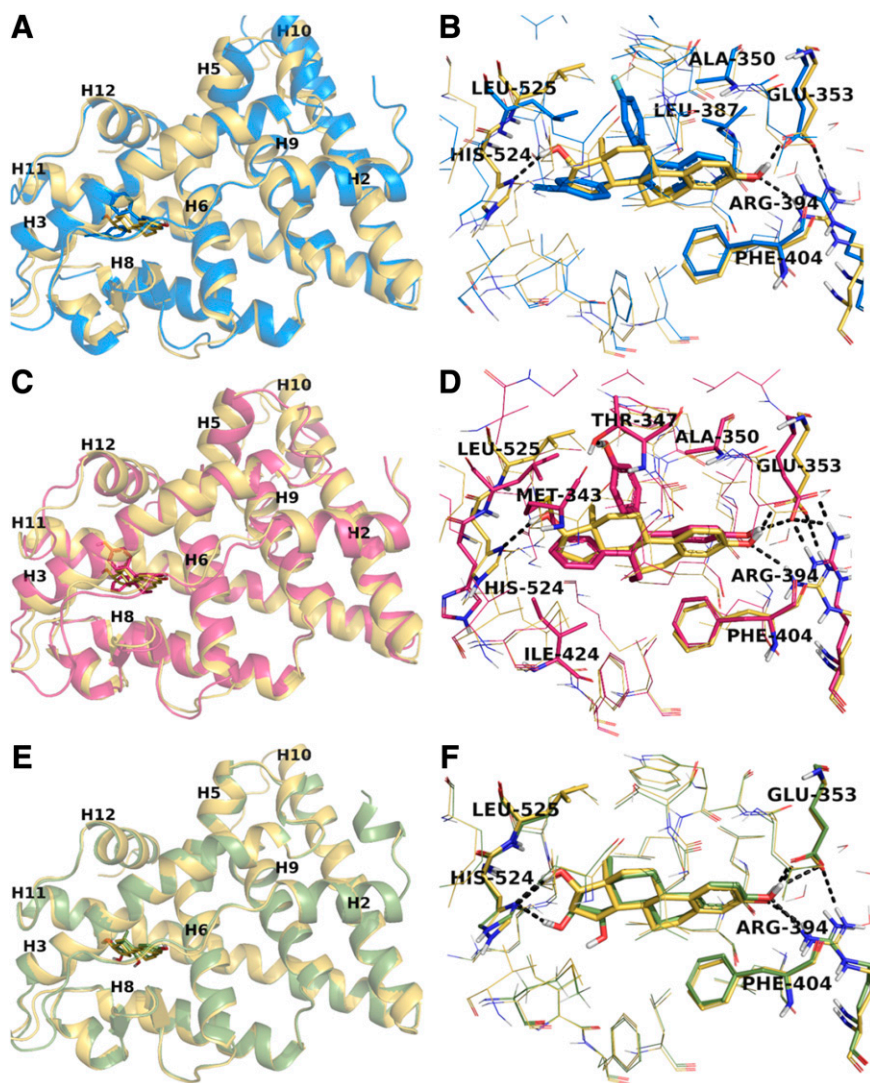
Fig. 6. Representations of ERα-LBD with E₂, E₄, BMI-135, and BPTPE. Comparison between the agonist conformation of ERα-LBD in complex with E₂, superimposed with BMI-135 (A), BPTPE (C), and E₄ (E) in similar conformations of the receptor. The helices forming the ligand-binding site are labeled together with helix 12 (H12), which defines the receptor conformation and those essential for the coactivator binding groove. The alignment in the binding site and the contacts between BMI-135 (B), BPTPE (D), E₄ (F), and critical amino acids of the binding pocket are revealed in comparison with the binding alignment of E₂. For BMI-135 and BPTPE, the most representative conformations extracted from MD trajectories are shown, whereas for E₂ and E₄, the experimental structures are presented. The ligand: receptor complexes are colored based on C atoms as follows: yellow for E₂, blue for BMI-135, magenta for BPTPE, and light green for E₄, whereas the N, O, and S atoms are colored in dark blue, red, and yellow, respectively. For clarity, the amino acids involved in critical contacts (i.e., H-bonds and π-π stacking) are shown as sticks together with those having contacts with occurrence frequencies during the MD trajectories larger than 40% of the simulation time. The remaining amino acids of the binding sites are shown as lines. The H-bonds redepicted as black dashed lines.

Fig. 10H). These flexible residues permitted the accommodation of the large etinylbenzoyl moiety in this part of the binding pocket.

A contact unique to BPTPE was the H-bond between the second phenolic group of the ligand and the OH group of Thr347 (Fig. 6D), whereas specific to E₄ was the involvement of the second OH group of the D ring into an extra H-bond to His524, adding stability to the ligand in the binding site (Fig. 6F). In addition, the hydrophobic contacts and π-π stacking interactions with Phe404 complemented the binding profile of these ligands (Supplemental Fig. 10, C, E, G, and I).

MD Simulations Analysis. To investigate the stability of BMI-135 in the binding site of ERα, the dynamics of the interactions, and how they compared with the interactions in the structures of E₂ and BPTPE, we performed MD simulations against the top-ranked ERα:BMI-135 complex, as previously described in *Materials and Methods*. The recorded trajectory was analyzed and compared with the trajectories previously reported (Maximov et al., 2020) for WT ERα bound to E₂ and BPTPE.

Firstly, we explored the conformational stability of the simulation. To ensure that the model had reached equilibrium, RMSDs of the protein backbone atoms, relative to their position in the first frame, were computed for trajectory. The RMSD evolution indicated that the system had reached equilibrium after approximately 5 nanoseconds, similar to the E₂ model (Supplemental Fig. 3A).

Next, to investigate the mobility of the protein and the dynamics of ligand binding, we monitored the RMSF of the residues along the trajectory (Supplemental Fig. 3A). Comparing the RMSF calculated for backbone atoms with the previously reported values for the runs of E₂ and BPTPE, we noticed a similar pattern for BMI-135 and E₂. There were several substantial fluctuations, which mainly overlapped with the flexible domains of the receptor (a significant peak located between residues 332–338 matches the loop connecting helices H2 and H3). The largest peak in all trajectories was situated between residues 456 and 469, part of the loop connecting H9 to H10, and missing in all experimental structures used in this analysis (Supplemental Fig. 3A). The high flexibility of this domain and the predicted coordinates for this loop could explain the observed fluctuation. Overall, the BMI-135 complex showed mobility domains matching with the E₂ system mainly positioned in connection loops, flexible regions of a protein. In addition, based on the previous analysis of the correlation between RMSF values and

B-factors for E_2 and BPTPE, we observed that the high RMSF values of protein fragments parallel with large B-factors.

Then, we explored the stability of the ligands relative to the protein and the binding site together with the internal fluctuations of ligands' atoms (Supplemental Fig. 3B). The analysis shows that BMI-135 did not fluctuate significantly and was stably bound in the active site, similar to E_2 and BPTPE, with average RMSD values of 0.8 ± 0.23 and 1.6 ± 0.34 Å, respectively (Supplemental Fig. 3B).

Analysis of BMI-135 Ligand-Protein Interactions in Modeled WT ERα Systems. We analyzed the binding dynamics of BMI-135 and assessed the stability of the interactions by monitoring the frequency of occurrence of that specific interaction throughout the trajectory. Overall, the computed variations of RMSF, based on the backbone and side-chain atoms, showed similar trends for E_2, BMI-135, and BPTPE (Supplemental Fig. 10A). The residues involved in H-bonds with the ligands (e.g., Thr347, Glu353, His524), π-π stacking, and hydrophobic contacts (e.g., Phe404, Ala350, Leu387) showed RMSF values that were smaller than average and fluctuated less, indicating stable contacts. This observation was also supported by the occurrence frequencies of these interactions monitored throughout the trajectory (Supplemental Fig. 11, A–C). A striking difference was noticed for BMI-135, which displayed the largest peak of side-chain RMSF for Arg394. This mobility indicated that Arg394 was not involved in a direct H-bond with the ligand and/or ionic bridges to Glu353, therefore not stabilizing it. However, H-bonds were sporadically monitored during the simulation between the ligand and Arg394 via a water bridge, with frequencies below 15%. Additionally, the bulkier substituents of BMI-135 displaced the amino acid and forced it not to adopt orientations proper for the binding.

Similarly to E_2, BMI-135 was stabilized by the H-bond to Glu353 and π-π stacking interactions with Phe404 but occurred in lower frequency. The hydrophobic contacts, mainly with residues Ala 350, Leu384, Leu 387, Met388, Leu391, Leu403, and Leu525, were stable for both ligands during the simulation time, however, in lower occurrence frequencies for BMI-135 (Supplemental Fig. 11, A and B). The H-bond to His524, which was very stable for E_2, was lacking for BMI-135 and BPTPE, but occasional hydrophobic contacts with the ethinyl-benzoyl moiety of BMI-135 were noticed. BPTPE mainly recapitulated the interactions mentioned above but with frequencies lower than those of E_2.

A distinctive feature of BPTPE is the H-bonding to Thr347, which occurred in over 95% of the trajectory (Supplemental Fig. 11C), indicating a very stable contact, and this was confirmed by the low RMSF value of the residue (Supplemental Fig. 10A). However, as previously shown, the H-bond to Thr347 prevented the formation of an H-bond between the side chains of Asn348 (H3) and Tyr537 (H11) (usually forming a stabilizing contact in the vicinity of H12) and, together with the phenol group of BPTPE, triggered a slightly different conformation of H12 (Maximov et al., 2020). Although the 4-fluoro-phenyl substituent of BMI-135 was oriented toward Thr347, the interaction Asn348-Tyr537 was not disturbed and occurred 52% of the simulation time but to a slightly lesser extent compared with E_2 (i.e., 70%); nonetheless, it is still significant. Another contact that added stability to the agonist conformation of the receptor was the interaction between the side chain of His524 and backbone of Glu419, which was found almost 80% of the time during the simulation of E_2. Surprisingly, this contact was observed in the trajectory of BMI-135 with a frequency of 72% of the simulation time.

Overall, these data show the confirmation of the BMI-135: ERα complex to be more similar to that of E_2, compared with that of BPTPE.

E_4 and BMI-135 Activate the UPR. Human UPR real-time profiler assays were used to assess the regulation of UPR genes with test compounds. Cell viability and proliferation assays showed a decline in MCF-7:5C cell DNA amount with E_2 and E_4 treatments at 72 hours (Fig. 7D). Furthermore, flow cytometry showed apoptosis at 72 hours (annexin staining 14.8% with E_2 and 12.6% with E_4 vs. vehicle control 4.5%) (Fig. 7E). The time point at 48 hours was chosen to investigate the terminal (or proapoptotic) UPR gene regulation with E_2 and E_4 treatments in MCF-7:5C cells, which precedes apoptosis by 72 hours.

After 48-hour treatment with 1 nM E_2 and 1 μM E_4 [i.e., these concentrations were shown earlier to trigger maximal cellular death (Fig. 2; Table 1)], the endoplasmic reticulum–associated degradation (ERAD) genes (downstream IRE1α/XBP1s and ATF6 p50), HTRA4 ($P < 0.001$), SYVN1 ($P < 0.001$), and HERPUD1 ($P < 0.001$), were downregulated (Fig. 7, B and C; Supplemental Fig. 5, A and B). The lipid or cholesterol metabolism genes (downstream IRE1α/XBP1s and ATF6 p50), MBTPS1 ($P < 0.001$) and SERP1 ($P < 0.001$), were downregulated with E_2 treatment, whereas only MBTPS1 ($P < 0.001$) was downregulated with E_4 (Fig. 7, B and C; Supplemental Fig. 5, A and B). The chaperone (chaperones are usually downstream IRE1α/XBP1s, PERK/P-eIF2α:ATF4, and ATF6 p50) gene SIL1 ($P < 0.001$) was downregulated with E_4 treatment (Fig. 7C; Supplemental Fig. 5B). By contrast, the genes CEBPB ($P < 0.001$) and INHBE ($P < 0.001$), which reflect high UPR stress, were upregulated (Fig. 7, B and C; Supplemental Fig. 5, A and B).

The heat map of MCF-7:5C cells with E_2 and E_4 treatments at 48 hours displays a general UPR gene downregulation (situated on the right side of the heat map) compared with vehicle control (situated on the left) (Fig. 7A). The majority of the profiler assays' genes belong to the lipid metabolism, ERAD, and chaperone gene groups, which are considered prosurvival mechanisms that help the cells cope with extrinsic or intrinsic cellular stress (Fig. 9). This general downregulation by 48 hours (Fig. 7, B and C; Supplemental Fig. 5, A and B) highlights MCF-7:5C cells' proapoptotic UPR phase and programming to undergo apoptosis by 72 hours (Fig. 7E).

Cell viability and proliferation assays showed a decline in MCF-7:5C cell DNA amount with BMI-135 treatment by 96 hours (Fig. 8D). Furthermore, flow cytometry showed apoptosis by 96 hours (annexin staining 17.1% with BMI-135 vs. vehicle control 5.7%) (Fig. 8E). The time point of 72 hours was chosen to investigate the proapoptotic UPR gene regulation with BMI-135 treatment in MCF-7:5C cells, which preceded apoptosis by 96 hours. Another time point of 48 hours was chosen to compare and contrast the UPR gene regulation with that by 72 hours and show how this regulation is dynamic and culminates over time.

After 48-hour treatment with 1 μM BMI-135, the ERAD genes EDEM1 ($P < 0.001$), HTRA4 ($P < 0.001$), SYVN1 ($P < 0.001$), and HERPUD1 ($P < 0.001$) were downregulated (Fig. 8C; Supplemental Fig. 5C). The lipid metabolism genes MBTPS1 ($P < 0.001$) and SERP1 ($P < 0.001$) were downregulated (Fig. 8C; Supplemental Fig. 5C). By contrast, the genes CEBPB ($P < 0.001$) and INHBE ($P < 0.001$) were upregulated (Fig. 8C;
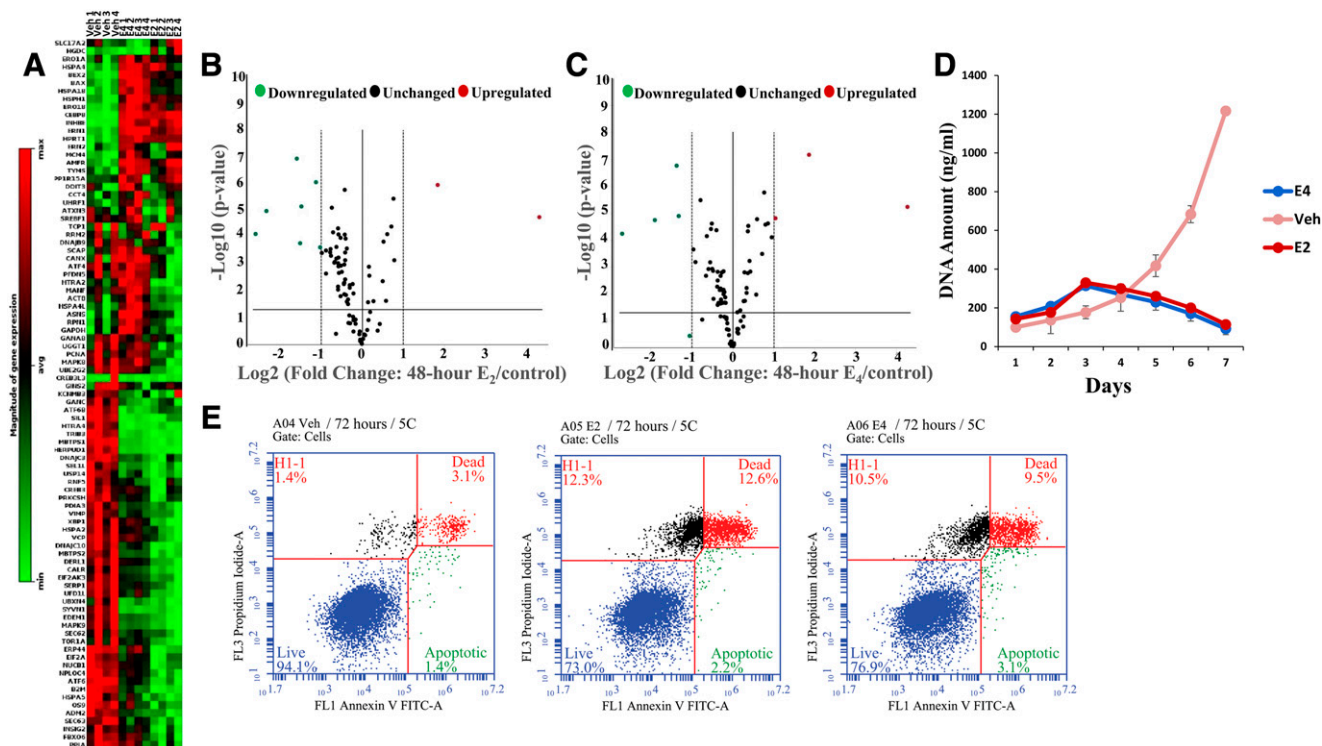
Fig. 7. Human UPR RT^2 PCR profiler PCR arrays, proliferation assays, and annexin V staining in MCF-7:5C cells with 48-hour, 96-hour, and 7-day E$_2$ and E$_4$ treatments. (A) A heat map providing a visualization of the fold changes in expression between select groups (from left to right; vehicle, E$_4$, and E$_2$, respectively) for every gene in the array in the context of the array layout. (B) A volcano plot of 48-hour E$_2$ treatment identifying significant gene-expression changes and displaying statistical significance vs. fold change on the y- and x-axes, respectively. The volcano plot combines a *P*-value statistical test with the fold-regulation change-enabling identification of genes with both large and small expression changes that are statistically significant. (C) A volcano plot of 48-hour E$_4$ treatment. (D) Effects of E$_2$ and E$_4$ alone after 7 days of treatment. (E) Flow cytometry of 72-hour E$_2$ and E$_4$ treatments. (B and C) Green represents downregulated, black unchanged, and red upregulated. Data are mean ± S.D. from three independent experiments performed in triplicate analyzed by one-way ANOVA. Veh, vehicle.

Supplemental Fig. 5C). Interestingly, there was a 9.46-fold (*P* < 0.05) downregulation of EIF2AK3 (PERK) (Supplemental Fig. 5C), which might play a role in MCF-7:5C cells' delayed course of apoptosis with BMI-135 treatment compared with E$_2$ and E$_4$. After a 72-hour treatment with 1 μM BMI-135, there was an intensified (or terminal) UPR gene regulation compared with 48 hours, with an upregulation of CEBPB (*P* < 0.001), INHBE (*P* < 0.001), PPP1R15A (GADD34, *P* < 0.001), DDIT3 (CHOP, *P* < 0.001), and ERN1 (IRE1α, *P* < 0.001). This is coupled with a downregulation of the ERAD genes, HTRA4 (*P* < 0.001), SEL1L (*P* < 0.01), and HERPUD1 (*P* < 0.001); the chaperone gene HSPA2 (*P* < 0.001); and the lipid metabolism gene MBTPS1 (*P* < 0.001) (Fig. 8B; Supplemental Fig. 5D).

The heat map of MCF-7:5C cells with BMI-135 treatment at 72 hours (Fig. 8A) displays a general UPR gene downregulation (situated on the right side of the heat map) compared with vehicle control (situated on the left). This general downregulation by 72 hours (Fig. 8B; Supplemental Fig. 5D) highlights MCF-7:5C cells' trajectory to undergo apoptosis by 96 hours (Fig. 8E).

Cell viability and proliferation assays showed a decline in MCF-7:5C cell DNA amount with BPTPE treatment by day 8 (Supplemental Fig. 4D). Furthermore, flow cytometry showed apoptosis by day 8 (annexin staining 31.5% with BPTPE vs. vehicle control 9.4%) (Supplemental Fig. 4E). The time point of day 7 was chosen to investigate the proapoptotic UPR gene regulation, which precedes apoptosis by day 8. Another time point of day 3 was chosen to compare

and contrast the UPR gene regulation with that of day 7 and show how this regulation is dynamic and culminates over time.

After a 3-day treatment with 1 μM BPTPE, there was a relatively minor UPR gene activation compared with the one seen by day 7 (Supplemental Figs. 4, B and C and 5, E and F). Interestingly, there was a 2.15-fold (*P* < 0.001) downregulation of EIF2AK3 with 3-day BPTPE treatment (Supplemental Fig. 5E), which might play a role in MCF-7:5C cells' delayed course of apoptosis with BPTPE treatment compared with E$_2$ and E$_4$. This is also observed with BMI-135's early treatment time point (Supplemental Fig. 5C). After a 7-day treatment with BPTPE, there was a downregulation of the ERAD gene HERPUD1 (*P* < 0.001), the lipid metabolism genes INSIG2 (*P* < 0.001) and MBTPS1 (*P* < 0.001), and the chaperone genes HSPA2 (*P* < 0.001) and DNAJB9 (*P* < 0.001) (Supplemental Figs. 4B and 5F).

The heat map of MCF-7:5C cells with BPTPE treatment at day 7 (Supplemental Fig. 4A) displays a general UPR gene downregulation (situated on the left side of the heat map) compared with vehicle control (situated on the right). This general downregulation by day 7 (Supplemental Figs. 4B and 5F) highlights MCF-7:5C cells' programming to undergo apoptosis by day 8 (Supplemental Fig. 4E).

The statistically significant regulated UPR genes with test compounds are stated and grouped at select time points (Fig. 9) to show the similar terminal UPR regulation preceding apoptosis.
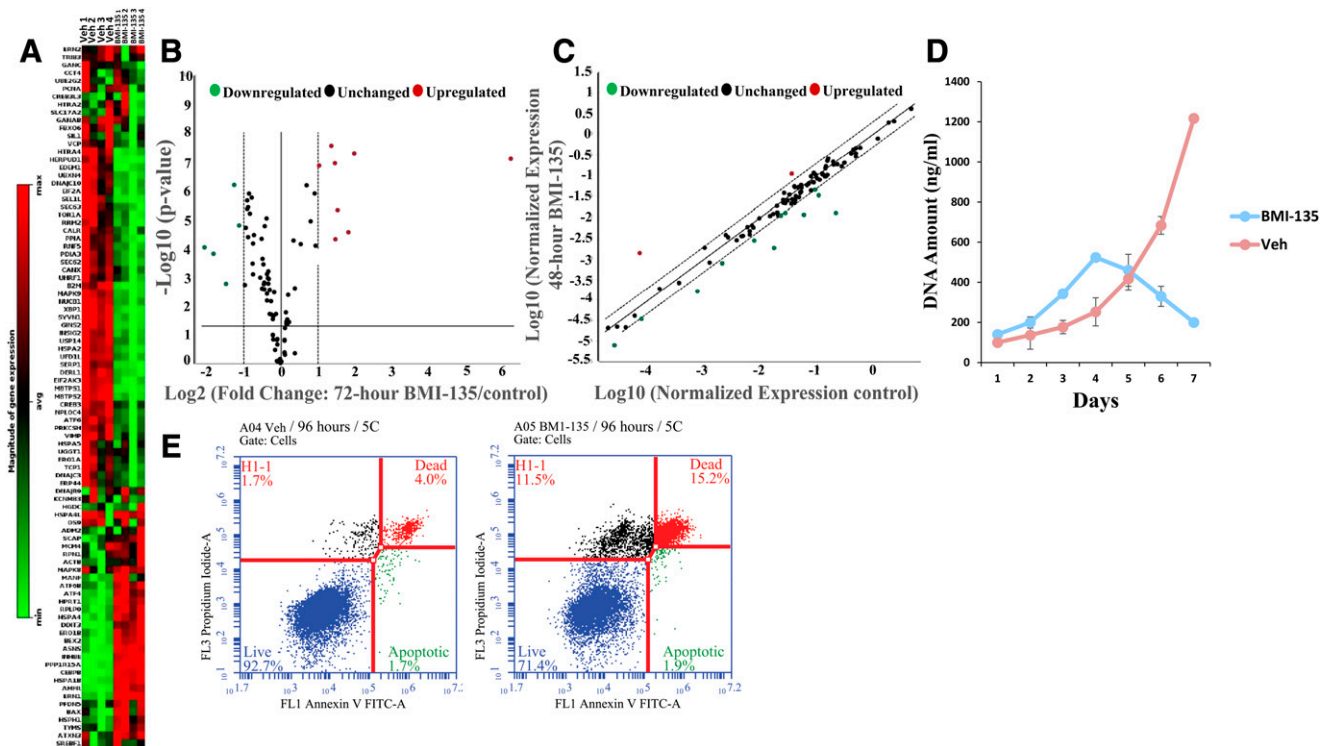
Fig. 8. Human UPR RT^2 PCR profiler PCR arrays, proliferation assays, and annexin V staining in MCF-7:5C cells with 48-hour, 72-hour, 96-hour, and 7-day BMI-135 treatments. (A) A heat map of 72-hour BMI-135 treatment, providing a visualization of the fold changes in expression between the select groups (from left to right; vehicle and BMI-135, respectively) for every gene in the array in the context of the array layout. (B) A volcano plot of 72-hour BMI-135 treatment. (C) A scatter plot of 48-hour BMI-135 treatment comparing the normalized expression of every gene on the array between the two select groups by plotting them against one another to quickly visualize large gene-expression changes. The central line indicates unchanged gene expression. The dotted lines indicate the selected fold-regulation threshold. Data points beyond the dotted lines in the upper left and lower right sections meet the selected fold-regulation threshold. (D) Effects of BMI-135 alone after 7 days of treatment. (E) Flow cytometry of 96-hour BMI-135 treatment. (B and C) Green represents downregulated, black unchanged, and red upregulated. Data are mean ± S.D. from three independent experiments performed in triplicate analyzed by one-way ANOVA. Veh, vehicle.

E$_4$ and BMI-135 Induce ThT Fluorescence as a Marker of UPR. ThT has been successfully used for the detection and quantification of EnR stress and the UPR in living cells (Beriault and Werstuck, 2013) given that it directly interacts with the accumulated misfolded protein amyloid during the UPR (Beriault and Werstuck, 2013).

The "blue" Hoechst 33342 dye was used for counterstaining as a live cell nuclear dye (channel A), the "green" ThT dye was used as a UPR-indicative dye (channel B), and a colocalization of ThT and Hoechst 33342 dyes is shown (channel C). 17β-Estradiol and E$_4$ were shown to induce ThT fluorescence by 48 hours, like the induction seen with positive control thapsigargin, and compared with vehicle control (Supplemental Fig. 6B). After 48-hour treatment, E$_4$ had the highest ThT relative intensity/cell of 1.244892, and this was followed by thapsigargin of 0.875072; E$_2$ of 0.741126; and BMI-135 of 0.497225, compared with vehicle control of 0.27594 (Table 2A).

BMI-135 induced a stronger delayed ThT fluorescence by 72 hours (Fig. 10B; Table 2B) compared with that seen by 48 hours (Supplemental Fig. 6B; Table 2A). The relative intensity/cell with 48-hour BMI-135 treatment was 0.497225 compared with vehicle control 0.27594 (Table 2A). However, the relative intensity/cell with 72-hour BMI-135 treatment was 4.878173 compared with vehicle control of 0.29573 (Table 2B). The relative intensity/cell over time is represented in Table 2.

E$_4$ and BMI-135 Induce Apoptosis in Multiple Endocrine-Resistant and Estrogen-Independent BC Models. Flow cytometry was used to determine whether the type of stress-induced cell death in MCF-7:5C, MCF-7:2A, and MCF-7:RAL cells was apoptosis when treated with 1 μM E$_4$ and 1 μM BMI-135.

In MCF-7:5C, 1 μM E$_4$ induced apoptosis (annexin staining 12.6% vs. vehicle control 4.5%) similar to the time course of 1 nM E$_2$ (annexin staining 14.8% vs. vehicle control 4.5%) (Fig. 7E), which was by 72 hours. However, MCF-7:5C's apoptosis with BMI-135 treatment (annexin staining 17.1% vs. vehicle control 5.7%) was delayed by 96 hours (Fig. 8E representing 96 hours; Supplemental Fig. 8D representing 72 hours). The antagonist 4OHT (as a negative control) and its pairing with E$_2$, E$_4$, and BMI-135 did not induce apoptosis by 72 or 96 hours, as predicted (unpublished data).

In MCF-7:2A, E$_4$ induced apoptosis (annexin staining 6.7% vs. vehicle control 0.8%) similar to the time course of E$_2$ (annexin staining 8% vs. vehicle control 0.8%) (Supplemental Fig. 8A), which was by day 9. However, MCF-7:2A's apoptosis with BMI-135 treatment (annexin staining 7.3% vs. vehicle control 2.2%) was delayed by day 13 (Supplemental Fig. 8B representing day 13; Supplemental Fig. 8C representing day 9). The antagonist 4OHT (as a negative control) and its pairing with E$_2$, E$_4$, and BMI-135 did not induce apoptosis by day 9 or 13, as predicted (unpublished data).
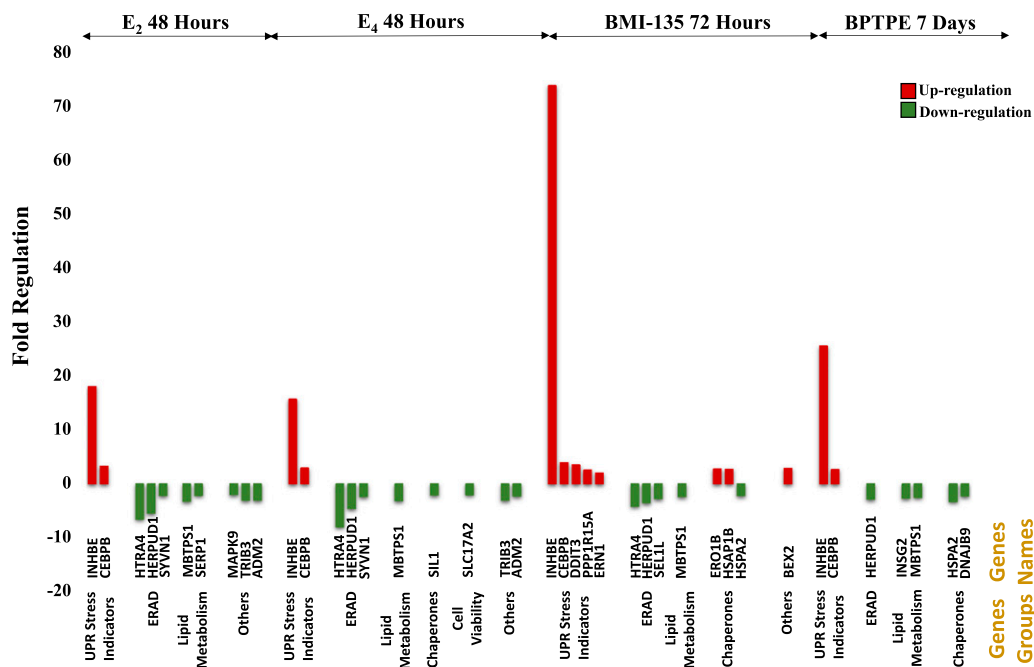
Fig. 9. A schematic representation of the statistically significant UPR genes and their gene groupings with test compounds. The *y*-axis displays fold regulation, and the *x*-axis states the UPR genes and their groupings, demonstrating a signature proapoptotic UPR regulation at different time points with test compounds. Green represents downregulation and red upregulation. The ERAD proteins decrease cellular stress by degrading severely misfolded or unfolded proteins, and chaperones do so by folding the misfolded or unfolded proteins that could be rescued (Hetz, 2012). Lipid metabolism-related proteins play a critical role in lipid metabolism and homeostasis to combat cellular stress (Hetz and Saxena, 2017). The downregulation of these UPR gene groups ($P < 0.05$) as well as the upregulation of UPR stress indicators (INHBE and CEBPB) ($P < 0.05$) form a UPR phase whose regulation is characterized as terminal/proapoptotic (Maly and Papa, 2014; Grootjans et al., 2016).

In MCF-7:RAL, E_4 induced apoptosis (annexin staining 7.6% vs. vehicle control 5.3%) similar to the time course of E_2 (annexin staining 9% vs. control 5.3%) (Supplemental Fig. 9A), which was by day 14. However, MCF-7:RAL's apoptosis with BMI-135 (annexin staining 8% vs. control 0.8%) was delayed until day 17 (Supplemental Fig. 9B representing day 17; Supplemental Fig. 9C representing day 14). The antagonists 4OHT and raloxifene and their pairing with E_2, E_4, and BMI-135 did not induce apoptosis by day 14 or 17, as predicted (Supplemental Fig. 9A). Interestingly, treatment of MCF-7:RAL cells with ICI for 3 weeks caused a decline in cell DNA amount ($P < 0.05$) (Supplemental Fig. 2C); however, this was not due to apoptosis (Supplemental Fig. 9D). Such observed effect of ICI in MCF-7:RAL could be attributed to growth inhibition by preventing cell replication.

Inhibition of PERK Pathway Blocks Apoptosis in MCF-7:5C with E_4 and BMI-135 Treatments. Blocking the UPR transducer PERK with 10 µM GSK G797800 in combination with 1 nM E_2 and in combination with 1 µM E_4 by 72 hours inhibited apoptosis (annexin staining 7.8% and 7.9%, respectively, vs. vehicle control 7%) (Supplemental Fig. 7A) compared with E_2- and E_4-alone treatments that trigger apoptosis (Fig. 7E) and compared with the negative control GSK G797800–alone treatment that does not trigger apoptosis (annexin staining 5.7% vs. vehicle control 7%) (Supplemental Fig. 7A).

Blocking PERK with 10 µM GSK G797800 in combination with 1 µM BMI-135 by 96 hours inhibited apoptosis (annexin staining 4% vs. vehicle control 5.7%) (Fig. 11A) compared with BMI-135–alone treatment that triggers apoptosis (Fig. 11A) and compared with GSK G797800–alone

treatment (annexin staining 5.5% vs. control 5.7%) (Fig. 11A).

Inhibition of IRE1α:XBP1s Pathway Enhances Apoptosis in MCF-7:5C with E_4 and BMI-135 Treatments. The compound MKC-3946 inhibits IRE1α by inhibiting basal XBP1 splicing. Blocking the UPR transducer IRE1α with 20 µM MKC-3946 in combination with 1 µM E_4 by 72 hours induces more apoptosis (annexin staining 34.1% vs. control 1.4%) (Supplemental Fig. 7B) compared with E_4-alone treatment that triggers apoptosis (annexin staining 18.6% vs. control 1.4%) (Supplemental Fig. 7B) and compared with MKC-3946–alone treatment that triggers apoptosis (annexin staining 8.8% vs. control 1.4%) (Supplemental Fig. 7B).

Blocking IRE1α with 20 µM MKC-3946 in combination with 1 µM BMI-135 by 96 hours induces more apoptosis (annexin staining 33.3% vs. control 1.4%) (Fig. 11B) compared with BMI-135–alone treatment (annexin staining 26.5% vs. control 1.4%) (Fig. 11B) and compared with MKC-3946–alone treatment (annexin staining 8.8% vs. control 1.4%) (Fig. 11B).

Discussion

Estetrol is a naturally occurring fetal estrogen, which is associated with a low risk of drug-drug interactions (CYP450 family) and a neutral impact on risk markers of venous thromboembolism (Singer et al., 2014; Coelingh Bennink et al., 2017; Verhoeven et al., 2018). BMI-135 is a member of a new class of estrogen mimics, which did not cause significant uterine proliferation (Molloy et al., 2014; Xiong et al., 2016). Estetrol and the ShERPA TTC-352 are currently being evaluated in endocrine-resistant MBC clinical trials (O'Regan et al., 2019;

Veh	Thapsigargin	BMI-135
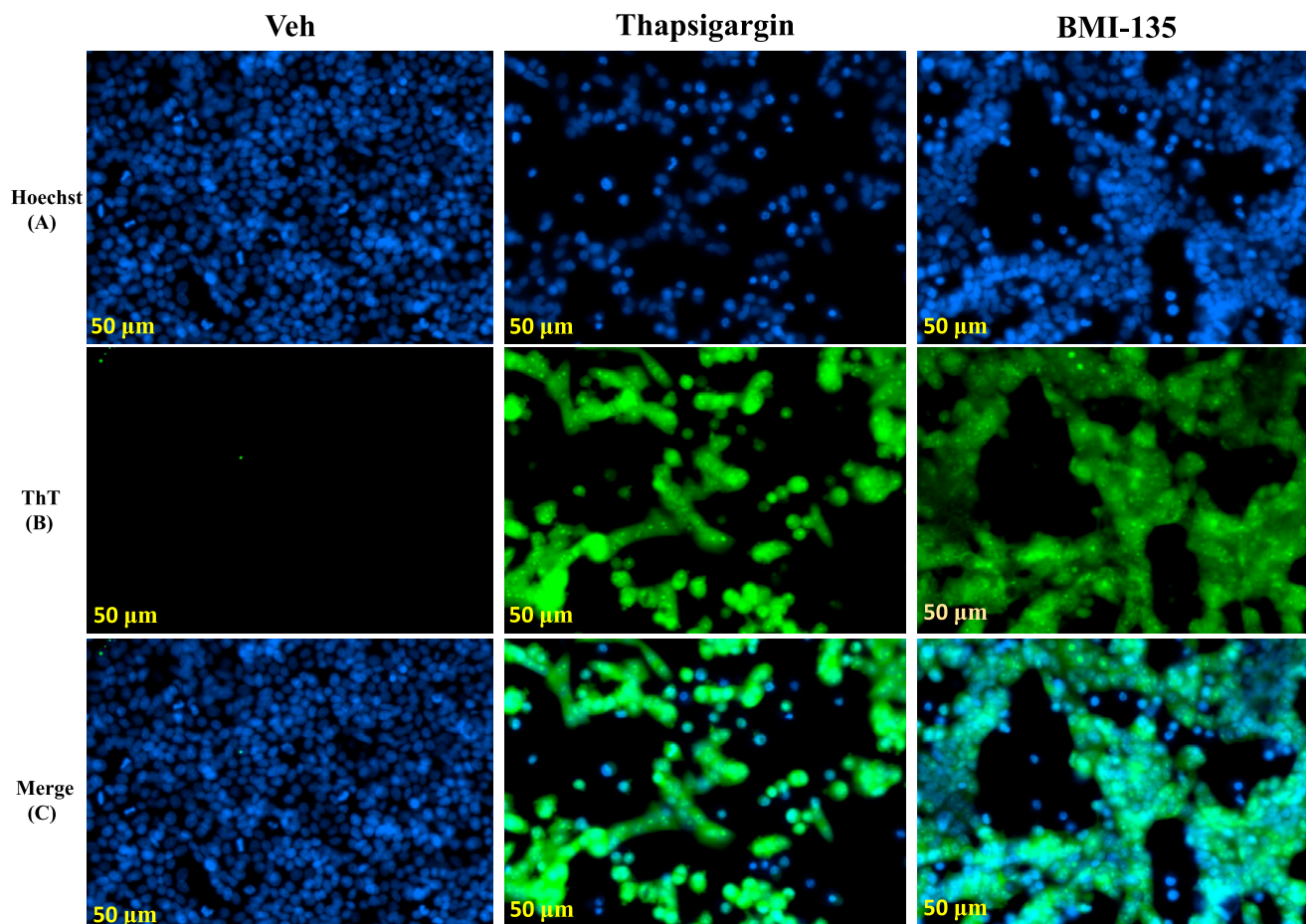
Fig. 10. Detection of UPR in live MCF-7:5C cells using ThT fluorescent dye after 72-hour treatments as measured by the ZEISS Celldiscoverer 7 microscope. (A) Hoechst 33342 dye single panel (blue). (B) ThT dye single panel (green). (C) A merge or colocalization ThT + Hoechst 33342 dyes panel (blue and green). Treatments included 0.1% DMSO (vehicle control), 1 μM thapsigargin (positive control; promoting EnR stress by disrupting EnR Ca^{2+} homeostasis), and 1 μM BMI-135. Scale bar, 50 μM. ThT relative intensity/cell, per treatment, is the mean of three biologic repeats with S.D. (Table 2B). Veh, vehicle.

Schmidt et al., 2020). Our study, in a wide range of endocrine-resistant and estrogen-independent BC cell models as well as an endometrial cancer cell model, shows E_4 and BMI-135 to be less potent full estrogen agonists (Figs. 2–5 and 6, B and F) with the induction of terminal UPR and apoptosis as their antitumor mechanism of action (Figs. 7–12; Supplemental Figs. 5, B and D and 6–9). Although BMI-135 exhibits a slightly delayed UPR-and-apoptosis biology compared with E_2 and E_4 (Figs. 7–11; Supplemental Figs. 6–9), it is still distinct from the much delayed UPR-and-apoptosis biology of the benchmark partial agonist BPTPE (Supplemental Fig. 4).

The application of long-term adjuvant endocrine therapy (Jordan et al., 1979) to treat ER-positive BC is invaluable for patient care. As a result, women's lives are extended or saved (Early Breast Cancer Trialists' Collaborative Group, 1998; Goss et al., 2003, 2005). Nonetheless, recurrence of endocrine-resistant stage IV BC is common (Pisani et al., 2002), hence the discovery of new therapeutic options remains a clinical priority.

Cell models (Pink et al., 1995; Liu et al., 2003; Lewis et al., 2005b; Ariazi et al., 2011; Fan et al., 2014) and athymic mice models (Gottardis and Jordan, 1988; Gottardis et al., 1989a,b; Yao et al., 2000) deciphered the evolution of acquired TAM resistance over years to eventually give rise to a vulnerability in BC: E_2-induced apoptosis (Jordan, 2008; Jordan, 2015).

Although estrogen is approved to treat BC, there is a reluctance to use estradiol as a salvage therapy in stage IV BC because of AEs. As a result, safer estrogenic alternatives are being considered.

Our goal was to compare and contrast the actions of E_4 and BMI-135 with the well characterized partial agonist BPTPE. Our earlier pharmacological studies classified ER-binding ligands into agonists, partial agonists, and antagonists (Jordan, 1984; Jordan et al., 1984, 1986; Murphy et al., 1990a) and are essential to decipher the current molecular mechanisms of E_2-induced apoptosis through the ER signal transduction pathway. These functional cell-based assays (Lieberman et al., 1983a,b; Jordan and Lieberman, 1984; Jordan et al., 1986) dovetailed with the subsequent X-ray crystallography studies of the agonist and antagonist ER complexes of the LBD (Brzozowski et al., 1997; Shiau et al., 1998). Our earlier biologic studies described E_2-induced apoptosis (Jordan, 2015). Our current study shows that E_4 and BMI-135:ERα complexes initiate and modulate the UPR (Figs. 7–12; Supplemental Figs. 5–7). This is an ERα-mediated (Supplemental Fig. 2) activation of the unfolded proteins' synthesis and thus of cellular stress.

The intrinsic activity of the ER complex was evaluated by comparing and contrasting TFF1 and GREB1 estrogen-regulated gene activation with E_2, BMI-135, BPTPE, and endoxifen
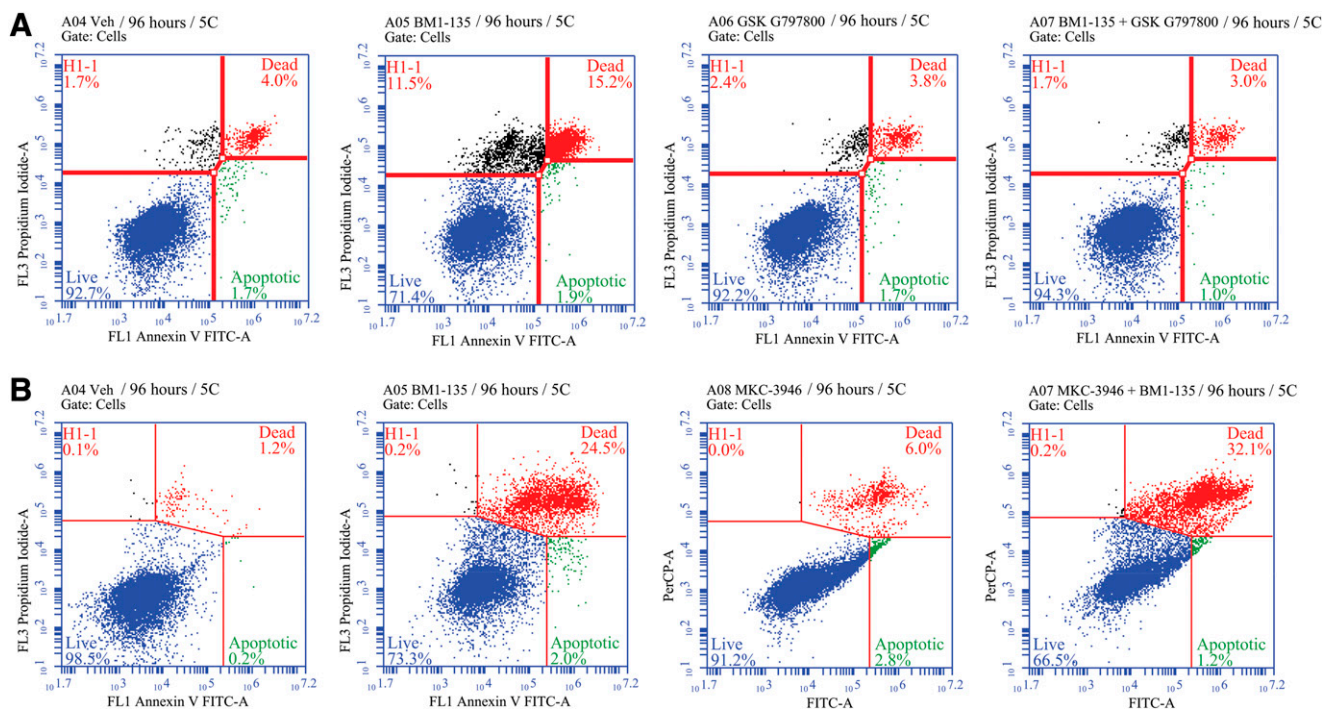
Fig. 11. Flow cytometry in MCF-7:5C cells with BMI-135 plus a PERK inhibitor or an IRE1α inhibitor after 96-hour treatments. (A) MCF-7:5C cells were treated with 0.1% DMSO (vehicle control), 1 μM BMI-135, 10 μM GSK G797800, and 1 μM BMI-135 + 10 μM GSK G797800 then stained with annexin V–FITC and propidium iodide and analyzed by flow cytometry. Viable cells (left lower quadrant) are annexin V–FITC− and PI−; early apoptotic cells (right lower quadrant) are annexin V–FITC+ and PI−; dead cells (left upper quadrant) are PI+, and late apoptotic cells (right upper quadrant) are annexin V–FITC+ and PI+. An increased, late apoptotic effect is observed in the right upper quadrant. (B) MCF-7:5C cells were treated with 0.1% DMSO (vehicle control), 1 μM BMI-135, 20 μM MKC-3946, and 1 μM BMI-135 + 20 μM MKC-3946. Data are mean ± S.D. from three independent experiments analyzed by one-way ANOVA. (A and B).

treatments in WT MCF-7 and LTED MCF-7:5C cells (Fig. 3). The pharmacology of each ligand as a full agonist (E_2, E_4, and BMI-135) or a partial agonist (BPTPE) or an antagonist with no intrinsic activity (endoxifen) mirrored the pharmacology in cells (Fig. 2).

Molecular modeling studies demonstrated that E_4, BMI-135, and BPTPE bind to the classic agonist conformation of ERα, similar to E_2 (Fig. 6, A, C, and E). The flexible docking and MD simulations performed for BMI-135:ERα complex show the dynamic profile of the system to be similar to E_2 (Supplemental Fig. 3A) with the ligand firmly bound to the active site (Supplemental Fig. 3B). Although BMI-135 is larger than E_2, the same contacts have been observed, with the notable exception of the H-bond to His524 (Fig. 6B). These H-bonds and hydrophobic contacts are stable for both ligands, with slightly larger frequencies of occurrence with E_2 (Supplemental Fig. 11, A and B), which indicates a stronger binding mode of E_2. BPTPE exhibits equivalent binding contacts to E_2 (Fig. 6, C and D) but forms a distinctive robust H-bond with Thr347 (Supplemental Fig. 11C), which induces the stability of the ligand binding but increases the mobility of H12 and the loop connecting H11 and H12, which affects the overall stability of the system. This is most likely responsible for the partial agonist profile of BPTPE. These data support the molecular classification of E_4 and BMI-135 as full agonists and further explain their observed biologic behavior.

A comparison of E_4, BMI-135, and BPTPE in multiple WT and LTED BC cell lines (Fig. 2; Supplemental Fig. 1) demonstrates the partial agonist actions of BPTPE on both

growth (Figs. 2, A–E and 3, A and B; Supplemental Fig. 1, A–C and F) and E_2-induced apoptosis (Figs. 2, F–H and 3, C and D; Supplemental Fig. 4, D and E). All experiments used BPTPE as a well characterized partial agonist (Jordan and Lieberman, 1984), which triggers delayed E_2-induced apoptosis in LTED BC cells compared with E_2 (Obiorah et al., 2014; Obiorah and Jordan, 2014) (Supplemental Fig. 4E). The mechanism is shown here to be through a delay in the induction of the proapoptotic UPR signaling (Supplemental Figs. 4, B and C and 5, E and F).

Delayed apoptosis with BPTPE (which contains a free para-hydroxyl on the phenyl ring) mirrors the delayed apoptosis with the synthesized angular triphenylethylene (TPE) derivative 3OHTPE (which contains the free para-hydroxyl) (Maximov et al., 2020). The other synthesized TPE derivative Z2OHTPE does not contain the free para-hydroxyl and causes early apoptosis, similar to E_2 (Maximov et al., 2020). This free para-hydroxyl in BPTPE and 3OHTPE is part of the anti-estrogenic side chain of endoxifen, which prevents the complete closure of ERα's H12 over the ligand:LBD (Supplemental Fig. 11C). This delays the coactivators' recruitment to the ER to form a transcriptionally active complex (Fig. 5B), which delays the ligand:ERα–induced transcription and translation of the unfolded proteins, resulting in delayed apoptosis (Supplemental Fig. 4).

Although BMI-135 does not exhibit the pharmacology of BPTPE (Figs. 2–5 and 6, A and B; Table 1), there is still a slight delay in the induction of the terminal UPR signaling and apoptosis, which is mediated by the BMI-135:ERα complex (Figs. 8, B and E and 10B; Supplemental Fig. 5D;
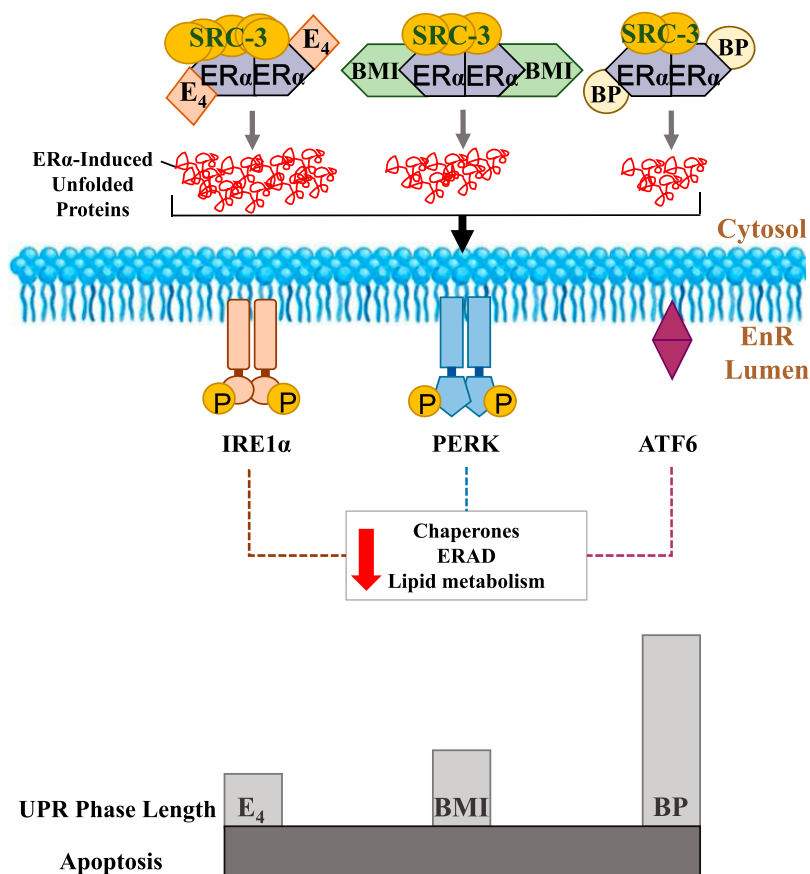
Fig. 12. Schematic representation of the study's concluded antitumor molecular mechanisms of E_4, BMI-135, and BPTPE in LTED endocrine-resistant BC MCF-7:5C. Estetrol:ERα complex recruits the most coactivator SRC-3 and thus induces the most accumulation of unfolded proteins (highest threshold of stress), followed by BMI-135:ERα (BMI-135 is referred to as BMI in the illustration) and BPTPE:ERα (BPTPE is referred to as BP in the illustration). This differential ligand:ERα:coactivator-induced endoplasmic reticulum stress activates the transducers of the UPR, with a downregulation of chaperons, ERAD, and lipid metabolism genes and proteins ($P < 0.05$), which are considered prosurvival mechanisms. This downregulation state constitutes the proapoptotic UPR phase, which is reached quickly with E_4, followed by BMI-135 and BPTPE, and eventually induces apoptosis.

Table 2B for the 72-hour time point vs. Fig. 8C; Supplemental Figs. 5C, 6B, and 8D; Table 2A for the 48-hour time point).

The ChIP assay (Fig. 5) is valuable in understanding the delayed apoptotic biology with BMI-135 and BPTPE. Earlier studies (Sengupta et al., 2013; Obiorah et al., 2014) demonstrated a reduction in the binding of the BPTPE:ERα:SRC-3 complex using the ChIP assay in MCF-7 cells, which is reproduced here (Fig. 5, A and B). A reduced DNA binding of the partial agonist complex occurs, which correlates with a reduction in the efficacy of the complex to synthesize misfolded or unfolded proteins, hence with a delay in the induction of the terminal UPR and apoptosis compared with E_2 (Supplemental Fig. 4). Although BMI-135 recruits equivalent quantities of ERα (Fig. 5A), there is a reduced recruitment of the coactivator SRC-3 compared with E_2 and E_4. Nonetheless, BMI-135:ERα's recruitment of SRC-3 is higher than that with BPTPE ($P < 0.05$) (Fig. 5B). This correlates with BMI-135's slightly delayed induction of the terminal UPR and apoptosis (Fig. 8).

The downregulation of the prosurvival mechanisms, chaperones, ERAD, and lipid metabolism genes ($P < 0.05$), alongside the upregulation of marker UPR stress proteins (INHBE and CEBPB) ($P < 0.05$) constitute the terminal/proapoptotic UPR phase and underscore the antitumor mechanism of E_2, E_4, BMI-135, and BPTPE (Figs. 7–9 and 12; Supplemental Figs. 4 and 5).

Apoptosis with E_4 and BMI-135 treatments was prevented by blocking the PERK pathway (Fig. 11A; Supplemental Fig. 7A). By contrast, blocking the IRE1α:XBP1s pathway after E_4 and BMI-135 treatments enhanced apoptosis (Fig. 11B; Supplemental Fig. 7B). These data demonstrate the modulation of apoptosis

with E_4 and BMI-135 through the modulation of UPR's subcellular sensors.

The timing of UPR-indicative ThT fluorescence with E_4 and BMI-135 is synchronic with that of their proapoptotic UPR gene regulation ($P < 0.05$). The ThT fluorescence and terminal UPR gene regulation were shown to be by 48 hours with E_2 and E_4 (before apoptosis by 72 hours), by 72 hours with BMI-135 (before apoptosis by 96 hours), and by day 7 with BPTPE (before apoptosis by day 8) (Figs. 7, 8, and 10B; Supplemental Figs. 4, 5, and 6B; Table 2).

Translational research (Gottardis et al., 1988) identified a potential link between TAM treatment and the occurrence of endometrial cancer in patients (Jordan and Assikis, 1995). Raloxifene does not have an increased risk of endometrial cancer in clinical trials (Cummings et al., 1999; Vogel et al., 2006). BMI-135 is a raloxifene derivative (Fig. 1) (Xiong et al., 2016) and was tested to determine whether the ShERPA BMI-135:ER:coregulators complex is an agonist in the human endometrial cancer cell line Ishikawa transfected with 5x-ERE (Fig. 4). BPTPE exhibited a partial agonist activity (Fig. 4A), but both E_4 and BMI-135 exhibited a less potent full agonist activity compared with E_2 (Fig. 4A). This effect is mediated via the Ishikawa ERα (Fig. 4B). Although BMI-135 was shown not to induce uterine growth in a mouse xenograft model (Xiong et al., 2016), based on this study's observations, it would be wise to require an endometrial screening for patients with BC receiving E_4 or BMI-135.

Raloxifene induces acquired resistance as evidenced by SERM-stimulated BC cell growth (Liu et al., 2003; Balaburski et al., 2010) (Fig. 2H; Supplemental Figs. 1F and 2C). Such

laboratory data have clinical significance because a case report of an antiestrogen withdrawal effect with raloxifene was reported (Lemmo, 2016). Raloxifene-resistant BC-stimulated growth has not been widely reported during the decades of treatment in patients with osteoporosis. This is surprising, but perhaps clinicians have not been aware of this form of SERM resistance. Nevertheless, our findings here (Supplemental Fig. 9, A and B) suggest that E_4 or an ShERPA could be deployed after raloxifene discontinuation to induce tumor regression through apoptosis in raloxifene-resistant BC. Furthermore, ICI could be deployed, as we have shown here that it has a growth inhibitory effect (Supplemental Figs. 1F, 2C, and 9D).

Estrogen receptor-positive BC constitutes more than 70% of all BCs (Clark et al., 1984). Rosenberg and coworkers (2015) projected BC cases in the United States to double by 2030 compared with cases in 2011. The majority will be ER-positive BC. The development of new agents to treat ER-positive endocrine-resistant MBC remains a priority. Overall, the results of our work support the continuation of future clinical trials with the new agents E_4 and ShERPAs.

Acknowledgments

Authorship Contributions

Participated in research design: Abderrahman, Jordan.
Conducted experiments: Abderrahman, Maximov, Hanspal, Fan.
Contributed new reagents or analytic tools: Curpan, Xiong, Tonetti, Thatcher.
Performed data analysis: Abderrahman, Curpan, Jordan.
Wrote or contributed to the writing of the manuscript: Abderrahman, Maximov, Curpan, Tonetti, Thatcher, Jordan.

References

Abderrahman B and Jordan VC (2016) The modulation of estrogen-induced apoptosis as an interpretation of the women's health initiative trials. *Expert Rev Endocrinol Metab* 11:81–86.

Abot A, Fontaine C, Buscato M, Solinhac R, Flouriot G, Fabre A, Drougard A, Rajan S, Laine M, Milon A, et al. (2014) The uterine and vascular actions of estetrol delineate a distinctive profile of estrogen receptor α modulation, uncoupling nuclear and membrane activation. *EMBO Mol Med* 6:1328–1346.

Anderson GL, Limacher M, Assaf AR, Bassford T, Beresford SA, Black H, Bonds D, Brunner R, Brzyski R, Caan B, et al.; Women's Health Initiative Steering Committee (2004) Effects of conjugated equine estrogen in postmenopausal women with hysterectomy: the Women's Health Initiative randomized controlled trial. *JAMA* 291:1701–1712.

Ariazi EA, Cunliffe HE, Lewis-Wambi JS, Slifker MJ, Willis AL, Ramos P, Tapia C, Kim HR, Yerrum S, Sharma CG, et al. (2011) Estrogen induces apoptosis in estrogen deprivation-resistant breast cancer through stress responses as identified by global gene expression across time. *Proc Natl Acad Sci USA* 108:18879–18886.

Balaburski GM, Dardes RC, Johnson M, Haddad B, Zhu F, Ross EA, Sengupta S, Klein-Szanto A, Liu H, Lee ES, et al. (2010) Raloxifene-stimulated experimental breast cancer with the paradoxical actions of estrogen to promote or prevent tumor growth: a unifying concept in anti-hormone resistance. *Int J Oncol* 37:387–398.

Beriault DR and Werstuck GH (2013) Detection and quantification of endoplasmic reticulum stress in living cells using the fluorescent compound, Thioflavin T. *Biochim Biophys Acta* 1833:2293–2301.

Brzozowski AM, Pike AC, Dauter Z, Hubbard RE, Bonn T, Engström O, Ohman L, Greene GL, Gustafsson JA, and Carlquist M (1997) Molecular basis of agonism and antagonism in the oestrogen receptor. *Nature* 389:753–758.

Chalasani P, Stopeck A, Clarke K, and Livingston R (2014) A pilot study of estradiol followed by exemestane for reversing endocrine resistance in postmenopausal women with hormone receptor-positive metastatic breast cancer. *Oncologist* 19:1127–1128.

Chlebowski Rowan T, Anderson Garnet L, Aragaki Aaron K, Manson JoAnn E, Stefanick Marcia L, Pan Kathy, Barrington Wendy, Kuller Lewis H, Simon Michael S, Lane Dorothy, et al. (2020) Association of Menopausal Hormone Therapy With Breast Cancer Incidence and Mortality During Long-term Follow-up of the Women's Health Initiative Randomized Clinical Trials. *JAMA* 324:369–380.

Clark GM, Osborne CK, and McGuire WL (1984) Correlations between estrogen receptor, progesterone receptor, and patient characteristics in human breast cancer. *J Clin Oncol* 2:1102–1109.

Coelingh Bennink HJ, Verhoeven C, Dutman AE, and Thijssen J (2017) The use of high-dose estrogens for the treatment of breast cancer. *Maturitas* 95:11–23.

Coelingh Bennink HJ, Verhoeven C, Zimmerman Y, Visser M, Foidart JM, and Gemzell-Danielsson K (2016) Clinical effects of the fetal estrogen estetrol in a multiple-rising-dose study in postmenopausal women. *Maturitas* 91:93–100.

Cole MP, Jones CT, and Todd ID (1971) A new anti-oestrogenic agent in late breast cancer. An early clinical appraisal of ICI46474. *Br J Cancer* 25:270–275.

Creinin MD, Rosing J, Jost M, Kinet V, Chatel G, and Foidart JM (2019) Estetrol combined with drospirenone: a new oral contraceptive with a favorable hemostatic profile. *Obstet Gynecol* 133:7S.

Cummings SR, Eckert S, Krueger KA, Grady D, Powles TJ, Cauley JA, Norton L, Nickelsen T, Bjarnason NH, Morrow M, et al. (1999) The effect of raloxifene on risk of breast cancer in postmenopausal women: results from the MORE randomized trial. Multiple Outcomes of Raloxifene Evaluation. *JAMA* 281:2189–2197.

Dutman E, Zimmerman Y, and Coelingh-Bennink H (2017) The effects of the human fetal estrogen estetrol (E4) in healthy men to estimate its potential use for the treatment of prostate cancer. *Eur Urol Suppl* 16:e362–e364.

Early Breast Cancer Trialists' Collaborative Group (1998) Tamoxifen for early breast cancer: an overview of the randomised trials. *Lancet* 351:1451–1467.

Ellis MJ, Gao F, Dehdashti F, Jeffe DB, Marcom PK, Carey LA, Dickler MN, Silverman F, Fleming GF, Kommareddy A, et al. (2009) Lower-dose vs high-dose oral estradiol therapy of hormone receptor-positive, aromatase inhibitor-resistant advanced breast cancer: a phase 2 randomized study. *JAMA* 302:774–780.

Engel LW, Young NA, Tralka TS, Lippman ME, O'Brien SJ, and Joyce MJ (1978) Establishment and characterization of three new continuous cell lines derived from human breast carcinomas. *Cancer Res* 38:3352–3364.

Fan P, Agboke FA, Cunliffe HE, Ramos P, and Jordan VC (2014) A molecular model for the mechanism of acquired tamoxifen resistance in breast cancer. *Eur J Cancer* 50:2866–2876.

Fan P, Griffith OL, Agboke FA, Anur P, Zou X, McDaniel RE, Creswell K, Kim SH, Katzenellenbogen JA, Gray JW, et al. (2013) c-Src modulates estrogen-induced stress and apoptosis in estrogen-deprived breast cancer cells. *Cancer Res* 73:4510–4520.

Gérard C, Mestdagt M, Tskitishvili E, Communal L, Gompel A, Silva E, Arnal JF, Lenfant F, Noel A, Foidart JM, et al. (2015) Combined estrogenic and antiestrogenic properties of estetrol on breast cancer may provide a safe therapeutic window for the treatment of menopausal symptoms. *Oncotarget* 6:17621–17636.

Goss PE, Ingle JN, Martino S, Robert NJ, Muss HB, Piccart MJ, Castiglione M, Tu D, Shepherd LE, Pritchard KI, et al. (2003) A randomized trial of letrozole in postmenopausal women after five years of tamoxifen therapy for early-stage breast cancer. *N Engl J Med* 349:1793–1802.

Goss PE, Ingle JN, Martino S, Robert NJ, Muss HB, Piccart MJ, Castiglione M, Tu D, Shepherd LE, Pritchard KI, et al. (2005) Randomized trial of letrozole following tamoxifen as extended adjuvant therapy in receptor-positive breast cancer: updated findings from NCIC CTG MA.17. *J Natl Cancer Inst* 97:1262–1271.

Gottardis MM, Jiang SY, Jeng MH, and Jordan VC (1989a) Inhibition of tamoxifen-stimulated growth of an MCF-7 tumor variant in athymic mice by novel steroidal antiestrogens. *Cancer Res* 49:4090–4093.

Gottardis MM and Jordan VC (1988) Development of tamoxifen-stimulated growth of MCF-7 tumors in athymic mice after long-term antiestrogen administration. *Cancer Res* 48:5183–5187.

Gottardis MM, Robinson SP, Satyaswaroop PG, and Jordan VC (1988) Contrasting actions of tamoxifen on endometrial and breast tumor growth in the athymic mouse. *Cancer Res* 48:812–815.

Gottardis MM, Wagner RJ, Borden EC, and Jordan VC (1989b) Differential ability of antiestrogens to stimulate breast cancer cell (MCF-7) growth in vivo and in vitro. *Cancer Res* 49:4765–4769.

Grootjans J, Kaser A, Kaufman RJ, and Blumberg RS (2016) The unfolded protein response in immunity and inflammation. *Nat Rev Immunol* 16:469–484.

Haddow A (1970) David A. Karnofsky memorial lecture. Thoughts on chemical therapy. *Cancer* 26:737–754.

Haddow A, Watkinson JM, Paterson E, and Koller PC (1944) Influence of synthetic oestrogens on advanced malignant disease. *Br Med J* 2:393–398.

Hetz C (2012) The unfolded protein response: controlling cell fate decisions under ER stress and beyond. *Nat Rev Mol Cell Biol* 13:89–102.

Hetz C and Saxena S (2017) ER stress and the unfolded protein response in neurodegeneration. *Nat Rev Neurol* 13:477–491.

Holinka CF, Diczfalusy E, and Coelingh Bennink HJ (2008) Estetrol: a unique steroid in human pregnancy. *J Steroid Biochem Mol Biol* 110:138–143.

Hosford SR, Shee K, Wells JD, Traphagen NA, Fields JL, Hampsch RA, Kettenbach AN, Demidenko E, and Miller TW (2019) Estrogen therapy induces an unfolded protein response to drive cell death in ER+ breast cancer. *Mol Oncol* 13:1778–1794.

Ingle JN, Ahmann DL, Green SJ, Edmonson JH, Bisel HF, Kvols LK, Nichols WC, Creagan ET, Hahn RG, Rubin J, et al. (1981) Randomized clinical trial of diethylstilbestrol versus tamoxifen in postmenopausal women with advanced breast cancer. *N Engl J Med* 304:16–21.

Iwase H, Yamamoto Y, Yamamoto-Ibusuki M, Murakami KI, Okumura Y, Tomita S, Inao T, Honda Y, Omoto Y, and Iyama KI (2013) Ethinylestradiol is beneficial for postmenopausal patients with heavily pre-treated metastatic breast cancer after prior aromatase inhibitor treatment: a prospective study. *Br J Cancer* 109:1537–1542.

Jiang SY, Wolf DM, Yingling JM, Chang C, and Jordan VC (1992) An estrogen receptor positive MCF-7 clone that is resistant to antiestrogens and estradiol. *Mol Cell Endocrinol* 90:77–86.

Jordan VC (1984) Biochemical pharmacology of antiestrogen action. *Pharmacol Rev* **36**:245–276.

Jordan VC (2003) Tamoxifen: a most unlikely pioneering medicine. *Nat Rev Drug Discov* **2**:205–213.

Jordan VC (2008) The 38th David A. Karnofsky lecture: the paradoxical actions of estrogen in breast cancer--survival or death? *J Clin Oncol* **26**:3073–3082.

Jordan VC (2015) The new biology of estrogen-induced apoptosis applied to treat and prevent breast cancer. *Endocr Relat Cancer* **22**:R1–R31.

Jordan VC (2020) Molecular mechanism for breast cancer incidence in the women's health initiative. *Cancer Prev Res (Phila)* DOI: 10.1158/1940-6207.CAPR-20-0082 [published ahead of print].

Jordan VC and Allen KE (1980) Evaluation of the antitumour activity of the non-steroidal antioestrogen monohydroxytamoxifen in the DMBA-induced rat mammary carcinoma model. *Eur J Cancer* **16**:239–251.

Jordan VC and Assikis VJ (1995) Endometrial carcinoma and tamoxifen: clearing up a controversy. *Clin Cancer Res* **1**:467–472.

Jordan VC, Dix CJ, and Allen KE (1979) The effectiveness of long-term treatment in a laboratory model for adjuvant hormone therapy of breast cancer, in *Adjuvant Therpy of Cancer II* (Salmon SE and Jones SE 19–26, Greene and Stratton, New York.

Jordan VC, Koch R, Mittal S, and Schneider MR (1986) Oestrogenic and anti-oestrogenic actions in a series of triphenylbut-1-enes: modulation of prolactin synthesis in vitro. *Br J Pharmacol* **87**:217–223.

Jordan VC and Lieberman ME (1984) Estrogen-stimulated prolactin synthesis in vitro. Classification of agonist, partial agonist, and antagonist actions based on structure. *Mol Pharmacol* **26**:279–285.

Jordan VC, Lieberman ME, Cormier E, Koch R, Bagley JR, and Ruenitz PC (1984) Structural requirements for the pharmacological activity of nonsteroidal anti-estrogens in vitro. *Mol Pharmacol* **26**:272–278.

Kraus MH, Popescu NC, Amsbaugh SC, and King CR (1987) Overexpression of the EGF receptor-related proto-oncogene erbB-2 in human mammary tumor cell lines by different molecular mechanisms. *EMBO J* **6**:605–610.

Lemmo W (2016) Anti-estrogen withdrawal effect with raloxifene? A case report. *Integr Cancer Ther* **15**:245–249.

Lewis JS, Meeke K, Osipo C, Ross EA, Kidawi N, Li T, Bell E, Chandel NS, and Jordan VC (2005a) Intrinsic mechanism of estradiol-induced apoptosis in breast cancer cells resistant to estrogen deprivation. *J Natl Cancer Inst* **97**:1746–1759.

Lewis JS, Osipo C, Meeke K, and Jordan VC (2005b) Estrogen-induced apoptosis in a breast cancer model resistant to long-term estrogen withdrawal. *J Steroid Biochem Mol Biol* **94**:131–141.

Lieberman ME, Gorski J, and Jordan VC (1983a) An estrogen receptor model to describe the regulation of prolactin synthesis by antiestrogens in vitro. *J Biol Chem* **258**:4741–4745.

Lieberman ME, Jordan VC, Fritsch M, Santos MA, and Gorski J (1983b) Direct and reversible inhibition of estradiol-stimulated prolactin synthesis by antiestrogens in vitro. *J Biol Chem* **258**:4734–4740.

Liu H, Lee ES, Gajdos C, Pearce ST, Chen B, Osipo C, Loweth J, McKian K, De Los Reyes A, Wing L, et al. (2003) Apoptotic action of 17beta-estradiol in raloxifene-resistant MCF-7 cells in vitro and in vivo. *J Natl Cancer Inst* **95**:1586–1597.

Lønning PE, Taylor PD, Anker G, Iddon J, Wie L, Jørgensen LM, Mella O, and Howell A (2001) High-dose estrogen treatment in postmenopausal breast cancer patients heavily exposed to endocrine therapy. *Breast Cancer Res Treat* **67**:111–116.

Maly DJ and Papa FR (2014) Druggable sensors of the unfolded protein response. *Nat Chem Biol* **10**:892–901.

Maximov PY, Abderrahman B, Hawsawi YM, Chen Y, Foulds CE, Jain A, Malovannaya A, Fan P, Curpan RF, Han R, et al. (2020) The structure-function relationship of angular estrogens and estrogen receptor alpha to initiate estrogen-induced apoptosis in breast cancer cells. *Mol Pharmacol* **98**:24–37.

Maximov PY, Myers CB, Curpan RF, Lewis-Wambi JS, and Jordan VC (2010) Structure-function relationships of estrogenic triphenylethylenes related to endoxifen and 4-hydroxytamoxifen. *J Med Chem* **53**:3273–3283.

Molloy ME, White BE, Gherezghiher T, Michalsen BT, Xiong R, Patel H, Zhao H, Maximov PY, Jordan VC, Thatcher GR, et al. (2014) Novel selective estrogen mimics for the treatment of tamoxifen-resistant breast cancer. *Mol Cancer Ther* **13**:2515–2526.

Murphy CS, Langan-Fahey SM, McCague R, and Jordan VC (1990a) Structure-function relationships of hydroxylated metabolites of tamoxifen that control the proliferation of estrogen-responsive T47D breast cancer cells in vitro. *Mol Pharmacol* **38**:737–743.

Murphy CS, Pink JJ, and Jordan VC (1990b) Characterization of a receptor-negative, hormone-nonresponsive clone derived from a T47D human breast cancer cell line kept under estrogen-free conditions. *Cancer Res* **50**:7285–7292.

Nishida M, Kasahara K, Kaneko M, Iwasaki H, and Hayashi K (1985) [Establishment of a new human endometrial adenocarcinoma cell line, Ishikawa cells, containing estrogen and progesterone receptors]. *Nippon Sanka Fujinka Gakkai Zasshi* **37**:1103–1111.

Obiorah I, Sengupta S, Curpan R, and Jordan VC (2014) Defining the conformation of the estrogen receptor complex that controls estrogen-induced apoptosis in breast cancer. *Mol Pharmacol* **85**:789–799.

Obiorah IE and Jordan VC (2014) Differences in the rate of oestrogen-induced apoptosis in breast cancer by oestradiol and the triphenylethylene bisphenol. *Br J Pharmacol* **171**:4062–4072.

O'Regan RM, Hurley R, Sachdev JC, Bleeker J, Tonetti D, Thatcher GR, Venuti R, and Dudek AZ (2019) Phase I study of TTC-352 in patients with estrogen receptor-positive metastatic breast cancer (Abstract). *Cancer Res* **79**:CT051.

Pink JJ, Jiang SY, Fritsch M, and Jordan VC (1995) An estrogen-independent MCF-7 breast cancer cell line which contains a novel 80-kilodalton estrogen receptor-related protein. *Cancer Res* **55**:2583–2590.

Pisani P, Bray F, and Parkin DM (2002) Estimates of the world-wide prevalence of cancer for 25 sites in the adult population. *Int J Cancer* **97**:72–81.

Roehm E (2015) A reappraisal of women's health initiative estrogen-alone trial: long-term outcomes in women 50-59 Years of age. *Obstet Gynecol Int* **2015**:713295.

Rosenberg PS, Barker KA, and Anderson WF (2015) Estrogen receptor status and the future burden of invasive and in situ breast cancers in the United States. *J Natl Cancer Inst* **107**:djv159.

Schmidt M, Hönig A, Zimmerman Y, Verhoeven C, Almstedt K, Battista M, Lenhard HG, Krijgh J, and Bennink HC (2020) Estetrol for treatment of advanced ER+/HER2- breast cancer (Abstract). *Cancer Res* **80**:P5-11–15.

Sengupta S, Obiorah I, Maximov PY, Curpan R, and Jordan VC (2013) Molecular mechanism of action of bisphenol and bisphenol A mediated by oestrogen receptor alpha in growth and apoptosis of breast cancer cells. *Br J Pharmacol* **169**:167–178.

Sengupta S, Sharma CG, and Jordan VC (2010) Estrogen regulation of X-box binding protein-1 and its role in estrogen induced growth of breast and endometrial cancer cells. *Horm Mol Biol Clin Investig* **2**:235–243.

Sherman W, Beard HS, and Farid R (2006a) Use of an induced fit receptor structure in virtual screening. *Chem Biol Drug Des* **67**:83–84.

Sherman W, Day T, Jacobson MP, Friesner RA, and Farid R (2006b) Novel procedure for modeling ligand/receptor induced fit effects. *J Med Chem* **49**:534–553.

Shiau AK, Barstad D, Loria PM, Cheng L, Kushner PJ, Agard DA, and Greene GL (1998) The structural basis of estrogen receptor/coactivator recognition and the antagonism of this interaction by tamoxifen. *Cell* **95**:927–937.

Singer CF, Bennink HJ, Natter C, Steurer S, Rudas M, Moinfar F, Appels N, Visser M, and Kubista E (2014) Antiestrogenic effects of the fetal estrogen estetrol in women with estrogen-receptor positive early breast cancer. *Carcinogenesis* **35**:2447–2451.

Song RX, Mor G, Naftolin F, McPherson RA, Song J, Zhang Z, Yue W, Wang J, and Santen RJ (2001) Effect of long-term estrogen deprivation on apoptotic responses of breast cancer cells to 17beta-estradiol. *J Natl Cancer Inst* **93**:1714–1723.

Verhoeven C, Schmidt M, Hönig A, Dünnebacke J, Dutman E, Krijgh J, and Coelingh-Bennink H (2018) Abstract OT1-04-01: Estetrol for treatment of advanced ER+ breast cancer. DOI: 10.1158/1538-7445.SABCS17-OT1-04-01

Vogel VG, Costantino JP, Wickerham DL, Cronin WM, Cecchini RS, Atkins JN, Bevers TB, Fehrenbacher L, Pajon ER Jr., Wade JL III, et al. National Surgical Adjuvant Breast and Bowel Project (NSABP) (2006) Effects of tamoxifen vs raloxifene on the risk of developing invasive breast cancer and other disease outcomes: the NSABP Study of Tamoxifen and Raloxifene (STAR) P-2 trial [published correction appears in *JAMA* (2006) 296:2926; *JAMA* (2007) 298:973]. *JAMA* **295**:2727–2741.

Wolf DM and Jordan VC (1993) A laboratory model to explain the survival advantage observed in patients taking adjuvant tamoxifen therapy. *Recent Results Cancer Res* **127**:23–33.

Xiong R, Patel HK, Gutgesell LM, Zhao J, Delgado-Rivera L, Pham TND, Zhao H, Carlson K, Martin T, Katzenellenbogen JA, et al. (2016) Selective human estrogen receptor partial agonists (ShERPAs) for tamoxifen-resistant breast cancer. *J Med Chem* **59**:219–237.

Yao K, Lee ES, Bentrem DJ, England G, Schafer JI, O'Regan RM, and Jordan VC (2000) Antitumor action of physiological estradiol on tamoxifen-stimulated breast tumors grown in athymic mice. *Clin Cancer Res* **6**:2028–2036.

Address correspondence to: V. Craig Jordan, Department of Breast Medical Oncology, University of Texas MD Anderson Cancer Center, 1515 Holcombe Blvd., Unit 1354, Houston, TX 77030. E-mail: VCJordan@mdanderson.org

Rapid Induction of the Unfolded Protein Response and Apoptosis by Estrogen Mimic TTC-352 for the Treatment of Endocrine-Resistant Breast Cancer

Balkees Abderrahman[1], Philipp Y. Maximov[1], Ramona F. Curpan[2], Sean W. Fanning[3], Jay S. Hanspal[1], Ping Fan[1], Charles E. Foulds[4], Yue Chen[5], Anna Malovannaya[6], Antrix Jain[7], Rui Xiong[8], Geoffrey L. Greene[3], Debra A. Tonetti[8], Gregory R.J. Thatcher[8], and V. Craig Jordan[1]

ABSTRACT

Patients with long-term estrogen-deprived breast cancer, after resistance to tamoxifen or aromatase inhibitors develops, can experience tumor regression when treated with estrogens. Estrogen's antitumor effect is attributed to apoptosis via the estrogen receptor (ER). Estrogen treatment can have unpleasant gynecologic and nongynecologic adverse events; thus, the development of safer estrogenic agents remains a clinical priority. Here, we study synthetic selective estrogen mimics (SEM) BMI-135 and TTC-352, and the naturally occurring estrogen estetrol (E$_4$), which are proposed as safer estrogenic agents compared with 17β-estradiol (E$_2$), for the treatment of endocrine-resistant breast cancer. TTC-352 and E$_4$ are being evaluated in breast cancer clinical trials. Cell viability assays, real-time PCR, immunoblotting, *ERE* DNA pulldowns, mass spectrometry, X-ray crystallography, docking and molecular dynamic simulations, live cell imaging, and Annexin V staining were con-

ducted in 11 biologically different breast cancer models. Results were compared with the potent full agonist E$_2$, less potent full agonist E$_4$, the benchmark partial agonist triphenylethylene bisphenol (BPTPE), and antagonists 4-hydroxytamoxifen and endoxifen. We report ERα's regulation and coregulators' binding profiles with SEMs and E$_4$. We describe TTC-352's pharmacology as a weak full agonist and antitumor molecular mechanisms. This study highlights TTC-352's benzothiophene scaffold that yields an H-bond with Glu353, which allows Asp351-to-helix 12 (H12) interaction, sealing ERα's ligand-binding domain, recruiting E$_2$-enriched coactivators, and triggering rapid ERα-induced unfolded protein response (UPR) and apoptosis, as the basis of its anticancer properties. BPTPE's phenolic OH yields an H-Bond with Thr347, which disrupts Asp351-to-H12 interaction, delaying UPR and apoptosis and increasing clonal evolution risk.

Introduction

Estrogen therapy can cause tumor regression in patients with breast cancer, who were long-term estrogen-deprived (LTED) with tamoxifen (TAM), which blocks estrogen binding to the breast cancer estrogen receptor (ER), or aromatase inhibitors (AI), which inhibit estrogen synthesis via the breast cancer aromatase enzyme system (1). Long-term adjuvant TAM therapy (2) became the translational strategy of choice for LTED treatment (3), whereby 5-year TAM therapy leads to a new phase of endocrine resistance, characterized by TAM-induced breast cancer growth and 17β-estradiol (E$_2$)–induced breast

cancer apoptosis (4). Today, AIs are widely used for LTED in treating postmenopausal women with ER-positive breast cancer. The Oxford overview analyses show that at least 50% of breast cancer recurrences occur more than 5 years after diagnosis (5). This prompted investigators to provide a guide (6) to improve the risk benefit of long-term adjuvant endocrine therapy in concordance with the patient's individualized risk for early- versus late-distant recurrence.

Estrogen triggers an endoplasmic reticulum (EnR) stress response, the unfolded protein response (UPR), and induces apoptosis in LTED breast cancer models (7). Numerous clinical trials (8–12) demonstrated the benefit of estrogen-induced tumor regression in patients with LTED breast cancer. However, estrogen therapy can have unpleasant gynecologic and nongynecologic adverse events. The research and development of safer estrogenic agents for the treatment of drug-resistant or metastatic breast cancer (MBC) remains a clinical priority, especially with breast cancer expected to double by 2030 than it was in 2011 (13), and MBC being associated with significantly higher health care costs (14). The majority of breast cancer will be ER-positive, which has a high risk of recurrence and residual relapse even with clinically low-risk disease (T1N0; ref. 15).

Three Selective Human ER Partial Agonists (ShERPAs; including pilot BMI-135 and clinically tested TTC-352; **Fig. 1**; ref. 16) are proposed as safer estrogen mimics for the treatment of endocrine-resistant breast cancer. In preclinical studies, TTC-352 demonstrated efficacy and tolerability (17). A clinical trial using TTC-352 in patients with hormone receptor–positive MBC, who had progressed on at least two lines of endocrine therapy, shows manageable safety and early clinical evidence of activity (11).

Estetrol (E$_4$; **Fig. 1**), a fetal estrogen that activates the nuclear ERα with a vasculoprotective effect, is proposed as a safer estrogen for the treatment of endocrine-resistant breast cancer (12), advanced prostate

[1]Department of Breast Medical Oncology, University of Texas MD Anderson Cancer Center, Houston, Texas. [2]Coriolan Dragulescu Institute of Chemistry, Romanian Academy, Timisoara, Romania. [3]Ben May Department for Cancer Research, University of Chicago, Chicago, Illinois. [4]Center for Precision Environmental Health and Department of Molecular and Cellular Biology, Baylor College of Medicine, Houston, Texas. [5]Adrienne Helis Malvin Medical Research Foundation, New Orleans, Louisiana. [6]Verna and Marrs McLean Department of Biochemistry and Molecular Biology, Mass Spectrometry Proteomics Core, Baylor College of Medicine, Houston, Texas. [7]Mass Spectrometry Proteomics Core, Baylor College of Medicine, Houston, Texas. [8]Pharmacology and Toxicology, University of Arizona, Tucson, Arizona.

Note: Supplementary data for this article are available at Molecular Cancer Therapeutics Online (http://mct.aacrjournals.org/).

Corresponding Author: V. Craig Jordan, University of Texas MD Anderson Cancer Center, 1515 Holcombe Blvd., Unit 1354, Houston, TX 77030. Phone: 713-745-0600; Fax: 713-794-4985; E-mail: VCJordan@mdanderson.org
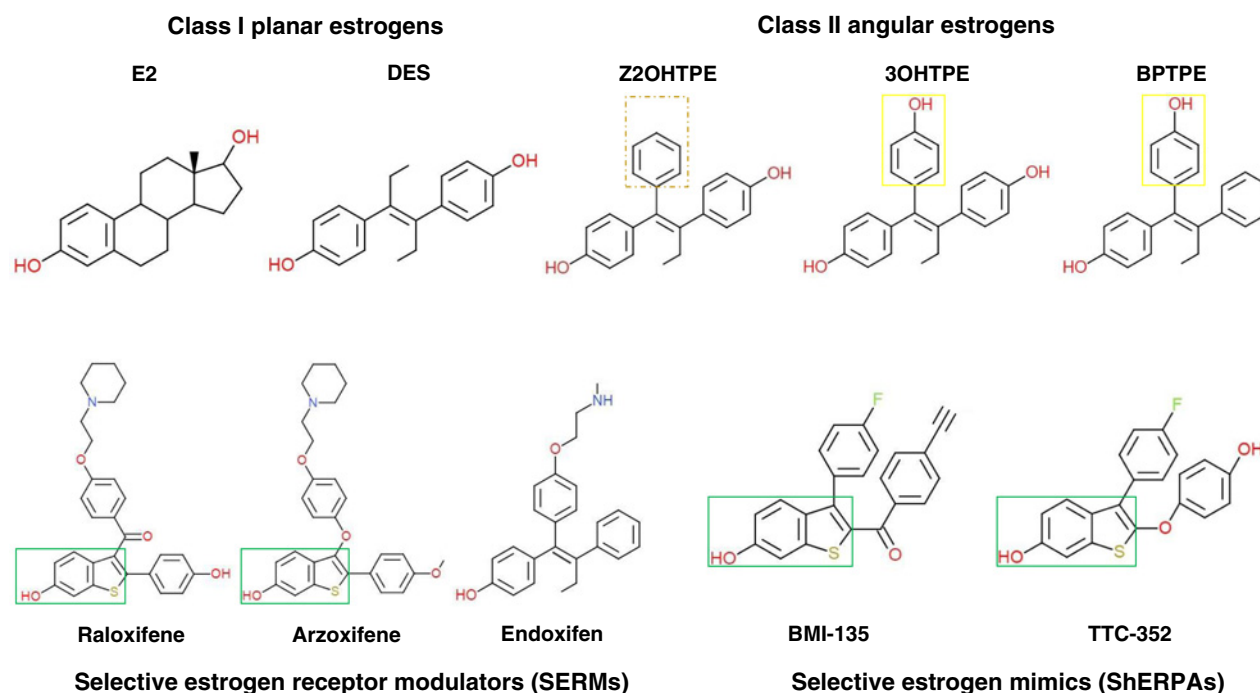
Figure 1.
Chemical structures of planar estrogens, angular estrogens, SERMS, and ShERPAs. The box (in green) highlights the benzothiophene scaffold embedded in raloxifene and arzoxifene structures, of which the ShERPAs' structures were based upon. The *continuous* box (in yellow) highlights the phenyl ring bearing OH of TPEs: trihydroxytriphenylethylene (**3OH**TPE) and **BP**TPE (46), which makes them angular estrogens/partial agonists. The *dashed* box (in brown) highlights the absence of OH on the phenyl ring of the Z-isomer of dihydroxytriphenylethylene (**Z2OH**TPE), which makes it an angular estrogen/full agonist like E_2 and diethylstilbestrol (DES; ref. 46).

cancer, and use for hormone replacement therapy as well as oral contraception. The combination of E_4 and progestin drospirenone is subject to FDA approval, with the possibility of E_4 becoming the first natural estrogen approved in a contraceptive product in the United States and the first new estrogen introduced in the United States in 50 years. A clinical trial using E_4, to treat advanced breast cancer, shows that the majority of patients experienced favorable subjective effects on wellbeing, and 1 patient completed the phase 1/IIA with stable disease after 24 weeks of treatment (12).

The ER in LTED breast cancer is at the crossroads of mediating the antitumor actions of therapeutics as well as breast cancer growth through ERα-activating mutations (18). Investigating ERα's regulation and DNA-or-ligand-binding profiles with ShERPAs and E_4 enhances our understanding of how these therapeutics influence cancer through ER.

ERα gene *ESR1* point mutations in the ligand-binding domain (LBD) lead to constitutive hormone-independent activation of ER and are identified in approximately 40% of MBC (19). These mutations are especially enriched in patients with breast cancer pretreated with AIs (20).

The expression level and stability of ER is modulated by estrogens and antiestrogens. Two regulatory mechanisms that govern the steady-state of ER messenger RNA (mRNA) and protein levels in breast cancer cells are documented (21). Model I ER regulation reflects the rapid downregulation of the steady state of ER mRNA and protein levels upon estrogen exposure, and is exemplified in MCF-7:WS8 breast cancer, ovarian carcinoma (PEO4), and the rat and mouse uterus. Model II ER regulation reflects the upregulation of the steady-state level of ER mRNA, alongside the maintenance of the ER protein level upon estrogen exposure, and is exemplified in T47D:A18 breast cancer. In MCF-7:WS8 and T47D:A18, the anti-estrogen 4-hydroxytamoxifen (4OHT) has little effect on the ER mRNA level, but accumulates the ER protein over time (21). The Selective ER Downregulator ICI 182,780 fulvestrant (ICI) has little effect on the ER mRNA level in MCF-7:WS8, whereas it causes its reduction in T47D:A18, and ICI dramatically reduces the ER protein level in both (21).

ERα's transcriptional control of diverse downstream gene expression is dictated by the ability of bound estrogens or antiestrogens (22) to recruit and assemble primary steroid receptor coactivators [steroid receptor coactivator-3 (SRC-3), also known as nuclear receptor coactivator-3 (NCOA3), and A1B1], followed by secondary coactivators [p300/E1A-binding protein p300 (EP300)], in what is known as minimal receptor–coactivator complex (23). This facilitates chromatin remodeling and transcriptional activation. A model was proposed for the assembly mechanism of the quaternary complex: the two ligand-bound ERα monomers each, independently, recruit one SRC-3 protein through the transactivation domain of ERα, and the two SRC-3s, subsequently, bind to different regions of one p300 protein via multiple contacts (23).

We investigate ShERPAs and E_4's influence on breast cancer through studying their ERα regulation and coactivators' binding profiles in biologically different breast cancer models. Furthermore, we present the first X-ray crystallography of TTC-352 with the mutant ER, its pharmacology, and molecular mechanisms of tumor regression in LTED endocrine-resistant breast cancer.

Materials and Methods

Materials

E_2, E_4, 4OHT, and raloxifene (Ralox) were purchased from Sigma-Aldrich. Endoxifen (Endox) was purchased from Santa Cruz Biotechnology, and ICI from Tocris Bioscience. Triphenylethylene bisphenol (BPTPE) was originally synthesized at the Organic Synthesis Facility, Fox Chase Cancer Center (Philadelphia, PA; ref. 24). The ShERPAs BMI-135 and TTC-352 were a gift from Drs. Debra A. Tonetti and Gregory R.J. Thatcher (University of Chicago, IL). The PERK inhibitor GSK G797800 was purchased from Toronto Research Chemicals. The IRE1α Inhibitor MKC-3946 was purchased from Calbiochem. Thioflavin T (ThT) was purchased from Sigma-Aldrich. For Western blotting, anti-ERα (sc-544), anti-eIF2α (D-3), and anti–β-actin (C-4) were purchased from Santa Cruz Biotechnology. Anti–phospho-eIF2α (Ser51; #9721), anti-ATF4 (D4B8), anti-CHOP (L63F7), and anti-cleaved PARP (Asp214; 19F4) were purchased from Cell Signaling Technology. Anti-XBP1 (isoforms nonspliced and spliced, ab37152) was purchased from Abcam. For immunoblotting validations for the ERE DNA pulldowns, the antibodies used were: anti-MLL4 (Millipore Sigma, ABE1867), anti-NCOA1 (Santa Cruz Biotechnology, sc-32789), anti-NCOA3 (custom-made in Bert W. O'Malley's laboratory, Baylor College of Medicine, Houston, TX; ref. 25), anti-MED6 (Santa Cruz Biotechnology, clone D-2), anti-MED17 (Novus Biologicals, clone 4D4), and anti-ESR1 (Santa Cruz Biotechnology, sc-543). For chromatin immunoprecipitation's (ChIP's) pulldowns, the antibodies used were: anti–SRC-3 (clone AX15.3, 1 μg/μL; 5 μg per reaction; Abcam), and normal mouse IgG as IP negative control (2 μg/μL; 5 μg per reaction; Santa Cruz Biotechnology).

Cell culture

Wild-type (WT) estrogen-dependent breast cancer MCF-7:WS8 (26); mutant p53 estrogen-dependent breast cancer T47D:A18 (27); estrogen-responsive, ER-positive, progesterone receptor (PgR)–positive, and HER2-positive luminal B breast cancer BT-474 (28); estrogen-responsive, ER-positive, PgR-positive, and androgen receptor–positive luminal A breast cancer ZR-75–1 (29); the first in vitro cellular model recapitulating acquired TAM resistance developed in athymic mice in vivo MCF-7:PF (30); antihormone-resistant estrogen-independent breast cancer MCF-7:5C (31); antihormone-sensitive estrogen-independent breast cancer MCF-7:2A (32); antihormone (raloxifene)-resistant, estrogen-independent breast cancer MCF-7:RAL (33); TAM-sensitive, estrogen-independent, ER-positive breast cancer LCC1 (34, 35); TAM-resistant and ICI-sensitive, estrogen-independent, ER-positive breast cancer LCC2 (36); and TAM and ICI cross-resistant, ER-positive breast cancer LCC9 (37) were cultured as described previously.

Cell viability and proliferation assays

The biological properties of compounds (E_2, BMI-135, TTC-352, BPTPE, 4OHT, endoxifen, and raloxifene) in cells lines were evaluated by assessing the DNA content of the cells, as a measure of cell viability, using a DNA fluorescence Quantitation kit (Bio-Rad Laboratories) as described previously (38). The DNA fingerprinting pattern of these cell lines is consistent with that reported by the ATCC. All cell lines were validated according to their short tandem repeat (STR) profiles at UT MD Anderson Cancer Center Characterized Cell Line Core (CCLC). The STR patterns of all cell lines were consistent with those from the CCLC standard cells (Supplementary Table S1). The calculated half maximal effective concentration (EC_{50}) for all test compounds, used in treating these cell lines, is summarized in Supplementary Table S2.

Quantitative real-time RT-PCR

Total RNA was isolated from MCF-7:WS8 and MCF-7:5C cells using MagMAX-96 Total RNA Isolation Kit (Applied Biosystems) and processed using Kingfisher Duo Prime magnetic particle processor (Thermo Scientific). The cDNA was synthesized using High Capacity cDNA Reverse transcription kit (Applied Bioscience). Quantitative real-time PCR assays were performed using Power SYBR Green PCR Master Mix (Applied Biosystems) and a QuantStudio 6 Flex real-time PCR System (Applied Biosystems). All primers were synthesized by Integrated DNA Technologies Inc. All data were normalized using reference gene 36B4.

Immunoblotting

Cells were treated with different compounds [E_2 (1 nmol/L), BMI-135 (1 μmol/L), TTC-352 (1 μmol/L), E_4 (1 μmol/L), BPTPE (1 μmol/L), 4OHT (1 μmol/L), endoxifen (1 μmol/L), raloxifene (1 μmol/L), ICI (1 μmol/L), thapsigargin (1 μmol/L), GSK G797800 (10 μmol/L), and MKC-3946 (20 μmol/L)], for different periods, and harvested in cell lysis buffer (Cell Signaling Technology) supplemented with Protease Inhibitor Cocktail Set I and Phosphatase Inhibitor Cocktail Set II (Calbiochem). Immunoblotting was performed as described previously (38). Analysis was validated by densitometry using Image J (National Institutes of Health). Densitometry data are presented in Supplementary Tables S3 and S4.

ERE DNA pulldowns

MCF-7:WS8 and MCF-7:5C cells were grown in 20 to 30 15-cm dishes, and nuclear extracts (NE) were made. The 4x estrogen response element (ERE) DNA pulldown assays were performed, by first immobilizing four copies of the Xenopus Vitellogennin ERE sequences onto Dynabeads M280 streptavidin as described previously (39). One milligram of NE from MCF-7:WS8 or MCF-7:5C cells, and 0.5 μg recombinant ERα protein (Invitrogen) were added to 4xERE-beads, with either vehicle controls (ethanol or DMSO), or E_2 (100 nmol/L), BMI-135 (1 μmol/L), TTC-352 (1 μmol/L), E_4 (1 μmol/L), BPTPE (1 μmol/L), and endoxifen (1 μmol/L), for a 1.5-hour incubation at 4°C. After performing three washes, the final coregulator-ERα-ERE DNA complexes were eluted from the beads in 30 μL 2x SDS-sample buffer for mass spectrometry (MS) as described previously (39). The detailed methodology is presented in Supplementary Materials.

MS

Label-free LC-MS was performed with quantification, by intensity-based absolute quantification (iBAQ; ref. 40), and the ERE/ER coregulator–binding reactions were analyzed as described previously (39). Samples were electrophoresed on 10% NuPAGE gels, 4 broad-region bands were excised, and the proteins were in-gel digested with trypsin. For each experiment, the peptides were combined into two pools and measured on a Thermo Scientific Orbitrap Elite mass spectrometer coupled to an EASY nLC1200 UHPLC system. The raw data were searched in Proteome Discoverer suite (PD2.2) with Mascot 2.5 engine. For peptide quantification, the PD 2.2 Peak Area Detector module was used, and for gene-centric inference and label-free quantitation based on the iBAQ method, the gpGrouper software was used. All raw MS and gpGrouper result files are deposited into the ProteomeXchange Consortium (http://proteomecentral.proteomexchange.org; ref. 41). Compiled results are provided in Supplementary Table S5.

X-ray crystallography

The 6 × His-TEV–tagged ER-Y537S LBD mutant was expressed in E. coli BL21 (DE3) and purified as described previously (42). The LBD

(5 mg/mL) was incubated with 1 mmol/L TTC-352 and 2.5 mmol/L GRIP peptide at 4°C overnight. The detailed methodology is presented in Supplementary Materials. Each structure was validated and deposited in the Protein Data Bank (accession code 7JHD).

Molecular dynamics simulations

Molecular dynamics (MD) simulations were performed for the following systems: hERαLBD in complex with E_2, TTC-352, and BPTPE, using the Desmond software (Schrödinger Release 2019–3, Schrödinger, LLC, 2019). The detailed methodology is presented in Supplementary Materials.

Live cell imaging and analysis to detect cellular stress

MCF-7:5C cells were seeded into three 15-μ slide 2-well chambered coverslip slides (Ibidi). After 24 hours, cells were treated with vehicle control [DSMO (0.1%)], positive control thapsigargin (1 μmol/L), TTC-352 (1 μmol/L), and 4OHT (1 μmol/L). After 72-hour treatment, ThT was prepared as described previously (43) and used in cotreating the cells for 1 hour. The Hoechst 33342 dye (Thermo Fisher Scientific) was prepared at a final concentration of 5 μg/mL and used in staining the cells for 15 minutes. Live cell images were taken at a 38 ms exposure under a 20X/0.7 objective with ZEISS Celldiscoverer 7 (Carl Zeiss AG). Fluorescent images were converted to 12-bit before being quantified by the ZEISS Zen Software Module-Image Analysis. Cells from each image were manually counted to normalize the fluorescent data per cell. Relative intensity per cell = ThT intensity/cell count was generated for each treatment per image. An average of the relative intensity per cell (using three images per treatment) was then calculated to give a final quantification. The excitation and emission settings were: Hoechst 33342 (Ex. 348 nm, Em. 455 nm), and ThT (Ex. 433 nm, Em. 475 nm).

Annexin V–binding assays to detect apoptosis

A FITC Annexin V Apoptosis Detection Kit I (BD Pharmingen) was used to quantify apoptosis of cells through flow cytometry. In brief, MCF-7:5C, MCF-7:2A, and MCF-7:RAL cells were seeded in 10-cm dishes. After 24 hours, the cells were treated with different compounds [E_2 (1 nmol/L), TTC-352 (1 μmol/L), 4OHT (1 μmol/L), raloxifene (1 μmol/L), GSK G797800 (10 μmol/L), and MKC-3946 (20 μmol/L)] for different time periods. Cells were suspended in 1x binding buffer, and 1×10^5 cells were stained simultaneously with FITC-labeled Annexin V and propidium iodide (PI) for 15 minutes at room temperature. The cells were analyzed using a BD Accuri C6 plus flow cytometer.

ChIP assays

The ChIP assay was performed as described previously (44, 45). The DNA fragments were purified using Qiaquick PCR purification kit (Qiagen). Then, 2 μL of eluted DNA was used for RT-PCR analysis. The primer sequences used are: GREB1 proximal ERE enhancer site amplification: 5′-GTGGCAACTGGGTCATTCTGA-3′ sense, 5′-CGACCCACAGAAATGAAAAGG-3′ antisense (Integrated DNA Technologies). The data are expressed as percent input, of starting chromatin material, after subtracting the percent input pulldown of the IP-negative control.

Statistical analysis

All reported values are mean ± SD. Statistical comparisons were assessed using two-tailed Student t tests. Results were considered statistically significant if the P value was less than 0.05.

Results

Effects of TTC-352 on cell viability in multiple breast cancer models

Cell viability assays were used to test the biological properties of compounds. TTC-352 exhibits a full agonist action, similar to E_2, across eight breast cancer cell lines that are estrogen-dependent (MCF-7:WS8, T47D:A18, BT-474, ZR-75–1, and MCF-7:PF), estrogen-independent (MCF-7:5C, MCF-7:2A, and MCF-7:RAL), endocrine-sensitive (MCF-7:2A), endocrine-resistant (MCF-7:PF, MCF-7:5C, and MCF-7:RAL), mutant p53 (T47D:A18), HER2-positive (BT-474), luminal A (ZR-75–1), and luminal B (BT-474).

The concentration 1 μmol/L for TTC-352 achieved either the maximal cellular growth (P value < 0.05 compared with vehicle control; Supplementary Fig. S1A–S1E) or the maximal cellular death (P < 0.05 compared with vehicle control; Supplementary Fig. S1F–S1H). TTC-352 was shown to be a less potent full agonist compared with E_2 (Supplementary Fig. S1 and Supplementary Table S2). The calculated EC_{50}s are summarized in Supplementary Table S2, and the detailed results are presented in Supplementary Materials.

TTC-352 induces the transcriptional activity of ER similar to E_2 in WT breast cancer MCF-7:WS8 and apoptotic-type breast cancer MCF-7:5C

qRT-PCR was used to assess the transcriptional activity of ERα on estrogen-responsive genes (TFF1 and GREB1) with TTC-352. After 24-hour treatment in MCF-7:WS8, TTC-352 significantly (P < 0.05) increased the levels of TFF1 and GREB1 mRNAs compared with vehicle controls (Fig. 2A–B). On the other hand, BPTPE induced a partial increase in the levels of TFF1 and GREB1 mRNAs, significantly (P < 0.05) less than that of E_2 and TTC-352 (Fig. 2A–B). The minimal concentration that produced a complete increase in the levels of TFF1 and GREB1 was at 10^{-6} mol/L for TTC-352 (P < 0.05 compared with vehicle control).

After 24-hour treatment in MCF-7:5C, TTC-352 significantly (P < 0.05) increased the levels of TFF1 and GREB1 mRNAs compared with vehicle controls (Fig. 2C–D). On the other hand, BPTPE induced a partial increase in the levels of TFF1 and GREB1 mRNAs, significantly (P < 0.05) less than that of E_2 and TTC-352 (Fig. 2C–D). The minimal concentration that produced a complete increase in the levels of TFF1 and GREB1 was at 10^{-6} mol/L for TTC-352 (P < 0.05 compared with vehicle control).

Overall, the induction of the levels of TFF1 and GREB1 mRNAs by TTC-352 in MCF-7:WS8 and MCF-7:5C is similar to that by full agonist E_2, only at a higher concentration.

Effects of TTC-352, BMI-135, and E_4 on ERα regulation in multiple breast cancer models

Western blotting and densitometry were used to assess the regulation of ERα protein levels with compounds. In MCF-7:WS8, TTC-352 was able to downregulate the protein levels of ERα after 72-hour treatment, compared with vehicle control, and similar to E_2 and E_4 (Model I; Fig. 3A and Supplementary Table S3). Whereas BMI-135 seems to have a different effect by slightly downregulating ERα's protein levels by 72 hours, compared with vehicle control (Supplementary Fig. S2A and Supplementary Table S4). This downregulation is less than that with BPTPE; nonetheless, BMI-135 does not accumulate the receptor compared to 4OHT and endoxifen (Supplementary Fig. S2A and Supplementary Table S4). This regulation trend with TTC-352, BMI-135, and E_4 in MCF-7:WS8 is
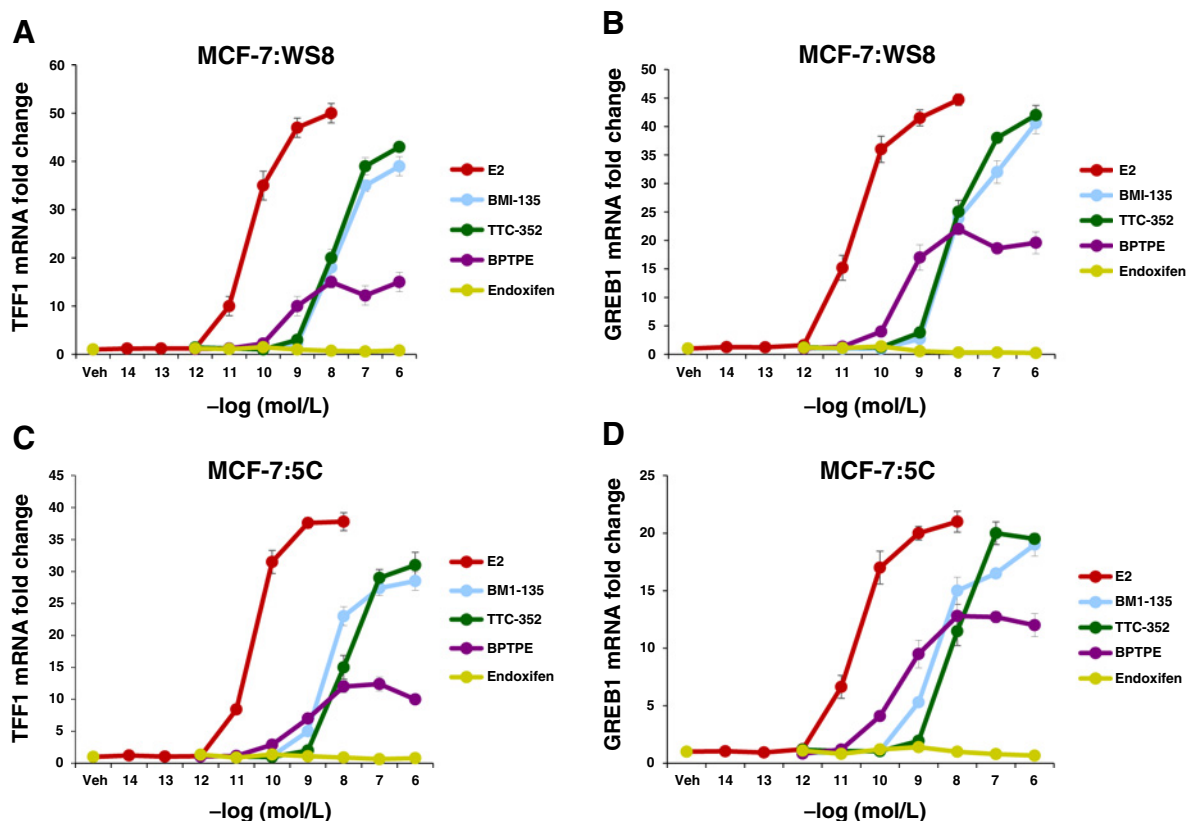
Figure 2.
Transcriptional activity of well-characterized estrogen-responsive genes *TFF1* and *GREB1* in WT MCF-7:WS8 and LTED endocrine-resistant MCF-7:5C with test compounds. **A,** mRNA expression of *TFF1* (or pS2) in MCF-7:WS8 cells after 24-hour treatment with 1 nmol/L E_2, and 1 μmol/L for other test compounds. **B,** mRNA expression of *GREB1* in MCF-7:WS8 cells after 24-hour treatment with 1 nmol/L E_2, and 1 μmol/L for other test compounds. **C,** mRNA expression of *TFF1* in MCF-7:5C cells after 24-hour treatment with 1 nmol/L E_2, and 1 μmol/L for other test compounds. **D,** mRNA expression of *GREB1* in MCF-7:5C cells after 24-hour treatment with 1 nmol/L E_2, and 1 μmol/L for other test compounds.

replicated in MCF-7 ATCC (Supplementary Fig. S2B and Supplementary Table S3).

In T47D:A18, TTC-352 and BMI-135 maintain the protein levels of ERα (Model II), compared with vehicle control, and similar to E_2 and E_4 (**Fig. 3B**, Supplementary Fig. S2C and Supplementary Tables S3 and S4). BPTPE, 4OHT, and endoxifen accumulate the receptor by 72 hours (Supplementary Fig. S2C and Supplementary Table S4).

In BT474, TTC-352 downregulates the protein levels of ERα by 72 hours, compared with vehicle control, and similar to E_2 and E_4 (Model I; **Fig. 3C**; Supplementary Fig. S2E; and Supplementary Tables S3–S4). Whereas BMI-135 seems to have a similar trend except that the protein levels by 72 hours are similar to vehicle control (Supplementary Fig. S2E and Supplementary Table S4). The protein levels are upregulated by 72 hours with BPTPE, and more so with endoxifen and 4OHT (Supplementary Fig. S2E and Supplementary Table S4).

In ZR-75–1, TTC-352 slightly downregulates the protein levels of ERα after 72-hour treatment, compared with vehicle control, and similar to E_2 and E4 (Model I; **Fig. 3D**; Supplementary Fig. S2D and Supplementary Tables S3–S4). Whereas BMI-135 seems to have a different trend whereby by 72 hours the protein levels become similar to vehicle control (Supplementary Fig. S2D and Supplementary Table S4). The protein levels are maintained by 72 hours with BPTPE,

4OHT, and endoxifen, compared with vehicle control (Supplementary Fig. S2D and Supplementary Table S4).

In MCF-7:5C, MCF-7:2A, and MCF-7:RAL, TTC-352, BMI-135, and E_4 downregulate the protein levels of ERα by 72 hours, compared with vehicle control, and similar to E_2 (Model I; **Fig. 3E–G** and Supplementary Fig. S3D–S3F). In MCF-7:2A, ER^{66} and ER^{77} protein levels with BMI-135, TTC-352, and E_4 are similarly regulated over time (Model I; **Fig. 3F**; Supplementary Fig. S3E; ref. 32). In these cell lines, the protein levels are slightly downregulated with BPTPE, and maintained or accumulated with endoxifen, 4OHT, and raloxifene (in MCF-7:RAL; Supplementary Fig. S3D–S3F).

In LCC1, LCC2, and LCC9, TTC-352, BMI-135, and E_4 downregulate the protein levels of ERα by 72 hours, compared with vehicle control, and similar to E_2 (Model I; **Fig. 3H–J**, Supplementary Fig. S3A–S3C, and Supplementary Table S3). In these cell lines, the protein levels are downregulated with BPTPE and maintained or accumulated with endoxifen and 4OHT (Supplementary Fig. S3A–S3C and Supplementary Table S3).

In 11 breast cancer cell lines, TTC-352 regulated the protein levels of ERα in a similar manner to E_2 (**Fig. 3** and Supplementary Table S3) and different from that with BPTPE (Supplementary Figs. S2–S3 and Supplementary Table S4), and ICI significantly downregulated the protein levels of ERα (**Fig. 3** and Supplementary Figs. S2–S3).
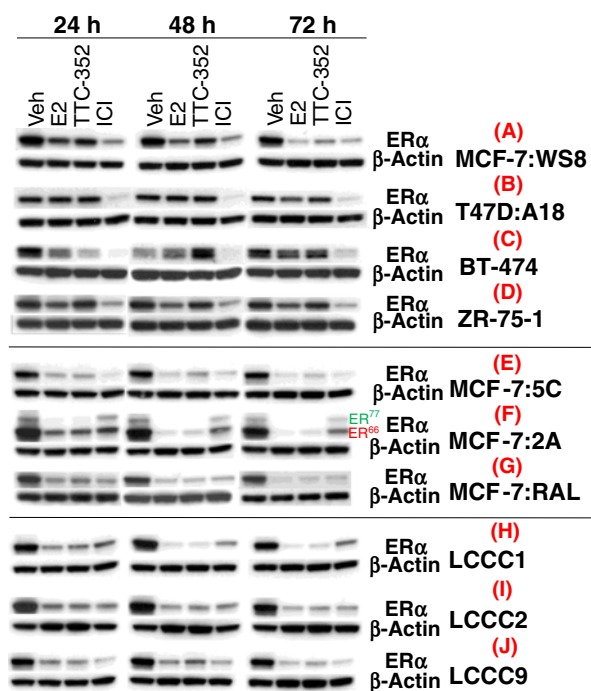
Figure 3.
ERα protein levels in multiple breast cancer cell lines after 24-, 48-, and 72-hour treatments with test compounds. **A,** ERα protein levels in MCF-7:WS8. **B,** ERα protein levels in T47D:A18. **C,** ERα protein levels in BT-474. **D,** ERα protein levels in ZR-75-1. **E,** ERα protein levels in MCF-7:5C. **F,** ERα protein levels in MCF-7:2A. **G,** ERα protein levels in MCF-7:RAL. **H,** ERα protein levels in LCC1. **I,** ERα protein levels in LCC2. **J,** ERα protein levels in LCC9. Densitometry data are presented in Supplementary Table S3.

Effects of TTC-352, BMI-135, and E_4 on coregulator recruitment to DNA-bound ER in WT breast cancer MCF-7:WS8 and apoptotic-type breast cancer MCF-7:5C

Cell-free *ERE* DNA pulldown (39) and LC-MS assays were used to assess the composition of coregulators recruited to ER bound to *ERE* DNA with compounds, using E_2 and endoxifen as positive and negative controls, respectively, for coactivator binding.

In MCF-7:WS8, E_2 recruited major coactivators such as NCOA1–3, the Mediator complex (MED; see subunits in **Fig. 4**), and Lysine Methyltransferase 2D (KMT2D or MLL4; **Fig. 4A**), which is consistent with prior proteomic publications (39). Endoxifen did not recruit these coactivators (**Fig. 4A**). BPTPE did not recruit many of the E_2-enriched coactivators and only a subset of endoxifen-enriched coregulators (**Fig. 4A**). Estetrol recruited NCOAs and KMT2D in a similar fashion to E_2, but failed to recruit many MED subunits at the level promoted by E_2 (**Fig. 4A**). TTC-352 and BMI-135 are different from BPTPE in terms of coactivator recruitment, chiefly recruiting NCOA1–2 and MED subunits, with NCOA3 not readily enriched compared with E_2 and E_4 (**Fig. 4A**).

In MCF-7:5C, E_2 recruited NCOA2–3, KMT2D, and the MED subunits, with slightly different distribution of affinities, whereas endoxifen repelled them, as expected for this Selective ER Modulator (SERM), and BPTPE did not have much of a coactivator binding (**Fig. 4A**). Estetrol recruited similar levels of NCOA3 and KMT2D, and many of the same MED subunits (**Fig. 4A**). TTC-352 and BMI-135

recruited NCOA3 and KMT2D at much lower levels than E_2 and E_4 (**Fig. 4A**). Interestingly, TTC-352 recruited more MED subunits than E_2, whereas BMI-135 displayed shared MED subunit recruitment with E_4 (**Fig. 4A**).

The recruitment of KMT2D, NCOA1, NCOA3, and MED17, in MCF-7:WS8 and MCF-7:5C, was further validated by immunoblotting (**Fig. 4B** and Supplementary Fig. S9).

Comparative analysis of the X-ray structures of hERαLBD in complex with ligands E_2, TTC-352, and BPTPE

The experimental X-ray structure (**Fig. 5G–I**) of hERαLBD in complex with TTC-352 shows the ligand binding to the agonist conformation of ERα [i.e., helix 12 (H12) is docked over the active site, in a grove between helices H5 and H11, leaning on H3, and closing the ligand inside the hydrophobic binding pocket; **Fig. 5A**]. The superposition with hERαLBD in complex with E_2 indicates minor differences between these two structures, with an average root mean square deviation (RMSD) of 0.55 Å; calculated based on Cα atoms. However, a difference has been noticed in the positioning of H12, with it being slightly displaced in the TTC-352:ERα structure by an average RMSD of 0.85Å, compared with the E_2:ERα structure (**Fig. 5A**). The binding mode of TTC-352 to the active site shares similar features with that of E_2. The benzothiophene moiety of TTC-352 overlaps well with the A and B rings of E_2, being involved in π–π stacking interactions with Phe404, and forming the H-bond network between the hydroxyl group and the side-chains of residues Glu353, Arg394, and a crystallization water molecule. The phenoxy ring occupies the same region of the binding pocket as the D ring of E_2, but it is buried slightly deeper in the active site, and oriented parallel with the imidazole ring of His524, favoring the formation of the H-bond with the hydroxyl group, like E_2 (**Fig. 5B**).

The analysis of the X-ray structure of hERαLBD in complex with BPTPE reveals good overlapping with the E_2:ERα structure with an average RMSD of 1.28 Å (**Fig. 5D**). Regarding the ligand-binding mode, BPTPE's alignment in the active site is comparable with E_2 and TTC-352 (**Fig. 5E**), preserving the same interactions with the exception of few noteworthy changes. First, the absence of the H-bond to His524, the residue's side-chain, is flipped out of the binding site, and the space freed is partially occupied by the phenyl ring of BPTPE. This observation could explain the displacement of BPTPE by 0.7 Å towards H11, compared with TTC-352. Second, the presence of an H-bond between the phenoxy ring of BPTPE and Thr347 (**Fig. 5E–F**). This contact leads to an alternative orientation of Thr347, with the methyl group pointing toward Tyr537, which results in a different conformation, and the displacement of Tyr537 relative to its position, compared with TTC-352:ERα or E_2:ERα (**Fig. 5C** and **F**). This repositioning at the base of H12, together with the reorientation of Leu540 due to the large phenoxy ring of BPTPE, alters the H-bond pattern in the vicinity. As a result, the H-bonds between Asp351 (H3) and the backbone of Leu539 and Leu540 (H12), which normally stabilize the orientation of H12 in the agonist conformation with E_2:ERα (**Fig. 5C**), are absent with BPTPE (**Fig. 5F**), but are present with TTC-352 (**Fig. 5C**).

MD simulations were performed to investigate the dynamics of hERαLBD and of ligand binding, specifically, the interactions responsible for binding, to highlight the differences that could discriminate between the ligands and explain their observed biological behaviors in tumor cells. The influence of the ligands on H12 conformation was also investigated, by monitoring the key interactions that are known to stabilize H12 in the agonist conformation (**Fig. 5C** and **F**).

A

Gene symbol	WS8								5C							
	EtOH	DMSO	E2	E4	TTC-352	BMI-135	BPTPE	Endoxifen	EtOH	DMSO	E2	E4	TTC-352	BMI-135	BPTPE	Endoxifen
ESR1	100.00	100.00	100.00	100.00	100.00	100.00	100.00	100.00	100.00	100.00	100.00	100.00	100.00	100.00	100.00	100.00
NCOA1			0.01	0.02		0.01										
NCOA2	0.20	0.05	0.25	0.39		0.09	0.04	0.06								
NCOA3	1.50	0.64	3.90	4.50	0.18	0.86	0.35	0.34	0.21	0.12	2.60	2.20	0.45	0.19	0.12	0.05
KMT2D	0.01	0.00	0.04	0.02	0.00	0.01	0.01	0.00	0.05	0.01	0.21	0.13	0.03	0.03	0.04	0.02
MED4	0.70	0.53	1.60	0.68	1.60	0.92	0.77	0.52	1.30	0.95	2.80	3.00	1.60	0.88	2.20	1.30
MED6	0.22	0.19	0.32	0.62	0.39	0.23	0.19	0.16	0.44	0.27	0.48	0.61	0.63	0.31	0.43	0.40
MED8	0.85	0.89	1.50	0.75	1.10	1.30	0.61	0.72	1.30	0.61	1.50	1.70	1.20	0.92	0.58	0.57
MED9	0.55	0.64	0.91	0.40	0.98	0.91	0.42	0.42	0.76	0.11	0.59	0.67	0.62	0.42	0.62	0.40
MED10	0.94	0.93	2.00	0.94	1.10	1.20	0.80	0.86	1.10	0.60	1.00	2.30	0.80	0.75	1.50	1.30
MED11	0.90	0.81	1.40	1.20	2.30	1.10	0.65	0.72	1.60	0.26	1.60	2.20	1.50	0.26	1.60	1.20
MED12	0.42	0.12	0.47	0.44	0.03	0.13	0.13	0.23	0.33	0.16	0.88	0.76	0.29	0.23	0.39	0.20
MED13	0.09	0.07	0.16	0.21		0.08	0.05	0.07	0.15	0.10	0.34	0.36	0.23	0.08	0.21	0.13
MED14	0.95	0.31	0.62	0.72	0.13	0.59	0.31	0.44	0.69	0.53	1.60	1.20	0.88	0.61	0.71	0.54
MED15	1.40	0.83	0.98	2.00	0.08	1.10	0.68	0.95	1.10	0.47	2.00	1.40	1.20	0.83	1.30	0.92
MED16	0.72	1.80	2.10	2.30	0.17	2.00	2.10	2.10	0.88	0.40	1.30	1.10	1.80	0.79	1.90	0.75
MED17	1.50	1.30	2.70	1.90	1.90	2.10	1.60	1.30	1.60	0.98	2.90	2.60	1.80	1.80	1.90	1.60
MED19	0.81	0.89	2.10	0.42	1.20	1.50	1.20	1.30	1.90	0.71	2.50	3.50	2.10	1.50	2.40	2.10
MED20	1.00	1.40	2.60	0.96	2.40	2.30	0.68	1.60	3.00	1.60	3.00	3.60	2.70	2.40	2.90	2.30
MED22	0.39	0.65	1.10	0.14	0.97	0.64	0.43	0.35	0.50	0.26	0.83	1.60	0.49	0.65	1.10	0.66
MED23	1.20	0.71	0.73	1.20	0.28	0.54	0.52	0.81	0.79	0.50	1.40	1.20	1.00	0.66	0.89	0.70
MED24	1.50	0.81	0.63	0.79	0.18	0.44	0.57	0.42	1.00	0.64	1.80	1.30	0.81	0.68	1.10	0.78
MED26	0.37	0.39	0.54	0.50	0.36	0.32	0.49	0.44	0.24	0.14	0.37	0.19	0.19	0.27	0.16	0.16
MED27	0.59	0.50	1.30	0.25	0.74	0.76	0.16	0.47	1.30	0.22	2.10	1.70	0.88	0.41	1.30	0.52
MED28	0.95	0.85	1.60	0.68	1.20	1.10	0.81	0.77	1.50	0.12	1.30	1.70	1.10	0.95	1.10	0.73
MED29	0.67	0.18	0.87	0.56	0.49	0.17	0.14	0.33	0.90	0.29	1.10	1.10	0.95	0.18	0.66	0.35
MED30	1.60	1.10	2.50	1.50	1.40	1.40	0.62	0.78	3.00	1.00	2.50	3.90	2.20	1.40	1.90	1.30
MED31	0.90	1.50	2.10	0.81	2.20	1.20	0.94	1.10	1.40	0.56	1.40	2.70	1.30	1.60	1.40	1.10

Fold change: 1 1.5 2 5 10 and above — Down / Up

Header colors:
COMPOUND - in EtOH vehicle
COMPOUND - in DMSO vehicle

B

WS8: 3% input, DMSO, E2, E4, BMI-135, TTC-352
5C: 3% input, DMSO, E2, E4, BMI-135, TTC-352

(kDa) 250 — KMT2D
150 — NCOA1
150 — NCOA3
75 — MED17
50 — ESR1

Figure 4.

Proteomics of major ER coregulators in MCF-7:WS8 and MCF-7:5C breast cancer with test ligands, and immunoblots of KMT2D, NCOA1 and 3, and MED17 to validate MS data. **A,** Proteomics of major coregulators differentially recruited to DNA-bound recombinant ER in MCF-7:WS8 and MCF-7:5C cells, treated with E_2 (100 nmol/L), E_4 (1 μmol/L), TTC-352 (1 μmol/L), BMI-135 (1 μmol/L), BPTPE (1 μmol/L), and endoxifen (1 μmol/L). Ethanol or DMSO served as the vehicle control. *ERE* DNA pulldown cell-free reactions were performed, and MS data are depicted as a heatmap for coregulator enrichment (light to dark red color) or repulsion (light to dark blue color). The values represent quantification with label-free iBAQ method, normalized to *ESR1* amount, and are shown (as estimated % relative to *ESR1*). Official gene symbols are shown (on the leftmost column). NCOA1–3, KMT2D, and MEDs were defined previously as E_2-enriched coactivators (25, 39). **B,** Immunoblotting to validate MS data of KMT2D, NCOA1 and 3, and MED17, recruited in MCF-7:WS8 and MCF-7:5C NE to DNA-bound ER (*ESR1*), when treated with E_2 (100 nmol/L), E_4 (1 μmol/L), TTC-352 (1 μmol/L), and BMI-135 (1 μmol/L). Protein size standards are shown (on the left side as kDa), and 3% input is shown (on the left side; representing 3% of WS8 or 5C NE that was added to each 4x*ERE* DNA bead).

Evaluation of the trajectory stability from MD simulations

Note that 165 ns MD simulations were performed for all systems. The RMSDs of the protein backbone atoms, relative to their position in the first frame, were monitored to evaluate the equilibration and stability of the simulations. The RMSD evolution for all simulations, together with the stability of H12 and amino acids of the binding sites, is displayed (Supplementary Fig. S4A–S4C) and detailed in Supplementary Materials. Briefly, the data indicate that all systems reached equilibrium and that the trajectories were stable (Supplementary Fig. S4A). Similar trends were observed for the systems of TTC-352 and E_2, whereas BPTPE showed more conformational changes in the segment corresponding to H12 (Supplementary Fig. S4B). No significant conformational changes were detected in the active site of all structures (Supplementary Fig. S4C).

To gain insights into the local flexibility of the receptor chain, root mean square fluctuation was monitored along the trajectories of all complexes (Supplementary Fig. S4D–S4F), with detailed results presented in Supplementary Materials. In summary, the data suggest that the large fluorophenyl moiety of TTC-352 induces more flexibility in the loop between H11 and H12, than the phenoxy ring of BPTPE. However, this is not translating into larger flexibility of H12, mainly because of the stabilizing effect of the H-bonds between Asp351, and the backbone of Leu539 and Leu540 with TTC-352, but not with BPTPE (**Fig. 5C** and **F**). Moreover, in the system of BPTPE, increasingly large fluctuations have been detected at the terminal residues of H12. This indicates more mobility in this region of the helix, which destabilizes and hinders the proper closing of H12 over the binding

pocket, leading to the inability of BPTPE complex to reach the full-agonist conformation of the receptor.

Analysis of E_2, TTC-352, and BPTPE binding modes from MD simulations

The interaction maps of the ligands with key residues of the binding site, together with the occurrences for specific contacts, are displayed (**Fig. 6**), and the detailed results are presented in Supplementary Materials. The MD simulations confirmed that the H-bonds to Glu353 and His524 are highly stable for TTC-352 and E_2 (**Fig. 6A–B**). As reported previously (46), the H-bond to Thr347 is the most stable interaction for BPTPE, being maintained during the entire simulation, which indicates a strong bond, whereas the H-bond to Glu353 shows a significantly decreased frequency, which indicates a weaker bond (**Fig. 6C**).

Analysis of the binding-free energy decomposition for E_2, TTC-352, and BPTPE

To gain a deeper understanding of the ligand–receptor interactions and highlight the subtle differences that could discriminate between these ligands, we performed ligand-binding energy calculations using the MM-GBSA method for the simulated systems. The contribution of each residue to the binding process was analyzed, by decomposing the binding energy into ligand-residue pairs, with the results displayed (Supplementary Fig. S5) and detailed in Supplementary Materials.

The data show that the H-bonding to Glu353 is the driving force of binding for TTC-352, similar to E_2. This interaction is crucial for
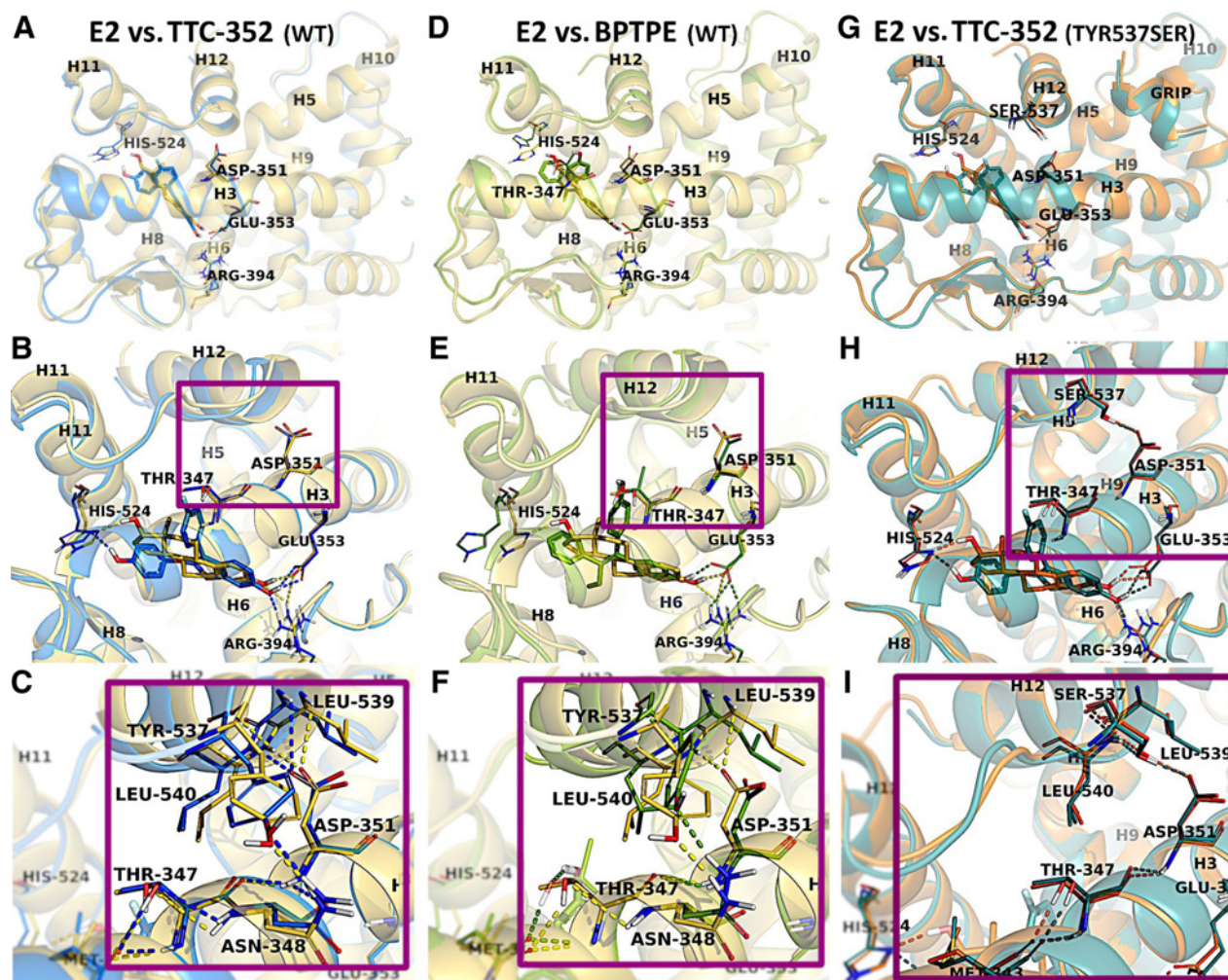
Figure 5.
Representation of ERα-LBD with E2, TTC-352, and BPTPE. Comparison of the WT structures of E2 (yellow), TTC-352 (blue), and BPTPE (green) bound to hERα. The superposition of the X-ray structures of hERαLBD:E2 with hERαLBD:TTC-352 (**A**), and of hERαLBD:E2 with hERαLBD:BPTPE (**D**). The closer views of the active sites show the binding modes of E2 (yellow), in comparison with TTC-352 (blue; **B**) and BPTPE (green; **E**), together with the H-bond contacts between H3 and H12 for E2, TTC-352 (**C**), and BPTPE (**F**). The superposition of the mutant *Tyr537Ser* X-ray structures of hERαLBD in complex with E2 (orange) and TTC-352 (teal; **G**), together with the binding site alignment of the ligands (**H**), and a close view of the H-bond interactions between Asp351 and Ser537 (**I**). Amino acid residues involved in direct interactions (i.e., H-bonds and hydrophobic contacts) are labeled and shown in sticks, together with the amino acids directly involved in H-bonds with H12. In the overall structures, H12 is labeled together with the helices that form the ligand-binding site (i.e., H3, H6, H8, H11) and part of the coactivator site (i.e., H5, H9, H10). The H-bonds are displayed (dashed lines) in yellow, blue, and green in the structures of E2, TTC-352, and BPTPE, respectively.

agonist binding. The H-bond between BPTPE and Glu353 is weaker, and the binding of BPTPE is governed by the H-bond to Thr347 (**Fig. 6C**). This leads to instability in this region of H3, which could have an impact on the conformation of Asp351 that is found in close proximity and could explain why the H-bonds to Leu539 and Leu540 are missing for BPTPE:ERα. In addition, the strong interaction with Thr347 stabilizes the ligand in the active site, but perturbs the local environment and disrupts the H-bond between Tyr537 and Asn348. Finally, the stability of H12 and proper closing specific for the agonist conformation are affected in the structure of BPTPE:ERα.

TTC-352 induces ThT fluorescence as a marker of UPR

Thioflavin T was used to detect and quantify the EnR stress or UPR in living cells, as it interacts directly with the accumulated misfolded protein amyloid during the UPR (43). The "blue" Hoechst 33342

fluorescent dye was used as a nuclear counterstaining dye in MCF-7:5C living cells (**Fig. 7**, channel A), the "green" ThT fluorescent dye was used as a UPR-indicative dye (channel B), and a colocalization of ThT and Hoechst 33342 dyes is shown (channel C).

TTC-352 induced ThT fluorescence by 72 hours compared with vehicle control, and somewhat similar to the induction seen with positive control thapsigargin (i.e., triggers EnR stress by disrupting EnR Ca^{2+} homeostasis; **Fig. 7B**). The ThT relative intensity/cell for thapsigargin was 3.320555, and 2.025762 for TTC-352, compared with 0.4725 for vehicle control.

TTC-352 triggers apoptosis in multiple estrogen-independent and endocrine-resistant breast cancer models

Flow cytometry was used to assess if the type of stress-induced cell death was actually apoptosis, when treated with 1 μmol/L TTC-352. In
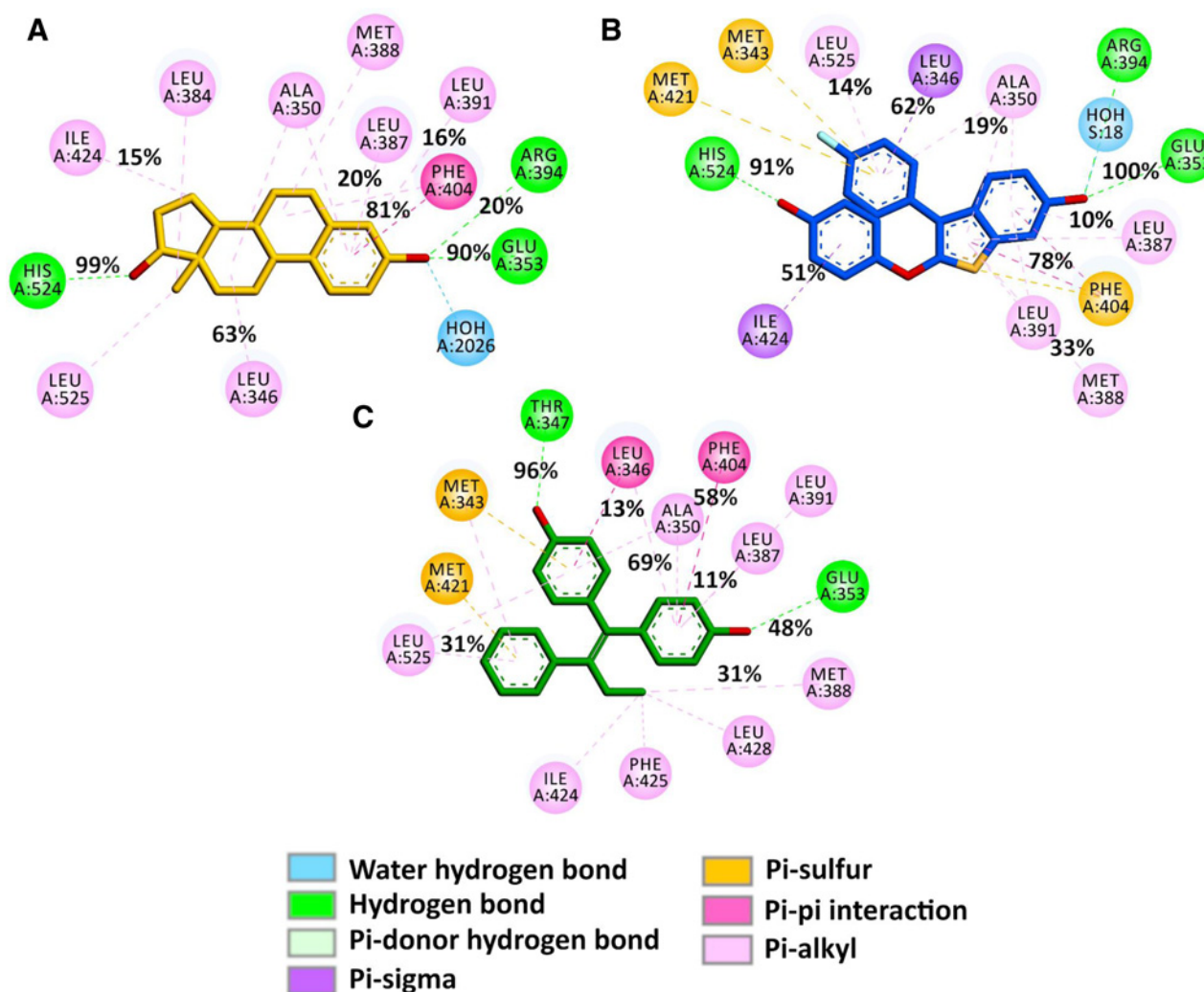
Figure 6.
2D ligand–ERα interaction maps highlighting key interactions between the ligands and ERα's amino acids during the simulations. These maps were generated from the recorded trajectories and the occurrences of the key contributing interactions between E$_2$ (**A**), TTC-352 (**B**), BPTPE (**C**), and the amino acids in the binding site of ERα, as shown.

MCF-7:5C, TTC-352 induces apoptosis (Annexin staining 22.9% vs. vehicle control 6.9%; **Fig. 8A**), similar to the time course of 1 nmol/L E$_2$ (Annexin staining 23.4% vs. control 6.7%; Supplementary Fig. S7A), which is in 3 days.

In MCF-7:2A, TTC-352 induces apoptosis (Annexin staining 21.2% vs. control 2.7%), similar to the time course of E$_2$ (Annexin staining 20.4% vs. control 2.7%; Supplementary Fig. S7B), which is in 9 days.

In MCF-7:RAL, TTC-352 induces apoptosis (Annexin staining 8.4% vs. control 1.5%), similar to the time course of E$_2$ (Annexin staining 9.1% vs. control 1.5%; Supplementary Fig. S7C), which is in 14 days.

Inhibition of PERK UPR pathway blocks apoptosis in MCF-7:5C with TTC-352 treatment

Blocking the UPR transducer PERK with 10 μmol/L GSK G797800 in combination with 1 μmol/L TTC-352 by 72 hours inhibited apoptosis (Annexin staining 6.9% vs. control 6.9%; **Fig. 8A**), compared

with TTC-352 alone treatment (**Fig. 8A**; Annexin staining 22.9% vs. vehicle control 6.9%), and compared with 10 μmol/L GSK G797800 alone treatment (Annexin staining 8.3% vs. control 6.9%; **Fig. 8A**).

PERK downstream targets p-eIF2α, ATF4, and CHOP as well as apoptosis target cleaved PARP are upregulated after 72-hour treatment with TTC-352, whereas the addition of GSK 797800 inhibits this UPR/apoptosis effect (**Fig. 8B**).

Inhibition of IRE1α:XBP1s UPR pathway enhances apoptosis in MCF-7:5C with TTC-352 treatment

Inhibiting the UPR transducer IRE1α, by inhibiting basal XBP1 splicing, with 20 μmol/L MKC-3946 in combination with 1 μmol/L TTC-352 by 72 hours, enhanced apoptosis (Annexin staining 35.5% vs. vehicle control 1.4%; **Fig. 8C**), compared with TTC-352 alone treatment (Annexin staining 27.9% vs. vehicle control 1.4%; **Fig. 8C**), and compared with 20 μmol/L MKC-3946 alone treatment (Annexin staining 8.8% vs. vehicle control 1.4%; **Fig. 8C**).
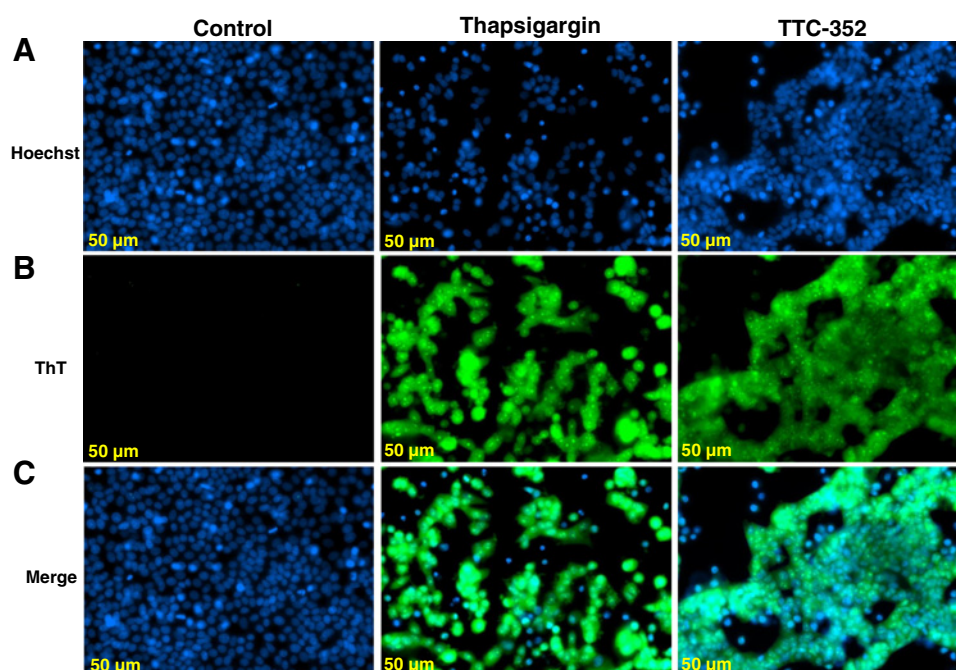
Figure 7.
Detection of EnR stress in live MCF-7:5C cells using ThT dye. **A,** Hoechst 33342 dye single panel (blue). **B,** ThT dye single panel (green). **C,** A colocalization panel of ThT and Hoechst 33342 dyes (blue and green). Treatments included vehicle control [DMSO (0.1%)], positive control thapsigargin (1 µmol/L), and TTC-352 (1 µmol/L). After 72-hour treatment, cells were cotreated with ThT (5 µmol/L) for 1 hour. The previous culture media were then swiped with Hoechst 33342 dye (5 µg/mL) in warm PBS for 15 minutes. Live cell imaging was done by the ZEISS Celldiscoverer 7 microscope. Scale bar, 50 µm.
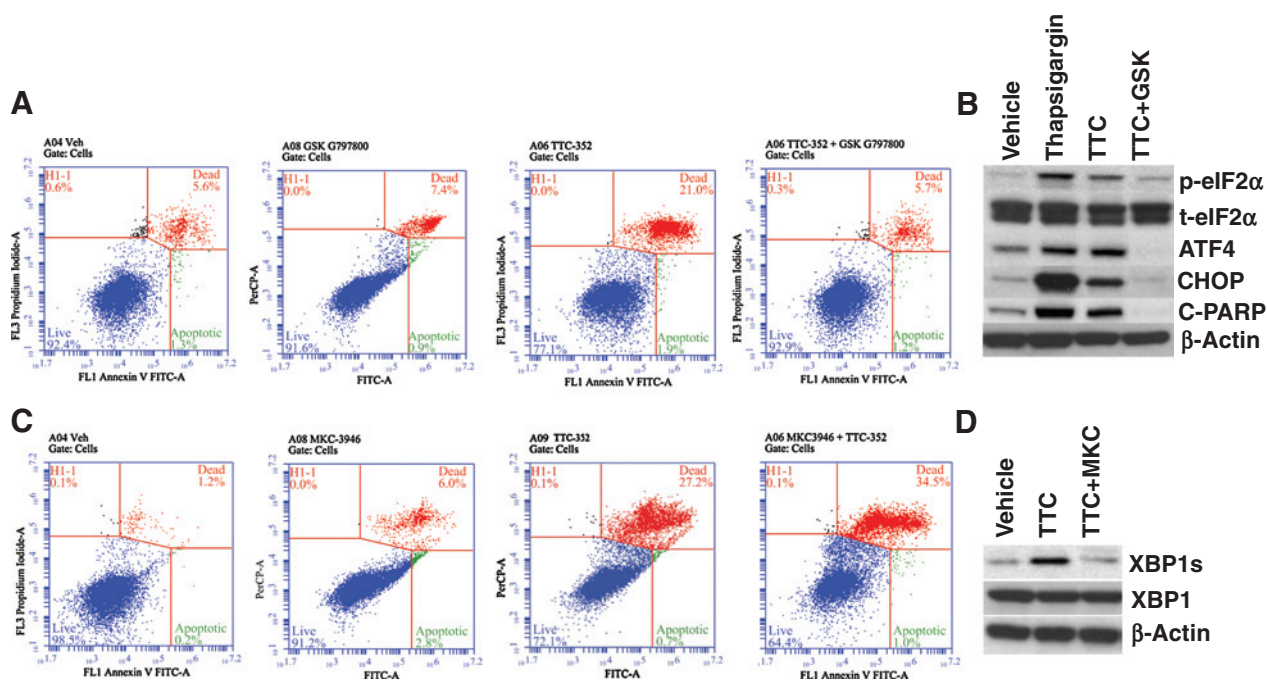
Figure 8.
Flow cytometry and Western blotting in MCF-7:5C cells treated with TTC-352 and its combination with a PERK inhibitor and an IRE1α inhibitor. **A,** MCF-7:5C cells were treated with vehicle control [DMSO (0.1%)], GSK G797800 (10 µmol/L), TTC-352 (1 µmol/L), and TTC-352 plus GSK G797800, for 3 days, and then stained with Annexin V–FITC and PI, and analyzed by flow cytometry. Viable cells (left bottom quadrant) are Annexin V–FITC− and PI−; early apoptotic cells (right bottom quadrant) are Annexin V–FITC+ and PI−; dead cells (left top quadrant) are PI+; and late apoptotic cells (right top quadrant) are Annexin V–FITC+ and PI+. An increased, late apoptotic effect is observed in the right top quadrant. **B,** p-eIF2α, total eIF2α, ATF4, CHOP, and cleaved PARP protein levels, in MCF-7:5C, after 72-hour treatments with vehicle control DMSO (0.1%), UPR +ve control thapsigargin (1 µmol/L), TTC-352 (1 µmol/L), and TTC-352 (1 µmol/L) plus GSK 797800 (10 µmol/L). **C,** MCF-7:5C cells were treated with vehicle control [DMSO (0.1%)], MKC-3946 (20 µmol/L), TTC-352 (1 µmol/L), and TTC-352 plus MKC-3946, and analyzed by flow cytometry. **D,** XBP1s, and XBP1 protein levels, in MCF-7:5C, after 72-hour treatments with vehicle control DMSO (0.1%), TTC-352 (1 µmol/L), and TTC-352 (1 µmol/L) plus MKC-3946 (20 µmol/L). **A** and **C,** ***, $P < 0.001$.
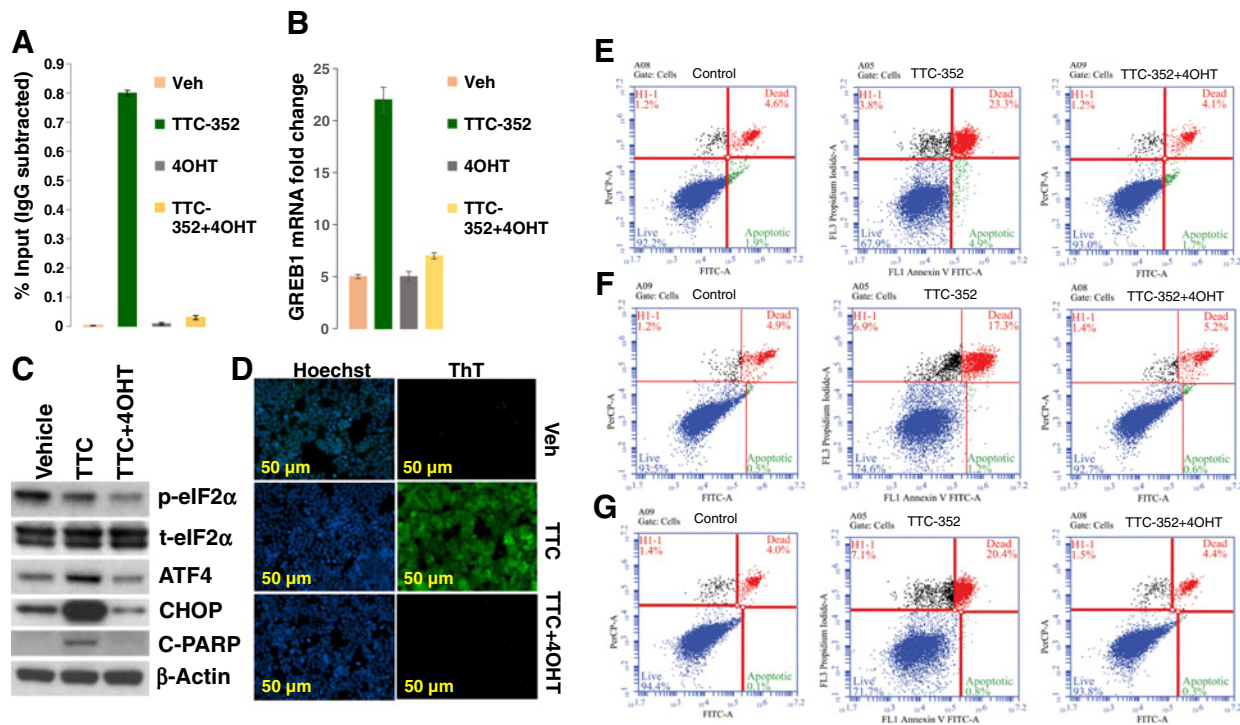
Figure 9.
Mediation of the transcriptional–translational, UPR, and apoptotic effects of TTC-352 via ERα. **A,** Recruitment of SRC-3, in MCF-7:5C cells, after 45-minute treatment with indicated ligands (1 μmol/L). Recruitment of SRC-3 was calculated as percentage of the total input after subtracting the IgG recruitment. **B,** mRNA expression of *GREB1*, in MCF-7:5C cells, after 24-hour treatment with ligands (1 μmol/L). **C,** p-eIF2α, total eIF2α, ATF4, CHOP, and cleaved PARP protein levels, in MCF-7:5C, after 72-hour treatments with vehicle control DMSO (0.1%), TTC-352 (1 μmol/L), and TTC-352 (1 μmol/L) plus 4OHT (1 μmol/L). **D,** Detection of UPR, in live MCF-7:5C cells, using ThT dye, after 72-hour treatments with vehicle control DMSO (0.1%), TTC-352 (1 μmol/L), and TTC-352 (1 μmol/L) plus 4OHT (1 μmol/L). Scale bar, 50 μm. **E,** MCF-7:5C cells were treated with vehicle control DMSO (0.1%), TTC-352 (1 μmol/L), and TTC-352 (1 μmol/L) plus 4OHT (1 μmol/L) for 3 days, and analyzed by flow cytometry. **F,** MCF-7:2A cells were treated with vehicle control DMSO (0.1%), TTC-352 (1 μmol/L), and TTC-352 (1 μmol/L) plus 4OHT (1 μmol/L) for 9 days, and analyzed by flow cytometry. **G,** MCF-7:RAL cells were treated with vehicle control DMSO (0.1%), TTC-352 (1 μmol/L), and TTC-352 (1 μmol/L) plus 4OHT (1 μmol/L) for 14 days, and analyzed by flow cytometry. **E–G,** ***, $P < 0.001$.

IRE1α downstream target XBP1 (or spliced XBP1) is upregulated after 72-hour treatment with TTC-352, whereas the addition of MKC-3946 inhibits this splicing effect (**Fig. 8D**).

Transcriptional–translational, UPR, and apoptotic effects of TTC-352 are mediated via ERα

TTC-352 was shown to function via ERα. The combination of TTC-352 and 4OHT blocked SRC-3 recruitment compared with TTC-352 alone treatment (**Fig. 9A**); inhibited *ERE* activation compared with TTC-352 alone treatment (**Fig. 9B**); blocked the antiproliferative effects of TTC-352 alone treatment (Supplementary Fig. S8A–S8C); inhibited the UPR PERK pathway activation (**Fig. 9C–D**); and prevented apoptosis (**Fig. 9C** and **E–G**).

Discussion

TTC-352 is a member of a new class of estrogen mimics (**Fig. 1**; 16), which is currently being evaluated in endocrine-resistant MBC clinical trials (11). This work reports: (i) the X-ray crystallography of TTC-352: mutant ER with clinical implications given that many patients with MBC harbor ER mutations (**Fig. 5G–I**; refs. 19, 20, 47); (ii) the molecular mechanisms of TTC-352′s breast cancer regression in patients with LTED (**Figs. 7–10**); and (iii) the key interactions at the molecular and atomic levels of the benchmark partial agonist BPTPE:

WT ER, involving Asp351 and H12 (**Figs. 5** and **6**), which explains the delayed ERα-induced UPR and apoptosis (48) compared with TTC-352 (**Fig. 8**).

Earlier pharmacologic studies classified ER-binding ligands into agonists, partial agonists, and antagonists (49), and complimented the subsequent X-ray crystallography studies of the agonist and antagonist ER complexes of the LBD (22, 50). Earlier biological studies described E_2-induced apoptosis (51). Current study concludes that TTC-352 is a less potent full estrogen agonist in numerous biologically different breast cancer models (**Figs. 2–6** and **9**; Supplementary Fig. S1; and Supplementary Table S2), with a rapid apoptotic effect (through the UPR) in estrogen-independent and endocrine-resistant breast cancer models (**Figs. 7–10** and Supplementary Fig. S7B–S7C).

This research area is of particular importance given that breast cancer is projected to double by 2030 than it was in 2011 (13). The majority will be ER-positive with a high risk of recurrence, even with clinically low-risk disease (T1N0; ref. 15). Moreover, treated metastases often harbor private "driver" mutations, compared with untreated metastases (52). In the case of ER-positive HER2-negative breast cancer, metastases treated with endocrine therapy acquire somatic single-nucleotide variants (47). This highlights the need to evaluate and develop new rapidly-acting breast cancer therapeutics such as estrogens. The recent long-term follow-up results of the Women's Health Initiative Trials (53, 54) reaffirm the clinical potential of novel
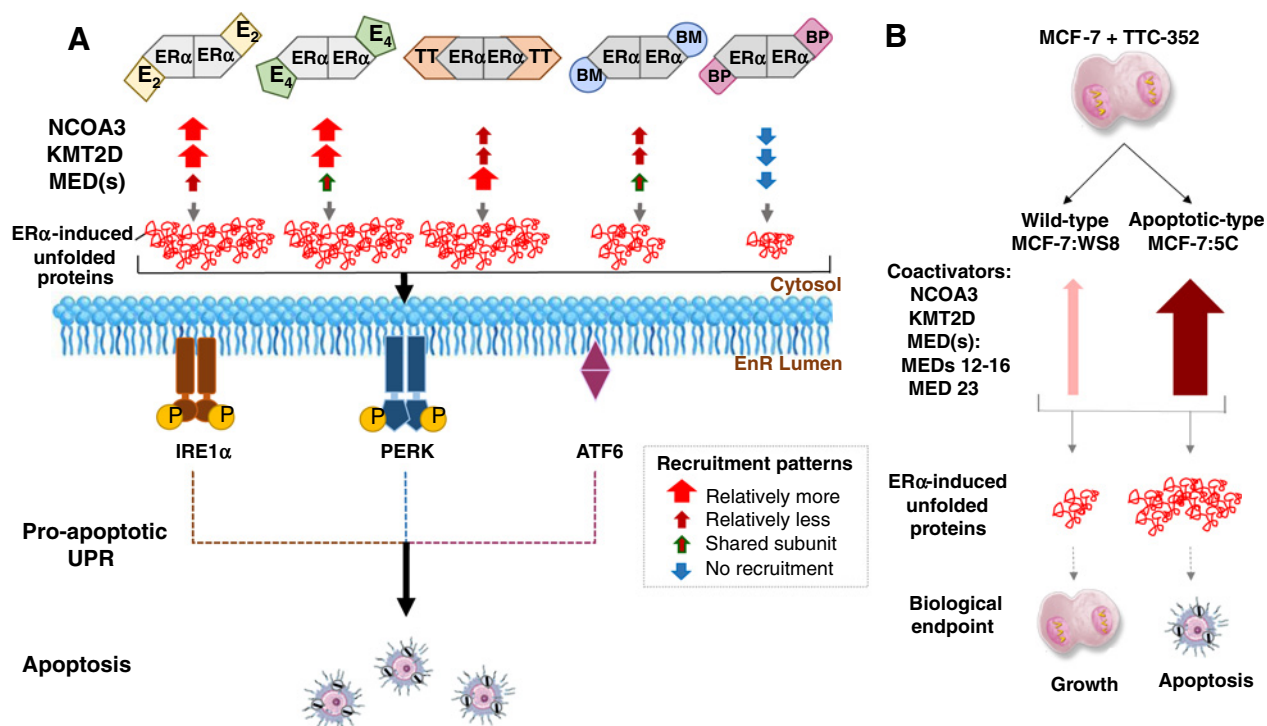
Figure 10.
Schematic representation of the study's conclusions highlighting major ER coactivator-binding differences in MCF-7:5C between E_2, E_4, ShERPAs, and BPTPE, and with ShERPA TTC-352 between WT MCF-7:WS8 and LTED endocrine-resistant MCF-7:5C breast cancer. **A,** E_2, E_4, ShERPA BMI-135, ShERPA TTC-352, and BPTPE major ER coactivators' recruitment, and antitumor molecular mechanism in MCF-7:5C. E_2:ERα and E_4:ERα complexes mainly recruit NCOA3, KMT2D, and many of the same MEDs, and induce a high threshold of stress, through the synthesis of unfolded and/or misfolded proteins, leading to rapid apoptosis. TTC-352 (referred to as TT in the illustration) recruited more MED subunits than E_2, but less NCOA3 and KMT2D than E_2 and E_4, with a similar threshold of stress and timing of apoptosis to E_2 and E_4. BMI-135 (referred to as BM in the illustration) recruited less NCOA3 and KMT2D than E_2 and E_4, and shared MED subunit recruitment with E_4, which generated a lower threshold of stress and delayed apoptosis (48) compared with E_2, E_4, and TTC-352. BPTPE (referred to as BP in the illustration) did not have much of a coactivator recruitment, which generates a very low threshold of stress and a much more delayed course of apoptosis (48) compared with E_2, E_4, TTC-352, and BMI-135. This differential ligand:ERα:coactivator-recruitment-and-induced EnR stress sets the therapeutics apart, in terms of the timing of activating the UPR, followed by inducing apoptosis. The box (in gray) highlights the observed recruitment patterns: thick arrow (red) represents relatively more recruitment, thin arrow (burgundy) is relatively less recruitment, thin arrow (burgundy with green border) is shared subunit recruitment, and thin arrow (blue) is no recruitment. **B,** TTC-352's paradoxical effect in WT growth-inducing breast cancer MCF-7:WS8 versus LTED apoptosis-inducing breast cancer MCF-7:5C. NCOA3, KMT2D, and many MEDs (especially MED12–16 and MED23) are recruited to ER, in MCF-7:5C treated with TTC-352 (thick arrow in maroon), compared with E_2, but these same coactivators are reduced upon the treatment of MCF-7:WS8 with TTC-352 (thin arrow in rose). This differential ligand:ERα:coactivator-recruitment-and-induced EnR stress phenotypically sets the two breast cancer models apart.

and safe estrogenic therapy in significantly reducing breast cancer incidence and mortality in patients with LTED.

MD simulations and MM-GBSA calculations for WT ERα in complex with TTC-352, E_2, and BPTPE are valuable methodologies to discover key ligand–receptor interactions, which aid the pharmacologic classification of TTC-352. Most importantly, they identify key structural components of estrogenic therapeutics that ensure the appropriate closure of the ERα LBD by H12 in LTED breast cancer. This closure is a prerequisite for the activation of ERE-mediated UPR and apoptosis, which is the basis of their antitumor properties.

The H-bonds of TTC-352's benzothiophene scaffold to Glu353, followed by the H-bond to His524, are the most stable contacts contributing to the binding mechanism of TTC-352, which are also the two binding features specific for the estrogenic activity of E_2 (E_2's A ring to Glu353; **Fig. 6A–B**). Such strong H-bond between TTC-352 and Glu353 induces stability in the LBD and, consequently, to H3. This supports the formation of the H-bonds between the side-chain of Asp351 (H3) to the backbone of Leu539 and Leu540 (H12), which stabilizes H12 in the full-agonist conformation (**Fig. 5C**). Such LBD-

stabilizing network of H-bonds is preserved with TTC-352, but more so with E_2, which explains the altered potency of TTC-352:ERα compared with E_2:ERα. By contrast, BPTPE's binding mechanism is governed by the H-bond of BPTPE's angular phenolic OH to Thr347, followed by the hydrophobic contacts, and a significantly weaker H-bond to Glu353 (**Figs. 5E** and **6C**). Although the H-bond between BPTPE's angular phenolic group and Thr347 stabilizes its binding, it disturbs the H-bond network within H3 and the stabilizing H-bonds to H12 (i.e., Asp351 to Leu 539 and Leu540). As a result, H12 is prevented from adopting the proper orientation specific for the ER full-agonist conformation (**Fig. 5F**). This is consistent with BPTPE's reduced recruitment of coactivators (**Fig. 4A**), and our previous reports (48) of its delayed activation of ERα-induced UPR and apoptosis as well as its functional modulation from a partial agonist (**3OH**TPE) to a full agonist (**Z2OH**TPE) by the removal of the para-phenol substitution (46).

Both, Asp351 and H12, play a critical role in modulating the estrogenic and antiestrogenic intrinsic efficacy of the ligand–ER complex. The natural mutation Asp351Tyr was discovered and

overexpressed in TAM-stimulated MCF-7 tumors grown in athymic mice (55). The molecular pharmacology of the WT ER (56) and Asp351Tyr ER (57) was established by stable transfection into ER-negative MDA-MB-231 breast cancer. Unexpectedly, Asp351Try ER converted the raloxifene:WT Asp351 ER complex from antiestrogenic to estrogenic (58). Subsequent X-ray crystallography of the raloxifene: ER LBD (22) demonstrated the critical role of the antiestrogenic side-chain containing a piperidine ring N to shield and neutralize Asp351, which prevented the closure of H12 and the subsequent *ERE* activation. Subsequent interrogation of the structural modulation of raloxifene and its interactions with Asp351 demonstrated how Asp351 modulates the estrogenic and antiestrogenic efficacy of the ligand–ER complex (59).

ESR1 somatic mutations, *Y537S* and *D538G*, stabilize ERα in the agonist state and are linked to acquired resistance to endocrine therapies (60). Mutations *Tyr537Ser* and *Asp538Gly* were most prevalent in breast cancer metastases (47), especially patients with AI-resistant breast cancer. These mutations improve the closure of H12 over ERα's LBD, through interacting with Asp351 and recruiting coactivators in the absence of estrogen, which increases the estrogen-like properties of the complex (47).

ERE DNA pulldowns and MS are valuable methodologies to determine if TTC-352 has an ERα:coactivators' binding profile of a full or partial agonist, and better understand why the TTC-352:ERα: coactivators' complex in the LTED endocrine-resistant MCF-7:5C is phenotypically apoptosis-promoting, whereas such complex in WT MCF-7 is phenotypically growth-promoting.

In MCF-7:WS8 breast cancer, TTC-352 and BMI-135 are different from BPTPE in terms of NCOA1–2 (or SRC-1–2) and MED subunit recruitments, with NCOA3 (or SRC-3) not being readily enriched with either ShERPAs compared with E_2 and E_4 (**Fig. 4A**). BPTPE did not recruit many of the E_2-enriched coactivators and only a subset of endoxifen-enriched coregulators (**Fig. 4**). In MCF-7:5C breast cancer, TTC-352 and BMI-135 recruited NCOA3 and KMT2D at much lower levels than E_2 and E_4, with TTC-352 recruiting more MED subunits than E_2, while BMI-135 displaying shared MED subunit recruitment with E_4 (**Fig. 4A**). BPTPE did not have much of coactivator binding (**Fig. 4A**).

TTC-352's differential recruitment of MED subunit types alongside their differential enrichment levels could explain its ability to cause a higher threshold of stress of ER-mediated unfolded proteins followed by earlier apoptosis, compared with that with BMI-135 (**Fig. 10A**). In MCF-7:5C, NCOA3, KMT2D, and many MEDs (especially MED12–16 and MED23) are recruited to ERα with TTC-352, compared with E_2, but these coactivators are reduced upon the treatment of MCF-7: WS8 with TTC-352 (Supplementary Table S5). TTC-352's higher recruitment of major ER coactivators in MCF-7:5C, compared with MCF-7:WS8, can explain its ability to cause a high threshold of stress of ER-mediated unfolded proteins followed by apoptosis, making it phenotypically apoptosis-promoting versus the growth-promoting MCF-7:WS8 (**Fig. 10B**). The altered recruitment patterns of major ER coactivators for transcriptional activation, with TTC-352, BMI-135, and E_4, in comparison with the levels promoted by E_2 or BPTPE, can better explain the observed differences in their potency and ERα-mediated UPR.

Our MD simulations data complement the MS data whereby the dynamics of H12 orchestrate ER's coactivator-mediated transcriptional activity. In the agonist complex structure, H12 forms one side of a hydrophobic coactivator-binding pocket, which allows the recruitment of an LXXLL motif present in many transcriptional cofactors (61). This is, especially, true with SRC-1–3 that possess three

LXXLL motifs, two of which bridge across the ER dimer (at least for an extended polypeptide containing all three motifs), which accounts for the 100-fold higher affinity relative to the single LXXLL-containing peptide (62). The overexpression of SRC-3 is observed in over 50% of breast cancers and leads to constitutive ER-mediated transcriptional activity in the agonist confirmation, conferring endocrine resistance in preclinical models and in patients treated with TAM (63). E_2, E_4, TTC-352, and BMI-135 in complex with ERα yield an agonist confirmation of the ligand–ER complex (**Figs. 5–6**; ref. 48) and, subsequently, recruit more coactivators (**Fig. 4A**), opposite to BPTPE. H12 acts as a molecular switch with the contribution of those H-Bond networks (**Fig. 6**) and such coactivators (**Fig. 4A**).

We demonstrate that the structure-function model of the synthetic estrogen mimic TTC-352 is a less potent full estrogen agonist compared with E_2, allowing H12 to seal the LBD, which recruits many E_2-enriched coactivators and induces rapid ERα-mediated UPR and apoptosis. This contradicts the model of the benchmark partial agonist BPTPE, not allowing H12 to seal the LBD properly, which does not recruit many E_2-enriched coactivators, and induces delayed ERα-mediated UPR and apoptosis. These data suggest that patients with breast cancer would potentially benefit more from full agonists like TTC-352 rather than partial agonists, because of BPTPE's delayed UPR-apoptotic effect. A partial agonist with delayed apoptosis might create a higher probability of tumor clonal evolution and acquired resistance (64).

Authors' Disclosures

Authors' Contributions

B. Abderrahman: Conceptualization, resources, data curation, software, formal analysis, supervision, validation, investigation, visualization, methodology, writing-original draft, project administration, writing-review and editing. **P.Y. Maximov:** Data curation. **R.F. Curpan:** Data curation, software, formal analysis, writing-original draft. **S.W. Fanning:** Methodology. **J.S. Hanspal:** Data curation. **P. Fan:** Resources. **C.E. Foulds:** Methodology. **Y. Chen:** Data curation. **A. Malovannaya:** Software, methodology. **A. Jain:** Data curation. **R. Xiong:** Resources. **G.L. Greene:** Methodology. **D.A. Tonetti:** Resources. **G.R.J. Thatcher:** Resources. **V.C. Jordan:** Conceptualization, supervision, funding acquisition, project administration, writing-review and editing.

Acknowledgments

References

1. Jordan VC, Brodie AM. Development and evolution of therapies targeted to the estrogen receptor for the treatment and prevention of breast cancer. Steroids 2007;72:7–25.
2. Jordan VC, Dix CJ, Allen KE. The effectiveness of long-term treatment in a laboratory model for adjuvant hormone therapy of breast cancer. In: Salmon SE, Jones SE, editors. Adjuvant therapy of cancer II. New York: Grune and Stratton; 1979. p. 19–26.
3. Early Breast Cancer Trialists' Collaborative Group. Tamoxifen for early breast cancer: an overview of the randomised trials. Lancet 1998;351:1451–67.
4. Yao K, Lee ES, Bentrem DJ, England G, Schafer JI, O'Regan RM, et al. Antitumor action of physiological estradiol on tamoxifen-stimulated breast tumors grown in athymic mice. Clin Cancer Res 2000;6:2028–36.
5. Early Breast Cancer Trialists' Collaborative Group, Davies C, Godwin J, Gray R, Clarke M, Cutter D, et al. Relevance of breast cancer hormone receptors and other factors to the efficacy of adjuvant tamoxifen: patient-level meta-analysis of randomised trials. Lancet 2011;378:771–84.
6. Sgroi DC, Sestak I, Cuzick J, Zhang Y, Schnabel CA, Schroeder B, et al. Prediction of late distant recurrence in patients with oestrogen-receptor-positive breast cancer: a prospective comparison of the breast-cancer index (BCI) assay, 21-gene recurrence score, and IHC4 in the TransATAC study population. Lancet Oncol 2013;14:1067–76.
7. Ariazi EA, Cunliffe HE, Lewis-Wambi JS, Slifker MJ, Willis AL, Ramos P, et al. Estrogen induces apoptosis in estrogen deprivation-resistant breast cancer through stress responses as identified by global gene expression across time. Proc Natl Acad Sci U S A 2011;108:18879–86.
8. Lonning PE, Taylor PD, Anker G, Iddon J, Wie L, Jorgensen LM, et al. High-dose estrogen treatment in postmenopausal breast cancer patients heavily exposed to endocrine therapy. Breast Cancer Res Treat 2001;67:111–6.
9. Ellis MJ, Gao F, Dehdashti F, Jeffe DB, Marcom PK, Carey LA, et al. Lower-dose vs high-dose oral estradiol therapy of hormone receptor-positive, aromatase inhibitor-resistant advanced breast cancer: a phase 2 randomized study. JAMA 2009;302:774–80.
10. Iwase H, Yamamoto Y, Yamamoto-Ibusuki M, Murakami KI, Okumura Y, Tomita S, et al. Ethinylestradiol is beneficial for postmenopausal patients with heavily pre-treated metastatic breast cancer after prior aromatase inhibitor treatment: a prospective study. Br J Cancer 2013;109:1537–42.
11. Dudek AZ, Liu LC, Fischer JH, Wiley EL, Sachdev JC, Bleeker J, et al. Phase 1 study of TTC-352 in patients with metastatic breast cancer progressing on endocrine and CDK4/6 inhibitor therapy. Breast Cancer Res Treat 2020;183:617–27.
12. Schmidt M, Hönig A, Zimmerman Y, Verhoeven C, Almstedt K, Battista M, et al. Abstract P5–11–15: estetrol for treatment of advanced ER+/HER2- breast cancer. Cancer Res 2020;80).
13. Rosenberg PS, Barker KA, Anderson WF. Estrogen receptor status and the future burden of invasive and in situ breast cancers in the United States. J Natl Cancer Inst 2015;107:djv159.
14. Reyes C, Engel-Nitz NM, DaCosta Byfield S, Ravelo A, Ogale S, Bancroft T, et al. Cost of disease progression in patients with metastatic breast, lung, and colorectal cancer. Oncologist 2019;24:1209–18.
15. Schroeder B, Zhang Y, Stal O, Fornander T, Brufsky A, Sgroi DC, et al. Risk stratification with breast cancer index for late distant recurrence in patients with clinically low-risk (T1N0) estrogen receptor-positive breast cancer. NJP Breast Cancer 2017;3:28.
16. Xiong R, Patel HK, Gutgesell LM, Zhao J, Delgado-Rivera L, Pham TND, et al. Selective human estrogen receptor partial agonists (ShERPAs) for tamoxifen-resistant breast cancer. J Med Chem 2016;59:219–37.
17. Tonetti DA, Xiong R, Zhao J, Gutgesell L, Dudek AZ, Thatcher GR. (Abstract e14090) Efficacy, maximal tolerated dose, and toxicokinetics of TTC-352 in rats and dogs, a partial ER agonist for metastatic ER+ breast cancer. J Clin Oncol 2017;35(suppl 15):509.
18. Jordan VC, Curpan R, Maximov PY. Estrogen receptor mutations found in breast cancer metastases integrated with the molecular pharmacology of selective ER modulators. J Natl Cancer Inst 2015;107:djv075.
19. Pejerrey SM, Dustin D, Kim JA, Gu G, Rechoum Y, Fuqua SAW. The impact of ESR1 mutations on the treatment of metastatic breast cancer. Horm Cancer 2018;9:215–28.
20. Niu J, Andres G, Kramer K, Kundranda MN, Alvarez RH, Klimant E, et al. Incidence and clinical significance of ESR1 mutations in heavily pretreated metastatic breast cancer patients. Onco Targets Ther 2015;8:3323–8.
21. Pink JJ, Jordan VC. Models of estrogen receptor regulation by estrogens and antiestrogens in breast cancer cell lines. Cancer Res 1996;56:2321–30.
22. Brzozowski AM, Pike AC, Dauter Z, Hubbard RE, Bonn T, Engstrom O, et al. Molecular basis of agonism and antagonism in the oestrogen receptor. Nature 1997;389:753–8.
23. Yi P, Wang Z, Feng Q, Pintilie GD, Foulds CE, Lanz RB, et al. Structure of a biologically active estrogen receptor-coactivator complex on DNA. Mol Cell 2015;57:1047–58.
24. Maximov PY, Myers CB, Curpan RF, Lewis-Wambi JS, Jordan VC. Structure-function relationships of estrogenic triphenylethylenes related to endoxifen and 4-hydroxytamoxifen. J Med Chem 2010;53:3273–83.
25. Gates LA, Gu G, Chen Y, Rohira AD, Lei JT, Hamilton RA, et al. Proteomic profiling identifies key coactivators utilized by mutant ERα proteins as potential new therapeutic targets. Oncogene 2018;37:4581–98.
26. Jiang SY, Wolf DM, Yingling JM, Chang C, Jordan VC. An estrogen receptor positive MCF-7 clone that is resistant to antiestrogens and estradiol. Mol Cell Endocrinol 1992;90:77–86.
27. Murphy CS, Pink JJ, Jordan VC. Characterization of a receptor-negative, hormone-nonresponsive clone derived from a T47D human breast cancer cell line kept under estrogen-free conditions. Cancer Res 1990;50:7285–92.
28. Lasfargues EY, Coutinho WG, Redfield ES. Isolation of two human tumor epithelial cell lines from solid breast carcinomas. J Natl Cancer Inst 1978;61:967–78.
29. Engel LW, Young NA, Tralka TS, Lippman ME, O'Brien SJ, Joyce MJ. Establishment and characterization of three new continuous cell lines derived from human breast carcinomas. Cancer Res 1978;38:3352–64.
30. Fan P, Agboke FA, Cunliffe HE, Ramos P, Jordan VC. A molecular model for the mechanism of acquired tamoxifen resistance in breast cancer. Eur J Cancer 2014;50:2866–76.
31. Lewis JS, Osipo C, Meeke K, Jordan VC. Estrogen-induced apoptosis in a breast cancer model resistant to long-term estrogen withdrawal. J Steroid Biochem Mol Biol 2005;94:131–41.
32. Pink JJ, Jiang SY, Fritsch M, Jordan VC. An estrogen-independent mcf-7 breast-cancer cell-line which contains a novel 80-kilodalton estrogen receptor-related protein. Cancer Res 1995;55:2583–90.
33. Liu H, Lee ES, Gajdos C, Pearce ST, Chen B, Osipo C, et al. Apoptotic action of 17beta-estradiol in raloxifene-resistant MCF-7 cells in vitro and in vivo. J Natl Cancer Inst 2003;95:1586–97.
34. Clarke R, Brunner N, Katzenellenbogen BS, Thompson EW, Norman MJ, Koppi C, et al. Progression of human breast cancer cells from hormone-dependent to hormone-independent growth both in vitro and in vivo. Proc Natl Acad Sci U S A 1989;86:3649–53.

35. Brunner N, Boulay V, Fojo A, Freter CE, Lippman ME, Clarke R. Acquisition of hormone-independent growth in MCF-7 cells is accompanied by increased expression of estrogen-regulated genes but without detectable DNA amplifications. Cancer Res 1993;53:283–90.

36. Brunner N, Frandsen TL, Holsthansen C, Bei M, Thompson EW, Wakeling AE, et al. Mcf7/Lcc2 - a 4-hydroxytamoxifen resistant human breast-cancer variant that retains sensitivity to the steroidal antiestrogen Ici-182,780. Cancer Res 1993; 53:3229–32.

37. Brunner N, Boysen B, Jirus S, Skaar TC, HolstHansen C, Lippman J, et al. MCF7/LCC9: an antiestrogen-resistant MCF-7 variant in which acquired resistance to the steroidal antiestrogen ICI 182,780 confers an early cross-resistance to the nonsteroidal antiestrogen tamoxifen. Cancer Res 1997;57: 3486–93.

38. Fan P, Griffith OL, Agboke FA, Anur P, Zou X, McDaniel RE, et al. c-Src modulates estrogen-induced stress and apoptosis in estrogen-deprived breast cancer cells. Cancer Res 2013;73:4510–20.

39. Foulds CE, Feng Q, Ding C, Bailey S, Hunsaker TL, Malovannaya A, et al. Proteomic analysis of coregulators bound to ERalpha on DNA and nucleosomes reveals coregulator dynamics. Mol Cell 2013;51:185–99.

40. Malovannaya A, Lanz RB, Jung SY, Bulynko Y, Le NT, Chan DW, et al. Analysis of the human endogenous coregulator complexome. Cell 2011;145:787–99.

41. Saltzman AB, Leng M, Bhatt B, Singh P, Chan DW, Dobrolecki L, et al. gpGrouper: a peptide grouping algorithm for gene-centric inference and quantitation of bottom-up proteomics data. Mol Cell Proteomics 2018;17: 2270–83.

42. Speltz TE, Fanning SW, Mayne CG, Fowler C, Tajkhorshid E, Greene GL, et al. Stapled peptides with gamma-methylated hydrocarbon chains for the estrogen receptor/coactivator interaction. Angew Chem Int Ed Engl 2016;55: 4252–5.

43. Beriault DR, Werstuck GH. Detection and quantification of endoplasmic reticulum stress in living cells using the fluorescent compound, Thioflavin T. Biochim Biophys Acta 2013;1833:2293–301.

44. Sengupta S, Sharma CG, Jordan VC. Estrogen regulation of X-box binding protein-1 and its role in estrogen induced growth of breast and endometrial cancer cells. Horm Mol Biol Clin Investig 2010;2:235–43.

45. Obiorah I, Sengupta S, Curpan R, Jordan VC. Defining the conformation of the estrogen receptor complex that controls estrogen-induced apoptosis in breast cancer. Mol Pharmacol 2014;85:789–99.

46. Maximov PY, Abderrahman B, Hawsawi YM, Chen Y, Foulds CE, Jain A, et al. The structure-function relationship of angular estrogens and estrogen receptor alpha to initiate estrogen-induced apoptosis in breast cancer cells. Mol Pharmacol 2020;98:24–37.

47. Toy W, Shen Y, Won H, Green B, Sakr RA, Will M, et al. ESR1 ligand-binding domain mutations in hormone-resistant breast cancer. Nat Genet 2013;45: 1439–45.

48. Abderrahman B, Maximov PY, Curpan RF, Hanspal JS, Fan P, Xiong R, et al. Pharmacology and molecular mechanisms of clinically-relevant estrogen estetrol and estrogen mimic BMI-135 for the treatment of endocrine-resistant breast cancer. Mol Pharmacol 2020;98:364–81.

49. Jordan VC, Lieberman ME. Estrogen-stimulated prolactin synthesis in vitro. Classification of agonist, partial agonist, and antagonist actions based on structure. Mol Pharmacol 1984;26:279–85.

50. Shiau AK, Barstad D, Loria PM, Cheng L, Kushner PJ, Agard DA, et al. The structural basis of estrogen receptor/coactivator recognition and the antagonism of this interaction by tamoxifen. Cell 1998;95:927–37.

51. Jordan VC. The new biology of estrogen-induced apoptosis applied to treat and prevent breast cancer. Endocr Relat Cancer 2015;22:R1–31.

52. Hu Z, Li Z, Ma Z, Curtis C. Multi-cancer analysis of clonality and the timing of systemic spread in paired primary tumors and metastases. Nat Genet 2020;52: 701–8.

53. Chlebowski RT, Anderson GL, Aragaki AK, Manson JE, Stefanick ML, Pan K, et al. Association of menopausal hormone therapy with breast cancer incidence and mortality during long-term follow-up of the women's health initiative randomized clinical trials. JAMA 2020;324:369–80.

54. Jordan VC. Molecular mechanism for breast cancer incidence in the women's health initiative. Cancer Prev Res (Phila) 2020;13:807–16.

55. Wolf DM, Jordan VC. The estrogen receptor from a tamoxifen stimulated MCF-7 tumor variant contains a point mutation in the ligand binding domain. Breast Cancer Res Treat 1994;31:129–38.

56. Jiang SY, Jordan VC. Growth regulation of estrogen receptor-negative breast cancer cells transfected with complementary DNAs for estrogen receptor. J Natl Cancer Inst 1992;84:580–91.

57. Catherino WH, Wolf DM, Jordan VC. A naturally-occurring estrogen-receptor mutation results in increased estrogenicity of a tamoxifen analog. Mol Endocrinol 1995;9:1053–63.

58. Levenson AS, Catherino WH, Jordan VC. Estrogenic activity is increased for an antiestrogen by a natural mutation of the estrogen receptor. J Steroid Biochem 1997;60:261–8.

59. Liu H, Park WC, Bentrem DJ, McKian KP, Reyes Ade L, Loweth JA, et al. Structure-function relationships of the raloxifene-estrogen receptor-alpha complex for regulating transforming growth factor-alpha expression in breast cancer cells. J Biol Chem 2002;277:9189–98.

60. Fanning SW, Mayne CG, Dharmarajan V, Carlson KE, Martin TA, Novick SJ, et al. Estrogen receptor alpha somatic mutations Y537S and D538G confer breast cancer endocrine resistance by stabilizing the activating function-2 binding conformation. Elife 2016;5:e12792.

61. Shiau AK, Barstad D, Radek JT, Meyers MJ, Nettles KW, Katzenellenbogen BS, et al. Structural characterization of a subtype-selective ligand reveals a novel mode of estrogen receptor antagonism. Nat Struct Biol 2002;9:359–64.

62. Nolte RT, Wisely GB, Westin S, Cobb JE, Lambert MH, Kurokawa R, et al. Ligand binding and co-activator assembly of the peroxisome proliferator-activated receptor-gamma. Nature 1998;395:137–43.

63. Osborne CK, Bardou V, Hopp TA, Chamness GC, Hilsenbeck SG, Fuqua SAW, et al. Role of the estrogen receptor coactivator AIB1 (SRC-3) and HER-2/neu in tamoxifen resistance in breast cancer. J Natl Cancer Inst 2003;95:353–61.

64. Rodriguez-Brenes IA, Wodarz D. Preventing clonal evolutionary processes in cancer: insights from mathematical models. Proc Natl Acad Sci U S A 2015;112: 8843–50.